ENGINE

ENhanced Geothermal Innovative Network for Europe

Workshop 3

Stimulation of reservoir and induced microseismicity

29 June - 1 July 2006

KARTAUSE ITTINGEN - SWITZERLAND

Workshop Proceedings

http://engine.brgm.fr

Collection actes / Proceedings

GEOWATT AG

SWISS GEOTHERMAL EXPERT GROUP

GEOTHERMAL ENERGY HYDROGEOLOGY ENGINEERING NUMERICS

ENGINE

ENhanced Geothermal Innovative Network for Europe

http://engine.brgm.fr

Workshop 3:

"Stimulation of Reservoir and Induced Microseismicity"

29 June – 1 July 2006

Kaurtause Ittingen – Zürich - Switzerland

Contribution book

Edited by: Clément Baujard and Thomas Kohl

GEOWATT AG
SWISS GEOTHERMAL EXPERT GROUP
GEOTHERMAL ENERGY HYDROGEOLOGY ENGINEERING NUMERICS

This document has been coordinated / edited by:

Clément **BAUJARD**, GEOWATT AG, Dohlenweg 28, CH-8050 Zürich, Switzerland

Thomas **KOHL**, GEOWATT AG, Dohlenweg 28, CH-8050 Zürich, Switzerland

PHONE: ++41 (0) 44 242 14 54

FAX: ++41 (0) 44 242 14 58

In bibliography, each contribution of this workshop will be referenced as the following example:
Asanuma, H., 2006. Analysis of induced microseismic events from HDR/EGS reservoirs by super resolution mapping techniques. From Baujard C. & Kohl T. (eds.) 2006, in Proceedings of the Engine Workshop 3 "Stimulation of Reservoir and Induced Microseismicity", 29 June - 1 July 2006, Zurich, Switzerland. ISBN 978-2-7159-0993-9. Orleans, BRGM Editions. Collection Actes/Proceedings. ISSN 1773-6161.

Keywords: Geothermal Energy; European Co-ordination Action; Renewable Energy; Enhanced Geothermal Systems (EGS); Unconventional Geothermal Resources (UGR); Drilling; Stimulation,Reservoir Assessment; Geothermal Exploration; Geophysical Methods; Geothermal Exploitation; Economics; Environmental Impacts; Social Impacts; Geothermal Education

Cover pictures
Thumbnail upper top: View of Zürich city, Switzerland, by S. Fleischmann.
Thumbnail lower top: Kartause Ittingen, Switzerland, by Ittingen Press Service.
Background: Basel Deap Heat Mining, Geothermal Power Plant under construction, Basel, Switzerland, by F. Ladner.

General support:

Thurgau

Swiss Confederation
Swiss Federal Office of Energy SFOE

http://engine.brgm.fr

Organization

Clément **BAUJARD** (baujard@geowatt.ch)
Thomas **KOHL** (kohl@geowatt.ch)
Sarah **SIGNORELLI** (signorelli@geowatt.ch)

GEOWATT AG

Scientific Committee

Thomas **KOHL** (kohl@geowatt.ch)
Ernst **HUENGES** (huenges@gfz-potsdam.de)
Sverrir **THORHALLSSON** (s@isor.is)

Engine Partners

BRGM
3, avenue C. Guillemin
BP 36009 - 45060 Orléans Cedex 2
FRANCE

GFZ
Telegrafenberg
14473 Potsdam
GERMANY

ISOR
Gresasvegi 9 – 108 Reykjavik
ICELAND

SIEP B.V.
Carel van Bylandtlaan 30
2596 HR Den Haag
NETHERLANDS

TNO
PO Box 6060
2600 JA Delft
NETHERLANDS

IGR DSC RAS
Imama Shamil str. 39-A
Makhachkala
RUSSIAN FEDERATION

CNR-IGG
Via G. Moruzzi 1 - 56124 Pisa
ITALY

CFG
3, avenue Claude Guillemin
BP 6429 - 45064 Orléans cedex 2
FRANCE

IE
Torgauer Str. 116
04347 Liepzig
GERMANY

ELTE
Egyetem tér 1-3 - 1053 Budapest
HUNGARY

CNRS
PO Box 20 - 23, rue du Loess
67037 Strasbourg
FRANCE

GGA-Institute
Stilleweg 2 - 30655 Hannover
GERMANY

GEIE
BP 38 - Route de Soultz
67250 Kutzenhausen
FRANCE

IGGL
T. Sevcenkos g. 13 - 03223 Vilnius
LITHUANIA

MeSy
Meesmannstr. 49 - 44807 Bochum
GERMANY

VUA
De Boelelaan 1085
1081 HV Amsterdam
NETHERLANDS

ENGINE

CRES
19th km, Marathonos Ave
19009 Pikermi Attikis
GREECE

NCSRD
Patriarchou Grigoriou &
Neapoleos st
Aghia Paraskevi - 15310 Attiki
GREECE

GPC
14, rue de la Perdrix, ZI Paris
Nord 2, Lot 109, BP 50030
95946 Villepinte CDG cedex
FRANCE

IFE
PO Box 40 - 2027 Kjeller
NORWAY

PGI
Rakowiecka 4
00-975 Warsawa
POLAND

GEUS
Oster Voldgade 10
1350 Copenhagen
DENMARK

UOR
Aramtei Romane, 5-9
410087 Oradea
ROMANIA

GEMRC IPE RAS
Box 30 - Troitsk
142190 Moscow Region
RUSSIAN FEDERATION

IVT RAN
Izhorskaya str. 13/19
125412 Moscow
RUSSIAN FEDERATION

JSC
9/1 Krasnokazarmennaya Str.
111250 Moscow
RUSSIAN FEDERATION

DHMA
Haering Geo-Project- Im Unter
Tollacher 2 8162 Steinmaur
SWITZERLAND

GEOWATT AG
Dohlenweg 28 - 8050 Zürich
SWITZERLAND

ORME
Hosdere Cad. 190/7-8-12
06550 Ankara
TURKEY

IGME
Rios Rosas, 23 - 28003 Madrid
SPAIN

CERTH
6th km Charilaou-Thermi Road
PO Box 361 -
57001 Thermi-Thessaloniki
GREECE

CONTRIBUTION SUMMARY

Introductory note for ENGINE workshop "stimulation of reservoir and induced microseismicity", Zurich, 2006

GEISSMANN Markus , Swiss Federal Office of Energy

In the past decades Switzerland has produced more electricity than it consumed. The production was made up by hydropower (60%) and nuclear power plants (40%). At present, two phenomena have raised the energy issue in the public awareness : 1. In 2005, Switzerland has for the first time had an import surplus of electrical energy, and 2. the lifetime of the first built nuclear power plants in Switzerland will end in 15 years time. A increasing gap between consumption and production can be foreseen.

Facing this situation, the Federal Office of Energy prepares energy perspectives to list options for planning a long-term and sustainable energy policy that meets the principal requirements of supply security, protection of the environment, economic viability and social acceptance. Four different scenarios show possible paths to Switzerland's energy future. One of these scenarios relies largely on renewable energy sources thogether with a strong increase in energy efficiency and aims to the so-called "2000W society".

In this 2000W scenario, geothermal energy plays a key-role among the other renewable energies. Only geothermal and hydropower plants can provide base load energy. But future climatic changes may have an unpredictable impact on the seasonal precipitations and on hydropower generation, and so geothermal energy might become even more important.

The Federal Office of Energy addresses the issue by conducting a R+D program on geothermal energy generation. The program strongly supported the preparatory work for the "Deep Heat Mining" Project in Basel, Switzerland, where a hot dry rock geothermal power plant is currently under construction. But the development of geothermal power generation into large scale application is still a huge task and it will take a long time.

Since the problems of energy supply and CO_2 emissions have a global scope, it seems natural that they should be solved by international collaboration. ENGINE is a classic example for such collaboration. The Federal Office of Energy is happy to host the ENGINE workshop on stimulation and microseismicity in Switzerland!

Zürich, June 30, 2006

SESSION I :
Review of stimulation techniques

ENGINE – **EN**hanced **G**eothermal **I**nnovative **N**etwork for **E**urope
Workshop 3, "Stimulation of reservoir and microseismicity"
Kartause Ittingen, Zürich, June 29 – July 1, 2006, Switzerland

Stimulation of geothermal wells in basaltic rock in Iceland

AXELSSON Gudni, ÍSOR, Iceland GeoSurvey, Reykjavík, gax@isor.is
THÓRHALLSSON Sverrir, ÍSOR, Iceland GeoSurvey
BJÖRNSSON Grímur, ÍSOR, Iceland GeoSurvey

Abstract

Stimulation operations are commonly part of the completion programs of geothermal wells drilled in the basaltic environment of Iceland. The purpose is to enhance the output of the wells either by improving near-well permeability that has been reduced by the drilling operation itself or to open up hydrological connections to permeable zones not intersected by the well in question. The methods used involve applying high-pressure water injection, sometimes through open-hole packers, or intermittent cold water injection with the purpose of thermal shocking. Stimulation operations are most commonly applied for a few hours to a few days while in a few instances stimulation operations have been conducted for some months. The stimulation operations often result in well productivity being improved by a factor of 2-3. Emphasis is placed on careful reservoir monitoring during stimulation operations. Seismic monitoring has only been applied in a few cases and examples are available where long-term water injection has caused a marked change in seismic activity as well situations where long-term high-pressure injection has caused no micro-seismic activity at all.

Keywords: geothermal, volcanic, stimulation, monitoring

Introduction

Iceland is a geologically young country (< 16 Myrs) lying on the Mid-Atlantic Ridge, which is the boundary between the North American and Eurasian tectonic plates. As a result of its location Iceland is tectonically and volcanically very active with abundant geothermal resources associated with this activity. A map of the country is presented in Fig. 1, which shows the volcanic zone passing through the country and the numerous geothermal areas.

The geothermal systems are classified as low-temperature or high-temperature systems. The low-temperature systems, which by definition have a reservoir temperature below 150°C, are all located outside the volcanic zone (see Fig. 1). About 250 such systems are known at present with the largest ones located in SW- and S-Iceland on the flanks of the volcanic zone, but smaller systems are found throughout the country. The heat-source for the low-temperature activity is believed to be the abnormally hot crust of Iceland, but faults and fractures, which are kept open by the continuously ongoing tectonic activity, also play an essential role by providing the channels for the water circulating through the systems and mining the heat at depth (Axelsson and Gunnlaugsson, 2000). The low-temperature resources are suitable for direct uses, such as space heating.

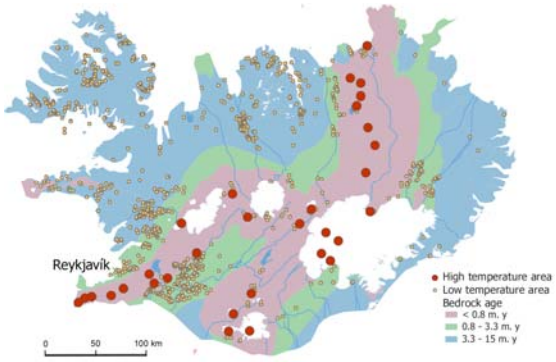

Figure 1. Locations of geothermal areas in Iceland. Also shown are the basic components of the geology of the island.

The high-temperature systems, which by definition have a reservoir temperature above 200°C, are located within the volcanic zone (Fig. 1). At least 26 high-temperature areas with steam fields are known at present in Iceland. These areas are directly linked to the active volcanic systems and the heat sources are believed to be mostly cooling magma bodies, i.e. intrusions of various shapes and sizes, as well as magma chambers. The high-temperature resources are suitable for electricity production, co-generation and industrial uses.

Geothermal resources account for just over half of the primary energy supply for the population of Iceland. The direct geothermal use in Iceland, mostly for space heating, totalled about 23,800 terajoules (TJ = 10^{12} J) in 2004, corresponding to 6,600 GWh/a. In addition, geothermal electricity production amounted to 1,484 GWh/a that same year (Ragnarsson, 2005). Geothermal electricity production is expected to have more than doubled in 2007.

This has required intensive exploration and drilling activity. It started during the middle of last century with intensive drilling commencing in the 1960's and 1970's. At the end of 2004 more than 570 geothermal production wells had been drilled in Iceland, with a total combined depth of about 550 km. In addition to this more than 900 exploration wells, deeper than 100 m, had been drilled in Iceland at this time.

Stimulation operations are commonly an integral part of the completion programs of geothermal wells drilled in Iceland, for high-temperature as well as low-temperature wells (Steingrímsson and Gudmundsson, 2005). The purpose is to enhance the output of the wells and the operations are usually conducted at the end of drilling. Emphasis is placed on careful well- and reservoir monitoring during stimulation operations in Iceland.

This paper reviews the stimulation operations conducted in geothermal wells drilled in the basaltic environment of Iceland, both the procedures used, the results and associated monitoring. A few representative examples are presented as well as results of a few cases of micro-seismic monitoring.

Stimulation operations

The purpose of geothermal production well stimulation is to enhance the output, or productivity, of the wells either by improving near-well permeability that has been reduced by the drilling operation itself (feed-zones clogged by drill cuttings or drilling-mud) or to open up hydrological paths to permeable zones not intersected by the well in question. In the case of injection wells the purpose is similarly to enhance the injectivity of such wells.

Methods and procedures

The following are the principal methods used for stimulation operations:

(A) Air-lift aided drilling and air-lift cleaning.

(B) Water circulation through drill string at well bottom.

(C) Well-head water injection, often at high pressure.

(D) Water injection above, or below, inflatable open-hole packers.

(E) Water injection through double packers.

(F) Intermittent cold water injection and well heating-up.

(G) Acidizing by well-head acid injection or acid injection through packers or coil-tubes.

Of these methods (A), (B), (C), (D) and (F) are regularly used in Iceland. Air-lift aided drilling (A), which has proven to be successful in preventing the clogging-up of feed-zone during drilling, is not a stimulation operation per se, but helps in maximizing well output. A schematic illustration of the setup for this procedure is presented in Fig. 2(a). Air-lift cleaning (A) and water circulation (B), at the end of drilling, help to restore feed-zone permeability reduced during drilling. Both these methods are a regular part of drilling operations in low-temperature fields in Iceland and the latter method (B) is also used during high-temperature drilling (see also (F)).

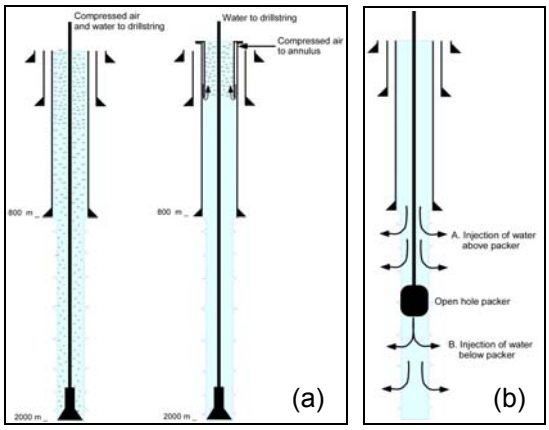

Figure 2. Schematic illustration of the setup for (a) air-lift aided drilling and (b) stimulation with an inflatable open-hole packer.

Methods (C) and (D) can be looked upon as proper stimulation methods. They both involve the injection of cold water, most often at high pressures, either through the well-head or above or below a packer placed at a specific depth. The pressures applied can be of the order of a few MPa, to some tens of MPa, with water flow-rates determined by the capacity of the equipment used and the water supply as well as the injectivity of the well involved. By using inflatable packers the stimulation can be focused on specific well intervals rather than the whole open section (see Fig. 2(b)). Method (C) is frequently used in drilling operations in Iceland while method (D) has mostly been used during low-temperature drilling. The latter method should be as applicable for high-temperature situations. These methods are not

as commonly applied as methods (A) and (B), however, being limited to wells with productivity below expectations. Some examples of low temperature stimulation operations are presented below.

Double packers (E) have hardly been used in stimulation operations in Iceland to-date, even though they have the potential of being more powerful as a stimulation tool then single packers. This is because they can be used to focus all the water injected into a specific, short interval, at higher pressures.

Intermittent cold water injection, with periods of thermal recovery in-between the injection periods (F), is one of the most common methods used for high-temperature well stimulation in Iceland. This method is aimed at causing cracking through thermal shocking. Some examples of this are presented below.

The stimulation of wells through acidizing (G) is in its infancy in Iceland, however. Its efficiency is, of course, limited in the basaltic environment of Iceland. It is used to remove calcite scale deposits within wells. Acidizing could be a powerful stimulation tool by dissolving scaling material in fractures.

Stimulation operations in Iceland are most commonly applied for a few hours to a few days while the drill rig is still on location. In some instances stimulation operations have been conducted for longer periods, from several days up to a few weeks. This is done after the drill rig has been moved from a well, and has mostly been limited to intermittent cold water injection and heating (F).

Low-temperature examples

The stimulation of low-temperature geothermal wells through inflatable packers (D) started as early as 1970. This was in the Reykir (Mosfellssveit) geothermal area, which has been utilized for space-heating in near-by Reykjavík since 1944. During the 1970's the Reykir field was redeveloped through the drilling of 39 large diameter wells ranging in depth from 800 to 2040 m. All these wells were stimulated by injection above and below inflatable packers with considerable success (Tómasson and Thorsteinsson, 1978).

In the Reykir stimulation operations an inflateable packer was set in-between two of the main feed-zones of a given well and water in-turn injected above and below the packer. Injection rates varied between 15 and 100 l/s and pressure increases at the feed-zones ranged from a few bar up to as high as 150 bar at the lowest permeability feed-zones treated (Tómasson and Thorsteinsson, 1978). A Reykir stimulation operation normally lasted a few days.

The results of the Reykir stimulation operations were appraised by two methods (Tómasson and Thorsteinsson, 1978):

(i) By comparing the eventual productivity of a well to the productivity at the end of drilling (before stimulation operations commenced). Thus the productivity was estimated to have generally improved by a factor of 30-40.

(ii) By comparing the final productivity of a well to the cumulative circulation losses during drilling. Thus the productivity was estimated to have increased as much as three-fold.

The drastic improvement indicated by appraisal method (i) may be mostly attributed to the reopening of feed-zones clogged by drill-cuttings during the drilling operation. The improvement estimated by method (ii) may mostly be attributed to increased feed-zone permeability, partly due to the removal of zeolite- and calcite-vein deposits and partly to increased permeability of near-well fractures in hyaloclastic rocks.

The results of the redevelopment of the Reykir geothermal field, both drilling and stimulation operations, were that the production capacity of the field increased from about 300 l/s by free-flow at the beginning of the 1970's to more than 1500 l/s by pumping in 1977.

Well SN-12 in the Seltjarnarnes low-temperature field in SW-Iceland was drilled to a depth of 2714 m in the fall of 1994. The well appeared to be almost non-productive at the end of drilling. A comprehensive ten day stimulation program was, therefore, initiated (Tulinius *et al.*, 1996). The program involved, firstly, high-pressure well-head injection and, secondly, high-pressure injection below a packer placed at 1412 m depth. After about twelve hours of well-head stimulation the pressure dropped suddenly, indicating that the well had been stimulated (see Fig. 3). At the same time the water level response increased suddenly in two near-by monitoring wells. The saw-tooth appearance of the well-head pressure results from the fact that not enough water was available to maintain the desired injection flow-rate uninterrupted. During the second stimulation phase (packer at 1412 m) the well appeared to be stimulated even further.

Well SN-12 eventually produced about 35 l/s with a drawdown of roughly 60 m, and the stimulation had increased the yield of the well by a factor of nearly 60 (see Fig. 4). Thus well SN-12, which appeared to be almost non-productive at the completion of drilling, had

turned into a good production well. It is believed that during the stimulation some previously closed fractures, or interbed contacts, reopened connecting well SN-12 to the main fracture system of the geothermal reservoir.

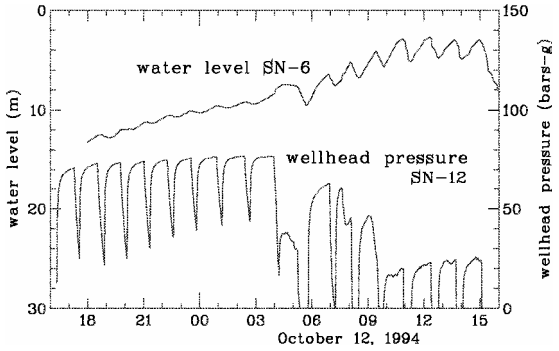

Figure 3. Water level in well SN-6 and well-head pressure of well SN-12, both in the Seltjarnarnes field SW-Iceland, during the well-head injection phase of the stimulation operations in well SN-12. From Tulinius et al. (1996).

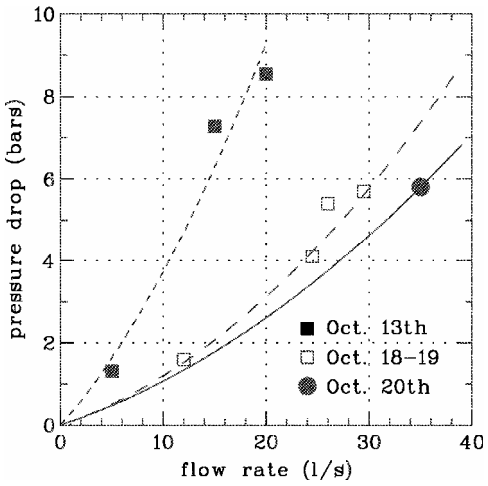

Figure 4. Results of production testing of well SN-12 in the Seltjarnarnes field during stimulation operations showing the gradual improvement in the potential of the well. Before the stimulations the well only yielded about 1.5 l/s with 150 m draw-down. From Tulinius et al. (1996).

High-temperature examples

The Krafla geothermal power plant in NE-Iceland, which has been in operation since 1977, now produces electricity at a rate of 60 MW_e. Krafla is a high-temperature system inside the active Krafla volcanic complex in the NE-part of the volcanic zone of Iceland (see Fig. 1). Reservoir temperatures in the Krafla-system range from 210 to 340°C. About 30 production wells have been drilled in the area to date and a large part of these have been stimulated at the end of drilling. The stimulation operations have almost exclusively involved cold water injection/circulation, with intermittent periods of thermal recovery used in many cases (F). Inflatable packers and high pressures have not been employed in the Krafla stimulations (one exception). During such stimulation operations the drill string is kept in the well, or drill pipes without a drill-bit or drilling motor are placed at a desired depth (usually near bottom), and the injection/ circulation alternated from being through the drill-string to being through the annulus between drill-string and borehole walls. After such cooling episodes injection is stopped to allow the well to heat up.

A good example from Krafla is well KJ-14, which was drilled to a depth of 2100 m in 1980 (Stefánsson *et al.*, 1982). At the end of drilling circulation losses were only about 4 – 8 l/s. During 3 days of stimulation, which included about 12 hours of heating up, circulation losses increased to about 40 l/s (see Fig. 5). Following the stimulation operation the transmissivity of the reservoir around the well was estimated as $khg/\upsilon = 3 \cdot 10^{-4}$ m^2/s, which indicated that well KJ-14 would be the most productive well drilled in Krafla up to that time. This was confirmed during production testing of the well when it yielded about 15 kg/s of steam.

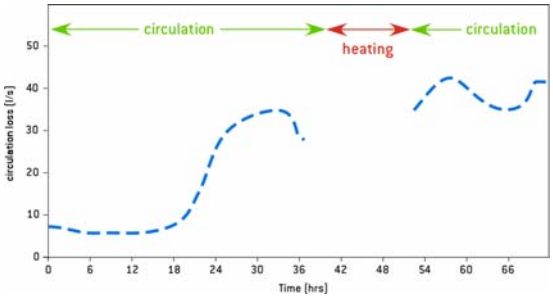

Figure 5. Circulation losses during stimulation of well KJ-14 in Krafla, NE-Iceland, at the end of August 1980. Based on Stefánsson et al. *(1982).*

The successful stimulation of well KJ-14, as well as other such high-temperature cases, has been partly attributed to the opening of pre-existing fractures by thermal stresses as well as creation of new fractures by thermal cracking. This is in addition to the reopening of feed-zones clogged by drill cuttings. It may be mentioned that Flores *et al.* (2005) present the results of a comparative, techno-economic study of different well stimulation techniques, partly based on information on stimulation operations in the Krafla field. They show that thermal fracturing is potentially the most attractive, but least understood, stimulation technique.

The Hengill volcanic system, which lies in the volcanic zone of SW-Iceland some 30 km east of Reykjavík, is another area were intense

high-temperature drilling has been ongoing during the last decades. Three geothermal production fields are associated with the Hengill system; (1) the Nesjavellir field where geothermal production started in 1990 and a 120 MW_e electrical and 290 MW_t thermal power plant is now in operation, (2) the Hellisheidi field where a 90 MW_e electrical power plant will start operating in 2006 and (3) the Hveragerdi field that is utilized for different direct purposes by the local community.

Stimulation procedures comparable to those used at Krafla have been used for many of the wells drilled at Nesjavellir and Hellisheidi, i.e. cold water injection/circulation with intermittent thermal recovery periods for a few days at the end of drilling. Recently the stimulation procedures have been modified in order to increase their potential for success. This involves continuing the stimulation of wells after drill rigs have been removed, often for a few weeks. Thus much longer heating and cooling periods can be realized, resulting in greater thermal stresses with more stimulation potential. In this case the cold water is injected through the well-head.

This modified stimulation procedure has been applied to some wells in the Hengill region, in particular wells with lower than average injectivity at end of drilling. One example is well HE-8, which was drilled to a depth of a little over 2800 m in 2003 (Björnsson, 2004). This is one of the deepest wells drilled in Iceland to date. The injectivity of the well at end of drilling was of the order of 1 – 2 (kg/s)/bar. After standard stimulation procedures involving a few heating/cooling cycles, as described above, well HE-8 was allowed to heat up for about 3 months. Following this 50 kg/s af 20°C water were injected into the well for about two weeks, which concluded the stimulation of the well. Pressure transient testing at the end of the stimulation program indicated an injectivity of 6 – 7 (kg/s)/bar for the well, a quite drastic improvement from the injectivity estimated at the end of drilling.

Again the stimulation of well HE-8 is partly attributed to the reopening of feed-zones clogged by drill cuttings and partly to increased near-well permeability resulting from thermal stresses/cracking. The re-opening of clogged feed-zones is believed to be particularly significant when high-speed bottom hole drilling motor assemblies are used instead of conventional drilling methods, as the former method produces smaller drill cuttings. This may explain 50-75% of the stimulation in the case of well HE-8.

A more recent Hengill example involves well HE-21, which was drilled to a depth of 2100 m in the Hellisheidi field in early 2006. The drilling of this well concluded without a significant loss of circulation. At first the well was stimulated for two days through a few cycles of cold water circulation and heating, during which injection rates varied between 40 and 70 l/s, with injection pressures as high as 5 bar. After the drill rig had been removed, and the open section of the well had been allowed to heat to 250-320°C, stimulation operations were continued. This involved two periods of cold water injection lasting 24 and 40 hours, respectively.

Data from the stimulation program for well HE-21 have not been fully analyzed yet, but a gradual rise in injectivity was observed, from near zero to 30 l/s. It may also be mentioned that the well was imaged by an acoustic televiewer, which revealed many near vertical fractures of variable orientation. Continuous thermal cracking over long depth sections was also seen.

At least three of the recent drilling and completion/stimulation operations in the Hengill geothermal region have interestingly generated substantial microseismic activity, detected by the national seismic network operated by the Icelandic Meteorological Office (see http://www.vedur.is). These are the two wells discussed above, wells HE-8 and HE-21, in addition to well NJ-24, which was drilled in 2005 in the Nesjavellir field. The first two cases will be discussed further below.

Results

During stimulation operations success can often partly be attributed to the re-opening of feed-zones, or fractures, that have been blocked by drill cuttings during drilling. In low-temperature situations this occurs when reservoir pressure is lower than the pressure of the water column in the well being drilled, a situation that can be avoided by air-lift aided drilling (see (A) in section 2.1 above). Such an unbalanced pressure situation is also the case during most high-temperature drilling operations and feed-zone blocking appears to be particularly severe when drilling motor assemblies with high penetration rates are used, as has been mentioned.

Besides re-opening (cleaning) of feed-zones blocked by drill-cuttings, stimulation operations often result in additional improvement in well injectivity and productivity. This ranges from no improvement to an improvement that is commonly by a factor of 2-3. In exceptional cases even greater improvement is realized. Such “secondary” stimulations are attributed to the creation of new hydrological connections to permeable structures not intersected by the well in question, either through the removal of scale-deposits in fractures or through the opening of existing fractures, or even creation

of new ones, through hydraulic or thermal stresses.

A higher "secondary" stimulation success ratio has been realized in the younger Quaternary formations of Iceland than in older Tertiary rocks. This is partly because fractures tend to be sealed in older formations in contrast with the younger ones. Yet it is also certain that crustal stress conditions play a key role here as in general in geothermal activity in Iceland and elsewhere. This has neither been studied systematically nor quantitatively in Iceland as of yet. More successful stimulation operations are to be expected where favourable stress conditions prevail, such as in the Quaternary regions of Iceland.

No clear picture has emerged on what geological conditions are most favourable for stimulations in high-temperature situations in Iceland. A clear correspondence between injectivity at the end of a stimulation operation and the productivity of a high-temperature well does not exist, in contrast to low-temperature wells where a simple one-to-one relationship exists. This can be clearly seen in Table 1 below, which shows relevant data for a number of production wells drilled in the Reykjanes high-temperature field in extreme SW-Iceland, where a 100 MW_e electrical power plant started operation in May 2006. The table seems to indicate that high injectivity wells have a productivity that is even higher than predicted by injectivity, while the wells with the lowest injectivity have even lower productivity indices.

Table 1. Information on geothermal production wells in the Reykjanes high-temperature field in SW-Iceland (II_1 = injectivity index at the end of drilling, II_2 = injectivity index at the end of stimulation operations and PI = productivity index based on production testing). Based on Hjartarson and Thórhallsson (2006).

Well	Depth (m)	Temp. (°C)	II_1	II_2	PI
RN-10	2050	310	-	6.6	2.3
RN-11	2250	295	-	>10	10
RN-12	2510	290	-	8-9	20-40
RN-13	2460	290	-	4-5	1-2
RN-14	2310	290	6	6-7	-
RN-15	2510	280	3.5	4	1
RN-16	2630	220	1.2	2	-
RN-18	1820	>285	5	5.4	1.5
RN-19	2250	250-260	5	5	-
RN-21	1710	275	6	13	6
RN-22	1680	305	10	10	15
RN-23	1920	305	-	38-48	50
RN-24	2110	>275	-	10-20	38

Monitoring

Well/reservoir monitoring

Emphasis is placed on careful well- and reservoir monitoring during stimulation operations in Iceland, both for the purpose of assessing the progress and results of the operations and to extract information on relevant reservoir properties as well. Tómasson and Thorsteinsson (1978), Tulinius *et el.* (1996) and Björnsson (2004) provide examples were such reservoir monitoring data is interpreted in the same manner as conventional pressure transient data. The following are the main parameters monitored during geothermal well stimulation operations in Iceland:

(1) Injection flow-rate, injection/well-head pressure or water level and injection temperature.

(2) Down-hole pressures with electronic or mechanical instruments. This was done as early as in the 1970's in the Reykir field (see above).

(3) Temperature- and pressure profiles for wells being stimulated.

(4) Pressure interference in selected monitoring wells, as well as flow monitoring for near-by production wells. See example in Fig. 3 above.

(5) Monitoring of well injectivity/productivity through repeated step-rate tests.

Not all of these items are monitored in every stimulation program, what is monitored is dictated by the scale of a program and often limited by various technical aspects. Monitoring item (1) is, of course, rudimentary, while item (2), if monitored, provides the most valuable information. Item (3) is used to locate the feed-zones involved.

Seismic monitoring

Seismic monitoring is generally not applied in geothermal stimulation operations in Iceland. Yet, micro-seismic monitoring has been implemented in conjunction with three geothermal injection projects. They are the following:

(a) A low-temperature reinjection experiment was conducted in the Laugaland field in central N-Iceland from late 1997 through 1999 (Axelsson *et al.*, 2000). During the experiment 6 – 21 kg/s of 15-20°C water were injected into two low permeability wells at well-head pressures of up to 28 bar. Part of the experiment involved the installation of an automatic network of six ultra-sensitive seismic monitoring stations

around the field, which was expected to detect all seismic events, down to size M_L = -1, caused by the reinjection. No such events were detected, however, indicating that either the pressure increase at depth in the fractured Laugaland reservoir was not sufficient to cause earthquakes, or that the deviatoric stresses needed to trigger such events had already been released through two decades of hot water production and greatly varying reservoir pressure at Laugaland.

(b) The Svartsengi high-temperature geothermal field in SW-Iceland is utilized for co-generation of heat and electricity. Portable seismographs were operated around the field for 4 months in 1993 in order to monitor microearthquake activity throughout a reinjection test during which up to 30 kg/s of about 100°C water were injected by gravity into well SG-6 (Brandsdóttir *et al.*, 2002). No detectable earthquakes occurred within the Svartsengi field during the test and it was concluded that the pressure changes resulting from the injection were probably well below the level needed to induce seismicity. The more than 20 bar draw-down in the field has reduced pore-pressure and consequently increased rock strength, which in-turn may have raised the fracture limit of rocks in the Svartsengi system.

(c) During the summer of 2004 a 20-station seismic array was deployed around the Krafla field with the purpose of monitoring seismic activity before, during and after a 10-day break in reinjection into well K-26 (Lees *et al.*, 2004). Work on the data collected is in progress, it aims at using various seismic data processing techniques, on the high-quality data collected, to map the main subsurface fracture system of Krafla. Natural seismic activity at Krafla is not high at the present time and most of the events recorded did appear to be related to the reinjection, even though a clear relationship between changes in injection rates and seismicity did not emerge.

Even though seismic activity has not been specifically monitored during the stimulation operations discussed here seismic activity, associated with such operations, has been detected by the national seismic network as already mentioned.

During the drilling and stimulation of well HE-8 in the Hellisheidi field, which has been described above, 22 small earthquakes were detected, both at end of drilling in July and August 2003 as well as during the stimulation attempt in November the same year (Björnsson, 2004). A total of 18 quakes were detected during the July-August period and 4 in November, in a 2x2 km area surrounding the well (see figures 6 and 7) at a depth between approximately 4 and 6 km. As the quake activity correlates strongly with the injection activity, it is concluded that fluid pressure changes inside the local reservoir fracture network have triggered these quakes, i.e. it is suspected that the water pressure exceeded the minimum horizontal stress. The exact nature of the quakes is to be defined, however.

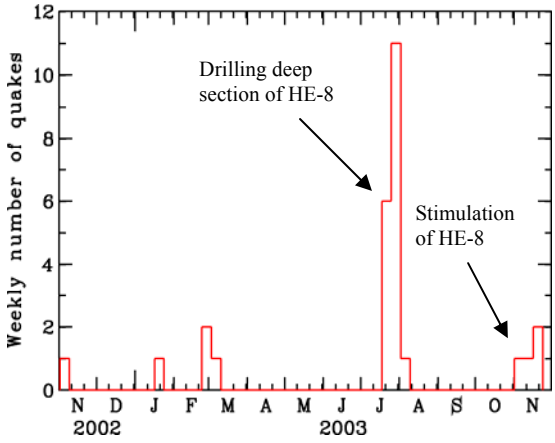

Figure 6. Weekly number of quakes in a 2x2 km area surrounding well HE-8 in the Hellisheidi field during drilling and stimulation. From Björnsson (2004).

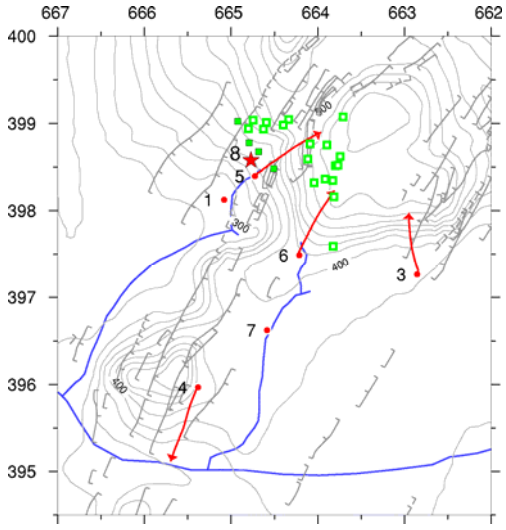

Figure 7. Well locations and quake epicenters near well HE-8 in the Hellisheidi field during drilling and stimulation. Wells are shown by red squares, quakes in July and August 2003 by open green boxes and in November by filled green boxes. From Björnsson (2004).

The correlation also implies that sufficient permeability, and direct pressure communication, exists between the two best feed-zones of well HE-8 at 1350 and 2000 m depth, on one hand, and the general 4-6 km depth of the quake centers, on the other hand. Large normal faults near well HE-8 that dip a few degrees to the east are suspected as likely surfaces of quake generation. The 4-6 km depth of penetration of fluid pressure changes suggests a considerably deeper geothermal reservoir than previously assumed.

An effort was recently made to better understand the coupled effect of current subsurface stress and the permeability distribution to cold water injection into well HE-21 in the Hellisheidi field, discussed above. As the well was flushed by cold water at completion several small quakes were located in the area. When cold water injection was repeated during a later stimulation phase (see above) no quakes were detected during 24 hours of injection. During a third injection test two mobile seismic stations were set up in the area for increased accuracy, onset of seismic activity was observed after more than 24 hours of injection. The activity continued for the remaining 40 hours of injection. Around 80 events were detected in the field data and interpretation is ongoing.

Quake epicenters during stimulation of well HE-21 are located at 3-6 km depth, substantially deeper than the water injection interval between 1 and 2 km depth, approximately. These data suggest that there is pressure communication between this injection interval and 3-6 km depth. If correct, the thermal resource may have considerable higher generation potential than currently assessed by models that reach a maximum of 2-3 km depth.

Concluding remarks

This paper has reviewed the stimulation techniques utilized in geothermal fields in Iceland. High-pressure injection through inflatable packers, is not as commonly applied in low-temperature wells as was the case 2-3 decades ago, partly because air-lift aided drilling has reduced the need for such stimulations. This method still has great potential in particular cases, however. Stimulation of high-temperature production wells through cyclic cooling and thermal shocking/fracturing has proven to be effective, especially when the stimulation period can be extended for several weeks after the drill rig has been removed. Seismic monitoring should be more commonly applied during long stimulation- and injection operations, since it may provide highly valuable resource information. The same applies to reservoir monitoring, such as interference monitoring.

Acknowledgements

The authors thank several colleagues at ÍSOR for information used here and Benedikt Steingrímsson of ÍSOR for a careful review of the paper.

References

Axelsson, G. and E. Gunnlaugsson (convenors), 2000: Long-term Monitoring of High- and Low-enthalpy Fields under Exploitation. International Geothermal Association, *World Geothermal Congress 2000 Short Course*, Kokonoe, Kyushu District, Japan, May, 226pp.

Axelsson, G., Ó.G. Flóvenz, A. Hjartarson, S. Hauksdóttir, G. Sverrisdóttir, F. Árnason, Á. Árnason and R. Bödvarsson, 2000: Thermal energy extraction by reinjection from the Laugaland geothermal system in N-Iceland. *Proceedings of the World Geothermal Congress 2000*, Kyushu-Tohoku, Japan, May-June, 3027-3032.

Björnsson, G., 2004: Reservoir conditions at 3-6 km depth in the Hellisheidi geothermal field, SW-Iceland, estimated by deep drilling, cold water injection and seismic monitoring. *Proceedings of the 29th Workshop on Geothermal Reservoir Engineering*, Stanford University, California, January, 8pp.

Brandsdóttir, B., H. Franzson, P. Einarsson, K. Árnason and H. Kristmannsdóttir, 2002: Seismic monitoring during an injection experiment in the Svartsengi geothermal field, Iceland. *Jökull*, **51**, 43-52.

Flores, M., D. Davies, G. Couples and B. Pálsson, 2005: Stimulation of geothermal wells, can we afford it? *Proceedings of the World Geothermal Congress 2005*, Antalya, Turkey, April, 8pp.

Gudmundsson, Á., 2001: An expansion of the Krafla power plant from 60 to 90 MW_e – geothermal considerations. *Geothermal Resources Council Transactions*, **25**, 741-746.

Hjartarson, A. and S. Thórhallsson, 2006: Production potential of Reykjanes wells. Status on April 28, 2006 (in Icelandic). Iceland GeoSurvey, memorandum April 28, 2006, Reykjavík, 2pp.

Lees, J., J. Rial, E. Thomson and M. Yang, 2004: The seismic imaging of the Krafla geothermal field. Progress report, Geothermal Seismology Group, Wave Propagation Labora-

tory, University of North Carolina, Chapel Hill, North Carolina, October 15, 2004, 21pp.

Ragnarsson, Á., 2005: Geothermal development in Iceland 2000-2004. *Proceedings of the World Geothermal Congress 2005*, Antalya, Turkey, April, 11pp.

Stefánsson, V., Á. Gudmundsson, B. Steingrímsson, G.K. Halldórsson, H. Ármannsson, H. Franzson and T. Hauksson, 1982: Krafla – well KJ-14. Drilling, research and production characteristics (in Icelandic). Orkustofnun report OS82061/JHD09, Reykjavík, 119pp.

Steingrímsson, B. and Á. Gudmundsson, 2005: Geothermal borehole investigations during and after drilling. *Proceedings of the UNU-GTP and KenGen Workshop for Decision Makers on Geothermal Projects and Management,* Naivasha, Kenya, November, 10pp.

Thorsteinsson, Th., 1975: Redevelopment of the Reykir hydrothermal system in southwest Iceland. *Proceedings of the Second UN Symposium on the Development and Use of Geothermal Resources*, San Francisco, California, May, 2173-2180.

Tómasson, J. and Th. Thorsteinsson, 1978: Drillhole stimulation in Iceland. *Proceedings of the ASME Energy Technology Conference and Exhibition*, Houston, Texas, November, 5pp.

Tulinius, H., G. Axelsson, J. Tómasson, H. Kristmannsdóttir and Á. Gudmundsson, 1996: Stimulation of well SN-12 in the Seltjarnarnes low-temperature field in SW-Iceland. *Proceedings of the 21st Workshop on Geothermal Reservoir Engineering*, Stanford University, California, January, 489-496.

ENGINE – **EN**hanced **G**eothermal **I**nnovative **N**etwork for **E**urope
Workshop 3, "Stimulation of reservoir and microseismicity"
Kartause Ittingen, Zürich, June 29 – July 1, 2006, Switzerland

Hydraulic fracturing in the hydrocarbon Industry

FOKKER Peter A. , TNO, Netherlands, peter.fokker@tno.nl

Abstract

This paper gives some of the issues present in the hydraulic fracturing design, application and evaluation procedures in the hydrocarbon industry.

Depending on the reservoir, hydraulic fracture treatments have as a goal either to bypass damaged permeability close to the well, or to create additional contact area between the reservoir and the well. While for the first goal the key is to maximize the fracture conductivity and thus the fracture width in the vicinity of the wellbore, the second goal requires large fractures, preferably connecting to an already existing network of natural fractures. Typically, such massive hydraulic fractures are placed in low-permeability reservoir.

The successful placement of a propped hydraulic fracture depends critically on the quality of the design input data. Such data contain knowledge about the in-situ stresses, the reservoir permeability, the elastic parameters, and the fracture propagation criteria. Minifrac tests are designed to disclose such parameters. To this end, the time-dependent behaviour of the pressure after a short injection test above the fracture pressure is analysed with specially designed software. Further important knowledge is the containing capacity of different layers in the subsurface, as these determine the height / length ratio of the fracture. A profile of the parameters, required to assess this, however, is often difficult to obtain.

Even with good design input data and a properly operated fracturing treatment, the results are not always in line with the predictions. Knowledge is usually built up in specific areas during subsequent hydraulic fracturing treatments and their careful evaluation. Method that can help considerably in this evaluation are tiltmeter mapping and microseismic monitoring, by which the dimensions of the created fracture can be estimated.

Keywords: hydraulic fracturing, stimulation, oil and gas

Introduction

Many oil and gas wells in the hydrocarbon industry are stimulated for better performance. One of the possibilities of stimulation is hydraulic fracturing. With hydraulic fracturing, a fluid is pumped into the formation with such high rate and pressure that the formation strength is exceeded and a fracture develops. Coarse material – proppant – is then pumped along with the fracturing fluid with the aim to keep the created fracture open after the fracturing treatment has been finalized. The fracture acts as an improved connection between the reservoir and the well, where the proppant keeps the fracture open and facilitates the high permeability required for the stimulation to be effective. The current paper highlights a number of issues that play a role in hydraulic fracturing applications in the hydrocarbon industry. After the presentation of some basic principles, different kinds of hydraulic fracturing application will be given. Some remarks will then be made about the design, the monitoring, and potential pitfalls. Particular attention will be given to issues that are related to issues playing a role in stimulation of geothermal wells. The paper will be completed with a number of concluding remarks.

Hydraulic fracturing

Central in the discussion about hydraulic fracturing is the stress present in the subsurface. At greater depths, the largest normal stress component is usually vertical. Thus, the medium and minimum normal stress components are both horizontal. Hydraulic fracturing is tensile fracturing (i.e. mode I; see Figure 1); in that case the orientation of the fracture is perpendicular to the minimum in-situ stress and is vertical.

The principle of fracturing is that a fluid is pumped into the well and the perforations at a high rate. When the increasing pressure exceeds the minimum in-situ stress and the tensile stress, the formation breaks and a fracture develops. The displacement of the fracture walls causes an increase in stress

ahead of the tip. This stress exhibits a singular behaviour, described in the stress intensity factor. As long as the singularity is larger than the critical stress intensity factor, the fracture propagates further. On its turn, the displacement of the fracture walls is directly coupled to the volume of the fracture and therefore the fracture propagation criterion must be combined with a volume balance calculation. The volume balance states that the increase of fracture volume is determined by the difference between the injection rate and the leakoff rate. On its turn, the leakoff rate is controlled by the invasion of the fracturing fluid into the formation and the development of a filtercake on the fracture wall. This coupled process can be summarized conceptually as

$$\frac{dV}{dt} = Q_{inj} - Q_{leakoff}$$

$$Q_{leakoff} = \int_{fracture} v_{leakoff}\, dA$$

$$v_{leakoff} = \left(p_{frac} - p_{res}\right) \cdot d_{penetrated}$$

$$d_{penetrated} = \int_{0}^{t} v_{leakoff}\, dt'$$

$$w = \frac{V_{fracture}}{A_{fracture}}$$

$$K_I = f\left(w, A\right)$$

$$L \text{ increases when } \quad K_I > K_{Ic}$$

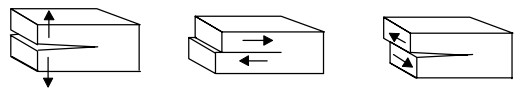

Mode I: Opening Mode II: Sliding Mode III: Tearing

Figure 1 Fracturing modes

There are a couple of issues that complicate the above described process. In the first place, the minimum in-situ stress does not need to be constant over the fracture area. The stress may in particular change on interfaces between subsurface layers. This makes the calculation of the propagation criterion far more difficult because the stress intensity factor depends critically on it. In the second place, the stress is not only influenced by the displacement of the fracture walls but also by the increase of pore pressure and the change in temperature when large amounts of fluid enter the reservoir. These effects are called poro-elasticity and thermo-elasticity. In the third place, the calculation of the leakoff rate is much more complicated then given above when the amount of fluid leaking to the reservoir is large in comparison to the volume of the fracture. In that case, the actual three-dimensional pressure field in the reservoir will determine the exact leakoff rate. This is in particular important when low-viscosity fracturing fluids like water are used.

The hydrocarbon industry has broad experience with hydraulic fracturing and many fracture models are around that simulate the fracturing process. Such simulators range from relatively simple single-layer tools to fully coupled simulators in which the fracturing process, the dynamic reservoir pressure response and the stress behaviour are taken into account [Ji et al, 2006]. In all cases, the more sophisticated the model, the more input is required. Very bad answers can be obtained when the input is wrong. Both a priori parameter estimation and a posteriori evaluation are critical to build a knowledge base in any area.

Types of Applications

The design and the execution of a hydraulic fracturing stimulation treatment is critically dependent on the goal that the operator wants to achieve. A number of classes can be distinguished in the hydrocarbon industry. The most classic application is massive hydraulic fracturing, which is primarily used in low-permeability reservoirs. The goal is to create a large fracture to enlarge the contact area between the well and the reservoir. Because of the low permeability of the reservoir, it is not so difficult to create a large contrast between the flow capacity of the fracture and of the reservoir. With the increasing application of horizontal wells, multiple fractures in a single well are often placed. This is achieved by progressive perforation from the toe to the heel of the well, and temporary shutoff of earlier treated intervals. Such shutoff can be accomplished with sand plugs, with removable packers, or with easily drillable composite bridge plugs.

For reservoirs with larger permeability, the problem is sometimes that the area around the well is damaged. Then a short fracture is created to bypass this damage. Special procedures are available to ensure that the width of the fracture is larger than the natural width with just clean fluid: proppant is already pumped in an early stage of the treatment such that it bridges the tip of the fracture and the stress intensity factor is smaller because only a part of the full fracture wall area is supported by the injection pressure. This is called tip-screen-out fracturing or frac-and-pack [Roodhart et al, 1994].

Another application, which may be of more interest to geothermal applications, is fracturing during water injection. Here, the injector is fractured without proppant, and this is therefore not stimulation in the strict sense. Many oil fields utilize water injection in order to maintain the reservoir pressure and to force the oil to the injector. However, to maintain the required injection rate, the pressure often needs to exceed the fracturing pressure. These cases require in particular the coupling with the reservoir behaviour that was described in the previous section. In some circumstances, water is used that has been produced associated with the produced oil. An even more complicating factor for the injection of produced water is that it may not be fully clean. Then the permeability around the fracture will decrease with the increasing amount of contaminants injected, and the interior of the fracture will progressively be plugged with contaminants that can not enter the reservoir pores [Gheissary et al, 1999] (Fig. 2).

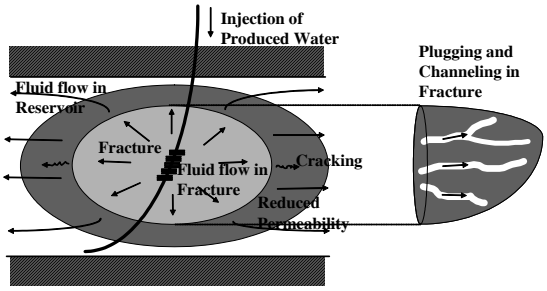

Figure 2 Processes associated with re-injection of produced water under fracturing conditions

In Texas, the fields in the Barnett shale play (Fig. 3) are completely different from most other fields known, and here a fracturing procedure typical for the area has been developed [Fisher et al, 2004]. The procedure is related to the way the fractures grow and to the response of the reservoir. The permeability of these fields is very low, in the μd range and they are only economic in combination with stimulation through hydraulic fracturing. Seismic monitoring has shown that the fractures that are induced in these fields grow in a complex network. With proper modeling, the fracture geometry can be approximately predicted, although the network development is still highly variable. It is the total network length and area, not just the conventional half-length of the fracture, which controls gas recovery and drainage patterns. Further, the fracture permeability is important, which has led the operators to use non-damaging fluids and low proppant loadings to perform their treatments.

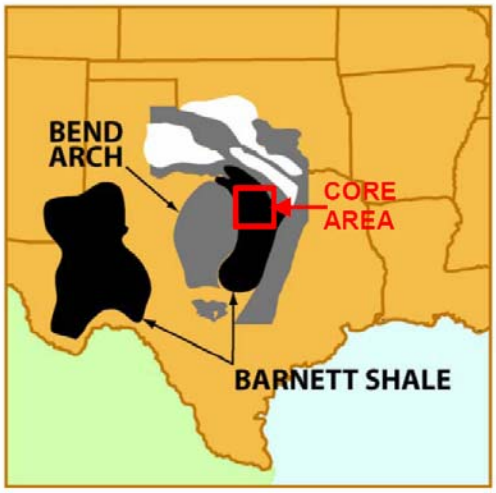

Figure 3 Geographical extent of Barnett shale [Fisher et al, 2004]

Considerations of Design

The goal of a hydraulic fracturing treatment is always an economic goal. In all cases, the design of the treatment should relate its costs to the expected benefits [Willis et al, 2005]. The benefits can be evaluated with simple analytic expressions [Prats, 1961], with comprehensive reservoir simulation, or with semi-analytic tools that allow some flexibility in the reservoir architecture and well completion [Fokker et al, 2005]. Users should realize that the productivity is critically dependent on the geology of the reservoir. Large reservoirs which exhibit flow barriers, for instance, may result in undrained reservoir parts. This can be countered by using multiple stages of fracturing from different positions in a horizontal well. McDaniel [2005] gives an overview of many techniques to achieve this, and he proposes a scorecard methodology to choose the best approach. His approach consists of evaluating the most important concerns and determining which technique copes best with them.

The fracture conductivity is an important number in evaluating what type of treatment should be chosen. It is a measure of the flow capacity of the fracture relative to the flow capacity of the reservoir and it is defined as

$$C_{fD} = \frac{k_f \cdot w}{k \cdot L}$$

According to Prats [1961], this number should be at least 1.6. However, the fracture conductivity is not a free-to-choose number – only the fracture length can be directly influenced by the job size. The width is dependent on the elastic modulus of the reservoir and the critical stress intensity factor,

and can only be indirectly be influenced by the choice of treatment design (like the tip-screen-out design mentioned above). The permeability of the resulting fracture is dependent on the grain size of the chosen proppant and on the cleanup behaviour of the fracturing fluid. A low-viscosity fluid (water) has the advantage that virtually no residue is left in the fracture interior; the drawback, however, is that proppant may fall out to the bottom of the fracture and large parts of the fracture close after pumping has stopped [Grieser 2003].

For the more detailed design of a fracturing treatment, more information is required. The parameters that influence the pressure most are the in-situ stress and the fracture net pressure. The latter is related to the critical stress intensity factor. These input data can be measured in a minifrac test. A small fracture without proppant is pumped into the reservoir and the pressure buildup and decline is closely measured. The speed of the pressure decline also provides information about the reservoir permeability or the leakoff behaviour of the fracturing fluid. The latter is of importance in establishing the fluid volumes necessary to achieve the required fracture dimensions. For these evaluations, comprehensive computer codes are available, mostly based on suitable scaling of the time. Figure 4 provides an example of such an analysis [Smith et al 2000].

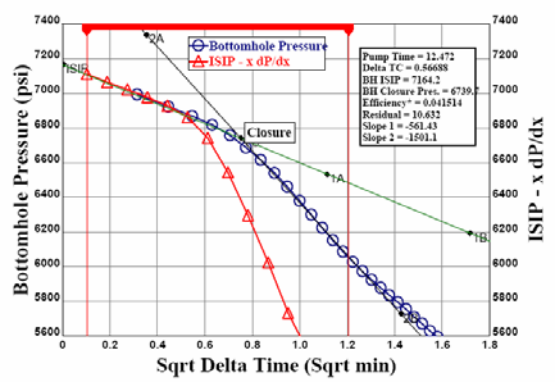

Figure 4 Minifrac test analysis with scaled time function [Smith et al 2000]

The structure of the reservoir can complicate the design of a hydraulic fracture considerably. When the reservoir exhibits layering, the stress may change at layer interfaces and it is very difficult to quantify such stress profiles. Naturally fractured reservoir may impact the development of the hydraulic fracture: depending on the stress situation, fractures may simply cross natural fractures, or follow the natural fracture over shorter or longer distances [Potluri et al 2005]. Further, pressurization of the reservoir due to the injection of large amounts of fluids, and the mechanical displacement of the fracture walls by the proppant, can change the stress profile and the associated direction of growth of the hydraulic fractures [Fisher et al, 2004]. It is such considerations that make hydraulic fracturing design difficult and that necessitate the buildup of a knowledge database in specific areas. This is the topic of the next Section.

Monitoring

The many uncertainties that are related to hydraulic fracture stimulation make the gradual buildup of a knowledge base crucial. This can only be achieved by careful evaluation of the treatment performance and the resulting productivity. A classic monitoring technique is the observation of the fracturing pressure. An increase in pressure, for instance, can indicate a tip-screen-out. Two other powerful techniques for monitoring the performance of the fracturing treatments during the operation are tiltmeters and microseismic monitoring [Warpinski, 1996; Warpinski et al, 2005].

With tiltmeters, the change in tilt is measured very accurately (Fig. 5) and it is inverted to a fracture geometry. Tiltmeters can be installed at the surface as well as in nearby offset wells. Surface tiltmeters permit larger flexibility in position but the distance to the source of the deformation makes them less precise. Surface tiltmeters have now been used for fracturing treatments down to a depth of 3000 m. For larger depths, tiltmeters in the treatment well or in an offset well are required.

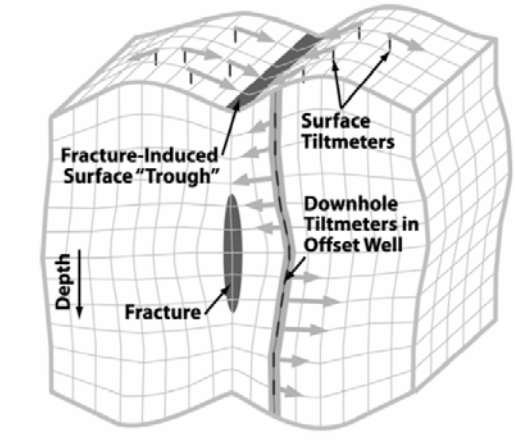

Figure 5 Deformation pattern induced by a vertical hydraulic fracture [Willis et al, 2005]

Microseismic fracture mapping provides an image of the fractures by detecting microseisms or micro-earthquakes that are triggered by shear slippage on bedding planes

or natural fractures adjacent to the hydraulic fracture. The location of the microseismic events is obtained using a downhole receiver array that is positioned at the depth of the fracture in an offset wellbore. Results from microseismic fracture mapping can be used to "calibrate" fracture growth models. Microseismic mapping has been instrumental in the development of understanding the fracturing in the Barnett shale. An example of the very complicated fracturing pattern that has been observed in one of the wells in that area is presented in Fig. 6.

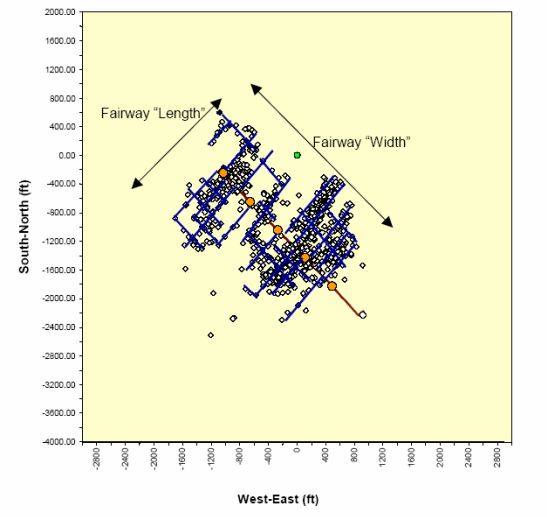

Figure 6 Plan view fracture map of a typical uncemented Barnett treatment with interpreted fracture structure [Fisher et al, 2004]

A method that is suitable to detect whether fractures are present in an injection well and where it is located is Hydraulic Impedance Testing (HIT). It is a completely non-invasive method, using only surface equipment to perform downhole fracture measurements. HIT can also provide a measurement of formation closure stress (minimum in-situ stress) to assist hydraulic fracture engineering and to monitor water injection wells.

Fracturing treatments must always be followed by a post-fracture analysis. A first evaluation can be with well testing, to determine the effective fracture size. This is important to know the effectiveness of the fracture placement [Bourdet, 2002]. The well test needs to be followed by monitoring the production of the fracture. A useful tool which relates the size of the stimulated region with gas production has been developed by Warpinski et al [2005]. The authors have named their method stimulated volume analysis (SRV). Six months of production are plotted against the stimulated volume as determined by microseismic mapping. Figure 7 shows how they obtained a fairly good correlation.

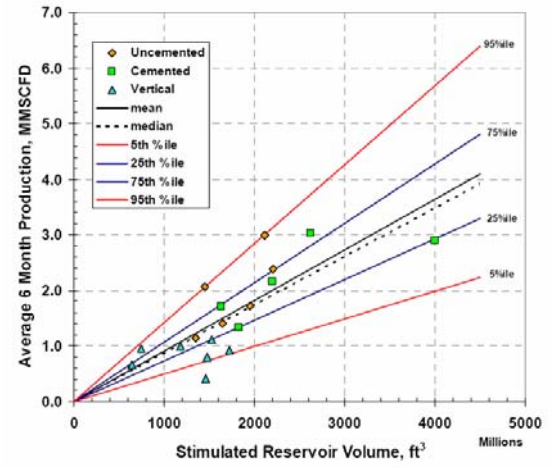

Figure 7 Stimulated Reservoir Volume plot [Warpinski et al, 2005]

Concluding remarks

Hydraulic fracturing treatments should be designed from their goal. In all cases, the goal of a hydraulic fracturing treatment is related to economics. The technical goal could be to increase the contact area between well and reservoir, to bypass damage, to create a large fracture network, or to maintain injection at a certain level. The goal of a fracturing treatment determines its size to a large extent. It also determines the type of treatment: should it be with high-viscosity liquid or with water; should there be high or low proppant concentrations; should the well be cemented or not; etcetera.

On a lower level, hydraulic fracturing should be designed with the right knowledge and input parameters. There are many fracture propagation models and many commercial software tools available that ease the design of a particular treatment. Still, a basic understanding of the rock mechanics and the design parameters is necessary. One needs to understand the impact of introducing the wrong value of a parameter, and the range of outcomes related to an uncertainty in the input. In particular, the relationship between the geology of the reservoir and the effectiveness of the hydraulic fracture is important.

Understanding the fracturing performance is helped by close monitoring. The pressure will always be recorded and a post-mortem analysis gives insight in the fracturing process. Monitoring during the fracturing process can also be done using tiltmeters and microseismic mapping. These are powerful techniques that give a direct measure of the spatial extent of the fracture.

The many uncertainties present in hydraulic fracturing call for the development of a knowledge base in areas where the technique is applied. Many case histories show that this incremental learning is one of the most important keys to success.

References

Bourdet, D. (2002), “Well test analysis: the use of advanced interpretation models”, Elsevier, Amsterdam.

Fisher, M.K., et al (2004), “Optimizing horizontal completion techniques in the Barnett shale using microseismic fracture mapping”, SPE 90051, SPE Ann. Techn. Conf & Exh, Houston.

Fokker, P.A., Verga, F. and Egberts, P.J.P. (2005) “New semi-analytic technique to determine horizontal well productivity index in fractured reservoirs”, SPE reservoir evaluation & Engineering, April, 123-131.

Gheissary, G., Fokker, P.A., Egberts, P.J.P., Floris, F.J.T., Sommerauer, G., and Kenter, C.J. (1999) “Simulation of fractures induced by produced water re-injection in a multi-layer reservoir”, SPE 54735, presented at the European Formation Damage Conference, The Hague, The Netherlands, 31 May – 1 June 1999.

Grieser, B., Hobbs, J., Hunter, J. and Ables, J. (2003), “The rocket science behind water frac design”, SPE 80933, SPE Production and Operations Symp., Oklahoma City, OK.

Ji, L., Settari, A., and Sullivan, R.B. (2006), “A New Approach to Hydraulic Fracturing Modeling — Fully Coupled With Geo-mechanical and Reservoir Simulation”, SPE 9428, SPE/EAGE Annual Conference and Exhibition, 12-15 June, Vienna, Austria.

McDaniel, B.W. (2005), “Review of current fracture stimulation techniques for best economics in multilayer, lower-permeability reservoirs”, SPE 98025, Eastern regional meeting, Morgantown, WV.

Potluri, N., Zhu, D., and Hill, A.D. (2005), “Effect of natural fractures on hydraulic fracture propagation”, SPE 94568, SPE Formation Damage Conference, Scheveningen, The Netherlands.

Prats, M. (1961) “Effect of vertical fractures on reservoir behavior - Incompressible fluid case”, SPE Journal (6/1961) 105 – 118.

Roodhart, L.P., Fokker, P.A., Davies, D.R., Shlyapobersky, J., and Wong, G.K. (1994), “Frac-and-pack stimulation: Application, design, and field experience” *J. Petr. Tech.* (March) 230-238.

Smith, J. E., Meyer, B.R., and Jacot, R.H. (2000), "Fracture pressure slope analysis for TSO’s in high-permeability formations,” SPE 63174, SPE Ann. Tech. Conf. & Exh., Dallas, TX.

Warpinski, N.R. (1996), “Hydraulic fracture diagnostics”, J. Petr. Sci. (October 1996), 907-910.

Warpinski, N.R., Kramm, R.C., Heinze, J.R., and Waltman, C.K. (2005), “Comparison of single- and dual-array microseismic mapping techniques in the Barnett shale”, SPE 95568, SPE Ann. Tech. Conf. & Exh., Dallas TX.

Willis, R.B., Fontaine, J., Paugh, L. and Griffin, L. (2005), “Geology and geometry: A review of factors affecting the effectiveness of hydraulic fractures”, SPE 97993, Eastern regional meeting, Morgantown, WV.

Review of Hydraulic stimulation Technology

RUMMEL Fritz, Ruhr Universität Bochum, Germany, fritz.rummel@ruhr-uni-bochum.de

Although explosives, acidizing and other methods have long been used in oil and gas well treatment, high pressure hydraulic stimulation was first time successfully intro-duced in the Hugoton Oil Field in Kansas by the Stanolind Oil & Gas Company (later on Pan American Petroleum Company) in 1948 (Clark, 1949). The technique was originally named Hydrafrac method. 16 years later more than 400.000 hydraulic frac-turing jobs have been performed in the free world. Early developments focussed on technological aspects like pumping capacities, hydraulic fluid viscosities and pumping rates, and proppant materials. Hubbert & Willis (1957) were the first to demonstrate conclusively the influence of tectonic stress to fracture orientation. The mathematical concepts based on Kirsch (1898), Sneddon (1946) or Barenblatt (1962) were devel-oped by Christianovich et al. (1959), Perkins & Kern (1961), Howard & Fast (1957), or Geertsma & de Klerk (1968). Fracture mechanics approaches to hydraulic fractur-ing were suggested by Aboud-Sayed et al. (1978), Rummel (1987), or Rummel & Hansen (1989). The powerful numerical simulator FRACPRO (RES 1991) is available commercially since app. 1990. A summary of oil and gas reservoir stimulation tech-nology is given by Economides & Nolte (1987). For geothermal energy exploitation from HDR-systems hydraulic fracturing was first applied within the LASL HDR project in 1975 ff (e.g. Burns 1990). The hydrofrac technique was experimentally investi-gated in the laboratory by Haimson (1968) and in-situ within the Falkenberg granite shallow geothermal frac project (Kappelmeyer & Rummel (1987), in the shallow French HDR project at Le Mayet de Montagne (Cornet 1988) or in the Cornwall gran-ite HDR project at about 2.5 km depth (Batchelor 1983). At Soultz-sous-Forêts almost 40 large-scale hydraulic stimulation experiments were carried out since 1988 which confirmed the concept of stimulation of pre-existing fractures for the creation of a large scale heat exchanger at depth (e.g. Baria et al. 1999). In this context hydraulic stimulation experiments as e. g. carried out in 9 km deep KTB borehole to induce microseismicity should be mentioned (Zoback & Harjes, 1997). Last not least the hy-draulic stimulation of dry water wells may become increasingly important for sustain-able water supply in many areas (Rummel 1997, Klee & Rummel (2005). The devel-opment of intelligent stimulation techniques and their physical understanding still is in demand for economic methane production from impermeable deep coal beds or for waste disposal into artificial fractures at great depth.

References :

Aboud-Sayed AS, Brechtel CE, Clifton RJ (1978): In-situ stress determination by hy-drofracturing: a fracture mechanics approach. JGR, 83, 2851-2862.

Baria R, Baumgärtner J, Rummel F, Pine RJ, Sato Y (1999): HDR/HWR reservoirs: concepts, understanding and creation. Geothermics, 28, 533-552, Pergamon.

Barenblatt GI (1962): The mathematical theory of equilibrium cracks in brittle fracture. Adv. Appl. Mechanics, 7, 55-129.

Batchelor AS (1983): Hot Dry Rock reservoir stimulation in the UK. Proc. 3rd Int. EC Seminar on Geoth. Energy, 681-711, Munich Nov. 1983.

Burns KL (1990): Hot Dry Rock Research – A compendium of publications Oct. 89 -Sept. 90, Los Alamos Nat. Lab. 1990 Fiscal year Report.

Christianovich SA, Zheltov YP, Barenblatt GI, Maximovich GK (1959): Theoretical principles of hydraulic fracturing of oil strata. Proc. 5th World Petr. Congr., New York, Section II 23, 289-296.

Clark, JB (1949): Hydrafrac process for well treatment. Div. Production, Am. Petr. Inst., paper 826-20-A, Spring Meeting Eastern District, Pennsylvania; Trans. AIME, 186, 1-3.

Cornet FH (1988): Projet Mayet de Montagne - etude in-situ de la perculation force d'eau en milieu granitique. Final Project Report, CEE-DGXII, AFME, CNRS.

Economides MJ, Nolte KG (1987): Reservoir stimulation. Schlumberger Educational Services Houston, SMP-7018.

Geertsma J, de Klerk F (1958): A rapid method of predicting width and extent of hy-draulically induced fractures. J. Petrol. Techn., 21, 1571-1581.

Haimson B (1968): Hydraulic fracturing in porous and nonporous rock and its poten-tial for determining in-situ stresses at great depth. PhD-thesis, Univ. Minnesota.

Howard GC, Fast CR (1957) Optimum fluid characteristics for fracture extension. Drilling & Production Practise, 261 ff.

Hubbert KH, Willis DG (1957): Mechanics of hydraulic fracturing. Trans. AIME, Vol. 210, 153-168.

Kappelmeyer O, Rummel F (1987): Terrestrial heat from impervious rocks – investi-gations in the Falkenberg granite massif. Geol. Jahrbuch, Reihe E/H 39, Schweizerbart Stuttgart.

Kirsch G (1898): Die Theorie der Elastizität und die Bedürfnisse der Festigkeitslehre Zeitschr. VDI, 42/29, 797-807.

Klee G. Rummel F (2005): Sustainable development of groundwater from hard rock formations. In: Rock Mech. with Emphasis on Stress (ed. Rummel), 223-234, Balkema.

Narashimhan TN (1987): Hydrodynamics of a vertical hydraulic fracture. Rep. Lawr. Berkeley Lab., Earth Sci. Div..

Perkins TK, Kern LR (1961): Width of hydraulic fractures. J. Petr. Techn., 937-949; Trans. AIME, 222 ff.

RES Resources Engineering Systems: Mechanics of fracturing and petroleum pro-duction. Seminar Hand-Out, Munich, June 1991.

Rummel F (1987): Fracture mechanics approach to hydraulic fracturing stress meas-urements. In: Fracture Mechanics of Rock (ed. Atkinson), 6, 217-239.

Rummel F (1997): Stimulation einer Mineralwasserbohrung mit geringer Schüttung. Der Mineralbrunnen, 10/97, 458-466.

Rummel F, Hansen J (1989): Interpretation of hydrofrac pressure recordings using a simple fracture mechanics simulation model. Int. J. Rock Mech., 26/6, 483-488.

Sneddon IN (1946): The distribution of stress in the neighbourhood of a crack in an elastic solid. Proc. Roy. Sic. London, A 187, 229-260.

Zoback MD, Harjes HP (1997): Injection induced earthquakes and crustal stress at 9 km depth at the KTB deep drilling site, Germany. JGR, 105/B8, 18477-18491.

ENGINE – **EN**hanced **G**eothermal **I**nnovative **N**etwork for **E**urope
Workshop 3, "Stimulation of reservoir and induced microseismicity"
Kartause Ittingen, Zürich, June 29 – July 1, 2006, Switzerland

Stimulation Techniques and implications from microseismicity

KOHL Thomas, Geowatt AG, Zürich, Switzerland, kohl@geowatt.ch;
BAUJARD Clément, Geowatt AG, Zürich, Switzerland

Abstract

Chemical and mechanical stimulations are commonly used in order to enhance hydraulic properties of EGS systems. Using chemical acids the reservoir conditions generally improve, however with largely varying success rates. Also, the success of permeability improvement by massive hydraulic injections ("mechanical stimulation") is not easily anticipated. Here, two main mechanisms are to be considered: shear fracturing (or faulting) and jointing (tensile fracture). Both methods increase the pore pressure in the rock, however at different levels. Depending on the stress regime, shear fracturing causes maximum pressures below the minimum stress component ($P \sim \sigma_{min}$). Slippage is induced in agreement with the Mohr (-Coulomb) Criterion on pre-existing mechanical discontinuities. The displacements generate larger apertures and possibly even new fractures. In contrast, jointing (tensile fracture) develops perpendicular to the least principal stress ($P > \sigma_{min}$). It is mostly applied in sedimentary rocks. Herewith, a single, far extending fracture can be created.

This paper provides an overview of stimulation techniques used in the past, classify them and define associated mechanisms. The focus is on mechanical stimulation. It describes results obtained through experiments, referenced in literature (using IGA and GRC databases, scientific literature and various reports). The generalization of the results is however not always possible since they depend on each site conditions (history, stress field, temperature…). Chemical stimulation techniques will be shortly examined.

Keywords: HDR, HFR, EGS, stimulation, review, stress field, geothermal

Introduction

Reservoir stimulation is a key technology in Hot Dry Rock (HDR) and/or Enhanced Geothermal Systems (EGS) development. Several research projects have been carried out over the past 30 years at widely different geological conditions and others are being planned.

This review compiles information and results obtained during stimulation campaigns performed since the beginning of HDR/EGS history, in the early 70's. Thus, data recorded and literature written on the following research projects were examined:

- Le Mayet-de-Montagne, France (1984-1987)
- Fenton Hill, New Mexico, US (1970-1993)
- Urach, Germany (1977-1986)
- Rosemanowes, UK (1976-1992)
- Soultz-sous-Forêts, France (1987-)
- Cooper Basin, Australia (running)
- Coso, California, US (running)
- Dixie Valley, Nevada, US (planned)
- Falkenberg, Germany
- Hijiori, Japan (1986-1999)
- Akinomya, Japan (1986-1991)
- Gamma, Japan (1983-1988)
- Ogachi, Japan (1990-1996)
- Fjällbäcka, Sweden (1983-1992)
- Gross Schönebeck, Germany (1990-)

As other sites exist all over the world, it is highly likely that new stimulation experiments will be realised in the next few years - if not months (essentially in Basel DHM, Switzerland and Desert Peak, California, US).

Two main types of stimulation technologies can be considered (Combs et al., 2004): mechanical stimulation techniques or chemical treatments.

Mechanical techniques can be:

- Hydraulic fracturing due to massive fluid injection in the wells
- Explosive fracturing
- Well mechanical treatment: re-deepening, jetting, scraping

Chemical techniques include:

- Matrix acidizing
- Clay shrinking and/or stabilization
- Scale inhibitors

We will here essentially focus on mechanical stimulation techniques.

Hydraulic fracturing

If the basic idea of hydraulic fracturing is quite common –high rate injections pressurizes the reservoir, leading to the creation of new fractures or to the enhancement of the permeability of pre-existing ones–, many way of proceeding, unknowns and variable make the results of this king of stimulation very hazardous to predict.

Presentation and preliminary classification

Reservoir stimulation mechanisms in Enhanced Geothermal Systems are quite closed to mechanisms described in the petroleum industry (Economides and Nolte, 1989), although a major difference exists between their purpose. Petroleum reservoir stimulation aims at increasing the permeability of a reservoir in order to allow the maximum oil recovery, which stands in rock pores, as geothermal reservoir stimulation aims at optimizing heat recovery, which is stored in the rock matrix.

Identification of stress regime

The main parameter that influences the preponderant failure mechanism in an EGS reservoir may be the stress regime, i.e. the relative values of vertical and horizontal stresses (see Figure 1).

Indeed, failure mechanisms can thus be classified:

Faulting (=shear fracturing)

Failure criterion:

$$\tau < C + \sigma_n'.\tan\varphi$$

$$\Leftrightarrow \frac{\sigma_{\max}'-\sigma_{\min}'}{2} = C.\cos\varphi + \frac{\sigma_{\max}'+\sigma_{\min}'}{2}.\sin\varphi$$

with τ being the shear stress, C the cohesion, φ the Mohr angle, σ_n', σ_{max}' and σ_{min}' the normal, maximum and minimum effective stress.

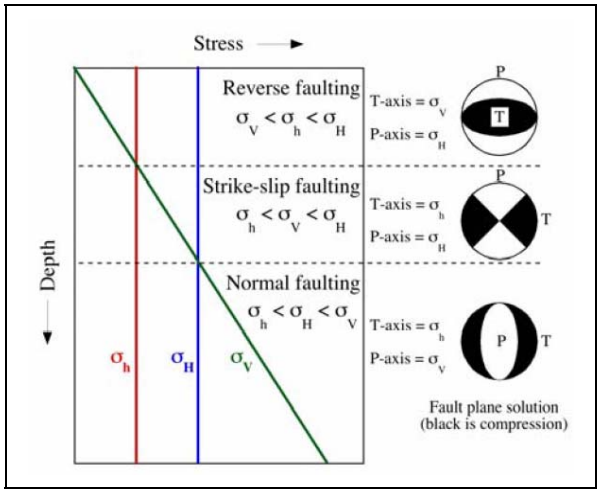

Figure 1: Conceptual representation of different stress regimes possible in HDR reservoirs: reverse, strike-slip and normal faulting (Karner, 2005)

Jointing

This mechanism is equivalent to tensile failure or extensional fracturing, or hydrofracturing.

Failure criterion:

$$P_{fracture} > \sigma_{\min} + S + (\alpha P_{Pore})$$

with S being the tensile strength or inherent resistance of the rock to propagation of a fracture and α the poroelastic constant.

Jacking

This mechanism corresponds to hydrofracturing with pre-existing fractures.

Failure criterion:

$$P_{fracture} \geq \sigma_{\min}$$

As one can observe on these various failure criterions, many parameters play a role in the rupture mechanism that is expected:

- Fluid pressure development in the reservoirs, that depends on:
  - injection rate,
  - injection time length
  - injection through the entire open section of the well, or through perforated casings, or through a casing section

isolated by packers, or in a plugged well with sand

  - fluid type (water, heavy brine, gel of various viscosity, presence of proppants)
  - fluid temperature, that may induce stress changes in the reservoir

- Stress field, that is different for each EGS site
- Rock and fractures parameters, like cohesion and Mohr angle, may highly influence results obtained, and could be modified by the use of proppant agents or acid treatments

Results obtained in the past

It is now quite commonly accepted in the scientific community that geothermal reservoir development due to massive hydraulic injections is most of the time due to reactivation of pre-existing fractures by shear of the fracture walls, induced by a diminution of the effective stress in the fracture.

As many stimulation campaigns have been performed on various EGS site all over the world, the purpose of this section is not to give an exhaustive index of the results of each test. The authors want to try to classify the main stimulation phases performed on geothermal reservoirs and the conclusions they led to, according to the considered reservoir properties (stress field, open or closed reservoir…) and to the type of stimulation realized (injected fluid, use of proppant, packers, flowrate…).

Hydraulic stimulation with a proppant agent

Three stimulation with a proppant agent were performed in Urach, Germany, in 1978 (Jupe et al., 1993). The Urach reservoir faces a normal faulting stress field ($\sigma_v > \sigma_H > \sigma_h$), characterized by a very low minimum horizontal stress, and a maximum horizontal stress nearly equivalent to the overburden. Proppant agent concentrations are related to be of 90 and 240 g/l of bauxite sand, in water or viscous gel. No results were obtained concerning the well injectivity, but the connection between wells could be increased after the last stimulation with proppant agent.

Three stimulations with proppant agent are also reported in le Mayet-de-Montagne, in France, in 1988 and 1989. This reservoir is quite an open system, with a normal faulting stress regime ($\sigma_v > \sigma_H > \sigma_h$). Each time, between 100 and 200 m^3 of water were injected, with a volume of proppant agent (sand) of 2, 7, and 40 tons of sand injected. If the first stimulation with proppant result was not significant, the second stimulation led to a great improvement of the recovery factor between wells, going from 20%, decreasing, to 58%, stable. Though, no improvement of the well injectivity was observed during any of the three stimulation campaigns (Jupe et al., 1993).

Proppant injections also occurred in Rosemanowes, UK. This geothermal reservoir is characterized by a strike-slip stress regime ($\sigma_H > \sigma_v > \sigma_h$). Proppant injections in production well RH15 are related to have had a good influence on the Rosemanowes reservoir responses, increasing the recovery factor from 70% to 85% (Willis-Richards et al., 1995).

Proppant injections also took place in the Gamma project reservoir, Japan (Jupe et al., 1993) and in the Fjallbäcka reservoir, Sweden (in combination with viscous gel injections) (Willis-Richards et al., 1995), that is characterized by an inverse faulting stress regime ($\sigma_H > \sigma_h > \sigma_v$) or a strike slip regime, but few literature was found to conclude on the positive or negative effect of these stimulations.

One could here notice that proppants injections with viscous gels can be performed in sedimentary reservoirs, like in the Rotliegend well situated in the eastern part of Germany (Legarth et al., 2003).

Hydraulic stimulation with a viscous gel

Viscous gels injections are often realized in combination with proppant injections. Low and high viscosity gels injections were performed in le Mayet-de-Montagne; these injections, when realized with a high viscosity gel, are reported to help jacking of fractures connected to the well, but finally quite low results were reported after these injections. High viscosity gels were also used in Rosemanowes, UK (Baria and Green, 1986), in order to increase chances of jacking and opening of fractures in tensile mode more than shearing, but recorded focal mechanisms were in fact consistent with strike-slip shear.

As geothermal conditions are most of the time extreme conditions –high temperatures, high stresses and highly corrosive fluids, there is a great need of material and techniques development. In that purpose, new gels and stimulation fluids based on saponite and smectite clays are tested (Hirano et al., 2000)

Hydraulic stimulation in a limited section of the well

Stimulation injection in perforated casing was performed in well Habanero 1 in the EGS of Cooper Basin, Australia (Wyborn et al., 2005). This geothermal field is characterized by an inverse faulting regime ($\sigma_H > \sigma_h > \sigma_v$). Following stimulation 1 (realized in the entire well open section), packers were introduced at the top of the well open section, and perforations of the casing above the casing shoe were made. This technique allowed showing up fractures in which inflow could reach 25 l/s during injections phases.

Hydraulic stimulation performed in Falkenberg, Germany took place in a 3 m long packed-off interval, which had previously been identified by core and BHTV logging as the center of a 50m long joint free interval, at 250m depth (Jupe et al., 1993). Falkenberg stress regime changes from an inverse faulting regime above 100 m, to a strike slip regime between 100 and 200 m, and to a normal faulting regime below. This technique allowed the creation of a new hydraulic fracture in the packer interval.

Packers were also tested on the injection well of the Hijori site, Japan, but, as packer rubbers were found to be damaged because of reservoir very high temperatures, no conclusion could be deduced from tests performed in that site. Packers were also used in le Mayet-de-Montagne, France, but their use combined with the injection of proppant makes any conclusion very hazardous.

The technique of injections in perforated and cemented casing was also used during phase 1 of the Fenton Hill project, and packers were used during phase two of the project, with relatively good results after several tests, as injectivity of the wellbore was 2 l/s/MPa and recovery factors was evaluated to 60%. Literature also reports (Jupe et al., 1993) stimulations in perforated casings and using packers in Urach, Germany, and the use of perforated casings was in that case thought to be responsible of high friction losses in the casing.

Another technique that could here be described is well plugging or well sanding/reaming/fracturing. This technique consists, in case of low inflow possibilities in the open section of the well, to sand up the well open section and then to ream out a part of the casing, in order to perform hydraulic stimulation in the reamed part of the casing. Its application is independent of evaluated stress regime of the reservoir. Such experiments were successfully performed at very small scale (flowrates lower than 3 l/s) in the Akinomiya site, Japan (Jupe et al., 1993). This technique of well sanding was also used in the Ogachi EGS, Japan and is very precisely described in literature (Kaieda et al., 2005). In this site, two reservoirs were successfully created at depth of 719 and 1000 m.

Hydraulic stimulation with water or brine only

As the cheapest fluid available in high quantity on earth is water, most of hydraulic stimulation phases in EGS were performed using fresh water, or with heavy brines, i.e. NaCl saturated water, reaching a density of 1200 kg/m^3 at 20°C. If quantities of available brine are often limited to the capacity of external tanks, one can find evidences that the injection of such a fluid into the reservoir before fresh water injection during stimulation phases can be established (Baujard and Bruel, 2005). Water injections offer the possibility of injecting great volumes of fluids in order to improve well injectivities, productivities or the recovery factor between wells. An other advantage of long-term fresh water injections in the reservoir is that this injected water can temporarily cool down the rock temperatures, leading to a thermal stimulation, due to contraction of rocks.

Though water injections allow high rate injections over long time periods, many uncertainties remain concerning the way of optimizing such injection in order to obtain good stimulation results.

The 5-km depth EGS reservoir of Soultz-sous-Forêts, France, has been developed using essentially fresh water and heavy brine injections, and some acid injections more recently (Baria et al., 2006). Thanks to these operations, connection could be achieved between two wells GPK2 and GPK3, the connection with the last well being problematic for the moment.

Massive hydraulic stimulations were also performed in well Habanero 1 of the Cooper Basin EGS, Australia (Asanuma et al., 2004; Wyborn et al., 2005), in the Ogachi geothermal reservoir (Kaieda et al., 2005; Tenzer, 2001) , in the Hijori EGS (Matsunaga et al., 2005), and in Fenton Hill (Robertson-Tait et al., 2000).

Hydraulic stimulation phases are planed in the Desert Peak reservoir, Nevada (Robertson-Tait et al., 2005) and probably in the Coso geothermal field, where low pressure stimulation experiments were realized (Rose et al., 2006) and stimulation test on shear of

the fractures were done on site (Rose et al., 2005).

Hydraulic stimulation expectations: information deduced from stimulation and questions

Of course, the first purpose of hydraulic stimulation is to enhance reservoir permeability. But, in addition to that, all of the previously defined stimulation techniques induce microseismicity. These microseismic events give extremely important information on reservoir parameters and structures, such as:

- Stress field orientation, thanks to development of microseismicity and orientation of in-situ fractures (Evans et al., 1999)
- Reservoir hydraulic diffusivity, thanks to the speed of extension of seismic cloud generated during stimulation phases (Shapiro et al., 1999)
- Isolation of large scale structures with multiplet clustering analysis (Moriya et al., 2003)
- Velocity structure of the reservoir can also be deduced from microseismic monitoring (Charlety et al., 2005)

On the other hand, very simple questions still remain unresolved:

- What is the exact nature of the link between flow paths and stimulation events ?
- How could high magnitude seismic events be avoided during reservoir development? Are they linked to injected volumes, flowrates, pressure-increase rate in the reservoir or more irrelevant parameters?
- What would be the best strategy to develop a reservoir in an efficient way: short term and very high rate stimulations, long term and moderate flowrate injections, or multi-well injections?

Microseismicity associated, Example Soultz

As microseismicity is generated during stimulation injections, the most common way to derive information on key reservoir parameters (extension depth, faults) is the determination of magnitude and location of generated microseismic events. These events describe generally local shear failure at individual fracture / fault planes.

Whereas the impact of magnitude from single large events are described only after a careful seismic analysis (i.e. Charléty et al., 2005), a generalization of seismic events can be performed by describing a “seismic density”. Recent studies (Kohl and Baujard, 2006) analyzed the density of the microseismicity recorded in Soultz-sous-Forêts during stimulation experiments in the deep reservoir. Figure 2 shows a transient evolution of the development of the microseismicity in Soultz during each well stimulation.

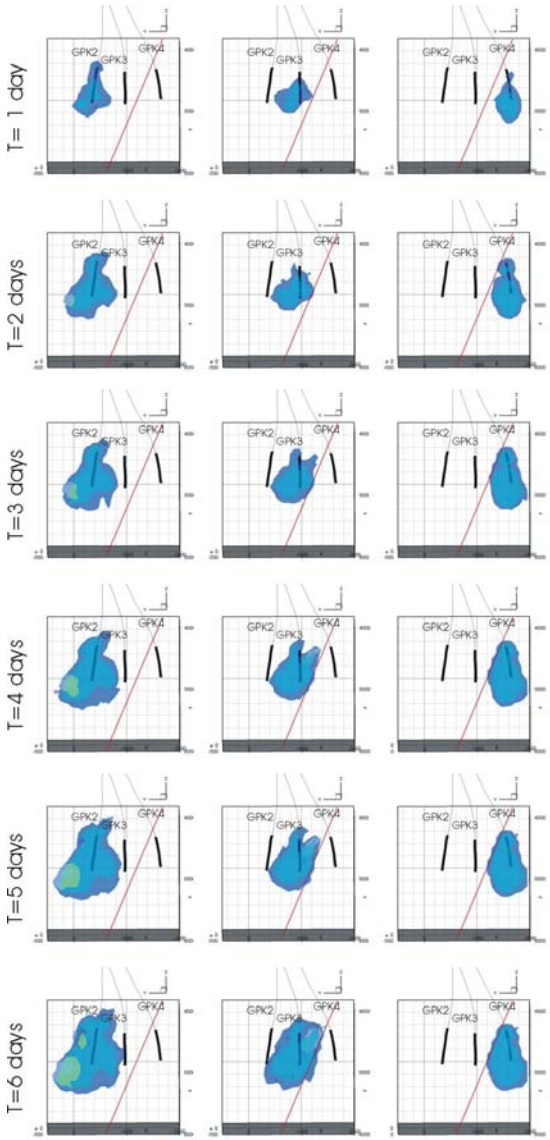

Figure 2: transient development of GPK2, GPK3 and GPK4 microseismic density distribution (Δx=100 m); Blue envelope: d = 3 events per 50 m side length cube; green envelope: d = 15 events per 50 m side length cube. Time is from beginning of injection.

Numerical analysis of this density of microseismicity development pointed at an aseismic zone at between GPK3 and GPK4, of orientation 96N64W, which may explain very poor hydraulic connection and low tracer recovery between these two wells. Microseismicity can be considered as a filter that favors the visualization of features parallel to Smax. However, faults perpendicular they may also have high hydraulic conductivity remains invisible. Yet, this kind of microseismic analysis is cannot provide non-unique information on the type of the hydraulic structure (drainage or no-flow boundary).

Other mechanical stimulation techniques

Explosive stimulation

Explosive well stimulation is a quite common technique of the petroleum industry. The use of explosive in geothermal wells is quite dangerous due to the instability of explosives at high temperatures in the wells, which represents a non-negligible danger for on-site workers. So far, this kind of treatments have been performed in a few geothermal wells and results were in fact very hazardous.

Explosive pre-treatment of well

An explosive pre-treatment of well was conducted on the site of Rosemanowes, UK. There was some microseismic evidence to suggest that this explosive stimulation may have acted as the focal point for subsequent growth of the reservoir during later stimulation phases (Jupe et al., 1993). No real conclusion on efficiency of this well pre-treatment was clearly showed out.

Explosive well stimulation

An explosive well stimulation was lead in several Geysers wells and is mentioned in literature (Hanold, 1980; Mumma et al., 1982). It is also reported that these explosive stimulation experiments resulted in a significant decrease of the well transmissivity, attributed to a possible blockage of two deep steam entry zones by rubble from the explosions (Entingh, 2000).

High energy gas fracturing

Realizing that explosives generally act so fast that they mainly pulverize and compress rock, Sandia scientists pursued the development and use of propellants that burn more slowly as a means to force fractures at least some distance from wellbore. This was called "high energy gas fracturing" (HEGF). The purpose of HEGF methods is to develop multiple, radial fractures around a borehole using a rapid pressure load. The advantage of this technique is that it was demonstrated that HEGF methods were likely to create fractures in every wanted direction, including in a direction perpendicular to the main stress direction, which could allow newly created fracture to intersect many hydraulically important fractures (Chu et al., 1987; Entingh, 2000).

References

Asanuma, H. et al., 2004. Microseismic Monitoring of a Stimulation of HDR Reservoir at Cooper Basin, Australia, by the Japanese Team, Geothermal Resources Council Transactions, Palm Springs.

Baria, R. and Green, A.S.P., 1986. Seismicity Induced During A Viscous Stimulation At The Camborne School Of Mines Hot Dry Rock Geothermal Energy Project In Cornwall, England, Progress in acoustic emission - The Japanese Society of NDI, pp. 407-429.

Baria, R. et al., 2006. Creation of an HDR reservoir at 5000 m depth at the European HDR project, 31th Stanford Geothermal Workshop, Stanford, California, US.

Baujard, C. and Bruel, D., 2005. Improving a numerical tool and evaluating impact of density changes of injected fluids in the hydraulic behavior of HDR reservoirs, 30th Stanford Geothermal Congress, Stanford, California, US.

Charlety, J., Cuenot, N., Dorbath, L. and Dorbath, C., 2005. Four dimensional velocity structure of the Soultz-sous-Forêts geothermal reservoir during the 2000 and 2003 stimulations, 30th Workshop on Geothermal Reservoir Engineering, Stanford University, Stanford, California.

Chu, T.Y., Jacobson, R.D. and Warpinski, N., 1987. Geothermal well stimulated using high energy gas fracturingv, Twelfth Workshop on Geothermal Reservoir Engineering, Stanford.

Combs, J., Garg, S.K. and Pritchett, J.W., 2004. Geothermal well stimulation technology: A preliminary review. Geothermal Resources Council Transactions, 28: 207-212.

Economides, M.J. and Nolte, K.G., 1989. Reservoir Stimulation.

Entingh, D.J., 2000. Geothermal well stimulation experiments in the united states, World Geothermal congress, Japan.

Evans, K. et al., 1999. Stress and rock mechanics issues of relevance ot HDR/HWR engineered geothermal systems: review of developments during the past 15 years. Geothermics, 28: 455-474.

Hanold, R.J., 1980. Explosive Stimulation of a geothermal well at The Geysers, Symposium on Geothermal well stimulation, San Francisco, California.

Hirano, N., Higashi, S. and Yamasaki, N., 2000. Plugging method for Hdr reservoir using hydrothermal processing of smectite clays to improve recovery efficient, World Geothermal Congress 2000, Kyushu - Tohuku, Japan.

Jupe, A.J., Willis-Richards, J. and Nicholls, J.D., 1993. Review of HDR Projects. ETSU G 164-P1, Department of Energy, CSM Associates Limited.

Kaieda, H. et al., 2005. Review of the Ogachi HDR Project in Japan, World Geothermal Congress 2005, Antalya, Turkey.

Karner, S.L., 2005. Stimulation techniques used in enhanced geothermal systems: perspectives from geomechanics and rock physics, 30th Workshop on Geothermal Reservoir Engineering, Stanford, California, US.

Kohl, D.T. and Baujard, C., 2006. Conditions for mechanical re-stimulation of GPK4, EHDRA scientific meeting.

Legarth, B., Tischner, T. and Huenges, E., 2003. Stimulation experiments in sedimentary, low-enthalpy reservoirs for geothermal power generation, Germany. Geothermics, 32: 487-495.

Matsunaga, I., Niitsuma, H. and Oikawa, Y., 2005. Review of the HDR Development at Hijiori Site, Japan, World Geothermal Congress 2005, Antalya, Turkey.

Moriya, H., Niitsuma, H. and Baria, R., 2003. 28th Workshop on Geothermal Reservoir Engineering, Stanford, California, US.

Mumma, D.M. et al., 1982. Geofrac--an explosive stimulation technique for a geothermal well, GRC Transaction.

Robertson-Tait, A., Klein, C. and McLarty, L., 2000. Utility of the data gathered from the fenton hill project for development of enhanced geothermal systems, World Geothermal Congress 2000, Kyushu-Tohoku, Japan.

Robertson-Tait, A., Morris, C. and Schochet, D., 2005. The Desert Peak East EGS Project: A Progress Report, World Geothermal Congress 2005, Antalya, Turkey.

Rose, P., McCulloch, J., Adams, M. and Mella, M., 2005. An egs stimulation experiment under low wellhead pressures, Thirtieth Workshop on Geothermal Reservoir Engineering, Stanford University, Stanford, California.

Rose, P., Mella, M. and McCullough, J., 2006. A comparison of hydraulic stimulation experiments at the soultz, france and coso, california engineered geothermal systemS, Thirty-first Workshop on Geothermal Reservoir Engineering, Stanford University, Stanford, California.

Shapiro, A., Royer, J.J. and Audigane, P., 1999. Large scale in-situ permeability tensor of rocks from induced microseismicity. Geophysical Journal International, 137: 207-213.

Tenzer, H., 2001. Development of Hot Dry Rock Technology. In: K. Popovski and B. Sanner (Editors), International Summer School on Direct Application of Geothermal Energy: International Seminar on Hot Dry Rock Technology. IGA - GtV, Bad Urach, pp. 213-226.

Willis-Richards, J., Green, A.S.P. and Jupe, A., 1995. A comparison of HDR geothermal sites, World Geothermal Congress 1995. IGA, Florence, Italy, pp. pp. 2601 - 2605.

Wyborn, D., Graaf, L.d., Davidson, S. and Hann, S., 2005. Development of Australia's First Hot Fractured Rock (HFR) Underground Heat Exchanger, Cooper Basin, South Australia, World Geothermal Congress 2005, Antalya, Turkey.

ENGINE – **EN**hanced **G**eothermal **I**nnovative **N**etwork for **E**urope
Workshop 3, "Stimulation of reservoir and induced microseismicity"
Kartause Ittingen, Zürich, June 29 – July 1, 2006, Switzerland

Hydraulic Fracturing and Formation Damage in a Geothermal Sedimentary Reservoir

REINICKE Andreas , GeoForschungsZentrum Potsdam, Germany, Andreas.Reinicke@gfz-potsdam.de
LEGARTH Bjoern, Shell EP Europe;
ZIMMERMANN Günter, GeoForschungsZentrum Potsdam Germany;
HUENGES Ernst, GeoForschungsZentrum Potsdam, Germany;
DRESEN Georg, GeoForschungsZentrum Potsdam, Germany

Abstract

In 2002 a Hydraulic Proppant Fracture treatment was applied to the Rotliegend sandstone aquifer of the geothermal research well Gross Schoenebeck 3/90. The site is located north of Berlin. The initial productivity of this well was significantly lower than expected from core measurements due to near wellbore damage. Therefore it was stimulated with 11 tons of ceramic proppants and over 200 m³ of high viscous gel. Simulations had predicted a productivity increase by a factor of 7-8, but the productivity was only doubled due to different reasons. One possible cause for missing the productivity goal is damage due to crushing, compaction and embedment of proppants into the rock matrix. To investigate this issue in more detail a new laboratory equipment was set up which allows determination of permeability of proppant pack and proppant rock interface under increasing effective stress. Acoustic emission (AE) activity is recorded during test execution. First tests show that fracture creation as well as proppant and rock crushing lead to considerable generation of fines and a clear permeability reduction. The AE events indicate that grain crushing and proppant embedment start at low effective stress (~5 MPa) at the fracture face. In this area fines are generated and flow paths get blocked. We expect that similar effects may reduce reservoir productivity due to flow impairments at the rock proppant interface.

Keywords: sedimentary geothermal reservoir, hydraulic proppant fracturing, fracture face damage, skin

Hydraulic Fracturing technology – a brief overview

Hydraulic fracturing is a standard technology in the hydrocarbon industry for more than 30 years to overcome effects of formation damage and low rock permeability and to increase the productivity of a reservoir [Economides & Nolte 2000]. The stimulation target is the creation of a fracture with a sufficient width during production. Two different concepts exist to stimulate a reservoir hydraulically depending on rock, formation and fluid properties.

1: Waterfracs (WF) or "self propped fracs": Low viscous gels without proppants or with a small proppant concentration are used to create long and small fractures in a low permeability reservoir. The aim of WF is to connect parts of the reservoir far from the borehole, to create a fracture network, to connect a natural joint network and to maximise the inflow area. In Hot Dry Rock [Baria, et al. 1999] applications WF treatments were applied to connect two wells in a tight hard rock (i.e. granite). Tab. 1 gives an overview to treatment parameters.

2: Hydraulic Proppant Fracturing (HPF): High viscous gels with high proppant concentrations are used to create highly conductive but short (compared to WF) fractures in a permeable reservoir with porous matrix. The fracture creates a connection between the well and the reservoir and overcomes the permeability damage in direct surrounding of the well (skin) [Dake 1978] increasing productivity. (See table 1 for treatment parameters.)

Treatment Parameters	Water Fracs (WF)	Hydraulic Proppant Fracs (HPF)
frac fluid viscosity η	1-10 cP	$\geq$ 100 cP
proppant concentration c	0 – 200 g/l	200 - 2000 g/l
fracture half length x_f	$\leq$ 250 m	$\leq$ 150 m
fracture width w_f	$\leq$ 1 mm	1 – 25 mm
fracture permeability k_f	10 – 10000 D	10 – 1000 D
fracture conductivity k_f*w_f	0.0001 – 10 Dm	0.01 – 25 Dm
reservoir permeability k	$\leq$ 1 mD	1 – 1000 mD

Tab. 1: Treatment parameters of waterfracs and Hydraulic Proppant Fracs

A key design parameter in well stimulation is the dimensionless fracture conductivity C_{fD} which relates the capacity of the fracture to transmit fluids into the wellbore with the ability of the formation to deliver fluid into the fracture [Economides & Nolte 2000].

$$C_{fD} = \frac{k_f \cdot w_f}{x_f \cdot k} \quad \text{Eq. 1}$$

For steady state conditions the optimum C_{fD} is 1, but in reality C_{fD} should be around 10 to guarantee good drainage during transient flow periods [Economides & Nolte 2000]. To reach this design goal a high conductivity contrast between fracture and formation is necessary.

The advantage of WF compared to HPF is a reduction of costs - costs for material are lower and realisation of these stimulations is easier. In addition the permeability of WF could be 10 – 100 times higher than permeabilities from HPF. Different studies have shown [Mayerhofer & Meehan 1998, Fredd, et al. 2001] that the field of application is limited to reservoirs with small permeability (< 1 mD). In these reservoirs it's important to maximise the inflow area for the slow diffusion process of fluid flow through the tight rock matrix. And due to low formation permeability and big fracture half length $C_{fD} \geq 10$ could be realised although width of self propped fracs is small. The success of the stimulation is dependent on the self propping potential of the reservoir rock. The self propping potential includes the shear potential of the formation as well as the toughness of the rock and a residual fracture width due to flushed particles. Consequently, a successful treatment depends on parameters that are difficult to manage.

In contrast HPF treatments allow a good control of stimulation parameters. The properties of the fracture can be predicted and optimised. With special Tip Screen Out (TSO) [Economides & Nolte 2000] design widths up to 25 mm are possible. Thus, a wide range of formations with respect to permeability can be treated using this technology. Stimulation parameters could be optimised for a certain reservoir to get a sufficient C_{fD}. But there more expensive and frac gels must be carefully selected to avoid damage due to chemical precipitations and gel residues.

Hydraulic stimulation treatments in the geothermal research well Gross Schoenebeck 3/90

Enhanced productivity of thermal water is necessary for the economic and sustainable generation of geothermal electricity. This requires a sufficiently high reservoir temperature (above 120 °C) and a high production rate of the deep fluids of at least 50 m³/h. An adequate temperature profile for this purpose is found in the former gas exploration well Groß Schoenebeck 3/90, about 80 km northeast of Berlin in the North-German Basin with formation fluids of 150 °C and porosities of up to 10 % [Zimmermann, et al. 2005]. The well is drilled through a series of Rotliegend sediments consisting of silt-, sandstones and conglomerate into vulcanite layers with 400 m open-hole section at the bottom

The initial productivity of the well was significantly lower than expected from core measurements and logs. Drilling operations produced a significant near wellbore damage resulting in a low productivity. Therefore, two HPF open hole treatments in the Rotliegend sandstones were conducted to bypass the skin zone and to connect undamaged reservoir regions. Since core and log measurements indicate reservoir permeabilities between 10 and 150 mD, a WF treatment was not applicable if a high C_{fD} should be achieved. In addition there exists no experience with WF treatments in sedimentary geothermal reservoirs.

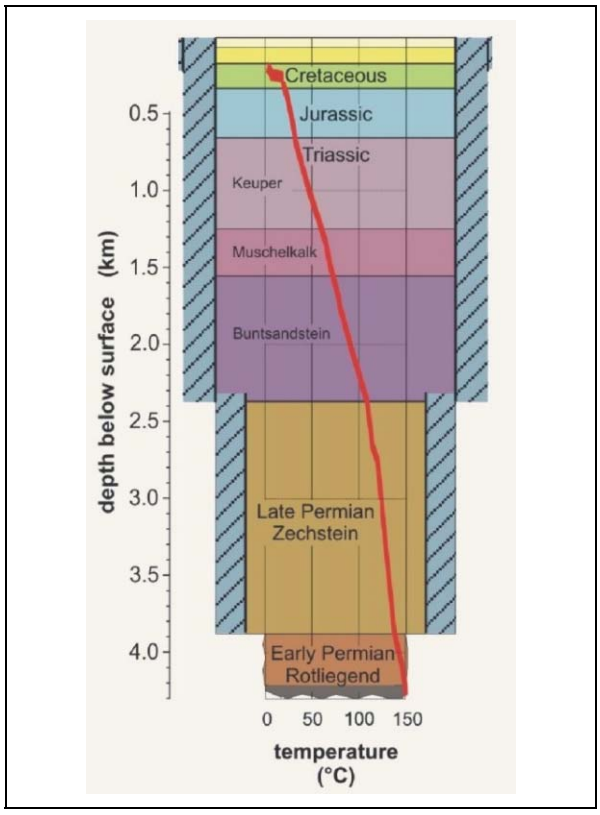

Fig.1) Lithology- and temperature-profile of the well Groß Schoenebeck 3/90

The test interval was isolated with a sand plug at the bottom of the well and with a mechanical packer at the top. About 200 m³ of

high viscosity fluid (polymers) with 11 tons of proppants were used for the well stimulation in two intervals. Since stimulation operations are accomplished in the open hole section under high temperature, a less aggressive frac design was applied to avoid a by-pass of the packer [Legarth, et al. 2005a].

Before and after stimulation production tests (casing lift tests with nitrogen) were performed to determine the stimulation effect. Fig. 2 displays a comparison of the flow log before and after the treatments. Before well stimulation no response in the Rotliegend sections above 4225 m could be seen, only at the transition zone between the conglomerates and the volcanic rock an inflow over 25 m is visible. After stimulation the flow log shows a response to a depth up to 4100 m indicating that the Rotliegend sandstones could be activated.

The stimulation effect was estimated by analytical modelling with the FRACPRO^{TM} - a 3D fracture simulator. From modelling the theoretically achievable Fold Of Increase (FOI) is determined. The FOI is the ration between the initial reservoir productivity and the reservoir productivity after the stimulation treatment. For given fracture dimensions values for the FOI between 7 and 8 were expected.

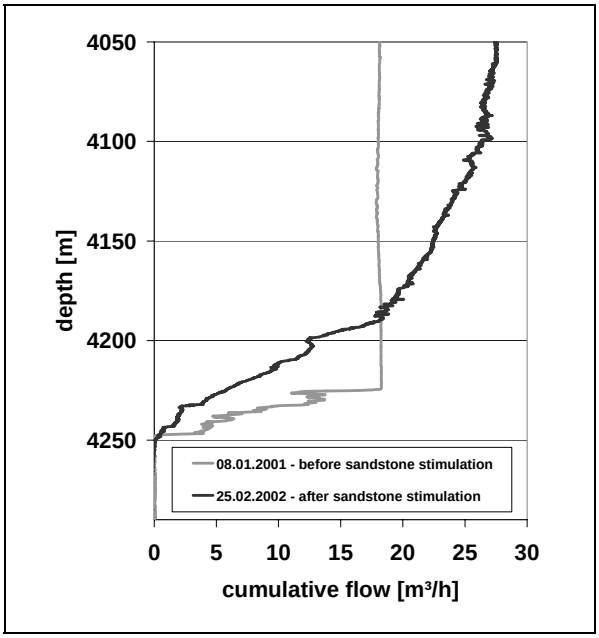

Fig. 2) Cumulative flow measured with a flowmeter during short term lift tests to obtain the inflow zones

But post-frac productivity was considerable lower than expected and a FOI of only 1.8 was reached. The modelling with FRACPRO^{TM} as well as the planning, execution and evaluation of the stimulation experiments is extensively explained by [Legarth, et al. 2005a, Legarth 2003].

Mechanical induced fracture face skin

Treatment failure could be very often attributed to fracture damage processes like: 1) poor clean-up after the treatment, geochemical alterations due to infiltration processes and precipitation, 2) mechanical damages like proppant pack failure. Especially in high stress and high temperature environments proppant crushing is an issue, 3) an additional damage mechanism results from a mechanically induced fracture face skin (FFS) between fracture and rock matrix. The general idea is that proppant embedment and grain/proppant crushing lead to a reduced permeability in the fracture face and during the production out of the reservoir this zone acts as a filter and the FFS zone grows into the formation.

The fracture face skin is referred to as impairment affecting flow normal to the fracture surface [Cinco-Ley & Samaniego 1977]. This damage of reservoir permeability can be caused by polymer leakoff and fluid saturation changes [Adegbola & Boney 2002]. Another damaging mechanism is a reduction in relative permeability changes generated by phase changes [Holditch 1979, Romero et al. 2003]. Furthermore various laboratory, field and theoretical studies address the field of fracture damage mechanisms [i.e. Meyn 1998, Fredd, et al. 2001]. Although there exist fracture face skin models mechanical effects have not yet been taken into account. Fig. 3 presents a view of the proppant rock matrix interface in a fracture. Under increasing effective closure stress grains and proppants get crushed and embedded and this leads to a compacted band in the fracture face. This effect is amplified by migration and deposition of fines from the formation into the damaged zone. The flow path becomes more tortuous and this results in a lower permeability at the fracture face.

A laboratory equipment was set up which allows determination of permeability development of the proppant pack and proppant rock interface under increasing effective stress. Fig. 4 gives a schematic view of this setup. A core with 50 mm diameter, and fractured in the middle and filled with proppants simulating a propped fracture in the reservoir. During an experiment a constant confining stress P_c is applied and the axial load is increased simulating increasing stress on proppant pack during draw down.

Permeability is measured in axial direction to investigate the effects of a mechanical FFS.

Acoustic Emission (AE) activity is recorded continuously to locate the damaging events.

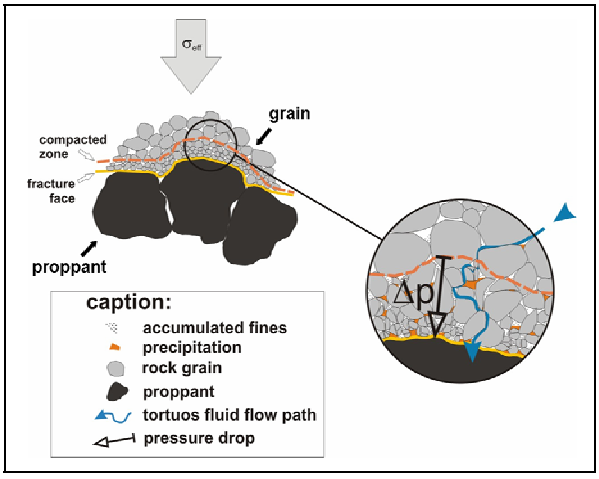

Fig. 3) Rock matrix proppant contact of a propped fracture. Proppant embedment and grain / proppant crushing leads to a reduced permeability in the fracture face. Modified from [Legarth, et al. 2005b].

A test is divided into 3 steps: 1) The mechanical properties of intact rock sample are determined and initial permeability is measured. 2) A 3-Point-Bending-test is applied creating a tensile fracture comparable to a hydraulic fracture. 3) The fracture is opened carefully, filled with 2 lb/ft² (~ 10 kg/m²) of intermediated strength proppants with a 20/40 mesh and closed aligned. The proppant concentration results in a 5 mm proppant bed with 6-7 layers. The setup is arranged as shown in Fig. 4 including the cups for the AE sensors.

Fig. 6 shows the recorded AE events, the AE density (projected into the zy-plane) as well as the permeability at defined effective stress levels, respectively. For this test Bentheim sandstone was used. This is a quartz rich sandstone with 95 % quartz, 3% kaolinite and 2% feldspar. The porosity is about 23 % [Klein, et al. 2001]. The Bentheim sandstone contains a small the amount of initial fines and only newly created fines will influence the permeability. A high permeability contrast between matrix and an arising FFS is expected.

The initial permeability (k_1) at effective stresses (σ_{eff}) of 5-50 MPa is about 1250 mD and shows only minor changes over the stress interval. Already at σ_{eff} of 5 MPa the permeability is reduced by a factor of 10 to 125 mD (k_t). This demonstrates that the fracture face is initially damaged due to fracturing. The AE events indicate that grain crushing and proppant embedment start at low σ_{eff} at the fracture face proppant contact. At high σ_{eff} a further reduction in permeability to 105 mD is observed. At this stress level the main AE activity moves from the fracture face into the proppant pack. Microscopic investigations after reopening the fracture show crushed proppants as well as crushed grains. Fines generated from quartz grains were detected in the proppant pack.

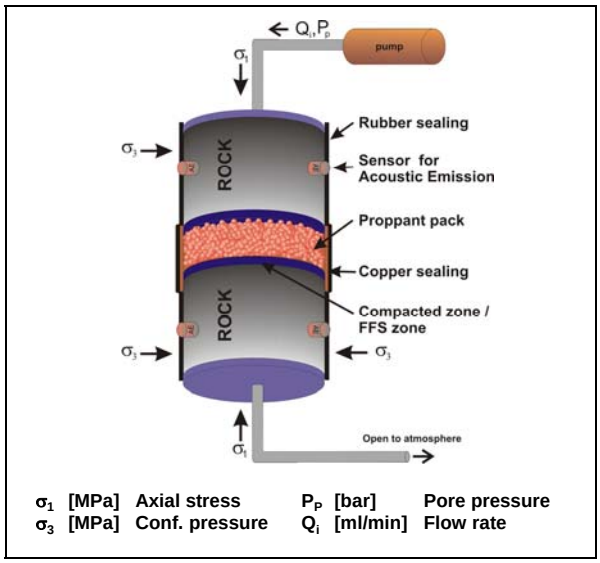

Fig. 4) Experimental setup for determination of the hydraulic permeability of the Fracture Face Skin zone (FFS) zone. Permeability during axial loading is measured, proppant and grain crushing is recorded with AE sensors

From the width of the cloud of AE-events the thickness of the damaged zone (L_2) could be estimated to 4 mm. With the knowledge of the measured initial permeability an estimation of the permeability of the FFS is possible. Proppant pack permeability was assumed as infinite. It is considerable higher (260 D at 50 MPa) than the rest of the system.

The setup is approximated as a series connection of hydraulic resistors resulting in following equation for the FFS permeability k_2:

$$k_2 = \frac{k_t k_1 L_2}{L_t(k_1 - k_t) + L_2 k_t} \quad \text{Eq. 2}$$

L_t is the length of the whole sample and L_1 is the lengths of the rock halves. With this formula a k_2 about 4 mD is calculated. That means the permeability in the FFS is reduced by a factor of 300 compared to the initial permeability due to the fracturing process itself as well as proppant embedment and grain crushing. Fig. 5 shows a proppant imprint into the rock matrix. The grains at the contact point are completely crushed and compacted. These imprints as indicator for proppant

embedment can be identified over the whole fracture face.

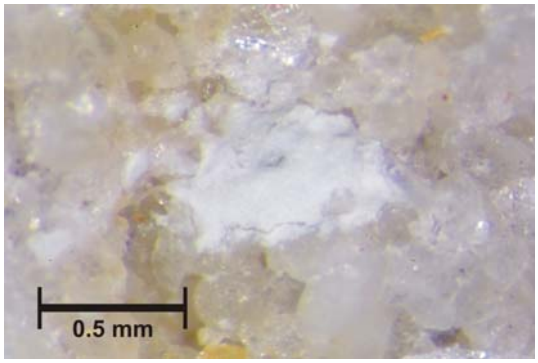

Fig. 5) Proppant imprint (embedment) into the rock matrix. The grains at contact of proppant and rock are completely crushed and compacted.

Conclusion

The open hole hydraulic proppant fracture treatments were successful applied at the geothermal research well Gross Schoenebeck 3/90. Propped fractures were created and the inflow performance of the well was enhanced. But desired post-frac productivity could not be achieved.

Treatment failure is very often caused by fracture damage processes, as reported in a wide range of literature. A possible damaging effect is a mechanically induced fracture face skin caused by rock matrix proppant interactions. A first test indicates that drastic reduction of sample permeability due to fracture creation as well as proppant embedment and proppant/grain crushing can be observed. The crushing of grains and/or proppants starts at low stress (~5 MPa). The AE events are concentrated at the fracture face and there moving into the proppant pack with increasing differential stress. Crushed rock particles (fines) were mobilized and transported into the proppant pack, embedment was identified.

The investigations represent a first approach to the analysis of mechanical interactions between proppants and rock matrix. Further tests with different rock types and a separate determination of proppant pack and fracture face permeability have to be conducted.

References

Adegbola, K. and Boney, C. (2002): *Effect of Fracture Face Damage on Well productivity*, SPE 73759

API RP-60 (1989): API *Recommended Practices for Testing High Strength Proppants in Hydraulic Fracturing Operations*, API Production Dept., Dallas

Baria, R., Baumgärtner, J., Rummel, F., Pine, R.J. and Sato, Y. (1999): *HDR/HWR reservoirs: concepts, understanding and creation*, Geothermics 28

Cinco-Ley, H. and Samaniego, V.F. (1977): *Effect of Wellbore Storage and Damage on the Transient Pressure Behaviour of Vertically Fractured Wells*, SPE 6752

Dake, L.P. (1978): *Fundamentals of Reservoir Engineering*, Elsevier Scientific Publishing Company, Developments in Petroleum Science, Vol. 8, Netherlands

Economides, M.J. and Nolte, K.,G. (2000): *Reservoir Stimulation*, 3rd Edition, Wiley and Sons Ltd., United Kingdom

Fredd, C.N., McConnell, S.B. and Boney, C.L., England, K.W. (2001): *Experimental Study of Fracture Conductivity for Water-Fracturing and Conventional Fracturing Applications*, SPE 74138

Holditch, S.A. (1979): *Factors Affecting Water Blocking and Gas Flow from Hydraulically Fractured Gas Wells*, JPT, p. 1515-1524

Klein, E., Baud, P., Reuschle, T. and Wong, T.-f. (2001): *Mechanical Behaviour and Failure of Bentheim Sandstone Under Triaxial Compression*, Phys. Chem. Earth, Vol. 26. No. 1-2, pp. 21-25

Legarth, B. (2003); *Erschließung sedimentärer Speichergesteine für eine geothermische Stromerzeugung, Dissertation*, Scientific Technical Report 03/09, GeoForschungs-Zentrum Potsdam, Deutschland

Legarth, B., Huenges, E. and Zimmermann, G. (2005a) *Hydraulic Fracturing in Sedimentary Geothermal Reservoirs: Results and Implications*, Int. Journal of Rock Mech., Vol. 42 p. 1028–1041

Legarth, B., Raab, S. and Huenges, E. (2005b): *Mechanical Interactions between proppants and rock and their effect on hydraulic fracture performance*, DGMK-Tagungsbericht 2005-1, Fachbereich Aufsuchung und Gewinnung, 28.-29. April 2005, Celle, Deutschland, pp. 275-288

Mayerhofer, M.J. and Meehan, D.N. (1998): Waterfracs – *Results from 50 Cotton Valley Wells, Proceedings*, SPE 49104

Meyn, V., (Editor), (1998): *Investigation of Fracture Conductivity Under In Situ Conditions as a Function of Frac- and Formation Parameters*, DGMK-Research Report 490,

Institut für Erdöl- und Erdgasforschung, Clausthal-Zellerfeld

Romero, D.J., Valkó, P.P. and Economides, M.J. (2003): *Optimization of the Productivity Index and the Fracture Geometry of a Stimulated Well With Fracture Face and Choke Skin*, SPE 81908

Zimmermann, G., Reinicke, A., Holl, H.-G., Legarth, B., Saadat, A. and Huenges, E. (2005): *Well test analysis after massive waterfrac treatments in a sedimentary geothermal reservoir*, Proceedings World Geothermal Congress 2005, Turkey

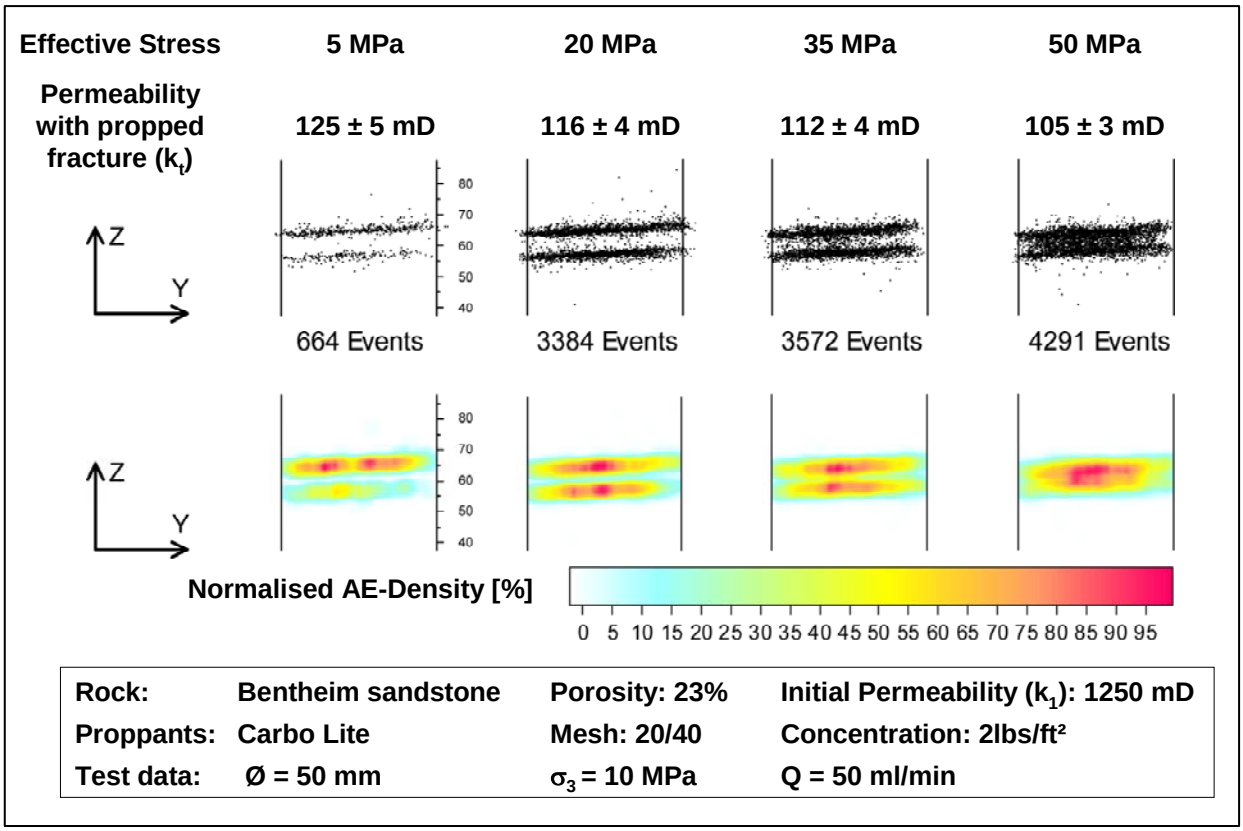

Fig.6) Comparison of initial permeability (k_1) of a Bentheim sandstone with permeability of the same sample with a propped fracture (k_t) at 10 MPa confining pressure. The AE-Locations and AE-Density during loading of the sample with a propped fracture are displayed. Permeability is reduced by a factor of 10 to 125 mD (k_t) at 5 MPa effective stress indicating that fracture face is initially damaged due to fracturing process itself. At high σ_{eff} a further reduction in permeability to 105 mD is observed. The AE events indicate that grain crushing and proppant embedment start at low σ_{eff} at the fracture face proppant contact. At high stress level the main AE activity moves from the fracture face into the proppant pack.

ENGINE – **EN**hanced **G**eothermal **I**nnovative **N**etwork for **E**urope
Workshop 3, "Stimulation of reservoir and induced microseismicity"
Kartause Ittingen, Zürich, June 29 – July 1, 2006, Switzerland

Modelling the geochemical effects of acid treatments and comparison with field observations at Soultz-sous-Forêts geothermal site

PORTIER Sandrine, CREGE, Neuchâtel, Switzerland, sandrine.portier@unine.ch
ANDRE Laurent, BRGM, Orléans, France
VUATAZ François-David, CREGE, Neuchâtel, Switzerland

Abstract

Acid treatments have been successfully applied in many cases to increase or to recover geothermal wells production rates to commercial levels. Chemical stimulation techniques were originally developed to address similar problems in oil and gas production wells. The applicability of these stimulation techniques to a hot and fractured reservoir is less well known. High temperatures increase the acid-rock reaction rate. The development of Enhanced Geothermal Systems (EGS) depends on the creation of permeable and connected fractures. Acid stimulation jobs intend to clean (pre-existing) fractures by dissolving filling materials (secondary minerals or drilling mud) and mobilizing them for an efficient removal by flow transport. Recent acid treatments were performed on the EGS wells at Soultz-sous-Forêts (France). This 200°C and 5-km deep granitic reservoir contains fractures partially filled with secondary carbonates (calcite and dolomite). In order to dissolve these carbonates and to enhance the productivity around the wells, each of the three boreholes (GPK2, 3 and 4) were successively treated with various amounts of hydrochloric acid. The FRACHEM code, a Thermo-Hydraulic-Chemical coupled code, has been developed especially to forecast the evolution of the Soultz reservoir. Reactive transport modelling with FRACHEM code has been used to simulate acid injection and its impact on brine-rock interactions. Comparisons between FRACHEM simulations and field observations have been tested to forecast the impact of acid treatments on reservoir properties. The main goal is to simulate the effect of acid injection on permeability evolution in fractures at pressure and temperature conditions of the Soultz geothermal site.

Keywords: Enhanced Geothermal Systems ; chemical stimulation ; acid injection ; brine-rock interactions ; coupled modelling ; reactive transport ; Soultz-sous-Forêts.

Introduction

The Enhanced Geothermal Systems (EGS) are dedicated to the exploitation of the heat present in low productivity reservoirs. A geothermal resource is quite different from an oil or gas reservoir or even a ground water reservoir. In an oil reservoir, once the oil has been extracted, the reservoir is exhausted. By contrast, in a geothermal reservoir the water or steam originally present in the reservoir can be replaced by surrounding cooler water or re-injected fluid that is heated by the reservoir rock, becoming again available for production (O'Sullivan and McKibbin, 1993). Despite all the differences between hydrocarbon and geothermal reservoir, the techniques used for extraction of fluids are similar; as are the exploration techniques and reservoir management approaches. Techniques comparable to those used in the oil industry are employed to drill and complete well in the productive reservoir. In both cases formation damage should be minimized in order to optimize well performance. A well may encounter multiple, widely spaced, fracture zones, resulting in flow rates that are too low. Stimulation techniques have the potential to remediate such causes for low flow-rate wells. Different techniques can be used to enhance the fracture network but the main ones are hydraulic fracturation and chemical treatment. The present paper will be focused on the chemical stimulation of geothermal wells. This technology, developed for more than one century by oil industry for the stimulation of oil and gas wells, is also used in geothermal wells. After a reminding of the different chemical stimulations performed on the GPK4 well at Soultz-sous-Forêts, numerical simulations using FRACHEM code have been carried out to estimate the impact of the

acidizing treatments on carbonates and reservoir properties.

Cleaning of geothermal wells

Well stimulation techniques

Resources exploitation of gas, oil and heat from deep reservoirs needs sometimes a permeability development around the production wells to ensure an efficient flow. The aim of this technology is to enhance the well productivity and to reduce the skin factor by removing near-wellbore damage and by dissolving scales in natural fractures. It consists to pump into the reservoir reactants such as strong acids (hydrochloric acid, HCl-HF mixture), organic acids (acetic acid, chloroacetic acid, formic acid, sulfamic acid) or chelatants (EDTA family). Besides the traditional acids, the chelatants are solutions used as formation cleanup and for stimulating wells especially in formations that may be damaged by strong acids (Frenier et al., 2001). They act as a solvent, increasing the water-wetting operations and dissolving (entirely or partially) some minerals containing Fe, Ca, Mg and Al.

These reactants can be pumped into the reservoir according to two procedures: below the fracturing flow rate and pressure of the reservoir (matrix acidizing) or above the fracturing flow rate and pressure (fracture acidizing). The main disadvantage of acid treatments is linked to the corrosion risk of the casing in particular with strong acids. Nevertheless, this risk can be reduced by addition of corrosion inhibitors or by using less-corrosive agents as chelatants, but their use increases the treatment cost.

Matrix acidizing

This process is performed below fracturing flow rate and pressure and is normally used for the removal of skin damage associated with work-over, well killing or injection fluids and also for to increasing formation permeability in undamaged wells.

The protocol of matrix acidizing has not really evolved since the beginning of the 1980's and is composed of three main steps: a preflush, with hydrochloric acid ; a mainflush with a hydrochloric – hydrofluoric acid mixture ; a postflush / overflush with soft HCl acid solutions or with KCl, NH_4Cl solutions and freshwater.

Treatment volumes, injection rates, acid placement techniques, acid system selection and evaluation of the results when stimulating geothermal wells, all follow the same criteria as for oil wells. The important difference is the formation temperature. High temperature reduces the efficiency of corrosion inhibitors (and increase their cost) as well as increasing the acid/rock reaction rate. The high acid rock reaction rate requires the use of a retarded acid system to ensure acid will not all be spent immediately next to the wellbore, but will penetrate deeper into the formation. Protecting the tubulars against corrosion is another serious challenge. This requires careful selection of acid fluids and inhibitors (Buijse et al., 2000), while cooling the well by injecting a large volume of water preflush may reduce the severity of the problem.

Fracture acidizing

Also called acid fraccing, this technique is widely used for stimulating limestone and dolomite formations or formations presenting above 85 % acid solubility. It consists to inject first a viscous fluid at a rate higher than the reservoir matrix could accept leading to the cracking of the rock. Continued fluid injection increases the fracture's length and width and injected HCl acid reacts all along the fracture to create a flow channel that extends deep into the formation. The key to success is the penetration of reactive acid along the fracture. However, the treatment volumes for fracture acidizing are much larger than the matrix acidizing treatment, being as high as 12'000 – 25'000 l/m of open hole (Economides and Nolte, 1987).

Chemical mechanisms involved in acidizing

The preflush, performed most often with a HCl solution, has to allow the displacement of the formation brine and the removing of calcium and carbonate materials in the formation. Acid reacts rapidly with carbonate rocks when it reaches the grain surface according to reactions:

$$CaCO_3 + HCl \rightarrow Ca^{2+} + Cl^- + HCO_3^-$$

$$CaMg(CO_3)_2 + 2HCl \rightarrow Ca^{2+} + Mg^{2+} + 2Cl^- + 2HCO_3^-$$

By dissolving calcite and dolomite, acid may create wormholes (Crowe et al., 1992) and new pathways. If the reaction rate is too quick, acid is immediately consumed in the vicinity of

the fracture, forming wormholes but preventing the aperture of new pathways and connection to other fractures.

The role of the preflush, by dissolving carbonates, also prevents their contact and their reaction with HF injected with the mainflush and therefore minimizes the risk of precipitation of calcium fluoride CaF_2, highly insoluble in water:

$$CaCO_3 + 2\ HF \rightarrow CaF_2 + 2\ HCO_3^-$$

During the mainflush, the HF acid reacts mainly with the associated minerals of sandstones (clays, feldspars and micas), rather than with quartz. The reaction rates of HF with clays or feldspars are 100 to 200 times faster than the one with quartz. It results from these reactions an enlargement and interconnections of the pores in the matrix, facilitating fluid flow. The risk of using HF acid is the strong affinity of Si and Al with F, which can cause the precipitation of silicium or aluminum complexes (SiF_6^{2-}, AlF^{2+}, AlF_2^+, AlF_3, AlF_4^-), then damaging the formation by plugging. This is why HCl is added to HF: hydrochloric acid keeps a low pH and prevents the formation of fluorosilicates, fluoroaluminates, and fluoride salts.

For the preflush operation in acidizing treatments, a solution of hydrochloric acid at a concentration of 10 to 15 % is most often used. For the mainflush, the mud acids generally range from 10% HCl – 5% HF to 12% HCl – 3% HF. Acidification of geothermal wells is not as frequent as of oil and gas wells, but the operations are borrowed from this industry.

Concerning the injected amounts, in the majority of the cases, the preflush volume was based on a dosing rate of 600 litres per metre of open hole (Malate et al., 1997; Barrios et al., 2002). The cleaning out of the geothermal wells needs about 900 litres per metre of target zone.

HCl and HF are two acids reacting quickly with carbonates and silicates. However, the objective of acid treatment is to increase porosity and permeability of the medium, deeply in the formation. Some retardants can be added to the mud acid to slow the reaction rate of acid with the minerals.

A key point is to inject a solution not containing HF explicitly but a compound able to generate HF at greater depth of penetration for a longer reaction time and a maximum dissolution of fines (Crowe et al., 1992). This retardant hydrolyzes in water when it enters in the reservoir to form HF according to the reaction:

$$HBF_4 + H_2O \rightarrow HBF_3OH + HF$$

Other retardant systems can be used as an emulsifier of the aqueous acid solutions in oil, the dissolving of the acids in a solvent (alcohol, gel…) or the injection of solutions of methyl acetate which hydrolyses slowly at very high temperatures to produce acetic acid.

Malate et al. (1998) also proposed an acid system applicable for moderate to deep penetrations. They used a phosphonic acid complex (HEDP) to hydrolyse NH_4HF_2 instead of HCl. HEDP has five hydrogens available that dissociate at different stochiometric conditions. Mixture of HEDP acid with NH_4HF_2 produces an ammonium phosphonate salt and HF.

Experiments of acid injection

The cleaning out of geothermal wells to increase their productivity after scaling deposits constitutes the main application of the acid treatments. This technique has been used extensively in some geothermal fields in the Philippines (Buning et al, 1995; Buning et al, 1997; Malate et al., 1997; Yglopaz et al., 1998; Malate et al., 1999, Jaime-Maldonado and Sánchez-Velasco, 2003, Amistoso et al., 2005), in El Salvador (Barrios et al., 2002) and in USA (Morris et al., 1984, Entingh, 1999). It presents interesting results, such as the well injectivity increasing by 2 to 12-folds according to the studied reservoirs (Table 1).

At the Larderello geothermal field (Italy), several stimulation methodologies have been used successfully by ENEL (Capetti, 2006). Among them, chemical stimulation operations were carried out by injection of acid mixtures. First, various laboratory tests were realised on reservoir rock samples to optimize the HCl/HF ratios and the effect on mineral dissolution. Field tests have shown impressive results on five deep wells for reservoir rocks composed of phyllites, hornfels and granites: the improvement of injectivity, respectively productivity ranged from a factor 4 to 12.

In the field of EGS, few chemical treatments have been applied to stimulate reservoirs. In 1976, at the Fenton Hill Hot Dry Rock site (USA), 190'000 l of 1 N carbonate sodium base solution was injected to dissolve quartz from the formation and to reduce the impedance of the existing system. About 1'000

kg of silica were dissolved and removed from the reservoir but without impedance reduction. In 1988, a matrix acidizing was performed on the Fjällbacka reservoir (Sweden): major and minor fractures of the granitic reservoir were filled with calcite, chlorite and clay minerals. About 2'000 l of HCl-HF acid were injected in Fjb3 to leach fracture filling. Returning rock particles showed some efficiency of this acid injection (Wallroth et al., 1999). Several wells at Coso field, affected by calcium carbonate scaling, were treated by acid methods. A total of 30 wells were treated with HCl and 24 gave successful results (Evanoff et al., 1995).

Geothermal Fields	Number of treated wells	Injectivity Index (kg/s/bar)	Improvement factor
Bacman (Philippines)	2	0.68 → 3.01	4.4
		0.99 → 1.4	1.4
Leyte (Philippines)	3	3.01 → 5.84	1.9
		0.68 → 1.77	2.6
		1.52 → 10.8	7.1
Salak (Indonesia)	1	4.7 → 12.1	2.6
Larderello (Italy)	5	11 → 54	5
		4 → 25	7
		1.5 → 18	12
		-	4
		11 → 54	5
Berlín (El Salvador)	5	1.6 → 7.6	4.8
		1.4 → 8.6	6.1
		0.2 → 1.98	9.9
		0.9 → 3.4	3.8
		1.65 → 4.67	2.8
Beowawe (USA)	1	-	2.2
Coso (USA)	30	24 wells	successful

Table 1: Results of HCl-HF treatments for scaling removal and connectivity development

The case of the EGS reservoir at Soultz

The geothermal research program for the extraction of energy from a Hot Fractured Rock at the Soultz-sous-Forêts site began in 1987 (Hettkamp et al., 2004). The project aims to convert heat to electricity from a deep fractured and granitic reservoir. To extract the heat from the reservoir, three deviated wells have been drilled at a depth of 5'000 m and their bottoms are separated by 650 m. The fractured reservoir encountered at this depth presents a temperature of 200°C. One well (GPK3) is dedicated to injection of cold water in the granitic reservoir whereas the two others (GPK2 and GPK4), located on both sides of injector, are used to pump hot water.

Stimulation experiments and injection tests

Recently acid treatments were performed at Soultz-sous-Forêts (France). This deep granitic reservoir contains fractures partially filled with secondary carbonates (calcite and dolomite). In order to dissolve these carbonates and to enhance productivity around the wells, each of the three boreholes (GPK2, 3 and 4) were treated with different amounts of hydrochloric acid. If GPK2 and GPK3 have shown weak variations of their injectivity, GPK4 presented a real increase of its injectivity after the treatments.

GPK4 well

In February 2005, an acid injection was tested to improve the injectivity around GPK4 well. The experiment began on 22 February 2005 with an injectivity test of the well before soft acidification. It consisted of the injection of 4'500 m^3 of water at increasing flow rates (9 l/s, 18 l/s, 25 l/s) in 24-hour steps. The injection of water acidified by the addition of approximately 2 g/l of hydrochloric acid started on 2 March 2005 at a flow rate of 27 l/s. It lasted 2 days, followed by one day of injecting fresh water at much lower rates in decreasing steps. A total volume of 5'200 m^3 was injected; with a total weight of acid (HCl) of 11 tons. When the wellhead pressure was back to the value observed during the previous injectivity test, an identical test was repeated on 13 March 2003: injection of 4'500 m^3 of water in flow rate steps of 24 hours at 9 l/s, 18 l/s and 25 l/s.

In May 2006, new tests began with a test of the well injectivity before acidification. The acid treatment was performed in four stages :

- Injection of 2000 m^3 of cold water deoxygenized at 12 l/s, 22 l/s then finally at 28 l/s.

- A preflush of 25 m^3 HCl diluted at 15 % (3 tons) (with deoxygenized water) was pumped ahead of

the HCl-HF acid mixture during 15 minutes at 22 l/s.

- A main flush consisted of the injection of 200 m^3 of Regular Mud Acid (RMA), (12 % hydrochloric (HCl)-3 % Hydrofluoric (HF) acid mixture treatment), with addition of a corrosion inhibitor, at a flow rate of 22 l/s during 2,5 hours.

- A postflush by injection of 2'000 m^3 cold water deoxygenized without inhibitor at a flow rate of 22 l/s then 28 l/s during 1 day.

When the wellhead pressure was back to a value identical to that observed in the previous injectivity test, a 3-day test identical to that of March 13, 2005 was repeated.

Results of acid stimulation treatments

Figure 1 shows the impact of the acidified water on the wellhead pressure during the first acid injection in GPK4 well. Despite the fact that the injection was performed in an over-pressurised reservoir, the injection pressure was decreasing during the last hours of the acidification test. Moreover, it is interesting to compare the data from two tests of water injection performed in the same conditions before (February 22, 2005) and after (March 13, 2005) the acid injection (Figure 1). Results (Gérard et al., 2005) show that after some 72 hours of water injection in the second test (24 hours at 9 l/s, 24 hours at 18l/s and 24 hours at 26 l/s), the GPK4 wellhead pressure was about 40 bars below the value observed in the same conditions before acidification. This represents a decrease of the apparent reservoir impedance seen from the wellhead by a factor ~1.5 (0.20 to 0.30 l/s/bar).

Figure 2 shows the impact of RMA acid job on the wellhead pressure by comparison before and after the second acid injection in GPK4 well. The repetition of the injectivity test showed that the difference in the over pressure values at the wellhead between the beginning of the test and the end were 16 bars. This represents a 35 % reduction of the wellhead pressure due to the acidification treatment. After some preliminary evaluation of downhole pressure changes, performed by Geowatt, this leads to a provisional estimate of GPK4 injectivity after chemical treatment of ~0.40 l/s/bar.

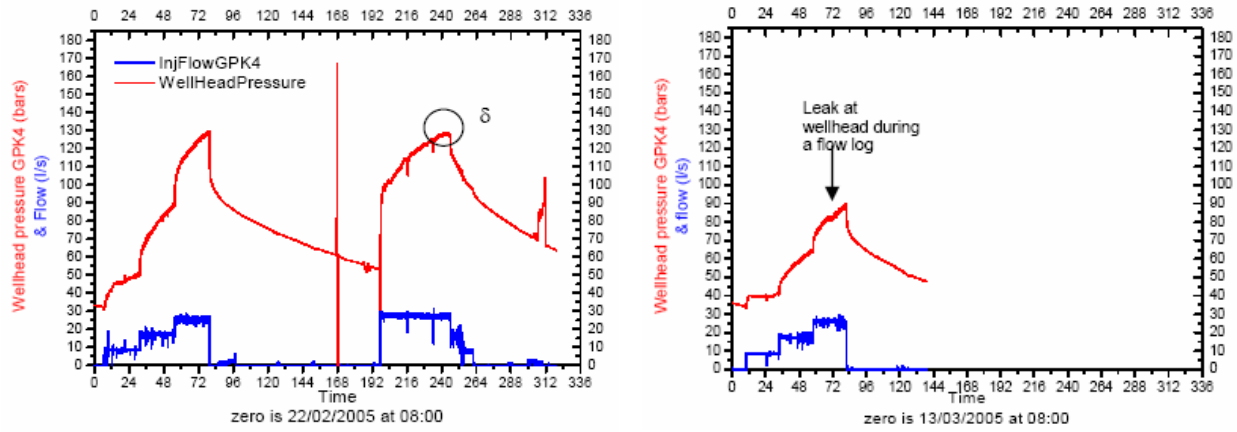

Figure 1: Impact of acidification test on GPK4; on the left, wellhead pressure before and during acidification injection, on the right, after acidification (Gérard et al, 2005).

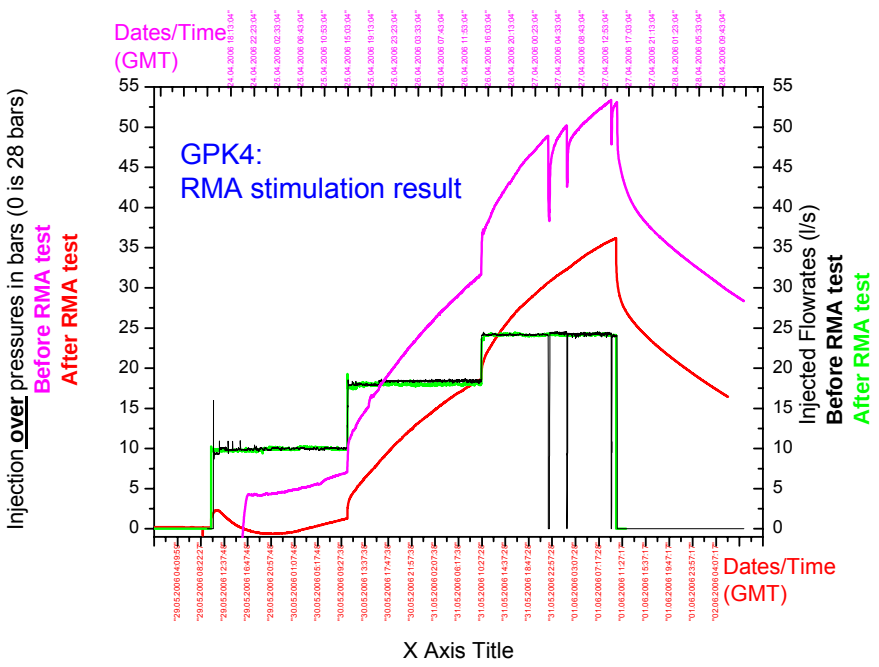

Figure 2: Impact of the RMA acidification test on the wellhead over pressure measured before and after the acidification test on GPK4 well (May 2006). (GEIE, 2006).

Modelling acidification impact on geothermal reservoir

The objective of the numerical simulation is to determine the impact of acid on the fracture minerals and on the reservoir properties.

Numerical modelling approach

To predict the impact of the acid treatment on the Soultz reservoir, the Thermo-Hydraulic and Chemical (THC) coupled code FRACHEM has been utilized. This THC code was built for the Soultz reservoir conditions. Instead of creating a totally new modelling programme, two existing codes, FRACTure and CHEMTOUGH2, have been combined in a new code called FRACHEM (Durst, 2002; Bächler, 2003; Rabemanana et al., 2003; André and Vuataz, 2005). FRACTure is a 3-D finite elements code and it determines thermal and hydraulic processes in fractured and porous rocks (Kohl and Hopkirk, 1995). CHEMTOUGH2 is a 3-D finite volumes code (White, 1995); it simulates the reactive transport and allows the variation of permeability according to chemical reactions occurring between fluid and rock of the reservoir. Considering the strong mineralization of brine and the high temperature of the reservoir, this last code has been modified by several implementations: thermodynamic model and computation of the activity coefficients of selected species in solution, kinetic model for dissolution and precipitation of minerals, as well as the relationship between porosity and permeability.

Knowing the high salinity of the brine of the Soultz system, The Pitzer formalism has been implemented in FRACHEM code to calculate the activity coefficients of selected chemical species; then, the precipitation/dissolution reactions of some minerals can be estimated. For the present time, the behaviour of eight minerals (calcite, dolomite, pyrite, quartz, amorphous silica, K-feldspars, albite and illite) is investigated. Detailed information on the determination of the reaction laws can be found in Durst (2002). At last, a supplementary module allows the determination of porosity and permeability variations linked with chemical processes occurring in the reservoir (André et al., 2005). The porosity variations are calculated and a combination of a fracture model and a grain model is used to determine the permeability evolution.

Simulation setup

Geometry

The same geometrical model as that presented in previous papers has been considered (André and Vuataz, 2005). The present application of FRACHEM is the modelling of a 2-D simplified model with a geometry close to the Soultz system. Injection and production wells are linked by fractured zones and surrounded by the impermeable granite matrix. The model is composed of 1250 fractured zones. Each fractured zone has an aperture of 0.1 m, a depth of 10 m, a porosity of 10%, and contains 200 fractures. This model allows an effective open thickness of about 125 m, while the mean openhole section of each well is about 600 m. Initially the temperature was set to the reservoir temperature of 200°C and the fractured zone contains the formation fluid.

One of these fractured zones is modelled with the assumption that the fluid exchange with the surrounding low permeability matrix is insignificant. Due to the symmetrical shape of the model, only the upper part of the fractured zone is considered in the simulation. The area is discretized into 222 2D elements (Figure 3).

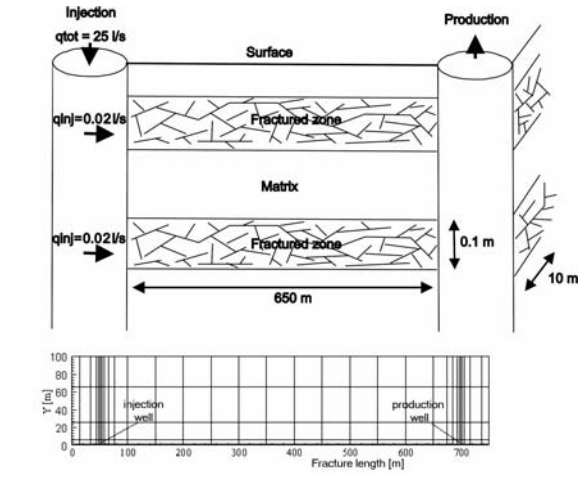

Figure 3: Simplified model and spatial discretization.

Considering a production rate of 25 l/s, the fluid was re-injected in each of the fractured zones at a rate of 2.10^{-2} l/s at a constant temperature of 65°C. During this simulation a constant overpressure of 8 MPa was assumed at the injection well and a hydrostatic pressure at the production well. Dirichlet boundary conditions were applied to the upper, left and right side of the model. The values of thermo-hydraulic parameters considered in the simulation are listed in Table 2.

Table 2: Thermo-hydraulic model parameters.

Parameters	Units	Fracture	Matrix	Fluid
Hydraulic conductivity	[m^2/Pa]	7.4 10^{-8}	10^{-15}	-
Thermal conductivity	[W/m.K]	2.9	3	0.6
Density	[kg/m^3]	-	2650	1000
Heat capacity	[J/kg.K]	-	1000	4200
Porosity	[%]	10	0	-

Rock composition

The mineralogical composition of Soultz granite given by Jacquot (2000) on GPK2 is assumed to be the same for the three wells (GPK2, GPK3 and GPK4) (Table 3). In the following simulations, the fluid is assumed to circulate within the hydrothermalised granite containing about 3.3 % of calcite and 0.8 % of dolomite.

Fluids composition

The fluid present in the formation is a NaCl brine with a pH of 4.9, a total dissolved solids of about 100 g/l and a temperature at the beginning of the simulation of 200 °C. The main characteristics of this fluid are given in Table 4.

The HCl solutions used to acidize the circulation fluid are highly diluted solutions (a fresh water) acidified to 2 g/l and to 15 g/l with concentrated HCl. These solutions are injected in the fractured zone at a temperature of 65 °C.

Table 3: Mean composition (in volume percent) of the different facies of granite in the Soultz reservoir (Jacquot, 2000).

Minerals	Healthy granite	Hydrothermalised granite	Vein of alteration
Quartz	**24.2**	**40.9**	**43.9**
K-Feldspar	**23.6**	**13.9**	
Plagioclases	**42.5**		
Illite		**24.6**	**40.2**
Smectite		**9.7**	**9.6**
Micas	**9.3**		
Calcite	**0.3**	**3.3**	**4.3**
Dolomite		**0.8**	**0.7**
Pyrite		**0.7**	**1.0**
Galena		**1.3**	**0.3**
Chlorite		**4.8**	

Table 4: Characteristics of the fluids used for the numerical simulations

Fluid		HCl solutions	Formation brine
Temperature (°C)		65	200
pH		1.3 to 0.4	4.9
Concentration (mg/kg)	Na^+	26.40	26400
	K^+	2.90	2870
	Ca^{2+}	4.75	6160
	Mg^{2+}	0.10	112
	Fe^{2+}	0.13	134
	SiO_2	0.36	364
	Cl^-	1455	54205
	SO_4^{2-}	0.07	63
	HCO_3^-	0.09	58

Simulation results of acid injections

We have been studying the impact of acid treatments on the Soultz reservoir properties near the injection well. The FRACHEM simulator is used to inject the adequate volume of acid in the model. The solutions are expected to circulate in a fractured zone composed of hydrothermally altered granite and their behaviour with respect to the minerals present in this granite is observed. When the desired volume is reached, the injection is stopped and the return to chemical equilibrium of the injected fluid is modelled. In the reservoir, a total pressure of 500 bars is assumed and the CO_2 partial pressure is fixed to 5 bars.

Concerning the acid solution used in the simulations, it should be noted that, for the time being, the code is not able to make the difference between the type of injected acid. It means that FRACHEM does not make the difference between hydrochloric and hydrofluoric acids. In this condition, the injection of an acid solution and the acid concentration are fixed by the H^+ concentration and by the total volume injected. Concentrated solutions are characterised by low pH solutions.

At last, it should be noted that the code calculates phases equilibrium between fluid and rock without taking into account the specific reaction rate of acid on carbonates. We suppose here that the reaction between acid and carbonates is instantaneous which is not a real disadvantage considering the high reactivity of HCl with carbonates and in particular with calcite.

Soft acidification

The duration of the numerical simulation was determined in order to simulate the real amount of acid injected in GPK4 in February 2005. The interpretation presented here are given for HCl injection of 60 hours at a flow rate of 25 l/s and at a concentration of 2g/l, equivalent to the 11 tons of HCl injected in GPK4 in February 2005.

The action of acid on carbonates has been investigated. Results show that acid solution dissolves carbonates in the first metres of the fractured zone. Around GPK4 (60 hours injection), the injected amount of HCl affects the first 3.5 metres around the injection well (Figure 4). Due to the respective reaction rate of each mineral, it should be noted that dolomite has dissolution rates two orders of magnitude smaller than calcite (Figure 5). Comparatively to a normal brine injection, after 60 h, the acid injection involves an increase of dissolved calcite and dolomite.

HCl acidification has a weak impact on other minerals: it only decreases the precipitation rate of K-feldspar, albite, illite and amorphous silica (Figure 6). Finally, quartz is not affected by this type of acidification (Figure 6).

All these dissolution processes cause an increase of about 2.0 % of rock porosity in the short interval of 0.5 m around the injection well and 0.1 % in the interval 0.5-1.5 m. This estimation of the reservoir changes is linked to the choice of the porosity model used in FRACHEM, namely the double fracture and grain model.

In conclusion, we can suppose that the volume of injected acid in the first soft acidizing test on GPK4 had only an impact on the first 4 metres around the injection well. With these rather small acid amounts, the impact on the reservoir properties seems to be limited, although the porosity increases in the close vicinity of the wells due to carbonates dissolution.

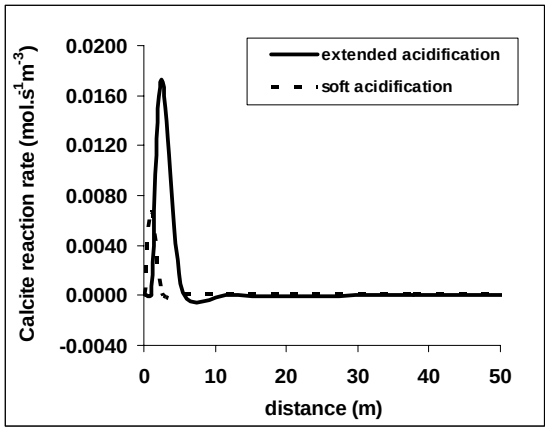

Figure 4: Variation of calcite reaction rate after acid injection.

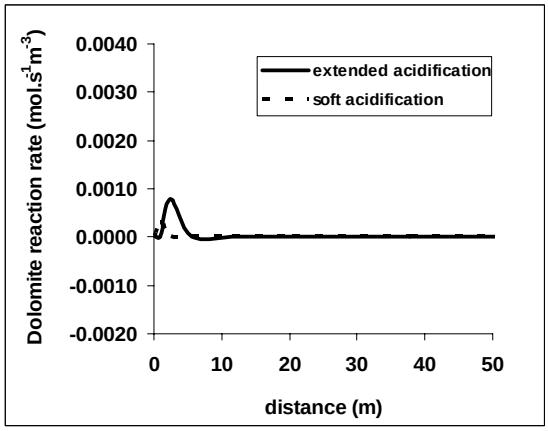

Figure 5: Variation of dolomite reaction rate after acid injection.

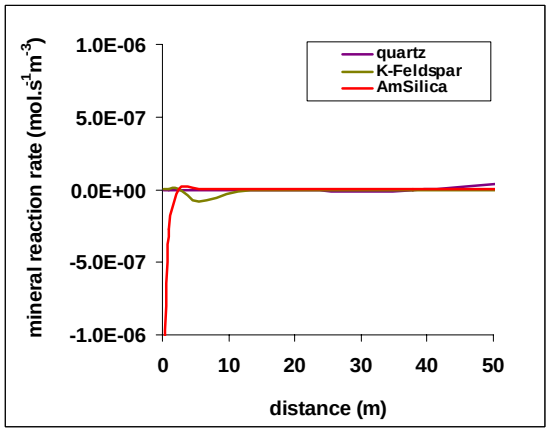

Figure 6: Variations of quartz, K-Feldspar and amorphous silica reaction rate after soft acid injection.

Influence of injection flow

The chemical stimulation of an EGS reservoir is effective if the acid can reach fractures distant from the injection well. In order to simulate this process, the flow was doubled meaning that the acid solution, at a concentration of 2 g/l, was pumped at 50 l/s. In these conditions, the 11 tons of acid are injected in 30 hours, compared to the 60 hours of the previous simulation. We observed that doubling the flow allows a farther transport of acid within the fracture. Less calcite is dissolved near the well but the impact of acid is visible up to 7.5 metres (Table 5). The same phenomenon applies to dolomite. Dissolution rate of this mineral is two orders of magnitude smaller than calcite. Consequently the impact of acid is still active beyond 15 metres along the fracture.

Table 5: Variation of the proportion of carbonates around the injection well according to variable transport flow

Distance from injection well (m)	Injection at 25 L.s^{-1}		Injection at 50 L.s^{-1}	
	Calcite (%)	Dolomite (%)	Calcite (%)	Dolomite (%)
0 0.5	- 19.70	- 5.73	- 18.80	- 6.00
0.5 1.5	- 1.40	- 0.12	- 1.02	- 0.10
1.5 3.5	- 0.15	- 0.15	- 0.37	- 0.06
3.5 7.5	0	- 0.10	- 0.10	- 0.05
7.5 15	0	0	0	- 0.05

Extended acidification

In May 2006, GPK4 well was stimulated by injecting 98 tons of HCl during a period of 2.5 hours. This second acidizing treatment used hydrochloric acid at a concentration of 12 % and hydrofluoric acid at a concentration of 3 %. After this injection, the acid is displaced within the formation by injecting about 2'000 m^3 of fresh water. The results showed a decrease of the injection pressure in the vicinity of the injection well, as the calcite was dissolved and progressively carried away. The response of the model to the acid addition has been examined.

Influence of high acid concentration

Knowing that the code is not able to make the difference between the type of injected acid, a numerical simulation was carried out to investigate the impact of this acid injection at a concentration of 15 g/l. This simulation was performed with fresh water. Its pH was lowered to 0.4, whereas the injection rate within the fractured zone was maintained to

2.10^{-2} l/s. Therefore, the flow was fixed at 25 l/s and the duration of the injection was 70 hours. The total amount of injected acid is equal to 98 tons. The results indicate that calcite is as usual, the most affected mineral by the acid injection. Respectively to the extended acidification, the increase of acid concentration seems to augment the dissolution processes in the first meter around the injection well, and the impact of acid is also noticeable farther in the formation (Figures 4, 5 and Table 6). The porosity increases mainly in the vicinity of the injection well of about 4.5 % (Figure 7) instead of the 2.0 % estimated with a soft acidification. This increase of porosity is expressed by an injectivity rise in the zones affected by acidizing treatment.

In conclusion, the extended acidification amplifies the amount of dissolved calcite of about 70 % around the injection well. We can also suppose that the volume of injected acid in the second test on GPK4 had an impact on the first 10 metres around the injection well. The simulation results were consistent with those of the experiment. The additional H^+ ions significantly modify the calcite reaction rate around the injection well. The additional acid reaction leads to significantly drop the pressure around the injection well (Figure 8). This brine acidification implies a decrease of about 4 bars near the injection well, corresponding to a reduction of about 5 % of the pressure in 70 hours. This result is linked to the enhanced dissolution of calcite within the fractured zone. As the reservoir permeability and porosity are controlled by the occurrence of mineral precipitation and dissolution, this stronger calcite dissolution implies an improvement of the reservoir properties, namely the hydraulic impedance of the injection well.

Table 6: Variation of the amounts of carbonates and quartz near the injection well according to the amount of acid injected.

Amounts of minerals (kg)	Calcite	Dolomite	Quartz
Soft acidification	-15.4	-13.8	+0.0207
Extended acidification	-145	-35.6	+0.0129

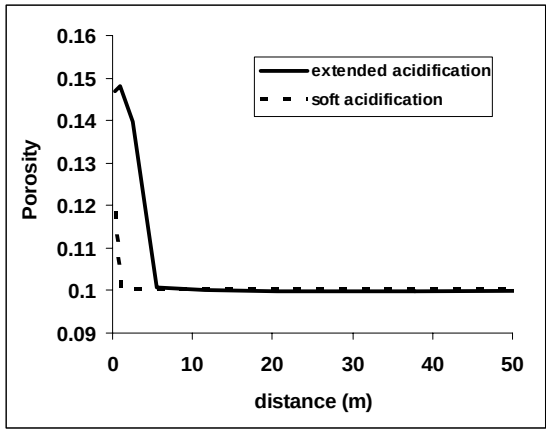

Figure 7: Porosity variation at different distance from the injection well after acid injection.

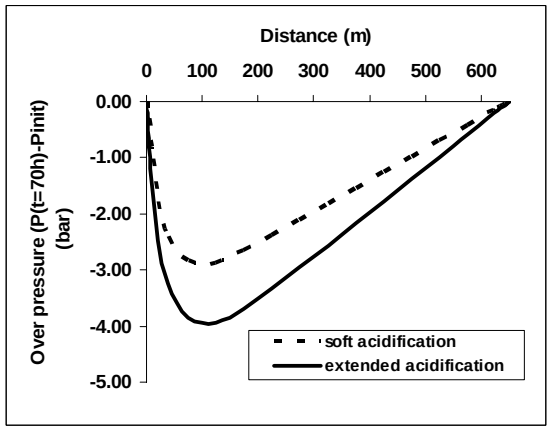

Figure 8: Variation of the pressure at different distance from the injection well after acid injection.

New improvements of the simulation

In order to improve simulation of the acidification processes, some new results of acid injections simulations using FRACHEM code are presented here. Porosity evolution resulting of acid injection has been observed according to three main parameters:

- acid concentration, varying from 2 to 15 g/l of HCl.

- flow imposed to the system, ranging from 10 to 50 l/s.

- duration of acid injection / circulation fluid in the fractured zone, reaching 0.5 to 10 days.

For a limited acid injection (10 l/s at 2 g/l), acid effect on dissolved carbonates and on penetration within the reservoir is very restricted. At this flow, a real impact on reservoir properties is only obtained for extended injections of many days and for high

acid concentrations. After an injection of 10 days of a solution at 15 g/l, all carbonates are dissolved in the first 0.5 metres around the injection well but only 65 % in the range 0.5 – 1.5 m. The relative weak effect of a small flow is shown here.

Nevertheless, for the other simulations at this flow, it seems that acid concentrations of about 7 to 15 g/l could have a positive impact up to 7.5 metres away from the injection well, and for a relatively limited injection time (5 days).

Injected acid reacts of course with carbonates (calcite and dolomite). According to mineralogical data, these compounds represent more or less 5 % of the hydrothermally altered granite. From this proportion and in case of a massive acid injection, all carbonates can be dissolved by acid solution leading to a porosity of about 0.15.

Obviously, the best results are obtained for long-term injections of high-concentration acid solutions. In these conditions, the impact radius can reach 15 metres around the injection well. Considering these conditions (for example 15 g/l and 50 l/s), it should be noted that the important amount of injected acid is able to dissolve carbonates (calcite + dolomite) up to 7 metres from the injection well, even for very limited injection times (2.5 days), (Figure 9).

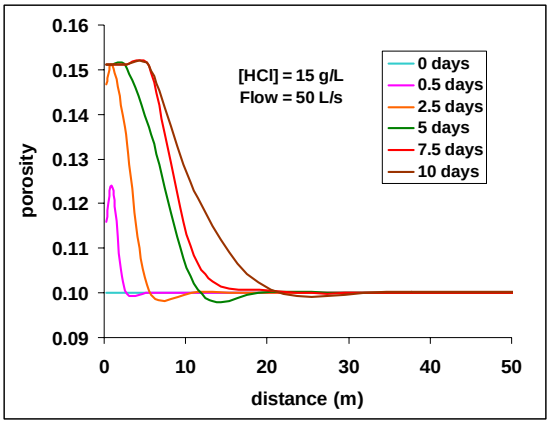

Figure 9: Porosity evolution of the fractured zone according to acid concentration and time of acid circulation and for a flow in the fractured zone of 50 L/s.

Finally, the increase of acid concentration involves an augmentation of dissolution processes but always in the first 5 metres around the injection well. Due to the high reactivity of HCl, the rock volume affected by acid is relatively small. An increase of the flow should allow a better dispersion of acid within the formation. The increase of the acid injection pressure to simulate a fracture acidizing allows a farther acid transport trough the fractures (Figure 10).

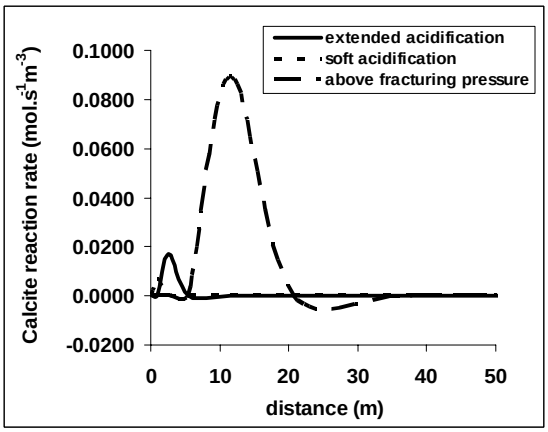

Figure 10: Variation of calcite reaction rate after acid injection below and above fracturing pressure.

Conclusions

Recent acid treatments have been successfully performed in geothermal granitic reservoirs such as at Soultz and encouraging results were obtained on GPK4 well.

Some numerical simulations using FRACHEM code were performed to better understand the acid behaviour within the reservoir. Considering the geometrical model used for the simulations and the different assumptions about fluid and rock compositions, some estimations have been proposed.

Simulations result indicate that carbonates are the most dissolved minerals by hydrochloric acid.

For GPK4 well, the first acid injection lasted 3 days at a concentration of 2 g/l (about 11 tons of acid injected in the reservoir). According to the simulation of this test, the amount of acid is just sufficient to dissolve half of the carbonates initially present in the range of 0 – 0.5 metres. Farther in the fracture, the impact is quasi nil.

Simulation of extended acid injection performed in May 2006 (about 98 tons of acid injected in the reservoir) seem to show a significant dissolution of carbonates around the injection well. The increase of acid concentration augments the reactivity in the

vicinity of the injection well and enhances the porosity.

Nevertheless, the high reactivity and a weak flow prevent the penetration of acid in the far field between the wells. This high reactivity also involves the risk of creating wormholes, able to increase the porosity but not always the permeability of the fractured medium.

Finally, we have demonstrated that acid injection can play a significant role in the development of porosity around injection wells. It was shown that HCl acid has the possibility to react with carbonates, dissolving them and opening new pores within the reservoir. The positive effect of acid injection on porosity is proportional to the amount of injected acid.

Looking for commercial production rates of the wells, other chemical stimulation techniques should be considered, such as fracture acidizing, more complex acid compounds and chemical retardants. These types of acid jobs should have a more pronounced effect on the fracture network of the far field and eventually connect injection to production wells.

Acknowledgements

The authors thank the State Secretariat for Education and Research and the Swiss Federal Office of Energy for funding this project (OFES-N° 03.04.60). The authors are also grateful to André Gérard of the GEIE at Soultz and Thomas Kohl of GEOWATT AG (Zürich) for their scientific support.

References

André, L., Vuataz, F.-D. (2005), "Simulated evolution of reservoir properties for the Enhanced Geothermal System at Soultz-sous-Forêts: the role of hot brine-rock interactions". Proceedings 30th Workshop on Geothermal Reservoir Engineering, January 31- February 2, 2005, Stanford University, Stanford, California.

André, L., Vuataz, F.-D. (2006), "Simulated evolution of reservoir properties for the Enhanced Geothermal System at Soultz-sous-Forêts: the role of hot brine-rock interactions". Geothermics, in press.

André, L., Rabemanana, V. and Vuataz, F.-D. (2005), "Geochemical modelling of water-rock interactions and implications on the properties of the Soultz fractured reservoir". Proceedings EHDRA Scientific Conference, March 17-18, 2005, Soultz-sous-Forêts, France

Amistoso, A.E., Aqui, A.R., Yglopaz, D.M. and Malate, R.C.M. (2005), "Sustaining steam supply in Palinpinon 1 production field, Southern Negros Geothermal Project, Philippines". World Geothermal Congress, Antalya, Turkey, 24-29 April, 2005.

Bächler, D. (2003), "Coupled Thermal-Hydraulic-Chemical Modelling at the Soultz-sous-Forêts HDR reservoir (France)", PhD Thesis, ETH-Zürich, Switzerland, 150 p.

Barrelli, A., Cappetti, G., Manetti, G. and Peano, A. (1985), "Well stimulation in Latera Field". Geothermal resources Council Transactions, Vol. 9- Part II, pp. 213-219.

Barrios, L.A., Quijano, J.E., Romero, R.E., Mayorga, H., Castro, M. and Caldera, J. (2002), "Enhanced permeability by chemical stimulation at the Berlin Geothermal Field, El Salvador". Geothermal Resources Council Transactions, Vol. 26, September 22-25, 2002.

Buijse, M., Maier, R. and Casero, A. (2000), "Successful high pressure, high temperature acidising with in situ crosslinked acid diversion". SPE paper 58804.

Buning, B.C., Malate, R.C.M., Lacanilao, A.M., Sta Ana, F.X.M. and Sarmiento, Z.F. (1995), "Recent experiments in acid stimulation technology by PNOC-Energy development corporation, Philippines". Proceedings World Geothermal Congress, Vol. 3, p. 1807-1812.

Buning, B.C., Malate, R.C.M., Austria, J.J.C., Noriega, M.T. and Sarmiento, Z.F. (1997), "Casing perforation and acid treatment of well SK-2D Mindanao 1 Geothermal project, Philippines". Proceedings 22nd Workshop on Geothermal Reservoir Engineering, January 27-29, 1997.

Capetti, G. (2006), "How EGS is investigated in the case of the Larderello geothermal field ?". Engine Launching Conferente, Orleans 12-15 February 2006, unpubl. presentation.

Crowe, C., Masmonteil, J. and Thomas, R. (1992), "Trends in Matrix Acidizing". Oilfield Review, October 1992, pp. 24-40.

Durst, P. (2002), "Geochemical modelling of the Soultz-sous-Forêts Hot dry Rock test site: Coupling fluid-rock interactions to heat and fluid transport". PhD thesis, University of Neuchâtel, Switzerland, 127p.

Economides, M. and Nolte, K. (1987), "Reservoir stimulation". Schlumberger Educational Services.

Entingh, D.J. (1999), "A review of geothermal well stimulation experiments in the United States". Geothermal Resources Council

Transactions, October 17-20, 1999, vol. 23, pp. 175-180.

Evanoff, J., Yeager, V. and Spielman, P. (1995), “Stimulation and damage removal of calcium carbonate scaling in geothermal wells: a case study”. World Geothermal Congress, Florence, Italy, pp. 2481-2485.

Frenier, W.W., Fredd, C.N. and Chang, F. (2001), “Hydroxyaminocarboxylic Acids produce superior formulations for matrix stimulation of carbonates at high temperatures”. SPE 71696.

GEIE. (2006), “Results of GPK4 RMA stimulation of May 2006”. Unpublished data.

Gérard, A., Fritz, B. and Vuataz, F.-D. (2005), “Results of soft acid injection tests performed at Soultz in wells GPK2, GPK3 and GPK4 – Extended summary: revised status on 14 March 2005- Proceedings EHDRA Scientific Conference”, March 17-18, 2005, Soultz-sous-Forêts, France.

Hettkamp, T., Baumgärtner, J., Baria, R., Gérard, A., Gandy, T., Michelet, S. and Teza, D. (2004), “Electricity production from hot rocks”. Proceedings, 29th Workshop on Geothermal Reservoir Engineering, Stanford University, Stanford, California, January 26-28, 2004, 184-193.

Jacquot, E. (2000), “Modélisation thermodynamique et cinétique des réactions géochimiques entre fluides de bassin et socle cristallin: application au site expérimental du programme européen de recherche en géothermie profonde (Soultz-sous-Forêts, Bas-Rhin, France)”. PhD thesis, Université Louis Pasteur-Strasbourg I, France.

Jaime-Maldonado, J.G. and Sánchez-Velasco, R. (2003), “Acid stimulation of production wells in Las Tres Vírgenes Geothermal field, BCS, México”. Geothermal Resources Council Transactions, Vol. 27, October 12-15, 2003.

Kohl, T. and Hopkirk, R. J. (1995), “FRACTURE" – A simulation code for forced fluid flow and transport in fractured, porous rock”, Geothermics, 24, 333-343.

Malate, R.C.M., Yglopaz, D.M., Austria, J.J.C., Lacanilao, A.M., and Sarmiento, Z.F. (1997), “Acid stimulation of injection wells in the Leyte Geothermal power project, Philippines”. Proceedings 22nd Workshop on Geothermal Reservoir Engineering, January 27-29, 1997.

Malate, R.C.M., Austria, J.J.C., Sarmiento, Z.F., DiLullo, G., Sookprasong, A. and Francia, E.S. (1998), “Matrix Stimulation Treatment of Geothermal Wells Using Sandstone Acid”. Proceedings 23rd Workshop on Geothermal Reservoir Engineering, January 26-28, 1998.

Malate, R.C.M., Sookprasong, P.A., Austria, J.J.C., Sarmiento, Z.F. and Francia, E.S. (1999), “Wellbore Soaking: a Novel Acid Treatment of Geothermal Injection Wells”. Proceedings 24th Workshop on Geothermal Reservoir Engineering, January 25-27, 1999.

Morris, C.W., Verity, R.V. and Dasie, W. (1984), “Chemical stimulation treatment of a well in the Beowawe Geothermal Field”. Geothermal Resources Council, Transactions, pp. 269-274.

O’Sullivan, M. and McKibbin, R. (1993), “Geothermal reservoir engineering”. Course notes, Institute of geothermal Engineering, University of Auckland, New Zealand.

Rabemanana, V., Durst, P., Bächler, D., Vuataz, F.-D., and Kohl, T. (2003), “Geochemical modelling of the Soultz-sous-Forêts Hot Fractured Rock system: comparison of two reservoirs at 3.8 and 5 km depth”. Geothermics, 32(4-6), 645-653.

Wallroth, T., Eliasson, T. and Sundquist, U. (1999), “Hot Dry Rock research experiments at Fjällbacka, Sweden”. Geothermics, 28(4), 617-625.

White, S.P. (1995), “Multiphase nonisothermal transport of systems of reacting chemicals”. Water Resources Research, 31, 1761-1772.

Yglopaz, D.M., Buning, B.C., Malate, R.C.M., Sta Ana, F.X.M., Austria, J.J.C., Salera, J.R.M., Lacanilao, A.M. and Sarmiento, Z.F. (1998), “Proving the Mahanagdong B Resource: A Case of a Large-Scale Well Stimulation Strategy, Leyte Geothermal Power Project, Philippines”. Proceedings 23rd Workshop on Geothermal Reservoir Engineering, January 26-28, 1998.

The importance of natural rock stress in the stimulation process, and the difficulty of its characterisation

EVANS Keith, Swiss Federal Institute of Technology, Zürich, Switzerland, keith.evans@erdw.ethz.ch

Hydraulic stimulation involves the injection of large volumes of fluid into the target rock mass. Experience has demonstrated that the operation is often highly effective in producing a permanent increase in rock mass transmissivity. The mechanism is thought involve the shearing of natural fractures which tends to produce dilation of the fracture walls and the opening of tubes at jogs in the fracture trace. The generation of microseismicity and the permanent nature of the transmissivity increases support this view. The shearing represents the relaxation of the natural shear stresses within the rock mass triggered by the weakening of the fracture by the elevated fluid pressure. The pore pressure increase required to initiate shear failure on favourably oriented fractures is often very small, perhaps as low as a few MPa. This reflects the tendency for the Earth's crust to be close to failure, a state which is referred to as being critically stressed. As such, the vast majority of the mechanical work of permeability/porosity creation is done by the natural stresses. The stress state thus determines which fractures shear and thus has a major influence of the geometry of the stimulated volume and flow paths that develop therein. It follows that knowledge of the stress state is essential if the process of reservoir creation is to be understood and modelled, which is a step towards developing the means to control it. The confident determination of the complete stress tensor is at best difficult and often not practical. Fortunately, limited knowledge of the stress tensor suffices for reservoir engineering purposes, but complete knowledge is needed for modelling. In this talk I will discuss the importance of the individual attributes of the stress tensor (e.g. the orientation of the maximum horizontal stress), and suggest strategies for their measurement.

Induced seismicity during EGS operation?

RYBACH Ladislaus, Geowatt AG, Zürich, Switzerland, rybach@geowatt.ch

Induced seismicity due to EGS stimulation is well known and useful: it can depict reservoir development in space and time. The event magnitudes rarely exceed M=3.0. Possible, even larger events due to EGS operation (for heat and/or power production) cannot be excluded. Experience in high-enthalpy fields show that prolonged fluid withdrawal or injection can lead to noticeable ground shaking. Examples from The Geysers/USA, Larderello/Italy, and Berlin/El Salvador will be presented.

For new EGS sites, the monitoring of local seismicity by a suitable seismometer array, starting well before stimulation/production activities, is indispensable to provide reliable base-line information on the pre-EGS situation. Besides, technical and social issues must be carefully addressed during EGS planning and realization.

There is a great need for specific research on possible seismic events, their causes and implications due to EGS operation. Substantial work is presently ongoing in the framework of the IEA Geothermal Implementing Agreement (GIA): Annex I “Environmental Impacts of Geothermal Energy Development” / Subtask D “Seismic risk from fluid injection into EGS” is especially devoted to corresponding activities. Some preliminary results will be outlined. A strong link should be established and cooperative efforts undertaken between ENGINE and the IEA GIA.

ENGINE – **EN**hanced **G**eothermal **I**nnovative **N**etwork for **E**urope
Workshop 3, "Stimulation of reservoir and induced microseismicity"
Kartause Ittingen, Zürich, June 29 – July 1, 2006, Switzerland

Understanding stimulation methods and microseismicity

BARIA Roy, Mil-Tech UK Ltd, Woking, England, roybaria@onetel.com
BAUMGAERTNER Jörg, Bestec GmbH
TEZA Dimitra, Bestec GmbH

Stimulation strategies

Stimulations are carried out in HDR/EGS systems so that the permeability between the wells can be enhanced to allow fluid circulation to place to extract the heat energy from the rock mass and transport it to the surface for power generation. This is done to meet certain economic targets and therefore has to attain right characteristics to minimize the parasitic losses during the circulation of fluid between the wells and yet the system be large enough to support up to 70-100 l/s for approximately 20 years.

Although one states that a stimulation is required to enhance permeability between the wells (ie an injector and a producer), in actual fact there two distinct zones which need to be addressed. The first one is near (the bottom) of the well and the second is between the two wells.

The enhancement of permeability near the well is carried out to reduce the friction losses between the well and the formation. This is of particular importance for production wells, as experience has shown that the permeability of the injector will always improve during the circulation due to thermal contraction and the higher pressure. On the other hand improvement of permeability between the wells with larger separations has always been a problem until recently, when this was successfully achieved at Soultz.

The enhancement of permeability near a well-bore can be increased by applying high pressure for a short period. Pressures can reach above the minimum earths stress and this helps to shear all joints from critically aligned to the direction of maximum earths stress. Methods used for achieving this varies from using low viscosity fluid such as fresh water to high viscosity jells. The flow rate and volume varies from 50-200 l/s and few hundred to a thousand m^3 respectively.

The enhancement of permeability between the wells has been a complex and difficult to implement. For example, wells with separation of 600 m would mean that one would have to deliver pressure well above that required for shearing at a distance greater than 300 m from the injection point between the wells. The shearing pressure will depend on values of the in-situ stresses, joint orientation and the overall permeability of the system (relatively open or closed system).

Shut-in curves from hydraulic tests carried out at around 3550 m and 5000m in Soultz show that the shallower system is relatively open but the deeper system is relatively tight.

The four months circulation test carried out in the shallower system in 1997 showed that the overall system impedance to circulate ~ 22 kg/s with a well separation of 450 m was 0.22 MPa/l/s. The tracer breakthrough was around 4.5 days. The result shows that good connectivity had been established between the wells. The impedance achieved was the best obtained anywhere in the world at that time and even more important; the value of the impedance was within the economic target required for this technology to be viable. The view was that with a three well system, the impedance will half and will be close to the economic target of 0.1 MPa/l/s.

Subsequently GPK2 was extended to 5000 m depth, stimulated twice, new well GPK3 was drilled in to the target zone defined by the microseismicity, in-situ stress and joint direction. The separation for the wells at the bottom was increased to ~ 600 m. During the stimulation of GPK3, a new technique was tried to improve the efficiency of stimulation technique, in conjunction with existing techniques. This was called focused stimulation and consisted of stimulating the two wells simultaneously. Following the stimulation of GPK3, a short circulation test was carried out showed that impedance between GPK3 & GPK2 was ~ 0.29 MPa/l/s. The separation between the wells had been increased by 150 m compared to the shallow system but the impedance had only increased by 0.07 MPa/l/s. Again, it was anticipated that

with a three well system, and following a prolonged circulation, the impedance would have fallen to the economic target of ~ 0.1 MPa/l/s.

The effectiveness of the focused stimulation was explained by numerical modeling which shows that a significant enhancement of the permeability can be achieved by a smaller volume and shorter period of stimulation, thus reducing the cost and risk of generating larger microseismic events.

Subsequently, the third well GPK4 was drilled in to the target zone defined by the microseismicity, in-situ stress and joint direction as before. GPK4 was stimulated twice using conventional technique with smaller volumes of fluid, and in both occasions poor connectivity was achieved between GPK3 & GPK4.

Focused stimulation technique was not used during these two stimulations of GPK4. Microseismic and other data indicate that here is a hydraulic barrier between the wells and this does not allow the pressure to buildup and shear the joints between the wells. Tracer test showed a breakthrough period of ~ 4 weeks, which is excessively longer than one would have expected. There are possible two methods to improve the connectivity between GPK3 and GPK4. A sustained high flow rate (70 -100l/s) injection in GPK4 with volume in the range of 30,000m^3, or a focused stimulation using around 30-50 l/s in each well for around a period of 24 –36 hours.

Other techniques to improve permeability are available from oil and gas, and mining industry. This includes chemical dissolution using acids, jell with proppants etc. One has to be exceedingly careful when using chemical treatment as very limited experience exists in igneous rocks and it is very likely to cause damage to the casing, cement and the asperities, which support the joint aperture and thus fluid transport.

Three examples are presented here one from Rosemanowes project and two from the Soultz site.

At Rosemanowes, circulations tests were carried out continuously for over five years. During this period, the produced hot water (~60ºC) was cooled using a cascade without realizing the effect this would have on the casing. The bottom of the injection well RH12 suffered a reduction of the cross-section of the casing by 60%. This was caused by the absorption of oxygen at the surface while exposed to the atmosphere when flowing over the cascade.

At the Soultz site, during the 4 months of circulation test in 1997, the injection well did not show the reduction of injection pressure, which was anticipated and observed in other HDR/EGS sites. Aquaprox, a chemical flocculants was added to the produced brine from GPK2 in an anticipation that this will help to coagulate very fine particle and these will trapped in the sock filters before the brine is injected in GPK1. The manufacturer of these chemicals had assured that this would have no effect on the injection well, although they had no experience with such a system. After two months of circulation, and comparing results from other HDR/EGS sites and observing the behavior of the flocculent in the sock filters by Terry Gandy, it was decided to stop injecting Aquaprox for two weeks. Within few hours, the injection pressure in GPK1 started to drop and with few days the injection pressure had halved from ~40 bars to ~20 bars. This is a clear example of how inexperienced use of chemicals can hinder a system rather than enhance the permeability.

The second example is during the injection test in GPK4 (2004) to evaluate the effectiveness of acid for improving the injectivity. The evaluation consisted of injecting a fresh water pulse, followed buy an acid pulse and this was followed by another fresh water pulse similar to the first one. The comparison between the first and the second fresh water pulse would indicate if there was any improvement in the injectivity. The initial look at the data suggested that there was an improvement but a flow log carried out during the this test showed that the acid had cause a leak in the casing (70 m above the casing shoe) and when this was accommodated in the calculation, the apparent improvement disappeared, leaving a hole in the casing.

Although acids are used to improve near well bore impedance in oil and gas industry and even in some geothermal industry, the delivery of the acid is normally done using tubing in the open hole to protect the casing and the cement. Again, inexperienced use of chemical can irreversibly damage rather than improve a system.

Microseismicity

The generation of microseismicity can explained by the shearing of existing joints when the pore is increased until the normal stress goes to zero causing the joint to fail. Although the generation of microseismicity can only be associated with pressure increase in joints, there are ample observations that indicate that flow channels do exist within the seismic clouds.

Microseismicity can be regarded as the result of a disturbance in the equilibrium of mechanical forces by the energy input in this system. Some of the input strain energy is absorbed and stored by the elastic readjustment of rock mass and some will be released as a seismic energy. The implication of his is that the large volume one injects, the more strain energy is imposed on the rock mass and thus increasing the possibility of larger events.

On the other hand it has to be recognized that critically oriented joints require significantly less pressure or the reduction of friction to slip and fail. Joints are held in place by the friction of the asperities and the use of chemicals to improve permeability may be counterproductive if the friction coefficient is reduced, etching away the fine undulations and thus reducing the effective aperture required to transport the fluid between the wells. The technique used for improving the near well-bore impedance may have slightly different mechanism as the thermal cooling takes place of the well-bore, it makes it possible for the fluid with acid to access virtually all orientation of joints. The dilated joints do not go very far in the formation and therefore they do not pose any threat to the stability of the aperture.

The understanding and the use microseismicity is a large topic and examples will be presented to demonstrate some of it's use.

Acknowledgement:

The Authors would like to acknowledge all those who have worked in this field over the last 30 years and it to them we thank for our understanding of the technology to date.

The authors would like to thank specifically S.Oates, T.Hettkamp, T.Gandy, R Young, F.Cornet, T.Tischner, A.Beauce, S.Michelet, M.Fehler. R.Jones, J.Garnish, T.Megel, T.Kohl and many others who have provided considerable input to some of the conclusions derived here.

SESSION II :
Case studies on reservoir stimulation

Results of flow-meters measurements in Soultz-sous-Forêts well GPK4 and implication for mechanisms of fracturing processes in crystalline rocks

JUNG Reinhard, BGR, Hannover, Germany, r.jung@bgr.de

No Contribution available.

ENGINE – **EN**hanced **G**eothermal **I**nnovative **N**etwork for **E**urope
Workshop 3, "Stimulation of reservoir and induced microseismicity"
Kartause Ittingen, Zürich, June 29 – July 1, 2006, Switzerland

Microseismicity and stimulation strategy: the case of Soultz-sous-Forêts, France

CHARLéTY Jean, EOST, Strasbourg, France, Jean.Charlety@eost.u-strasbg.fr
DORBATH Louis, IRD-LMTG, Strasbourg, France

Abstract

After a basic presentation of the definition of an earthquake we present the induced seismicity at the geothermal site of Soultz-sous-Forêts for the four stimulations carried out since 2000. The aim of this presentation is to clarify some particular and important characteristics that rule the seismicity. These characteristics are the fact that an earthquake is the motion of one block against another due to local stress variation. Therefore the exact representation of an earthquake is not a point but a plane with particular dimension and orientation. Furthermore the seismicity obey some power-law distribution such as the Gutenberg-Richter. From this law it can be shown that the area follows the same power-law distribution. It is also noted that microearthquakes are ruled by the same physic laws and so the induced seismicity. Therefore a lot of information can be inferred from the results hereafter shown.

Introduction

The aim of this article is to give an clear insight on the seismicity and tends to give a simple definition of the word earthquake. To achieve this purpose, we present some global idea about the seismicity theoretically and in the nowadays conceptual view. Then, we present the case of Soultz-sous-Forêts. Does the induced seismicity follow the general law of the seismology? Is it different and what kind of information can we infer from it?

Theory

This part is highly inspired by the article of Udías (2002).

Shear Dislocation

If an earthquake is produced by a fracture, a mechanical representation of its source can be given in terms of fractures or dislocations in an elastic medium. The theory of elastic dislocation was developed by Volterra in 1907. A displacement dislocation consists of an internal surface inside an elastic medium across which there exists a discontinuity of displacement but stress is continuous. The focal region consists in an internal surface Σ with two sides (positives and negatives). This surface can be considered as derived from a certain volume V_0 that is flattened to form a surface with both side stuck together without any volume. Coordinates on this surface are ξ_k and the normal at each point $n_i(\xi_k)$. From one side to the other of this surface there is a discontinuity in displacement or slip

$$u_i^p(\xi_k,t) - u_i^m(\xi_k,t) = \Delta u_i(\xi_k,t) \quad (1)$$

where the supscript p (plus) and m (minus) refer to the displacement at each side of the surface Σ. If there are no body forces and if the stresses are continuous through Σ (their integral is null) for an infinite medium, the displacement at a given point distant from the dislocation, say at the location of the observer, the recorded displacement can be written as

$$u_n(x_s,t) = \int_{-\infty}^{\infty} d\tau \int_{\Sigma} u_i(\xi_s,\tau) C_{ijkl}(\xi_s) G_{nk,l}(x_s,t;\xi_s,\tau) dS \quad (2)$$

From this formulation it can be seen that the seismic source is represented by a dislocation or discontinuity in displacement given by the slip vector Δu on the surface Σ, which corresponds to the relative displacement between the two sides of a fault. This is a nonelastic displacement that, once produced, does not go back to the initial position. In a general sense for each position on the surface, the normal to the surface Σ can vary and so the displacement discontinuity. Usually, the normal to the surface $\mathbf{n}(\xi_k)$ is constant meaning that the surface Σ is a plane. Green's function G includes the propagation effects of the medium from points (ξ_k) of surface Σ to point (x_k) where the elastic displacements u_i are evaluated.

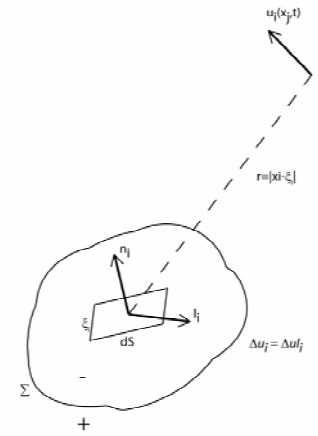

Figure 3 Representation of a shear dislocation. (From Udías, 1999)

Let us consider the seismic source represented by a shear dislocation fracture, with fault plane Σ of area S and normal **n**, slip $\Delta\mathbf{u}(\xi_i,t)$ in the direction of unit vector **l**, not necessarily contained on the plane. For an infinite homogeneous isotropic medium, displacement according to the previous formulation is

$$u_k = \int_{-\infty}^{\infty} d\tau \int_{\Sigma} \mu \Delta u \left(l_i n_j + l_j n_i\right) G_{ki,l}\, dS \quad (3)$$

If the distance from observation point to the source is long in comparison with the source dimension ($r >> \Sigma$) and the wavelengths are also long ($\lambda >> \Sigma$), the problem can be approximated by a point source whose displacement can be written as:

$$u_k = \mu S \left(l_i n_j + l_j n_i\right) \int_{-\infty}^{\infty} \Delta u(\tau) G_{ki,l}(t-\tau) d\tau \quad (4)$$

Displacements are given by temporal convolution of slip with the derivatives of the Green function. The geometry of the source is now defined by the orientation of the two unit vectors **n** and **l**, respectively the orientation of the fault plane and that of slip. The slip discontinuity can be decomposed in a constant part $\Delta \dot{u}$, the slip rate, and a time varying term, the source time function, STF. Introducing this formulation allows to define the scalar seismic moment $M_0 = \mu \bar{u} S$.

Seismic Moment Tensor

We can define the moment tensor density corresponding to a dislocation with slip Δu on a surface Σ of normal **n**:

$$m_{ij} = C_{ijkl} \Delta u_k n_l \quad (5)$$

where C_{ijkl} is the four order tensor of elastic coefficient, Δu_k the slip vector, and n_l the normal to the fault plane.

For an isotropic medium, if the slip direction is given by unit vector **l**, we obtain

$$m_{ij} = \Delta u[\lambda\, l_k n_k \delta_{ij} + \mu(l_i n_j + l_j n_i)] \quad (6)$$

where λ and μ are the Lamé's parameters. The tensor can be decomposed in an isotropic and a deviatoric part. The first one describes the volume change. If **l** and **n** are perpendicular, this term is zero and the source represents a shear fracture. With the moment tensor we can represent various types of sources.

Focal mechanism

Equation 3 and 4 show that the seismograms recorded at various distances and azimuths can be used to study the geometry of faulting during an earthquake. This is known as the focal mechanism. This operation uses the fact that the pattern of radiated seismic waves depends on the fault geometry. The main and simplest method relies on the first motion, or polarity, of body waves.

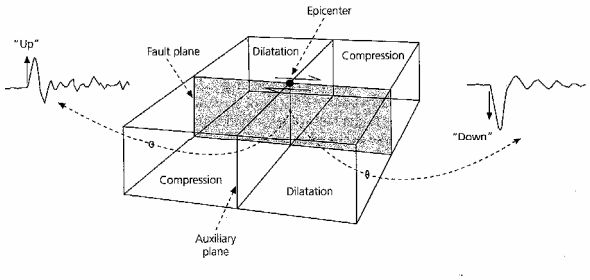

Figure 4 First motions of P waves observed at seismometers located in various directions about the earthquake provide information about the fault orientation. The two nodal planes separate regions of compressional and dilatational first arrivals (from Stein and Wysession, 2003).

The basic idea is that the polarity (direction) of the first P-wave arrival varies between seismic stations at different directions from an earthquake. These first motions define four quadrants, two compressional and two dilatational. The division between quadrants occurs along the fault plane and a plane perpendicular to it. In these directions, because the first motion changes from dilation to compression, seismograms show small or zero first motion. These perpendicular planes, called nodal planes, separate the compressional and dilatational quadrants. If these planes can be found, the fault geometry is known. However from equation 6, it is obvious that **l** and **n** can be interchanged. Therefore, from the focal mechanism the fault plane cannot be determined uniquely.

Discussion

Fault definition and reservoir

The theory presented here points out the fact that an earthquake is, by definition, the motion of a

plane against another. This definition implies that the exact representation of an earthquake is not a point but a plane with a particular orientation (strike and dip) and dimension. Even if the theory considers that the source is a point inasmuch as the distance of observation is much longer than the fault dimensions, this argumentation may be fallacious in the sense that for the size of the reservoir the dimensions of the fault can be important.

Fault dimension

The surface involved by the fault motion can be known by the way of the scalar seismic moment $M_{0,}$ which is, actually, the product of the area of the fracture, S, by the mean over the area of the fracture of the amount of displacement caused by the earthquake, Δu, and by the shear modulus, μ. Dimensional considerations (Kostrov, 1974) show that Δu is proportional to the stress $\Delta\sigma = (\overline{\sigma}^0 - \overline{\sigma}^1)$ removed as a result of the earthquake from the fracture surface (the stress drop), and is also proportional to the linear dimension of the fracture, for which a natural approximation is the square root of the area:

$$\overline{u} = c\frac{\Delta\sigma}{\mu}S^{1/2} \quad (7)$$

hence, the scalar seismic moment can also be written

$$M_0 = c\Delta\sigma\, S^{3/2} \quad (8)$$

where c is a constant.

Fault geometry

The information about the fault geometry is obtained by the focal mechanism but, unfortunately, the nodal planes cannot be distinguished from one another. The focal mechanism represents directly the geometry of the fault and of the slip, *i.e.* if the slip vector is contained in the fault or not. In the case that the slip vector is not contained on the fault plane, the distribution in four quadrants of the focal mechanism is not conserved. Thus this particular aspect of the focal mechanism is important to draw the existence of a mode I (opening of the fracture).

Cause of faulting

The occurrence of an earthquake depends mainly on the variation of the stress condition either in the surrounding of the plane of weakness (fracture, fault), or in the medium considering the creation of fracture. This variation can be of several kinds from the variation of the pore pressure to the variation of the stress itself because of stress concentration due to asperity, difference of material, etc. An earthquake is, actually, the response of the medium to the deformation undergone. When this deformation is higher than its strength, the medium fails and generates an earthquake. However the strength of the medium varies with different parameters such as strain rate, and chemical constitution (Scholz, 1990). Scholz (1990) also points out that the effect of water, ubiquitously present in the lithosphere, can generate chemical reaction that must control the strength of rock in the earth. This particular feature may be taken into account for geothermal reservoir behaviour. For this, the characteristic time of chemical reaction between water and contituant (calcite, ilite, ...) must be known.

Earthquake size and complexity

Size and Self similarity

One of the main problem encountered in seismology consists in the understanding of the nucleation of earthquake. From a prediction point of view as from a theoretical one, this question remains open. There are two opposing views as to what controls the size of an earthquake (Steacy and McCloskey,1998): either the size is determined at the outset of instability by the size of the nucleation zone (Ohnaka 1992; Ellsworth and Beroza 1995; Beroza and Ellsworth 1996) or there is no difference between the nucleation process of small and large earthquakes and a large event is simply a small one which expands as the result of chance interactions between rupture-front stresses and local variations in fault strength (Abercrombie and Mori 1994; Mori and Abercrombie 1997). For the first assumption, two models are proposed. In the 'cascade' model, earthquake ruptures involve a hierarchy of subevent sizes and the breakaway phase is generated by the first large slip event. In the 'pre-slip' model, the nucleation is generated when an area that is slipping aseismically accelerates to the dynamic rupture velocity; the size of the final earthquake is determined by the size of this slipping patch. For the second assumption, they have found no systematic differences in the initiation of large and small events.

Several studies have discussed the relation between the size of the rupture area and the value of the scalar seismic moment, M_0. From this plot, for example Abercrombie (1995, figure 11) or Stork and Ito (2001), a trend is obvious between both parameters. The expression established earlier linking M_0 and a characteristic length, $S^{1/2}$, states that if a trend exists it means that the stress drop is approximately constant and independent of earthquake size. This observation is the most powerful argument for the self-similarity of earthquakes.

Complexity

The question that arises from the discussion of the size of an earthquake concerns the complexity of a micro-earthquake. Sato and Mori (2006) or Singh et al. (1998) have shown that the rupture involved for a micro-earthquake can be as complex as for a larger one. The difference comes from the attenuation of the medium that tends to cut off higher frequency.

Power-law scaling

An alternative approach to earthquake mechanics is to assume that the crust is a complex self-organizing system that can be treated by techniques developed in statistical physics. The basic hypothesis is that deformation processes interact on a range of scales from thousands of kilometres to millimetres or less. Evidence in support of this hypothesis comes from the universal validity of scaling relations. The most famous of these is the Gutenberg-Richter frequency-magnitude relation:

$$\log\left(\dot{N}_{CE}\right) = -bm + \log(a) \quad (9)$$

where $\dot{N}_{CE}$ is the cumulative number of earthquakes with magnitude greater than m occuring in a specified area and time, and b and a are constants. b is called the b-value and ranges commonly from 0.8 to 1.2. Mandelbrot (1982), Turcotte (1997) have explored the idea that complex phenomena often exhibit fractal (power-law) scaling in magnitude, space and time. For earthquakes, fractal scaling of their magnitudes imply the validity of the relation:

$$\dot{N}_{CE} = CA_E^{-D/2} \quad (10)$$

where $\dot{N}_{CE}$ is the cumulative number of earthquakes with rupture area greater than A_E occurring in a specified area and time; C and D are constants, with D the fractal dimension. Aki (1981) showed that D is equivalent to 2b. The universal applicability of the Gutenberg-Richter relation implies that the number of earthquakes scales with their rupture area according to power-law (fractal) scaling.

This power-law shows that the microearthquakes are in much more number than the greatest ones. However from the definition of the scalar seismic moment the role of the small events contributes neither to seismic moment sums nor to long-term displacement rates along active faults. Consequently the deformation undergone by the medium tectonically or not is only accommodated by the largest events. The smaller earthquakes redistribute the forces that exist along active faults, including plate boundary (Hanks, 1992). The smaller earthquakes are just as important as larger ones in redistributing the driving forces along active faults.

Seismogenic failure is a self-similar, scale invariant process with a natural area scaling for frequency of occurrence would seem to be a straightforward consequence of stochastically well behaved heterogeneity within the Earth and of the brittle failure process.

The Case of Soultz-sous-Forêts

Self-similarity condition

From several years it has been argued that the seismicity in Soultz-sous-Forêts has a particular behaviour in terms of source mechanics. Results, summarized in Michelet et al. (2004), from the automatic study of the spectral contains of displacement recorded by the downhole seismological stations show that the invariant is not the stress drop but the source dimension. Therefore the largest scalar seismic moment are due to large stress drop and not large surface of rupture. This particular point differs from several other observations and contradicts several studies for such a range of magnitude (Abercrombie 1995; Hough *et al.* 1999; Jost *et al.* 1998). The same study from the surface seismological network has been performed to confirm this point. Since it takes place at the top of the granite, it is obvious that the data from the downhole seismological network has not been filtered by the 1.4 km of sediment. Nevertheless, if the energy of the seismic signal is much greater than the energy of the noise signal, the filter effect can be corrected by the estimation of the attenuation factor (Q).

The constant-stress-drop scaling relation has been confirmed by an overwhelming number of studies and has become an accepted model for small to large earthquakes (Kanamori and Anderson 1975; Pearson 1982; Gibowicz and Kijko 1994). Evidence for constant-stress-drop scaling was also shown by Abercrombie (1995) based on observations of $-1 < M_l < 5.5$ events with hypocentral distances from 5 to 120 km in the Cajon pass scientific drill hole at 2.5 km depth in granite. Constant stress drop implies a self-similar rupture process independent of size, and seismic moment M_0 proportional to the cube of the source radius after Brune (1970, 1971). More recently, Prejean and Ellsworth (2002) used data from a 2 km deep borehole in Long-Valley caldera, California, to determine the stress drop and apparent stress of earthquakes from M_w 0.5 to 5.0 and reached similar conclusions. In contrast, a marked decrease of stress drop with decreasing seismic moment (breakdown in self similarity) has been reported by some authors for small

earthquakes with seismic moment below 10^{13} Nm (Chouet *et al.* 1978; Fletcher *et al.* 1986, Dysart *et al.* 1988; Gibowicz and Kijko 1994). However other authors considering the same range, or even lower, of seismic moment have shown that there is no breakdown in self similarity (Gibowicz 1995). Constant source radii with magnitude seismic moment indicates a strong dependence of stress drop on seismic moment.

Spectral analysis

Data

The main problem for that kind of study comes from the sensor and from the acquisition chain involved for the recording of the data. The transfer function of the whole chain has to be perfectly known. For this purpose, we have chosen to use only the data from a velocimeter CMG-3T manufactured and calibrated by Güralp. This device has a constant response for the frequencies of interest, say from 1 to 90Hz. The sampling rate is 200 points per second. Considering the work of Abercrombie (1995), from the range of magnitude, M_l, 0-3, the corner frequencies range from some hertz for the larger microearthquake to hundreds of hertz for the smallest. Consequently the Güralp velocimeter is the more appropriate device of the surface network. In this study we have analysed the frequency spectra of the data for 15 microearthquakes randomly chosen in the whole seismic catalog of 2000 and 2005. We have nevertheless taken records with a good signal to noise ratio and chosen the events in order to cover a large part of the magnitude range. The signals used are only S waves because they have a higher signal energy than the P waves.

Method

We have followed the methodology defined by Abercrombie (1995). The length of the time window used is dependent on the earthquake magnitude since larger events have longer source durations. Around 0.2-0.3 second windows are used for the smallest events and 0.5 second windows for the largest events. The processing has been performed with sac (Goldstein and Minner, 1996). The signal has been integrated once in the time domain and then Fourier transformed. The Q value is estimated in order to have a decay at high frequency in ω^{-2}. The value of Q is about 250. This value corresponds to the geometrical average along the ray path taking a common value for Q of 500 in the granite and an extreme value of 50 in the 1.4 km of sediment. Then the estimation of the corner frequency has been visually determined.

Result

The source parameters, seismic moment and source radius, are calculated from the long period amplitude and the corner frequency. The relations used are those described in Abercrombie [9] with the following value of parameters: density 2700 kg .m^{-3}, v_s 3400 ms^{-1}. The hypocentral distance is set to 5500 m for all the events.

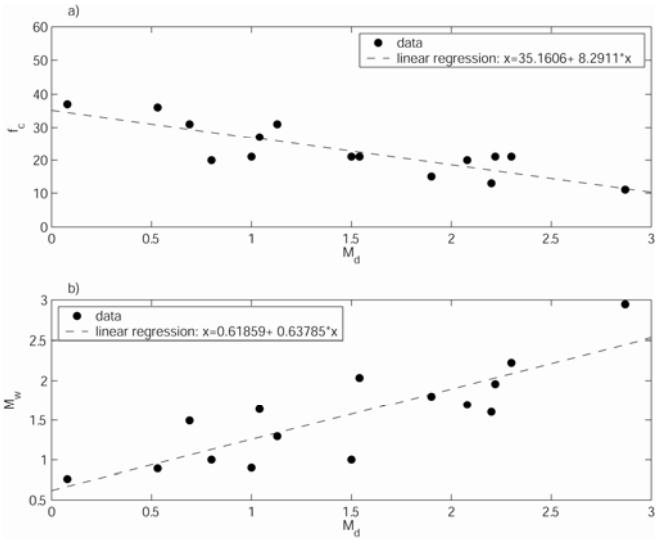

Figure 5 a) S wave corner frequency as a function of duration magnitude. b) Moment magnitude as a function of duration magnitude

The seismic moments range from 10^{10} to 10^{14}, corresponding to M_w 0.7 to 2.9. We can derive the relationship between the duration magnitude, M_d, and the moment magnitude, M_W. The relation is written in the figure 3b. The duration magnitude is determined with the length of the coda. The figure 3a shows the corner frequency values obtained as a function of M_d. Figure 4 shows seismic moment and source radius for the 15 microearthquakes studied. The results are consistent with a constant stress drop. Even if the precision of the determination of the different parameters are not optimal, the results give a good idea of the process. The results can be directly compared with the results of Abercrombie (1995), Prejean and Ellsworth (2002) and Stork and Ito (2004) for that range of moments and source radii. Our results, which can appear scatter but are included in the cloud of the others studies, and these studies do not show any breakdown in self similarity. Therefore the microearthquakes, based on the data from the seismological surface network, can be considered as following the commonly used seismological laws in terms of physical properties of the faulting mechanic.

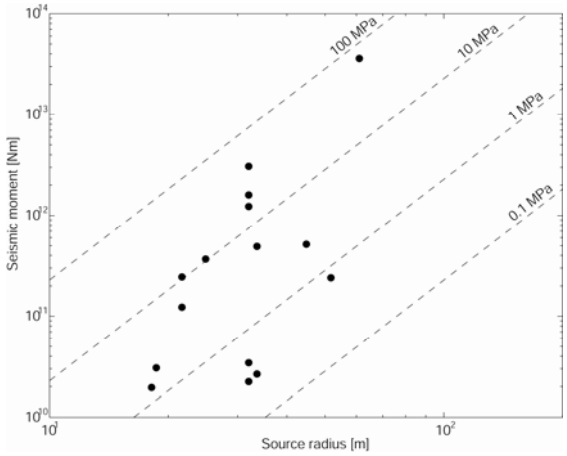

Figure 6 Seismic moment and source radius. The dashed lines are calculated from equation 4 of Abercrombie (1995) and are from 0.1 to 100 MPa

Empirical Green's function

A recorded seismogram is the result of the temporal convolution of three different operators: the Green's function, which includes the propagation effect of the medium from the source to the receiver, the source time function (STF), whose time duration is proportional to the length of the rupture and a third operator allowing to take into account the site effect and the sensor response.

Considering that the third operator is invariant, a much smaller earthquake located near the larger one and recorded by the same seismological station can be considered as a Green's function inasmuch as its STF can be approximated as a dirac. Therefore the STF can be computed from the deconvolution of the larger event by the smaller.

This method has been used in order to retrieve and confirm the results of the spectral analysis (figure 4). The maximum distance between both events is less than 100 metres and the difference in magnitude is more than 1. Assuming a rupture velocity of 3 $km.s^{-1}$, the lower bound estimate of the rupture length is computed from the time duration of the retrieved STF. This result and the one given by the spectral analyses are similar (table1).

Table 1: Comparison between the rupture length of three events for both methods.

Event	***L (spectral analysis)***	***L (STF)***	***magnitude***
2 juin 2003 21h29	r=49 m d=98 m	153 m	2,5
10 juin 2003 19h32	r=50 m d=100 m	125 m	2,4
10 juin 2003 19h32	r=97 m d=194 m	203 m	2,9

Gutenberg-Richter

The second argument for the fact that the seismicity induced by hydraulic stimulation is ruled by the self-similarity law consists in the build-up of the Gutenberg Richter law for each stimulation (figure 5). Even though the b value is high ranging from 1 to 1.2, the cumulative number of earthquake follows the power-law distribution.

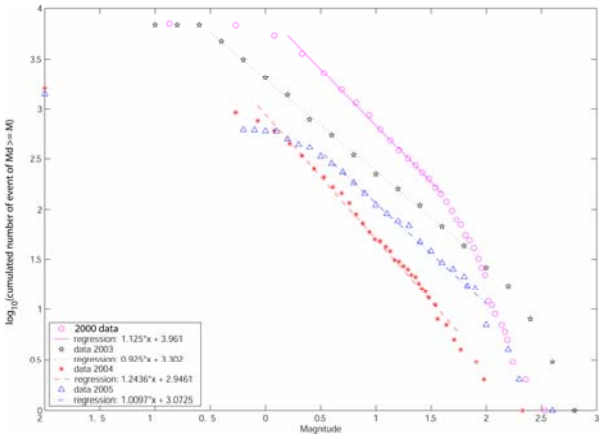

Figure 7 Gutenberg Richter law for the 4 stimulations.

Seismicity

From the spectral analysis results and the linear relationship between the duration magnitude and the moment magnitude, the scalar seismic moment can be estimated and thus the area of each event (equation 8). These estimations rely on an extrapolation of the results found earlier and must not be overemphasized. Nevertheless, they tend to show some important trend and behaviour.

First the smaller earthquakes do not contribute in the moment sum (figure 6) and only play a role in redistributing the driving forces since the self-similarity of the seismicity is valid and thus the considerations of Hank (1992) about the role of the small earthquakes. In figure 6, the example is taken from the 2003 experiment but it is the same for the other stimulations.

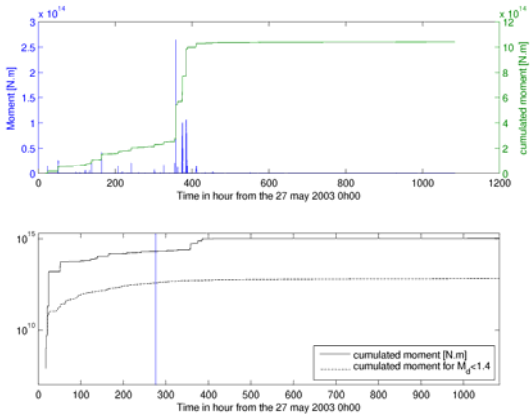

Figure 8 Top: in blue is represented the moment versus time of each event. In green, is represented the cumulated moment on the whole period of time. Bottom: effect of the largest earthquakes on the cumulated sum. Around two orders of magnitude exist between them. Example with the data of 2003.

From the estimation of the characteristic length of the fractures, a distribution law can be drawn. The constant c has been estimated in order to calibrate the size with those determined by the spectral analysis. Figure 7 shows that equation 10 is valid with a value of D of 1.2. This value for the stimulation of the year 2003 is higher than the one obtained from the Gutenberg-Richter but is based on some approximate relationships. In figure 7, the example is taken from the 2003 experiment but it is the same for the other stimulations.

Figure 6 shows clearly that the deformation undergone by the reservoir is mainly compensated by the largest earthquakes. Therefore this seismicity is of great importance for the understanding of the reservoir behaviour.

Figure 8 shows the distribution of this seismicity in the reservoir and tend to indicate a non random distribution of their location. Charléty *et al.* (in submission) shows that this seismicity put the shed on large features that likely rule the large scale circulation of the fluid. This seismicity represents the events with a magnitude higher than 1.4, *i.e.* with a source dimension of about 40 metres.

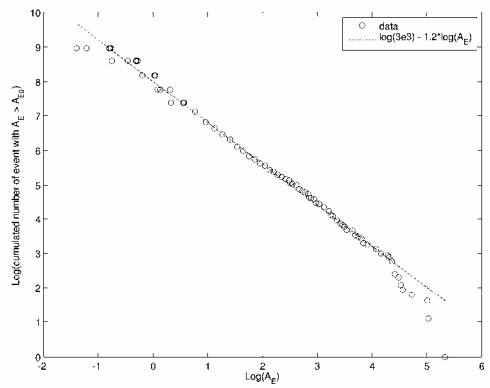

Figure 9 Implication of the Gutenberg-Richter relation meaning that the number of earthquakes scales with their area according to power-law scaling. Example on the data of 2003.

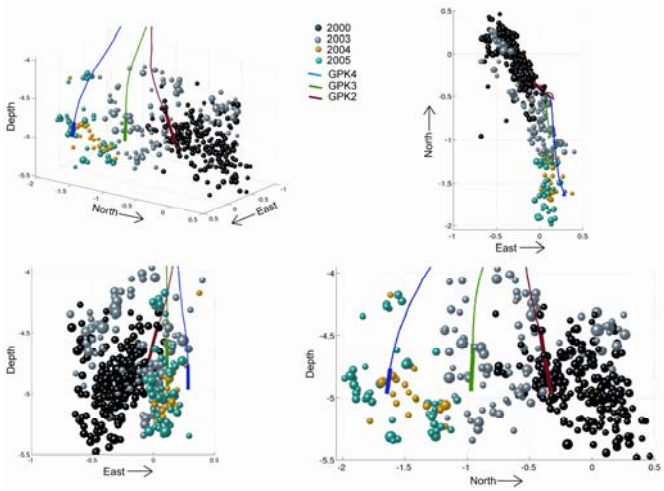

Figure 10 Largest events for the 4 stimulations performed on the deep reservoir at Soultz-sous-Forêts.

Focal mechanism

The focal mechanism of the events of magnitude larger than 1.4 is systematically determined from the P-wave polarities with the assumption of a double couple (quadrantal distribution of the polarities). Up to now, we have been able to determine such a mechanism for each event. This means that this earthquake mechanics is predominant but it does not mean that another one is not conceivable. Figure 9 shows some focal mechanisms for the stimulation of 2004 and for the events of magnitude greater than or equal to 1.4.

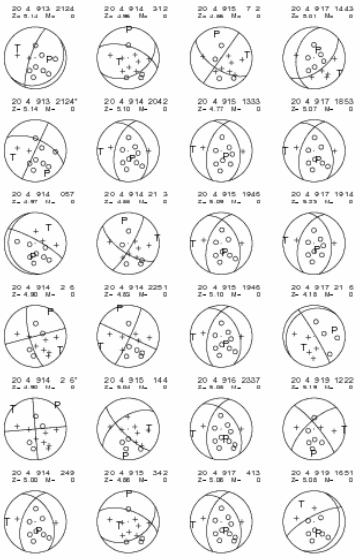

Figure 11 Focal mechanisms of the 2004 stimulation of GPK4

Conclusion

After a basic presentation of the definition of an earthquake we present the induced seismicity at the geothermal site of Soultz-sous-Forêts for the four stimulations carried out since 2000. This presentation wants to clarify some particular and important characteristics that rule the seismicity. These characteristics are the fact that an earthquake is the motion of one block against another due to local stress variation. Therefore, the exact representation of an earthquake is not a point but a plane with particular dimension and orientation. Furthermore, the seismicity obey some power-law distribution such as the Gutenberg-Richter. From this law it can be shown that the area follows the same power-law distribution. It is also noted that microearthquakes are ruled by the same physic laws and so the induced seismicity. Therefore, a lot of information can be inferred from the results shown.

References

Abercrombie, RE., (1995), "Earthquake source scaling relationships from -1 to 5 M_L using seismograms recorded at 2.5 km depth", *J. geophys. Res.*, **100**, 24015-24036.

Abercrombie, R, Mori, J., (1994), "Local observation of the onset of a large earthquake: 28 june 1992 Landers, California", *Bull. Seism. Soc. Am*, **84**, 725-734.

Aki, K., (1981), "A probabilistic synthesis of precursory phenomena.", in "Earthquake prediction" (D.W. Simpson and P.C. Richards, Eds), pp 566-574, American Geophysical Union, Washington DC.

Beroza, GC, Ellsworth, WL, (1996), "Properties of the seismic nucleation phase", *Tectonophysics*, **261**, 209-227.

Brune, J.N., (1970), "Tectonic stress and the spectra of seismic shear waves from earthquakes.", *J Geophys Res.*, **75**, 4997-5009.

Brune, J.N., (1971), "Correction", *J Geophys Res.*, **76**, 5002.

Charléty, J., Cuenot, N., Dorbath, L., Dorbath, C., Haessler, H., Frogneux, M., "Larger earthquakes occured during the hydraulic stimulation of wells GPK2-3-4 at the geothermal site of Soultz-sous-Forêts.", *submitted* to International Journal of rock mechanics.

Chouet, B., Aki, K., Tsujiura, M., (1978), "Regional variations of the scaling law of earthquake source spectra.", *Bull. Seis. Soc. Am.*, **68**, 49-79.

Dysart, P.S., Snoke, J.A., Sacks, I.S., (1988), "Source parameters and scaling relations for small earthquakes in the Matsushiro region, southwest Honshu, Japan.", *Bull. Seis. Soc. Am.*, **78**, 571-589.

Ellsworth, WL, Beroza, GC, (1995), "Seismic evidence for an earthquake nucleation phase", *Science*, **268**,851-855.

Fletcher, J.B., Haar, L.C., Vernon, F.L., Brune, J.N., Hanks, T.C., Berger, J., (1986), "The effects of attenuation on the scaling of source parameters for earthquakes at Anza, California.", In *Earthquake Source Mechanics*, Das, S., Boatwright, J. and Scholz, C.H. (Editors), Am. Geophys. Union Monograph, **6**, 331-338.

Gibowicz, S.J. and Kijko, A. (1994), "An introduction to mining seismology, *Academic Press*, San Diego.

Gibowicz, S.J., (1995), "Sacling realtions for seismic events induced by mining", *PAGEOPH*, **114**.

Goldstein, P. and Minner, L., (1996), "SAC2000: seismic signal processing and analysis tools for the 21st century." *Seis. Res. Let.*, **67**, 39.

Hank, TC, "Small earthquake, tectonic forces", *Science*, **256**, 1430-1432.

Hough, S. E., Lees, J.M., Monastero, F., (1999), "Attenuation and source properties at the Coso Geothermal Area, California". *Bull. Seis. Soc. Am.*, **89**, 1606-1619.

Jost, M.L., Büßelberg, T., Jost, Ö., Harjes, H.-P., (1998), "Source parameters of Injection-Induced Microearthquakes at 9 km depth at the KTB deep drilling site, Germany.", *Bull. Seis. Soc. Am.*, **88**, 815-832.

Kanamori, H. and Anderson, D.L., (1975), "Theoretical basis of some empirical relations in seismology.", *Bull. Seis. Soc. Am.*, **65**, 1073-1095.

Kostrov, VV, (1974), “Seismic moment and energy of earthquakes, and seismic flow of rock”, *Izv. Earth Physics*, **1**, 23-40.

Mandelbrot, BB, (1982), “The fractal geometry of nature”, W.H. Freeman, New York.

Michelet, S., Baria, R., Baumgaertner, J., Gérard, A., Oates, S., Hettkamp, T., Teza, D., (2004) “Seismic source parameter evaluation and its importance in the development of an HDR/EGS system”. In *29th Stanford Workshop on Geothermal Reservoir Engineering*. Stanford University, Stanford, California.

Mori, J., Abercrombie, R., (1997), “Depth dependence of earthquake magnitude-frequency distributions in California: implication for rupture initiation.”, *J. geophys. Res.*, **102**, 15081-15090.

Ohnaka, M., (1992), “Earthquake source nucleation: a physical model for short-term precursors”, *Tectonophysics*, **211**, 149-178.

Pearson, C., (1982), “Parameters and a magnitude moment relationship from small earthquakes observed during hydraulic fracturing experiment in crystalline rock.”, *Geophys. Res. Lett.*, **9**, 404-407.

Prejean, S.G. and Ellsworth, W.L., (2002), “Observations of earthquake source parameters at 2 km depth in the Long Valley Caldera, eastern California.”, *Bull. Seis. Soc. Am.*, **91**, 165-177.

Sato, K., Mori, J., (2006), “Relationship between rupture process complexity and earthquake size.”, *J. geophys. Res.*, **111**, B05307, doi:10.1029/2005JB003614.

Scholz, C.H., (1990), “ The mechanics of earthquakes and faulting”, Cambridge University Press, Cambridge.

Singh, SK, Ordaz, M., Mikumo, T., Pacheco, J., Valdés, C., Mandal, P., (1998), “Implicatins of composie source model and seismic-wave attenuation for the observed simplicity of small earthquakes of reported duration of earthquake initiation phase.”, *Bull. Seism. Soc. Am*, **88 (5)**, 1171-1181.

Steacy, SJ, McCloskey, J., (1998), “What controls an earthquake’s size? Results from a heterogeneous cellular automaton”, *Geophys. J. Int.*, **133**, F11-F14.

Stein, S., Wysession, M., (2003), “Ian introduction to seismology, earthquakes and earth structure.”, Blackwell Publishing, Oxford (U.K.).

Stork, L. and Ito, H., (2004), “Source parameter scaling for small earthquakes observed at the western Nagano 800-m-deep borehole, central Japan.”, *Bull. Seis. Soc. Am.*, **94**, 1781-1794.

Turcotte, D.L., (1997), “Fractal and chaos in geology and geophysics”, 2nd ed. Cambridge University Press, Cambridge.

Udías, A. (2002), “Theoretical seismology: an introduction”, in International handbook of earthquake and engineering seismology, edited by Lee, WHK, Kanamori, H., Jennings, PC, Kisslinger, C., Academic Press.

Control of induced seismic hazard associated with the hydraulic stimulation of a hot fractured rock geothermal reservoir

OATES, Steve ,Shell, Rijswijk, Netherlands, steve.oates@shell.com
BOMMER, Julian, Imperial College, London
CEPEDA, Jose Mauricio, Universidad Centroamericana, El Salvador)
LINDHOLM, Conrad, NORSAR, Norway
BIRD, Juliette, Imperial College, London
TORRES, Rodolfo, LaGeo, El Salvador
MARROQUIN , Griselda , Servicio Nacional de Estudios Territoriales, El Salvador
RIVAS José,LaGeo, El Salvador

In 2003 hydraulic stimulations were carried out in El Salvador's Berlin geothermal field as part of a project to explore the feasibility of commercial hot fractured rock energy generation. A key requisite was that the induced seismicity associated with the reservoir stimulation at depths of 1–2 km should not produce levels of ground shaking at the surface that would present a threat or serious disturbance to those living in and around the field. A pump control system - which we refer to as the traffic light system - was implemented which utilised real time seismic monitoring data and ground motion estimates calibrated using accelerograph measurements. Thresholds of tolerable ground motion were inferred from guidelines and regulations on tolerable levels of vibration and from correlations between instrumental strong-motion parameters and intensity, considering the vulnerability of the exposed housing stock. These thresholds were defined in terms of peak ground velocity (PGV) and incorporated into the traffic light system through locally derived predictive equations for PGV in terms of event magnitude. The system also took into account the frequency of occurrence of the induced earthquakes. During the stimulation activities we encountered a much lower level of induced seismicity than anticipated such that the boundaries of the traffic light system were not tested but we argue that an approach such as this is a viable method for ensuring that hydraulic stimulation is conducted in an environmentally responsible manner. The major shortcoming of this type of approach is that it does not address the issue of seismicity occurring after the end of the pumping operation. This presentation is based on the material reported in the paper "Control of hazard due to seismicity induced by a hot fractured rock geothermal project", by Julian J. Bommer, Stephen Oates, Jose Mauricio Cepeda, Conrad Lindholm, Juliet Bird, Rodolfo Torres, Griselda Marroquin and Jose Rivas, which is about to appear in the journal, Engineering Geology.

ENGINE – **EN**hanced **G**eothermal **I**nnovative **N**etwork for **E**urope
Workshop 3, "Stimulation of reservoir and induced microseismicity"
Kartause Ittingen, Zürich, June 29 – July 1, 2006, Switzerland

Detection of flow pathway structure upon pore pressure distribution estimated from hydraulically induced microseismic events and application to the Soultz HDR field

ITO Takatoshi, Institute of Fluid Science, Tohoku University, Japan, ito@ifs.tohoku.ac.jp

Abstract

In the hydraulic stimulation, massive fluid is injected into subsurface rock through drilled wells. Then a number of microseismic events are commonly observed. By analyzing those data of microseismic events, we can estimate the orientation, i.e. dip and strike, of the fracture which slides to induce microseismic event. From the estimated fracture orientation, taking into account the in situ stresses and the Mohr-coulomb criterion to describe the critical condition of fracture sliding, we can estimate the pore pressure at the location of sliding fracture and at the time when the sliding occurs, in other words, when the microseismic event occurs. The estimated values of pore pressure are sorted in a certain manner for each equally divided spatial region, i.e. block or cell, to give spatial distribution of pore pressure and its variation with time during hydraulic stimulation. Furthermore, we have shown that the location of flow pathways and the hydraulic conductivity along them could be estimated from the pore pressure distribution estimated from microseismic events.

Keywords: stimulation, microseismic event, pressure propagation, flow pathway

Introduction

Fracture networks are used for underground heat exchangers, i.e. reservoirs, in the Enhanced Geothermal Systems (EGS). Each fracture composed of the network is spread over a relatively large area of several hundreds square meters, but its aperture is limited to several millimeters at maximum. There is no way to detect directly such a thin structure nor the fluid flow in it from ground surface through a huge rock mass with few thousands meters in thickness, while those factors are important for construction of the EGS. On the other hand, a number of microseismic events are observed during hydraulic stimulation. It is believed that the occurrence of those events is associated with the fluid flow through fracture networks caused by the stimulation. Therefore it may be possible to estimate the fluid flow from the observed micoseismic events. To this end, we have considered the sequence in which hydraulic stimulation leads to the occurrence of microseismic events. Then, based on those consideration, we have come up with an idea to integrate the data of microseismic events for estimating pore pressure propagation along the fracture network associated with hydraulic stimulation (Ito et al., 2004, Osada et al., 2005, Ito et al., 2006). Furthermore, we have shown that the location of flow pathways and the hydraulic conductivity along them could be estimated from the pore pressure distribution estimated from microseismic events. To do this, we assume an appropriate model of flow pathway structure and adjust it as the pore pressure distribution computed by the model agrees well with that estimated from micro-seismic events (Ito et al., 2004). In this paper, those concepts and procedure which have been proposed in our previous works, will be summarized, and the outline of the analyses in which we have applied the proposed method to the Soultz HDR site in France will be presented.

Concept and procedure

Estimation of pressure distribution

Microseismic events are considered to be occurred by the following sequence; hydraulic stimulation drives pressure propagation through fracture network, then the pore pressure in pre-existing fractures is increased, the additional pressure affects to reduce friction between the fracture planes, as a result, shear slipping occurs on the fractures, and finally the slipping generates elastic waves to be observed as the microseismic events.

Friction between fracture planes is given by $\mu(S_n - P_p)$, where μ is the coefficient of friction along the fracture plane, S_n is the normal stress of fracture and P_p is pore pressure in the fracture (**Fig. 1**). The friction decreases with increasing P_p until P_p reaches the critical pore pressure P_c at which the friction decreases to be balanced with the shear stress of fracture, τ, and then shear slipping occurs on the fracture. Such a critical condition is well known as the Coulomb criterion, and is given by

$$|\tau| = \mu(S_n - P_c) \quad (1)$$

The stress components S_n and τ are given as functions of the fracture orientation and the regional state of stress as follows;

$$\tau = \left\{\lambda_1^2\lambda_2^2(S_1 - S_2)^2 + \lambda_2^2\lambda_3^2(S_2 - S_3)^2 + \lambda_3^2\lambda_1^2(S_3 - S_1)^2\right\}^{\frac{1}{2}} \quad (2)$$

$$S_n = \lambda_1^2 S_1 + \lambda_2^2 S_2 + \lambda_3^2 S_3 \quad (3)$$

where S_i (i = 1, 2, 3, $S_1 > S_2 > S_3$) are principal components of the regional stresses, and λ_i (i = 1, 2, 3) are direction cosines between normal to the fracture plane and the axes of S_1, S_2 and S_3 respectively.

On the other hand, the detailed analysis of the microseismic events allows us to detect not only the seismic location but also the dip and strike of the fracture on which shear slipping occurs to cause the microseismic events. Thus if the principal stresses S_i and those orientations are given in another way, the direction cosines λ_i can be determined from the analysis of the microseismic events. In this case, the stresses S_n and τ are to be known from Eqs. (2) and (3), and therefore, the value of P_c can be estimated so as to satisfy Eq. (1) assuming an appropriate value of μ e.g. $\mu = 0.8$. This fact implies that we can estimate the value of pore pressure at the location and time of each microseismic event. This idea has been originally proposed by Cornet and Yin (1995), and recently we have proposed an idea how to integrate the estimated value of P_c for each microseismic event into a spatial distribution of pore pressure induced by hydraulic stimulation (Ito et al., 2004, Osada et al., 2005). To do this, we have introduced the concept of 'block' (or 'cell' in other words). We divide the region of interest into square blocks with the same size as schematically shown in **Fig. 2 (a)**, and we assume that the microseismic events involved in each one of the blocks are induced by the elevated pore pressure brought by a flow pathway passing through the block. When the estimated values of P_c of the microseismic events involved in a block are plotted on the pressure - time diagram, the results may be as illustrated by cross marks in **Fig. 2(b)**. The values of P_c should be equal to or lower than the pore pressure P in the flow pathway passing through the block. It is hard to predict specifically the relationship between P and P_c,

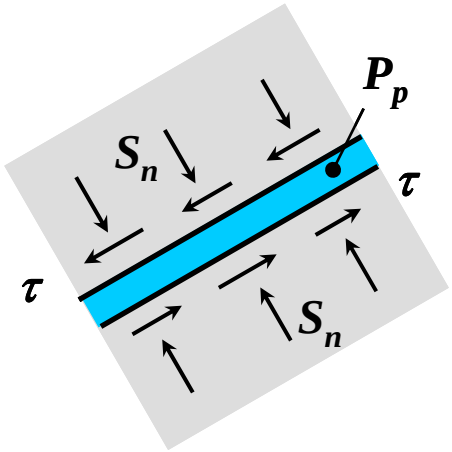

Figure. 1. Fracture subjected to stress and pressure.

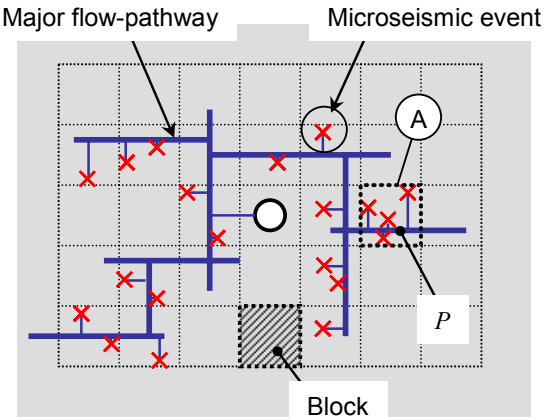

(a)

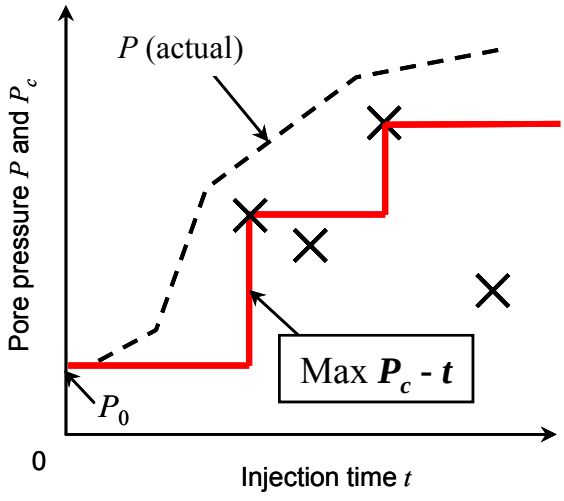

(b)

Figure. 2. (a) Concept of 'block', and (b) the relationship between the pore pressure P in the flow pathway and the critical pore pressure Pc estimated from each one of microseismic events involved in the block 'A' shown in A.

which should be a function of unknown factors such as hydraulic conductivity in the branches connecting the pathway and the fractures in principle. However, it is reasonable to consider that microseismic events associated with larger P_c should occur according to an increase in P. Therefore, when we collect the maximum value of P_c in the past at each time, its variation with time such as the solid line in Fig. 2(b), should have a similar tendency with the actual variation of P such as the dashed line in Fig. 2(b). In this reason, we assume that the dashed line, i.e. the variation of P with time, could be estimated approximately as the solid line in each one of the blocks, and by compiling those results, the regional pressure distribution could be estimated finally. Hereafter we will refer to the relationship shown by the solid line in Fig. 2(b) as the maximum $P_c - t$ relationship for simplicity. The more detailed discussion with this concept is referred to Ito et al. (2004) and Osada et al. (2005).

Estimation of flow pathways

On the other hand, pore pressure distribution should change according to location of flow-pathways and distribution of hydraulic conductivity along them. Therefore, we could estimate flow-pathway structure as it gives a good explanation of the pore pressure distribution estimated from microseismic events. To this end, we assume an appropriate model of flow-pathway structure and adjust it as the pore pressure distribution computed by the model agrees well with that estimated from microseismic events.

Fig. 3(a) illustrates a model of flow-pathway structure for a 2D case. Again we divide the region in concern into square blocks as they are consistent with the blocks used for the estimation of pore pressure distribution from microseismic events (see Fig. 2(a)). We assume hydraulic conductivity between the adjacent blocks, and the conductivity is modeled by a slit-like flow-pathway (**Fig. 3(b)**) which is hereafter referred to the pathway-unit. The pathway-unit is assumed to be located connecting each center of the adjacent blocks, and it has a constant width w everywhere but its height H varies one by one according to the degree of local hydraulic conductivity. There is additional fluid storage connecting with the pathway-unit, which represents fluid volume in the fractures whose one side is open to flow-pathway but the opposite side is closed, and so fluid flow is not expected through them. The storage volume is defined per unit length of the pathway-unit, and is denoted by v_s. This parameter is of course independent of

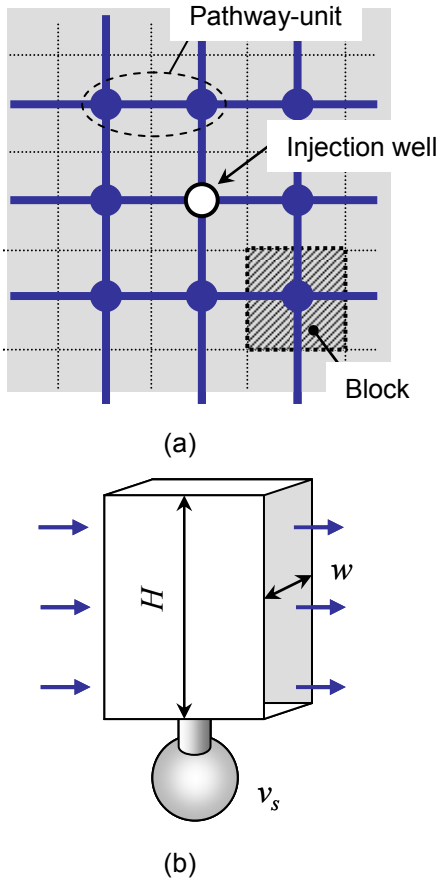

Figure. 3. (a) A 2D model of flow pathway, and (b) structure of the pathway-unit shown in Fig. (a).

hydraulic conductivity, but it is necessary, since such a kind of fluid volume controls the mean velocity of pressure propagation. In the present study, the volume is assumed constant everywhere.

Application to the Soulz HDR site

Pressure distribution

The Soultz project began in 1989 when well GPK1 was drilled to 2000 m, penetrating 400 m into the crystalline granite basement of the Rhine graben. In 1992, the well was extended to a total depth of 3600 m and the casing shoe set at 2850 m, leaving some 750 m open hole. In September, 1993, a major hydraulic stimulation test which is to be the object of the present study, was carried out, and then fresh water was injected into the rock formation through the open hole section of well GPK-1 for a period of 17 days. There are microseismic events of 12,837 in total, whose locations were successfully detected (Jones et al., 1995). We examined the focal mechanism using the P-wave first motion data of those events, and then for a subset of 2,285 events, we succeeded in finding the fault plane solutions as the orientation of fractures on

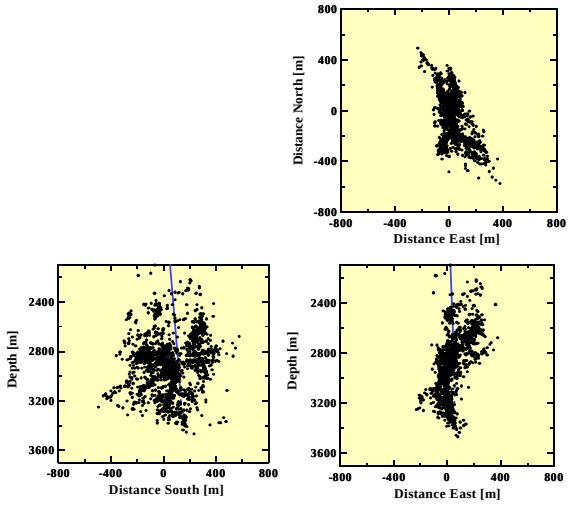

Figure. 4. Location of microseismic events observed during the stimulation of GPK-1 in 1993.

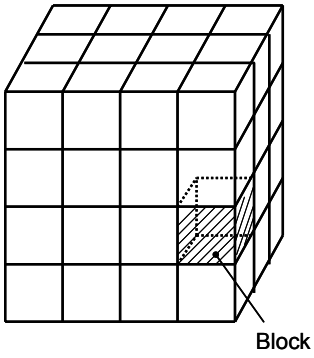

(a)

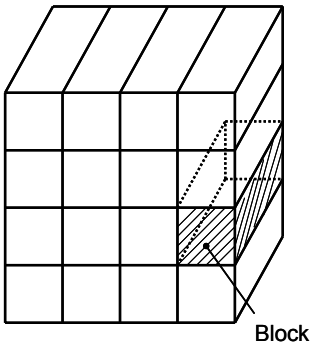

(b)

Figure. 5. Division into the blocks with the shape of (a) cubic and (b) rectangular parallel piped.

which shear sliding occurred to cause the microseismic events (**Fig. 4**). For each one of the fractures whose orientations were determined as the focal plane solution, the critical pore pressure required for the fracture to slide, P_c, was evaluated.

The shape and size of the blocks for the estimation of pore pressure distribution are basically arbitrary as long as they are the

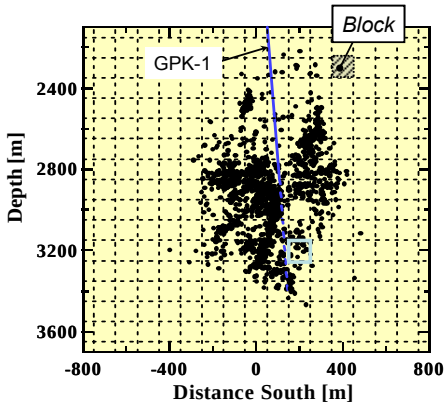

(a)

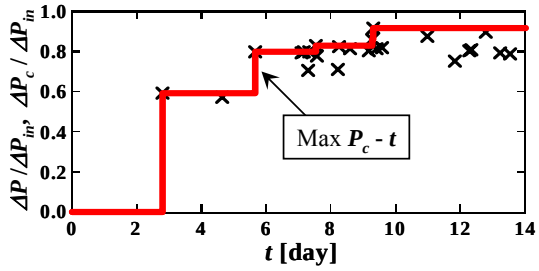

(b)

Figure. 6. (a) Division of the blocks, and (b) estimated pore pressure variation in the block located at the horizontal and vertical positions of "Distance south"=200 m and "Depth" = 3200 m in Fig. (a).

same everywhere (**Fig. 5**). For this analysis we assumed here two-dimensional division of the blocks for simplification so that the block is set to be a rectangular parallelepiped as schematically shown in Fig. 5(b). Taking into account the fact that the microseismic events distributed in the region which is wide in the N-S direction but thin in the E-W direction as can be seen from Fig. 4, the blocks are set to be oriented so that their long side is aligned in the E-W direction. The cross section of the block is 100 x 100 m^2, and the length of the block is such that each one of the microseismic events is involved in one of the blocks. On these arrangements, we estimated the pore pressure variation with time for each one of the blocks. **Fig. 6** shows an example. In the figures, we plotted (ΔP_c /ΔP_{in}) and (ΔP /ΔP_{in}) in ordinate and the elapsed time t in abscissa, where the ΔP_c and ΔP denote (P_c - P_0) and (P - P_0) respectively and P_0 is the initial value of pore pressure, ΔP_{in} denotes (P_{in} - P_{in0}), P_{in} is the well-head pressure at the injection well and P_{in0} is the well-head pressure before the injection is started. The value of ΔP_{in} is here set to be 9 MPa. The cross marks represent the estimated values of the critical pore pressure, P_c, to cause the microseismic events

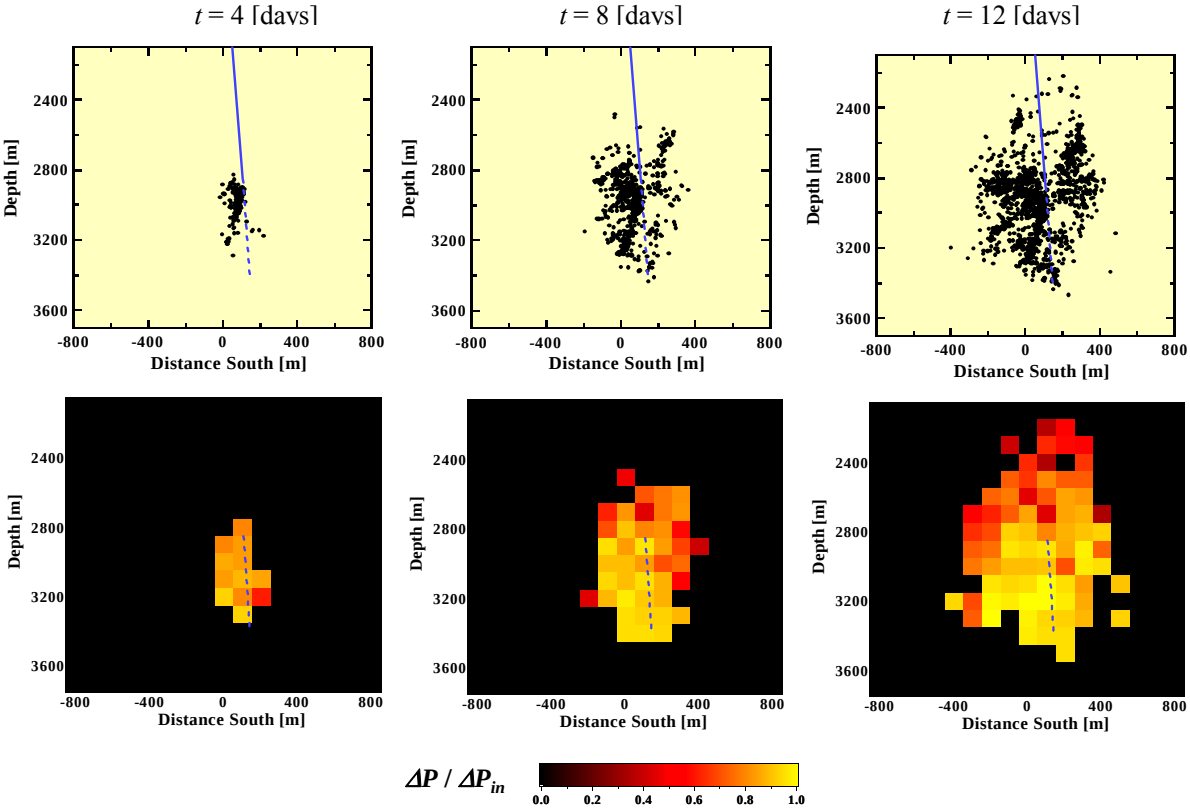

Figure 7. (Top) Locations of microseismic events which occurred until the indicated time, and (bottom) pore pressure distribution estimated from those microseismic events.

involved in the block, and the solid lines represent the P_c-t relationship which is obtained by connecting the maximum value of P_c in the past at each time. The maximum P_c -t relationship should represent approximately the variation of the pore pressure inside the flow pathway at the location of the block. In the same way, we estimated the maximum P_c -t relationship for each one of the blocks where the microseismic events are involved. The results are summarized in the set of figures at the lower side of **Fig. 7**, where those figures show the spatial distribution of the estimated pore pressure at the selected time of t = 4, 8 and 12 [days]. The set of figures at the upper side of Fig. 7, show the locations of microseismic events which occurred until each one of the selected times. The dashed lines denote the open hole section of the injection well. From those results, we can see that relatively high pressure was induced in the blocks including the open hole section of the injection well. The high pressure propagated into the surrounding region gradually with time, and then there appeared a pressure gradient in the outward direction from the location of the open hole section. Such a tendency is reasonable, since the injected fluid flowed out from the open hole section into the surrounding rock formation. The pressure gradient in the upward direction appeared more clearly in the results. It should be noted here that the gradient did not arise from hydrostatic pressure gradient with depth, since we used here the index of ΔP for representing pressure distribution and the ΔP denotes the increment of pore pressure from its initial value, i.e. hydrostatic pressure.

Flow pathway structure

We assumed the 2D model of flow pathway structure as shown in Fig. 3(a), and optimized the height H and the storage volume v_s of the model as the pore pressure distribution computed by the model agrees well with the pore pressure distribution estimated from microseismic events. In order for simplification, it was assumed that H depends on the location but v_s is uniform everywhere. For the model optimization, we used the pore pressure distribution at t = 4, 8 and 12 [days] shown in Fig. 7 and also the pore pressure distribution at t = 5, 7 and 10 [days] estimated from the microseismic events in the same way to obtain Fig. 7. Note that by using the pore pressure distribution not only at a certain time but several different times, we can optimize a lot of unknowns of H and v_s with more accuracy.

Fig. 8(a) shows the distribution of H which was obtained finally by the model optimization. The blue color shows a region in which the microseismic events were observed, in other words, the pore pressure distribution was estimated. As can be seen easily, the flow

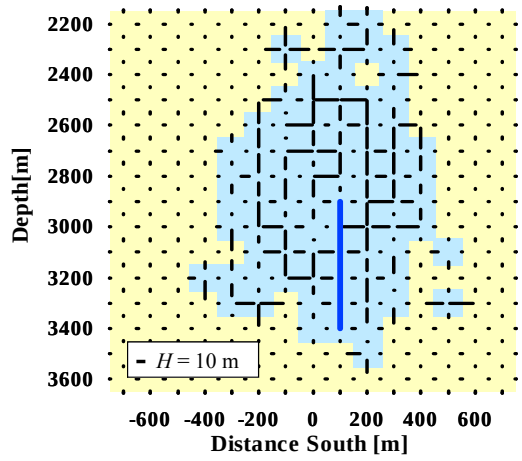

(a)

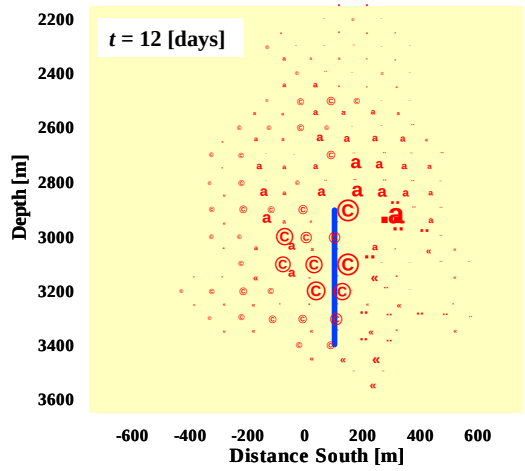

(b)

Figure. 8. (a) Estimated flow pathway, and (b) simulated flow distribution assuming the 1993 stimulation.

pathway structure can be estimated for that region basically. Each tick mark in the figure denotes the location of the assumed slit-like flow pathway, where its length is proportional to the height of flow pathway, H. The storage vole v_s was estimated to be 400 m^3/m. A thick blue line denotes the open hole section of the injection well, i.e. GPK-1. The result shows that conductive flow pathways are aligned in vertical direction rather than the horizontal direction. On the other hand, if the flow pathway could be detected, in principle we could estimate fluid flow through the flow pathways at arbitral conditions. Thus **Fig. 8(b)** shows the estimated distribution of fluid flow through the flow pathways of Fig. 8(a) assuming that GPK-1 is pressurized at the condition of ΔP_{in} = 9 MPa as same as the hydraulic stimulation in 1993, where the arrow in red shows the flow direction and its length is proportional to the flow rate. This figure shows that the large amount of fluid enters the rock mass from the upper part of the open hole section of GPK-1. This result is consistent with the fact recorded in flow logs that some 60 % of the injected fluid entered the rock mass at the upper zone of the open hole section (Jones et al., 1995, Evans et al., 2005). The entering fluid tends to flow upward in accordance with the anisotropy of higher conductivity in vertical direction.

Conclusions

We presented here a method to estimate the pressure propagation in reservoirs during hydraulic stimulation by using the data of microseismic events. The estimated pressure distribution allows us to infer the fluid flow in reservoirs caused by the hydraulic stimulation. Furthermore, by using the estimated pressure distribution, we can estimate quantitatively the spatial distribution of hydraulic conductivity in reservoirs. To do this, we assume an appropriate model of flow pathway structure and optimize it as the pore pressure distribution computed by the model agrees well with that estimated from microseismic events. Thus if the flow pathways can be detected accurately, based upon the results, we can carry out case studies such as estimating the best arrangement of injection and production wells, the recovery rate and the flow impedance etc. The achievement of this kind of techniques should improve drastically the procedure to design and control the HDR systems, and it should bring a big thrust to drive the HDR development.

Acknowledgement

We would like to acknowledge the members of the MURPHY/MTC International Collaborative Projects for their support and encouragement.

References

Cornet, F.H. and Yin, J. (1995), "Analysis of Seismicity for Stress Field Determination and Pore Pressure Mapping," *Pure Appl. Geophys.*, **145**, 677-700.

Evans, K.F., Genter, A. and Sausse, J. (2005), "Permeability Creation and Damage due to Massive Fluid Injections into Granite at 3.5 km at Soultz," *J. Geophys. Res.*, **110**, B04203.

Ito, T., Osada, K. and Hayashi, K. (2004), “Detection of Flow-pathway Structure upon Pore-pressure Distribution Estimated from Hydraulically-induced Micro-seismicity,” *Proc. the 6th North American Rock Mech. Symp. (NARMS)*, Houston, ARMA/NARMS 04-602 (CD-ROM).

Ito, T., Chiba, T., Osada, K. and Hideshi, K. (2006), “A New Approach for Monitoring Pressure Propagation in Reservoirs Based on Microseismic Events Caused by Hydraulic Stimulation,” *Proc. the 31st Workshop Geother. Reservoir Eng.*, Stanford, pp.372-377 (CD-ROM).

Jones, R. H., Beauce, A., Jupe, A., Fabriol, H. and Dyer, B.C. (1995), “Imaging induced microseismicity during the 1993 injection tests at Soultz-sous-Forêts, France,” *Proc. World Geother. Cong.*, Florence, pp. 2,665-2,669.

Osada, K., Ito, T., Hayashi, K. and Baria, R. (2005), “Mapping of Propagating Pressure in Reservoir from the Data of Microseismic Events in the 1993 Hydraulic Stimulation at the Soultz HDR Site,” *Geother. Resour. Coun. Trans.*, **29**, 109-114

ENGINE – **EN**hanced **G**eothermal **I**nnovative **N**etwork for **E**urope
Workshop 3, "Stimulation of reservoir and induced microseismicity"
Kartause Ittingen, Zürich, June 29 – July 1, 2006, Switzerland

Enhancement of productivity after reservoir stimulation of the hydro-thermal reservoir Gross Schönebeck with different fracturing concepts

ZIMMERMANN Günter, GeoForschungsZentrum Potsdam, Germany, zimm@gfz-potsdam.de

Abstract

A series of stimulation experiments were carried out at the well Groß Schönebeck, a geothermal research well in the north-eastern part of Germany. The aim was the development of concepts for the productivity enhancement of geothermal wells in that region. In a first attempt hydraulic proppant-gel fracturing treatments were conducted in two sedimentary reservoir zones with high permeability at about 4 km depth. These treatments were performed under challenging conditions in the open hole section at a temperature of about 150°C. They proved to be on the one hand technically demanding and on the other hand less successful than expected due to a suboptimal design. Most likely, the small injection volumes combined with a low proppant density did limit the success of these operations. Nevertheless, the productivity of the well could be increased by a factor of two. The characterisation of the inflow zones after the proppant fracs and derived values for the minimal horizontal stress led to a completely different frac concept. Massive waterfrac treatments were now applied over the entire open hole interval of the well below 3874 m to the final depth at 4294 m. Again, a significant increase of productivity was achieved, demonstrating that waterfracs can be a successful and effective stimulation concept for the geological situation. Evidence of the creation and properties of a very long vertical fracture were retrieved from pressure response analyses demonstrating a bilinear flow regime. The stimulation effect in terms of a productivity increase was determined for the described concepts and improvements are derived for similar field experiments.

Keywords: reservoir stimulation, hydro-thermal, waterfrac, gel-proppant frac

Introduction

Sustainable and environmentally friendly energy can be generated from the conversion of Earth's heat (from formation fluids) into electricity. The preconditions for an economic generation of geothermal electricity are sufficiently high temperatures and flow rates of about 50 m^3h^{-1} and 150 °C (Köhler & Saadat, 2003).

The required temperature for this purpose can be found in the North German Basin in 4000 m to 5000 m. At this depth the initial permeability of the rocks is generally insufficient for the necessary flow rates. However, stimulation operations to improve the near wellbore regions can lead to a sufficient productivity increase.

Concepts have to be developed to enhance the existing flow. This can be summarized by the term *hydraulic fracturing*. During stimulation experiments fluids under high pressure penetrate into the rock and generate or extend fractures. These procedures are well known in hydrocarbon industry (e.g. Economides & Nolte, 1989) as well as in the Hot Dry Rock (HDR) technology (Hettkamp et al., 2004; Baumgärtner et al. 2004). However, the objective for using hydrothermal reservoirs requires a special stimulation technique to be able to produce considerable higher amounts of fluids compared to hydrocarbon reservoirs. In contrast to the HDR technology the aim was not to create an underground heat exchanger but to get access to formation fluids in the reservoir. The most important parameters in these experiments include fracture fluids volume, injection rate, viscosity (water with added polymers), the composition of chemical variants or added proppants, and the selection of the depth interval to initiate new fractures. In the following, we summarize the stimulation experiments carried out over the recent years in the well Groß Schönebeck 3/90. A detailed description of the work presented here is in the process of publication (Zimmermann et al., 2006).

Initial reservoir conditions

The former gas well Groß Schönebeck 3/90 drilled in 1990 was re-opened and deepened to 4294 m at the end of the year 2000 to get access to the Rotliegend formation. The well encounters the typical sequence of various

geological formations known in the North German Basin. A series of 2370 m of Quarternary to Triassic sediments is under lain by 1492 m of the Zechstein salinar. The following section of this well, which was foreseen for testing, comprises 400 m of Rotliegend formation (siltstones, sandstones, conglomerates and 60 m of underlying volcanic rocks) up to the final depth of 4294 m (Huenges et al., 2002; Holl et al., 2004). This section below 3874 m was an open-hole section at times of the intended stimulation treatments of the well with access to the reservoir rocks. In 2003 this section had to be cased with a perforated liner due to instabilities of the borehole wall in the siltstone layers. During this treatment the well was deepened to 4309 m and reached the top of the carbon.

The initial hydraulic condition of the well was tested with a casing lift test in January 2001 over the whole open hole section between 3874 m to 4294 m. During the test a total volume of approximately 167 m³ of fluid was extracted over 12.3 hours with an average flow rate of 13.5 m³/h and a maximum pressure draw down of 14 MPa. Hence, the resulting productivity index achieved 0.97 m³/(h MPa) at maximum pressure drawdown. Subsequently, a flow log was run which showed outflow of the conglomerates and the volcanic sequences of the reservoir (Fig. 1). The rocks of the Rotliegend Sandstones intended for use as the geothermal reservoir were totally blocked (Huenges et al., 2002; Zimmermann et al., 2003). The reason for this blockade is believed to be the mud infiltration during the long standstill period of approximately 10 years. Permeability measurements on cores from the well showed mean values of 10^{-14} m^2 (10 mD) and documented the general usability of these reservoir rocks (Trautwein, 2005; Trautwein & Huenges, 2005).

Transmissibility was calculated from the shut-in period of the initial test and estimated to 4 – 6 x 10^{-14} m³ (0.04 – 0.06 Dm). Due to the short time of production no stable conditions can be assumed and hence the determined transmissibility is only a rough estimate of the close borehole conditions.

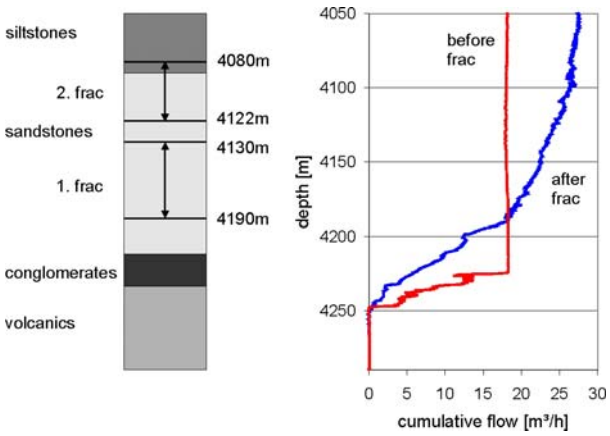

Figure 1. Left side: frac intervals during the stimulation treatments in 2002; right side: cumulative flow before and after the frac treatments.

Stimulation treatments

Sandstone stimulation

The first stimulation experiments were of conventional kind, i.e. on the basis of expertise of the hydrocarbon industry. Two experiments were performed in January 2002 using proppant-gel-frac techniques in two intervals of the Rotliegend sandstones (Fig. 1) (Zimmermann et al., 2003; Legarth et al., 2005). Experimental design comprised the isolation of the bottom boundary of the interval of interest by filling the bottom of the well with sand. The top of the interval was sealed with a mechanical packer. High viscosity fluid (gel) with proppant was employed for stimulation. The flowmeter-log indicated a significant increase of inflow due to this frac operation (Fig. 1). Visualisation by Borehole Televiewer (BHTV) and Formation Micro Imager (FMI) confirmed the creation of an open vertical fracture with a height of more than 100 m and in the direction of the maximum horizontal stress (S_H = 18.5° ± 3.7°) (Holl et al., 2003; 2004). Nevertheless the observed flow rates were not sufficient for economic power production (Zimmermann et al., 2003), but the productivity index could be enhanced to 2.2 m³/(h MPa) due to the stimulation treatments. The mean flow rate obtained during the casing lift test was 22.4 m³/h at a differential pressure of 10.5 MPa at the end of the test. A total volume of 307 m³ was produced at the duration of the test of about 14 hours, which is a similar time of production as during the previous casing lift test. Hence this result can be compared to the previous test indicating a doubling of the productivity index of the well. Legarth et al. (2003) conclude that the limited achievement was strongly influenced by the proppant properties during the treatment and

prevented a better result of the stimulation treatments.

Massive waterfrac treatment

The first treatment started in January 2003 with a moderate injection test with a flow rate of 3.6 m³/h over a period of 200 hours. The aim of this pre-test was to obtain initial injection properties of the reservoir and to compare these results with the former short term and long term production tests carried out in spring and summer 2002. After 48 hours the injectivity index was 1.15 m³/(h MPa) and decreased to 0.83 m³/(h MPa) at the end of the test after 200 hours (Tischner, 2004). The observed injectivity corresponds to the productivity derived in former production tests at similar low differential pressure. For this reason it can be assumed that the hydraulic response of the reservoir is similar for production and injection for a pressure change up to 10 MPa (decreasing for injection as well as increasing for production).

Thereafter, the first massive waterfrac treatment was performed in whose progression a total amount of 4284 m³ fluid was injected under high pressure into the reservoir. In the first part a pressure step test with gradually increasing injection rates up to 24 l s^{-1} was performed. The results show that starting with an injection rate of 8 l s^{-1} the pressure increase is reduced due to an enhanced injectivity of the formation. This effect can be interpreted as a mechanical reaction of the rock due to an opening of the existing generated artificial fractures as well as the extension of pre-existing fracture in the conglomerates and volcanic rocks at the bottom of the well (Huenges et al., 2006).

In a subsequent flow back test 250 m³ of water was produced within a time of 5 hours and a mean flow rate of 50 m³/h. This indicates in comparison with tests after the sandstone frac treatment a significant increase of productivity. Productivity index is above 4 m^3/(h MPa) during the whole test. This is an indication that the massive water injection produced additional fractures, so that the experiment was rated successful and represented roughly another doubling of the productivity index. However, borehole breakouts occurred resulting in an obstruction just at the upper part of the tested section at about 3900 m depth. Therefore, further technical borehole operations were necessary. In October 2003 the obstruction in the well was removed and the well was deepened to 4309 m and an additional liner from 3850 m down to the final depth was installed. Prior to the liner installation, an extensive logging program was performed in order to get information about the geological structure and the lithology of the borehole section of interest. The liner was installed with perforated tubes in the lower part beneath 4135 m installation depth (diameter of holes 15 mm; 93 holes per metre circumferential) to ensure the hydraulic contact to the formation. In the stabilized well the massive water frac experiment was continued in fall 2003 (Fig. 2).

The massive injection treatment was continued with a pressure step rate test to obtain the fracture opening pressure (Huenges et al., 2005). Thereafter, a massive stimulation test of 30 ls^{-1} to 40 ls^{-1} over several days and one short peak of up to 80 ls^{-1} for approximately 2 minutes were performed. The total injection volume accumulated to 7291 m³. Initially, it was intended to perform the last high rate flow injection over 8 hours, but due to a cable break during the first few minutes the test had to be abandoned. The pressure step rate test indicates multiple fracture opening events. Fracture closure pressure was determined by pressure decline analyses during shut-in at 6.4 MPa above formation pressure. According to model calculation (Legarth et al., 2005) the pressure data of the stimulation treatment demonstrated the existence of an artificial fracture. Assuming one single vertical fracture, it spans vertically over a height of 120 m in north-south direction and extends horizontally at least 160 m into the formation. The mean fracture aperture is in the range of approximately 5mm during the stimulation treatment at an injecting flow rate of 30 l/s.

Within a 24 hours flow back test 859 m³ water was produced back from the formation indicating another increase of productivity in comparison with former tests. Due to the cable break and loss into the well the pressure response is affected by frictional loss. After the cable loss a step down test was performed. This pressure response can be used to correct the frictional effects. This non linear effect is potentially turbulent flow due to the resistance of the cable above the open hole section of the well. This quadratic behaviour of flow versus pressure was applied to obtain undisturbed pressure values in the subsequent flow back test. The results show that the stimulation treatments yielded an increase of productivity up to 14 m^3/(h MPa) determined at fracture closure pressure. The productivity index decreases with decreasing differential pressure giving a clear indication of a closing fracture. Hence it can be concluded that a self propping effect is nonexistent for the fractures of the Rotliegend sandstones and only a residual fracture conductivity remains. At the

end of stable flow conditions at a flow rate of 50 m³/h the remaining productivity index is 7.5 m³/(h MPa), which corresponds nearly to another doubling.

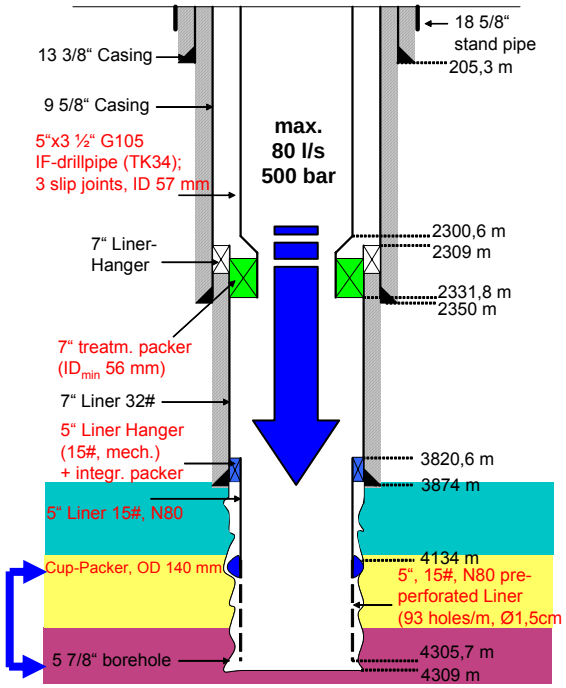

Figure 2. Casing profile of the massive water frac treatment. Access to the reservoir is given through the pre-perforated liner at the bottom.

The pressure response of the flow-back test reveals a clear indication of a bilinear flow signature ($p \sim t^{0.25}$; according to Cinco-Ley & Samaniego-V., 1981) during the first part of the test (Tischner, 2004). At the end of the injection and especially at the end of the shut-in the pressure signature shows a pseudo radial flow response ($p \sim \ln t$; e.g. Horne, 1995).

Fracture conductivity was calculated according to the bilinear flow analysis to 0.4 Dm, the fracture half length is 142 m. From pseudo radial flow phase the maximum transmissibility was estimated to 0.065 Dm from curve fitting (Tischner, 2004).

Interpretation of stimulation operations

The initial production test before stimulation showed inflow only from the volcanic rock section of the reservoir. Since these rocks only have negligible matrix permeability this inflow is due to natural fractures of the volcanic rocks. The sandstone layers were totally blocked.

After stimulation treatments of the sandstones the flow log showed a clear indication of additional inflow from the sandstones. Furthermore the productivity index had increased. At low differential pressure the situation is different: the inflow from the sandstones decreases and the artificial fractures close. Hence the productivity index is similar to that of the initial situation. This interpretation is supported by the determination of the associated transmissibility before and after stimulation, which shows similar values. Transmissibility was calculated in each case from the shut-in after the production test and represents a value at low differential pressure.

The massive waterfrac treatments were performed in the whole open section of the well which included the sandstone layers and the volcanic rocks. These treatments led to an additional access to the sandstone intervals and the volcanic rocks in the vicinity of the borehole due to the generation of additional artificial fractures.

After these waterfrac treatments the effect in the sandstones is twofold: at high differential pressure the artificial fractures give access to the sandstone reservoir with a corresponding fracture half length of approximately 150 m. This leads to an additional increase in productivity index at high differential pressure and hence enables the access to the reservoir. At low differential pressure the fracture half lengths and the fracture apertures are reduced, so most parts of the fractures are not effective and the connection to the reservoir is blocked again.

This interpretation is supported by the results of a temperature log during a production test, which shows a clear indication of inflow from the bottom of the open hole section of the well (Fig. 3). Due to the obstruction below 4260 m the measured bottom of the interval was limited to 4255 m. The most significant change in the temperature profile and hence the most productive inflow was detected from 4212 m to the bottom at 4255 m yielding an effective inflow interval of 43 m. The limitation of this inflow to the conglomerates reveals that the contribution of the fractured intervals of the sandstone layers due to the proppant frac treatment can almost be neglected at low differential pressures, i.e. the artificial sandstone fractures are closed at these conditions.

Only in the near vicinity of the well the fractures are effective and improve the access

to the borehole. But this is only a skin reduction and is limited to the near borehole environment and hence does not transcend the blockage of the sandstone reservoir.

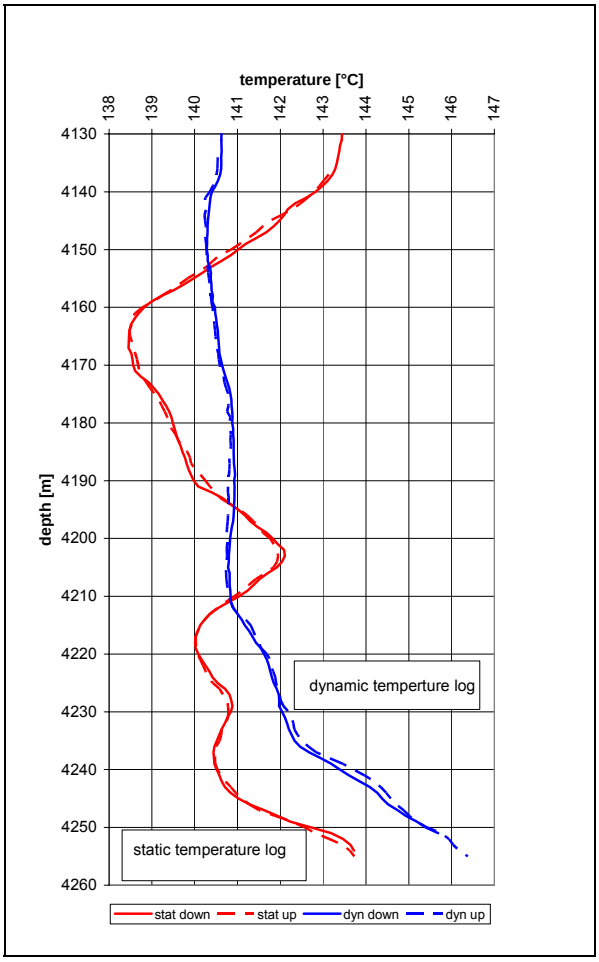

Figure 3. Temperature profile of the open hole section during a production test.

In the conglomerates and the volcanic rocks at the bottom of the well new additional fractures were created. At low differential pressure only these sections give a contribution to the transmissibility. According to the low matrix permeability of these rocks this contribution is low and only the fracture system with a calculated extension of approximately 300 m is effective.

The transmissibility of the whole open hole section including the sandstones and the volcanic rocks has not changed substantially after all these fracture treatments and hence this is a further confirmation of the closure of the stimulated sandstone layers and a still existing blockade in the vicinity of the well at low differential pressure.

Conclusion

Development of a technology to stimulate deep geothermal reservoirs in sedimentary basins is the purpose of installing the down-hole geothermal laboratory in the former gas exploration well in Groß Schönebeck 3/90.

The results reflect the learning curve from several reservoir treatments. These experiments are major steps towards developing a procedure to increase the thermal water productivity from a prior low permeable sedimentary reservoir. For “engineering” this kind of reservoir type we recommend a method of massive waterfrac with a proppant treatment at the end to ensure 1) connection to the reservoir by generating long fractures and increasing overall transmissibility 2) tie-back of generated fracture system to the well 3) sustaining fracture conductivity by proppant placement.

The obtained values of productivity seem to show the feasibility of geothermal power production from a sedimentary geothermal reservoir. The concept for power production from the Groß Schönebeck reservoir comprises a doublet of wells. The second well should be completed as a production well. The existing well can be used as an injection well.

References

Baumgärtner, J., Jung R., Hettkamp, T. & Teza, D., 2004. The Status of the Hot Dry Rock Scientific Power Plant at Soultz-sous-Forêts, *Z. Angew. Geol.*, Vol. 2, 12-16.

Cinco-Ley, H., Samaniego-V, F., 1981. Transient Pressure Analysis for Fractured Wells, *Journal of Petroleum Technology*, 1749-1766.

Economides, M.J., Nolte, K.G., 1989. *Reservoir Stimulation*, 2nd edn, Schlumberger Educational Services, Houston, Texas.

Hettkamp, T., Baumgärtner, J., Baria, R., Gerard, A., Gandy, T., Michelet, S., Teza, D., 2004. Electricity Production from Hot Rocks, *Proc. 29th Workshop on Geothermal Reservoir Engineering*, Stanford University, Stanford, California, January 26-28, 2004 SGP-TR-175.

Holl, H.-G., Hurter, S., Saadat, A., Köhler, S., Wolfgramm, M., Zimmermann, G., Trautwein, U. Winter, H., Legarth, B. & Huenges, E., 2003. First hand experience in a second hand borehole: Hydraulic experiments and scaling in the geothermal well Groß Schönebeck after reopening, *Proceedings of the International Geothermal Conference, IGC-2003 Reykjavik, Multiple integrated uses of geothermal resources*, S01, paper 060, 8-13.

Holl, H.-G., Moeck, I., Schandelmeier, H., 2004. Geothermal well Groß Schönebeck 3/90: A low enthalpy reservoir (Rotliegend, NE Germany), *Proceedings 66th EAGE Conference & Exhibition*, F032, Paris.

Horne, R.N., 1995. *Modern Well Test Analysis*, 2nd edn, Petroway Inc., Palo Alto, California.

Huenges, E., Hurter, S., 2002. In-situ Geothermielabor Groß Schönebeck 2000/2001, *Scientific Technical Report,* GeoForschungsZentrum Potsdam, STR02/14.

Huenges, E., Hurter, S., Saadat, A., Köhler, S., Trautwein, U., 2002. The in-situ geothermal laboratory Groß Schönebeck: learning to use low permeability aquifers for geothermal power, *Proc. Twenty-Seventh Workshop on Geothermal Reservoir Engineering,* Stanford University, Stanford, California, January 28-30, 2002, SGP-TR-171.

Huenges, E., Trautwein, U., Legarth, B., Zimmermann, G., 2006. Fluid pressure Variation in a Sedimentary Geothermal Reservoir in the North German Basin: Case Study Groß Schönebeck, *Pure and Applied Geophysics*, in press

Köhler, S., Saadat, A., 2003. Thermodynamic Modeling of Binary Cycles – Looking for Best Case Scenarios, *Proceedings of the International Geothermal Conference, IGC-2003 Reykjavik*, *Multiple integrated uses of geothermal resources*, S01, Paper061, 14-19.

Legarth, B., Huenges, E., Zimmermann, G., 2005. Hydraulic Fracturing in Sedimentary Geothermal Reservoirs, *International Journal of Rock Mechanics and Mininig Sciences*, Vol. 42, 7-8, 1028-1041.

Legarth B., Tischner, T., Huenges, E., 2003. Stimulation experiments in sedimentary, low-enthalpy reservoirs for geothermal power generation, Germany, *Geothermics*, Vol. 32, 4-6, 487-495.

Tischner, T., 2004. Stimulationsexperimente und hydraulische Untersuchungen in den Vulkaniten der Bohrung Groß Schönebeck, *Abschlussbericht*, Bundesanstalt für Geowissenschaften und Rohstoffe, Hannover.

Trautwein, U., 2005. Poroelastische Verformung und petrophysikalische Eigenschaften von Rotliegend Sandsteinen, *PhD thesis*, Technische Universität Berlin.

Trautwein, U., Huenges, E., 2005. Poroelastic behaviour of physical properties in Rotliegend sandstones under uniaxial strain, *International Journal of Rock Mechanics and Mining Sciences*, Vol. 42, 7-8, 924-932.

Zimmermann G., Hurter, S., Saadat, A., Köhler, S., Trautwein, U., Holl, H.-G., Wolfgramm, M., Winter, H., Legarth, B., Huenges, E., 2003. The in-situ geothermal laboratory Groß Schönebeck- stimulation experiments of sandstones in 4200 m depth, *Proc. Twenty- Eight Workshop on Geothermal Reservoir Engineering*, Stanford University, Stanford, California, SGP-TR-173.

Zimmermann, G., Tischner, T., Legarth, B., Huenges, E.; 2006. Enhancement of productivity due to stimulation of a hydro-thermal reservoir with different fracturing concepts, *Geophys. J. Int.*, submitted

Hydraulic Stimulation and Geophysical Fracture Monitoring in the GeneSys-Project

ORZOL Jens, GGA-Institute, Hannover, Germany, j.orzol@gga-hannover.de;
JUNG Reinhard, GGA-Institute, Hannover, Germany;
BUNESS Hermann, GGA-Institute, Hannover, Germany;
JATHO Reiner, BGR, Hannover, Germany;
TISCHNER Torsten, BGR, Hannover, Germany;
KEHRER Peter, BGR, Hannover, Germany

The objective of the GeneSys-Project is to develop concepts for the geothermal exploitation of low permeable sedimentary rocks. In a second step it also aims to supply direct heat to the GeoCenter Hannover, located in the Northern German Sedimentary Basin. Porosity and per-meability of the rocks at depth interesting for geothermal use however, are too low to allow classical hydrothermal use. Therefore concepts developed by EGS-projects in mainly crystal-line rocks need to be transferred to the adjacent tight sedimentary rocks. The creation of large fracture areas using the waterfrac technology is considered as the key challenge. To test transferability, a 4100 m deep research well is operated in the Northern German Sedimentary Basin. An extensive test program including massive waterfrac tests and Geophysical fracture monitoring has been carried out in the last years. Waterfrac tests were performed using un-treated freshwater. Injection rates went up to 50 l/s at wellhead pressures of 330 bar during fracture propagation. Test analysis shows that the tensile fracture that was created covers an area in the order of 100.000 m² and has a vertical extension of approximately 200 m. For microseismic fracture monitoring a network consisting of eight stations was installed. At each station 4.5 Hz 3D geophones were installed in a 100 m deep well and in addition seismometers were placed at the surface. Despite the detection level of the network being low enough to detect events with magnitudes observed during stimulation tests in crystalline rock (e.g. in Soultz project), only a very low number of events was registered. Stress conditions suggest that shearing seems to be unlikely. It is concluded that the propagation of the tensile fracture is aseismic. Measurements of the variation of the self-potential along two perpendicular profiles in the vicinity of the well, and tiltmeter measurements along a profile completed the geophysical fracture monitoring program. For the later methods a number of methodological challenges were identified. Hence no direct information about fracture geometry was derived. For the stimulation of the well planned at the Hannover site, a microseismic network will also be installed. Likewise more experience will be gained about the stimulation process in low permeable sediments.

ENGINE – **EN**hanced **G**eothermal **I**nnovative **N**etwork for **E**urope
Workshop 3, "Stimulation of reservoir and induced microseismicity"
Kartause Ittingen, Zürich, June 29 – July 1, 2006, Switzerland

Simulation of mineral precipitation in geothermal installations: The Soultz-sous-Forëts case

STAMATAKIS Emmanuel , NCSR Demokritos, Attica, Greece, manos@ipta.demokritos.gr;
BJØRNSTAD Tor , Institttut for Energiteknikk, Kjeller, Norway,
CHATZICHRISTOS Christos , Institttut for Energiteknikk, Kjeller, Norway,
MULLER Jiri , Institttut for Energiteknikk, Kjeller, Norway
STUBOS Athanassios , NCSR Demokritos, Attica, Greece

Abstract

Simulations of $CaCO_3$ scale formation during flow in geothermal installations are going to be performed. The development of the reaction scheme is based on lab-scale experiments. In this work, a dynamic optimization of the fouling process in the Soult-sous-Forêts geothermal plant is being considered using the gPROMS distributed process modeling capabilities. *gPROMS* (**g**eneral **PRO**cess **M**odeling **S**ystem) is a simulation tool widely used for creating and executing models of any level of complexity, particularly in areas characterized by complex physical and chemical phenomena as those encountered in geothermal environments. Once an accurate predictive model is available it can be used for many different activities in analyzing and optimizing a wide range of aspects of design and operation. The result is improved design solutions, such as equipment dimensions, control tuning values and set point trajectories, with capital and operational savings that will be realized over the lifetime of the plant.

The work considers also some of the issues associated with the generation and reliability of the laboratory data used in the construction of the model. The new laboratory scale data have been acquired from a series of tube blocking experiments using a nuclear technique.

Keywords: mineral precipitation, geothermal scaling

Introduction

The Soultz-sous-Forêts geothermal field is on the Alsace region in northeast France. The field is a Hot Dry Rock (HDR) reservoir and its location is shown in figure 1. The reservoir extends along NNW/SSE, about 500 m wide, 1500 m long and 1500 m tall.

The fracture network at Soultz-sous-Forêts has been explored down to 5000 m depth. The predicted temperature of 200° C was measured at a depth of 4950 m. Within the volume, which has been investigated the network appears to be stable and to have the desired properties. GPK2 is planned as a production well for the Scientific Pilot Plant. The final planned Scientific Pilot Plant module is a 3-well system consisting of one injector and two producers, one on each side of the injector. All wells are started from a single platform using the existing deep well GPK2 as one of the producers. A hydraulic stimulation was led in July 2000 for GPK2 well, one year after deepening it up to 5000 m. The geochemical results obtained during the monitoring of the fluid produced from this well have been provided to our research group in order to study calcite scaling tendency. It was found that $CaCO_3$ is one of the most annoying scales for that field.

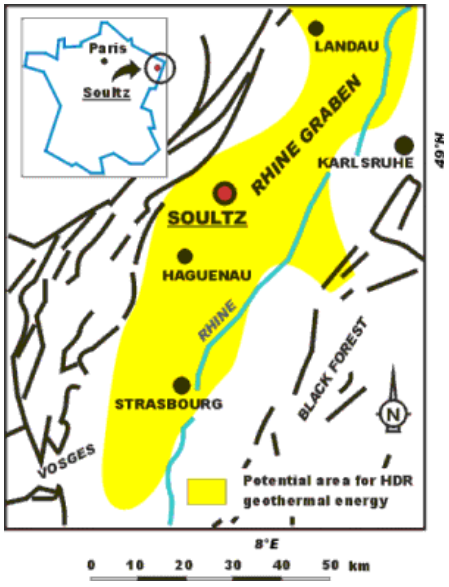

Figure 1. The European HDR-project is situated in Soultz-sous-Forêts, France, at the western border of the Rhine Graben.

According to Vetter (Vetter & Kandarpa, 1980), calcium carbonate scale ($CaCO_3$) is one of the most common and most annoying scales in

geological environments such as oilfield and geothermal applications. In the reservoir, the geothermal fluid is in chemical equilibrium with its surroundings at specific temperature and pressure. It may or may not be saturated with respect to any given minerals. But as the geothermal fluid is produced the equilibrium is disturbed by going to a lower temperature and pressure. In order to manage a potential scale problem, it is important to know when, where and how much $CaCO_3$ will be deposited during production. Effective prediction of scaling requires a reliable thermodynamic model for the prediction of the scaling tendency, a kinetic model for the prediction of scaling rate and a transport model to simulate flow along the flow path. Considerable work has been carried out in our laboratories to understand all physicochemical factors influencing calcite deposition using nuclear monitoring techniques (Stamatakis et al., 2006). The new data acquired from those experiments are incorporated into certain existing calcite kinetic models in order to check their performance. In addition, the profile of the scale formed in our tube blocking tests are monitored and going to be compared with the predicted results from the simulations. Finally, a dynamic optimization of the fouling process in the Soultsous-Forêts geothermal plant will be demonstrated using the gPROMS advanced distributed process modeling capabilities. *gPROMS* (**g**eneral **PRO**cess **M**odeling **S**ystem) is a simulation tool widely used for creating and executing models of any level of complexity, particularly in areas characterized by complex physical and chemical phenomena as those encountered in geothermal environments. Once an accurate predictive model is available it can be used for many different activities in analyzing and optimizing a wide range of aspects of design and operation. The result is improved design solutions, such as equipment dimensions, control tuning values and set point trajectories, with capital and operational savings that will be realized over the lifetime of the plant.

Figure 2 shows the topology (using gPROMS) of the corresponding geothermal facility design at Soultz. The overall objective of this study is the scaling management optimization (optimize the surface processes in order to minimize the impact of calcite scaling). It is understood that the only parameter available for optimization is the pressure, which currently is held at 20 bars in order to avoid scaling.

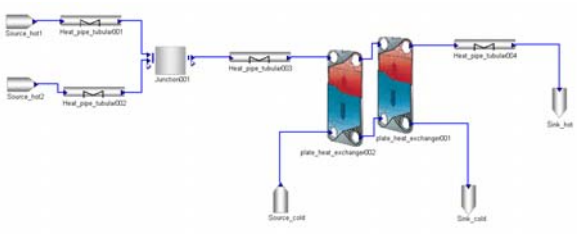

Figure 2. Designed topology of the geothermal facility using gPROMS.

The chemical system

The sparingly soluble $CaCO_3$ may form when a solution is supersaturated with respect to this, that is, when the product of the precipitating ions concentrations exceeds the solubility product. Atkinson & Mecik (1994, 1997) tried to find the effect of temperature and pressure on $CaCO_3$ dissolution. They supported that in the presence of a gas phase in the system $CaCO_3$ equilibrium can be written as:

$$CaCO_{3(s)} + CO_{2(g)} + H_2O \leftrightarrow \leftrightarrow Ca^{2+}_{(aq)} + 2HCO_3^-{}_{(aq)} \quad [1]$$

While in the absence of a gas phase as:

$$CaCO_{3(s)} + CO_{2(aq} + H_2O \leftrightarrow \leftrightarrow Ca^{2+}_{(aq)} + 2HCO_3^-{}_{(aq)} \quad [2]$$

The temperature dependence of these equilibria is given in Table 1 together with the equilibrium that connects reactions [1] and [2].

The main complication here is the occurrence of $CO_{2(g)}$ in reaction [1]. The molar volume of $CO_{2(g)}$ varies greatly with both temperature and pressure. The effect of pressure on $CaCO_3$ dissolution from the work of Atkinson & Mecik are summarized in Table 2.

Table 1. Temperature-dependent constants for lnk

$\ln k = \frac{\Delta A \ln T}{R} + \frac{\Delta B T}{2R} + \frac{\Delta C}{2RT^2} - \frac{\Delta I_h}{RT} - \frac{\Delta I_g}{R}$, (T in K)

Solid	ΔA	ΔB	ΔC ($\times 10^{-6}$)	ΔI_h	ΔI_g
Calcite	-239.623	0.18866	9.0767	83810.8	-1540.62
$CaCO_{3(s)} + CO_{2(g)} + H_2O \leftrightarrow Ca^{2+}_{(aq)} + 2HCO_3^-{}_{(aq)}$, K_1					
Range: 0 - 300°C					
Calcite	282.476	-0.7958	-14.5318	-102360	1772.44
$CaCO_{3(s)} + CO_{2(aq)} + H_2O \leftrightarrow Ca^{2+}_{(aq)} + 2HCO_3^-{}_{(aq)}$, K_1					
Range: 0 - 200°C					
	-80.384	0.18166	6.1255	31661.2	-495.94
$CO_{2(g)} \leftrightarrow CO_{2(aq)}$, K_H					
Range: 0 - 250°C					

Table 2. Effect of pressure on $CaCO_3$ dissolution

$CaCO_{3(s)} + CO_{2(g)} + H_2O \leftrightarrow Ca^{2+}_{(aq)} + 2HCO_3^-{}_{(aq)}$, K_1
$\ln\left[\frac{K_P}{K_1}\right] = \frac{-\left[\Delta\overline{V}^0_{s,1} - \Delta\overline{V}^0_{CO_{2(g)}}\right]}{RT}(P-1) + \frac{\Delta\overline{K}^0_{s,1}}{2RT}(P^2-1)$
$\Delta\overline{V}^0_{s,1} = -26.69 + 0.146365t - 15.7085\times10^{-4}t^2 - 1.0566\times10^{-6}t^3$
$\Delta\overline{K}^0_{s,1}\times10^{-3} = 11.8837 + 2.853\times10^{-2}t - 8.5531\times10^{-4}t^2 + 5.3145\times10^{-6}t^3$
$\Delta\overline{V}^0_{CO_{2(g)}}$ from interpolation of the CO2 molar volumes reported by Angus et al. (1976)
$\Delta\overline{V}^0_{s,1}$ in cm^3mol^{-1}, $\Delta\overline{K}^0_{s,1}$ in $cm^3bar^{-1}mol^{-2}$, t in °C
Range: 0 - 150°C, 1 - 200bar
$CaCO_{3(s)} + CO_{2(aq)} + H_2O \leftrightarrow Ca^{2+}_{(aq)} + 2HCO_3^-{}_{(aq)}$, K_1
$\ln\left[\frac{K_P}{K_1}\right] = \frac{-\Delta\overline{V}^0}{RT}(P-1) + \frac{\Delta\overline{K}^0}{2RT}(P^2-1)$
$\Delta\overline{V}^0 = -61.9 + 20.231\times10^{-2}t - 24.45\times10^{-4}t^2 - 0.603\times10^{-6}t^3$
$\Delta\overline{K}^0\times10^{-3} = 13.517 + 3.222\times10^{-2}t - 15.1385\times10^{-4}t^2 + 12.919\times10^{-6}t^3$
$\Delta\overline{V}^0$ in cm^3mol^{-1}, $\Delta\overline{K}^0$ in $cm^3bar^{-1}mol^{-1}$, t in °C
Range: 0 - 225°C, 1 - 2000bar

The experimental system

Two different nuclear techniques have been designed and evaluated in the lab for the real-time measurements of scale formation under flow conditions. Both methods are capable to visualize the distribution of the scale deposits, a result that is not readily obtained by methods commonly used in conventional dynamic scaling experiments. Furthermore, the techniques are sensitive to scaling, resulting generally in shorter induction times compared currently employed methods (based on pressure drop). The methodologies can be easily used for the laboratory investigation of the scaling processes occurring in geological systems, including oilfield, geothermal and hydrology applications and for all kind of mineral scales (Stamatakis et al., 2006).

Calcite formation has been investigated in the lab-scale in absence and presence of scale inhibitors. A number of runs have been successfully performed where the desired experimental conditions have been evaluated and tested using both techniques.

Mathematical modeling

A fouling model must take into account all the relevant factors along the flow path in geothermal installations, such as fluid velocity, fluid composition, pressure and temperature. It is generally agreed that fouling is controlled by balk or layer reactions or a combination of both. For small supersaturations, there is no precipitation in the fluid bulk and ionic species seem to be consumed only through a pipe surface reaction in creating a crystalline deposit (scale). For larger supersaturations, scale formation on the pipe surface proceeds as a combination of ionic and particulate deposition (Kostoglou & Karabelas, 1998).

The key step in studying fouling is to capture the interrelationship between the chemical reactions, which give rise to deposition and the fluid mechanisms encountered along the flow path. Here, the necessary heat and mass transfer equations are coupled with the equations which describe the formation of calcite deposits in the transfer pipelines and heat exchanger. The reaction/mass transfer scheme is shown in Figure 3. The overall model involves a coupled set of partial and ordinary differential and algebraic equations which can be described in gPROMS using its distributed process modelling capabilities. Those capabilities permit a detailed description of the fouling phenomena, and their variation over time and spatial position, leading to an accurate characterization of their effect on e.g. heat transfer.

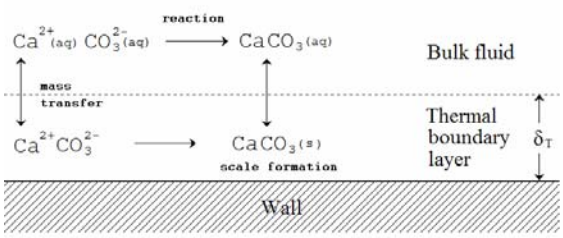

Figure 3. The calcite reaction scheme used in the fouling model.

Parameter estimation

Before using the model to predict the dynamic behaviour of the process, we need to validate it and estimate the values of several unknown model parameters based on the data gathered from our experimentations. This type of analysis can be easily performed using the built-in parameter estimation capabilities of gPROMS. Thus, the mathematical model is used to estimate the values of the unknown parameters, such as heat transfer coefficients, that best match the experimental data over time.

Optimal design and operation of the plant

The optimization procedure proposed determines the optimal operating system pressure in order to minimize the impact of calcite scaling. The complexity of the dynamic optimization problem arises primarily from the distributed and highly nonlinear nature of the system model. There are two main issues which must be taken into consideration when establishing optimal control strategies for this problem. The first issue is to ensure that no precipitation occurs and the system operates above its bubble point at all times. The second

issue is to seek for the best economic performance. However, because of the complexity of the underlying physical process, it is often difficult to define simple strategies in order to address these two issues and take at the same time into account all operating constraints.

References

Atkinson G., Mecik M. (1994), "$CaCO_3$ scale formation: How do we deal with the effects of pressure?", *Conf. Corrosion 94.*, **Paper 610**, 12pp..

Atkinson G., Mecik M. (1997), "The chemistry of scale prediction", *J. Petrol. Sci. Eng.*, **17**, 113-121.

Kostoglou M., Karabelas A.J. (1998), "Comprehensive Modeling of Precipitation and Fouling in Turbulent Pipe Flow", *Ind. Eng. Chem. Res.*, **37**, 1536-1550.

Stamatakis E., Bjørnstad T., Chatzichristos C., Muller J. and Stubos A., "Scale Detection in Geothermal Systems: The Use of Nuclear Monitoring Techniques", *presented during the Launching Conference of the European Project: Enhanced Geothermal Innovative Network for Europe (ENGINE),* Orleans, France, 13-15, February 2006.

Vetter O.J., Kandarpa V. (1980), "Prediction of $CaCO_3$ Scale Under Downhole Conditions", *Soc. Petr. Eng. Of AIME*, **SPE 8991**, 155-165.

ENGINE – **EN**hanced **G**eothermal **I**nnovative **N**etwork for **E**urope
Workshop 3, "Stimulation of reservoir and microseismicity"
Kartause Ittingen, Zürich, June 29 – July 1, 2006, Switzerland

Pre-Stimulation Analyses of a Low Permeability Geothermal Well at Desert Peak, Nevada

ROBERTSON-TAIT Ann, GeothermEx, Inc., Richmond, California, USA, art@geothermex.com
JOHNSON, Stuart D., ORMAT Nevada, Inc, Reno, Nevada, USA

Abstract

Keywords: EGS, Enhanced Geothermal Systems, HDR, Hot Dry Rock, Desert Peak, Nevada, binary geothermal power plant

An industry-DOE cost-shared project is underway to evaluate the technical feasibility of developing an EGS power generation project on the eastern side of the Desert Peak geothermal field. An existing well (DP23-1) is the focus of much of the Phase I investigation, including re-interpretation of lithology, acquisition and analysis of a wellbore imaging log, and conducting and analyzing a step-rate injection test. In addition, numerical modeling has been undertaken to estimate heat recovery and make generation forecasts for various stimulated volumes and well configurations. The target formations for hydraulic stimulation in well DP23-1 lie below an unstable phyllite which bottoms at about 1,740 m (5,700 feet). The formations beneath this unit include a section of Jurassic/Triassic metamorphic rocks (of which the phyllite is a part) and an underlying, younger (Cretaceous?), massive granodiorite that intrudes the older rocks above. This granodiorite unit extends from 2,140 m (7,020 feet) to TD (2,939 m or 9,641 feet) in DP23-1 and is likely to have considerable lateral extent. A wellbore image log obtained over a significant portion of the open hole has been analyzed in terms of the distribution and orientation of natural fractures and borehole failure phenomena (tensile fractures and breakouts). The features analyzed from the image log have been used to evaluate the orientation of the stress field and constrain the magnitudes of the principal stresses. These analyses permit an evaluation of the effects of pore pressure increase on pre-existing fractures, and, in conjunction with lithology, mineralogy, drilling rate and geophysical log data, have been used to identify the most prospective interval for stimulation. Future plans for Phase II include undertaking a "mini-frac," re-completing the well in preparation for hydraulic stimulation, and planning, conducting, monitoring and evaluating a massive hydraulic stimulation. Should the stimulation result in the creation of a large enough reservoir, a second and perhaps a third well would be drilled and stimulated, and the system would be tested for several months to determine its capacity. In Phase III, a 2-5 MW stand-alone binary power plant would be designed and constructed at Desert Peak East, and in Phase IV, the power would be either sold to a utility customer or used to supply the parasitic power needs of the existing Desert Peak hydrothermal power plant. A recent additional focus of the project involves evaluating the feasibility of stimulating a non-commercial wells drilled in the hydrothermal portion of the field (DP27-15).

Introduction

ORMAT Nevada Inc. (ORMAT) has received funding from the US Department of Energy (DOE) on a cost-shared basis to investigate the technical and economic feasibility of creating an artificial underground heat exchanger in the eastern part of the Desert Peak geothermal field, located about 130 km (80 miles) ENE of Reno, Nevada. This project has as its ultimate goal the development of 2 to 5 MW of EGS-derived power from a stand-alone binary power plant supplied by a well doublet or triplet. Focusing initially on well DP23-1, a hot but tight hole about 2.5 km (1.5 miles) east of the producing hydrothermal wells at Desert Peak (Figure 1), a systematic evaluation of the EGS potential of this area is nearing completion. This Phase I evaluation includes:

- analysis of existing geological data, including new petrologic analyses of samples from well DP23-1 and a nearby core hole (35-13TCH);
- review of previously collected geophysical data;
- mechanical testing of cores from 35-13TCH (none are available from well DP23-1);
- obtaining and evaluating a new wellbore image log in well DP23-1 to determine stress field orientation and evaluate the intrinsic fracture population;

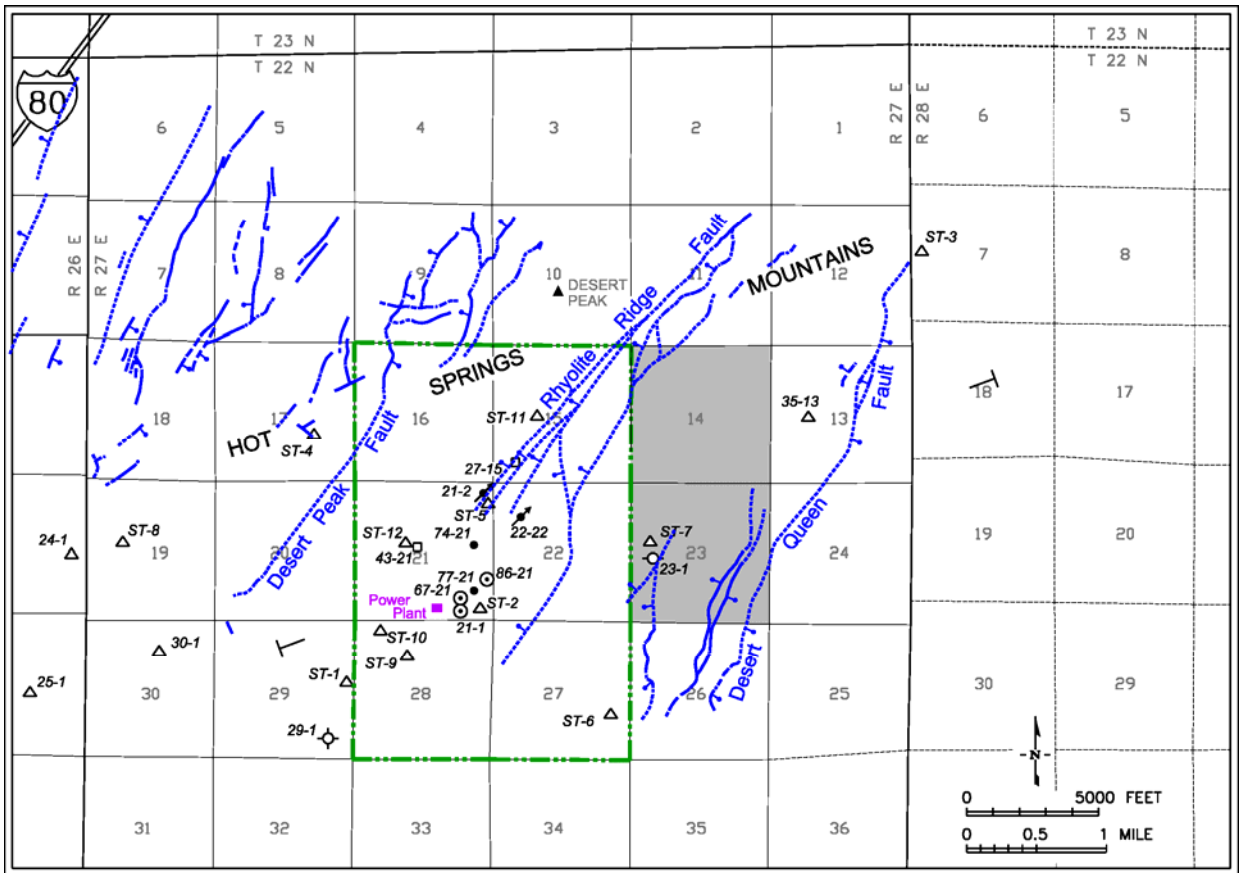

- conducting an injection test of well DP23-1 to determine baseline (pre-stimulation) well and reservoir characteristics;
- numerical modeling of heat recovery to develop generation forecasts for various well configurations over a range of stimulated volumes; and
- preparation of a detailed plan to guide the next activities at the field (Phase II).

We present herein a review of the analyses made to date and summarize the lessons learned in the course of the project.

Basic Data from Well DP23-1

Well DP23-1 was completed in May 1979 with a 13-3/8-inch production casing from the surface to 908 m (2,980 feet). Below this is a 12-1/4-inch open hole to 1,613 m (5,292 feet), an 8-1/2-inch open hole to 2,445 m (8,022 feet) and a 7-7/8-inch open hole to TD (2,931 m or 9,641 feet). Circulation losses occurred while drilling between 2,533 and 2,586 m (8,310 and 8,485 feet) and losses continued to 2,809 m (9,215 feet). Below this depth, the drilling fluid was changed from mud to aerated water, and it is not possible to discern if or where any fluid losses occurred in this lower interval.

During drilling and after completion, various attempts were made to flow test the well, sometimes with air or nitrogen assist. During testing in November 1979, the well bridged off below the 13-3/8-inch casing shoe. In December 1984, a 9-5/8-inch liner was hung and cemented from 810 to 1,309 m (2,658 to 4,293 feet) to cover the bridging zone. The depth for the bottom of this liner was chosen on the basis of temperature (the well reaches 400°F [204°C] at 4,300 feet [1,311 m]; see Figure 2). There were no returns of drilling fluids while cleaning out bridges down to 4,608 feet (1,406 m). After setting and cementing the 9-5/8-inch liner, the bottom of the hole was cleaned out with full returns to 2,755 m (9,040 feet), and with about 95% returns below that depth.

A step-out from the known productive area at Desert Peak, well DP23-1 was unable to sustain flow at commercial rates and pressures. Several flow tests were made before installing the 9-5/8-inch liner; during the November 1979 test, the well flowed unassisted. After the workover was completed, a brief injection test was conducted. While injecting at 5 barrels per minute (bpm), the wellhead pressure varied between 100 and 150 psig. The following day, the injection rate was increased to 20 bpm and the corresponding wellhead pressure was about 600 psig. A temperature survey was

collected during the first injection period and is included in Figure 2 (the blue survey).

Well DP 23 1 is drilled through a thick section of Tertiary sediments and volcanics to a depth

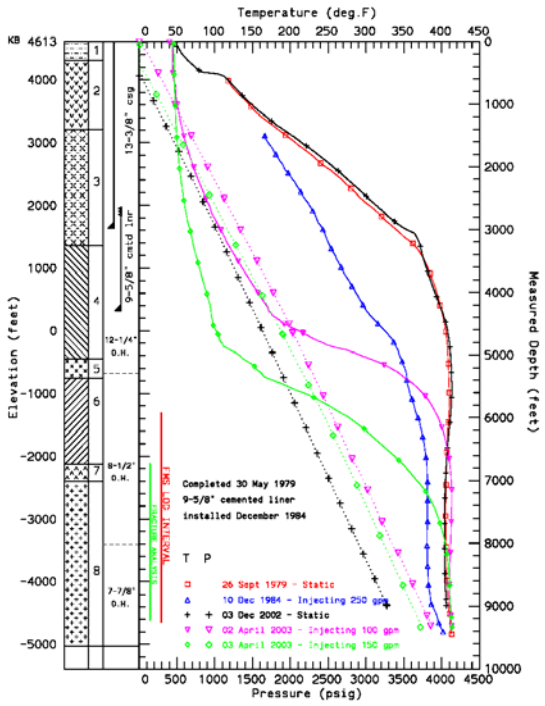

Figure 2: Lithology, completion and downhole survey data, well DP 23-1. April 2003 FMS log interval shown (lower left) by red line; data subset for fracture analysis shown by green line. Formations: 1 Truckee + Desert Peak; 2 Chloropagus Formation; 3 Rhyolite Unit; 4 pT1 Metasediments; 5 Quartz Monzodiorite (pT2); 6 pT2 Metasediments; 7 Hornblende Diorite (pT2); 8 Two-Mica Granodiorite (see Lutz et al., 2003 for full descriptions of these units).

of about 1,000 m (3,300 feet). As shown in Figure 2, a high, conductive temperature gradient persists throughout this section; temperature at the base of the Tertiary (the bottom of formation 3) is about 190°C (370°F). The temperature gradient decreases in the pre-Tertiary section, where a maximum temperature of 216°C (421°F) is observed at about 1,615 m (5,300 feet). A modest temperature reversal occurs below this maximum, and there is a long, nearly-isothermal section at about 207°C (405°F) extending from 2,430 to 3,130 m (7,000 to 9,000 feet), below which the temperature increases again, reaching about 211°C (412°F) at TD. A comparison of static temperature surveys from September 1979 and December 2002 (the red and black surveys on Figure 2) shows that temperatures have remained stable with time, although the 2002 survey suggests that there is a small amount of circulation around the 9-5/8-inch x 13-3/8-inch liner lap (which had not been installed when the September 1979 survey was run). Also shown in Figure 2 are temperature surveys collected during injection in December 1984 after installing the 9-5/8-inch liner (blue survey) and in April 2003 during the recent injection test (pink and green surveys). The static water level sits at about 180 m (600 feet).

Geological Analysis

A simplified lithologic column for DP23-1 is included in Figure 2. Formation picks were developed based on mud log data, recent petrological analysis (summarized below), and geophysical logs collected at the time of drilling in 1979, some of which are included in Figure 3. The following summary of the pre-Tertiary section, which includes the target formations for hydraulic stimulation, is taken largely from Lutz *et al.* (2003).

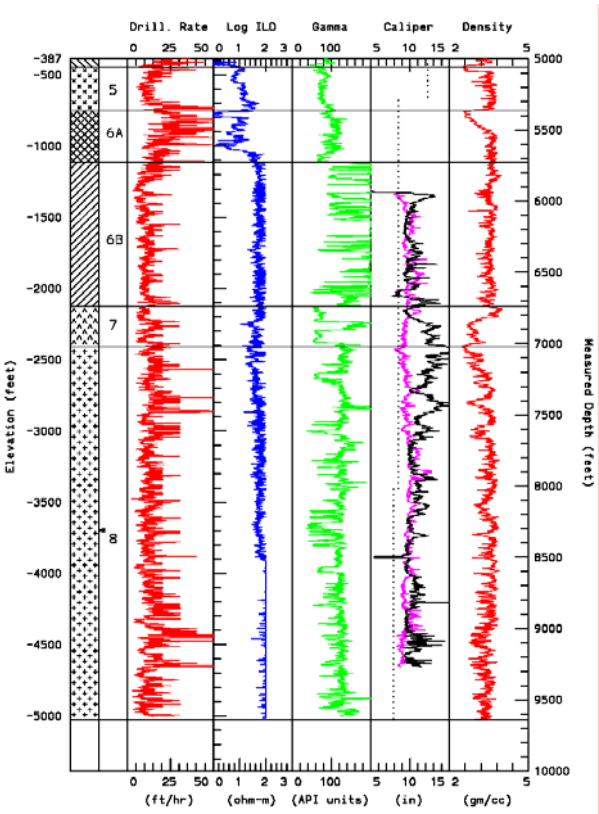

Figure 3: Lithology, penetration rate, geophysical logs and caliper data below 5,000 feet, well DP23-1. Nominal hole diameter shown by the dotted line in the caliper window.

The pre-Tertiary metamorphic section in DP23-1 is formed of two distinct subgroups with a sharp contact between them. The upper subgroup (pT1), which covers a depth range of 994 to 1,542 m (3,260 to 5,060 feet), is dominated by marine metasediments that have undergone regional greenschist facies

metamorphism. The lower subgroup (pT2) extends to 2,140 m (7,020 feet) and is composed of a series of Jurassic/Triassic phyllite, schist and mafic-to-intermediate plutonic rocks, all more strongly metamorphosed than the pT1 section. This is underlain and intruded by a two-mica granodiorite that is similar to Cretaceous intrusive rocks typical of the Sierra Nevada batholith found to the west in Nevada and California.

Several formations of interest from an EGS perspective were identified in the pT2 subgroup and below. The first is a quartz monzodiorite extending from 5,060 feet to 5,380 feet in well DP23-1 (formation 5), which was also found in 35-13TCH from 3,123 to 3,484 feet. The second is a hornblende diorite unit extending from 6,800 feet to 7,020 feet in well DP 23 1 (formation 7); this is not observed in 35-13TCH owing to the relatively shallow depth of the core hole. Beneath these units is a third formation of interest: the two-mica granodiorite (referred to herein simply as granodiorite), which is less altered, less veined and more massive than the two intrusive units above. Thin dikes near the bottom of 35-13TCH imply the presence of this granodiorite beneath the bottom the core hole (Lutz *et al.*, 2003). Therefore, this unit is likely to have considerable lateral extent.

A moderate temperature (430-460ºF; 220-240ºC) propylitic-phyllic alteration assemblage consisting of chlorite, pyrite, calcite, epidote and sericite is present in the granodiorite and overlying rocks in DP23-1. The propylitic alteration appears to be younger than the magmatic-hydrothermal alteration and may represent cooling of the granodiorite after its initial emplacement. The upper 300 m (1,000 feet) of the granodiorite body is moderately sericitized. Most of the primary biotite and some of the hydrothermal biotite has undergone retrograde alteration to chlorite and calcite. There is a general decrease in chlorite with depth in the granodiorite and also a slight increase in epidote below about 2,740 m (9,000 feet). The granodiorite is microbrecciated in sheared or fractured zones at 2,207 m (7,240 feet) and 2,332 m (7,650 feet), and the comminuted rock is cemented with chloritic gouge. The youngest veins in the granodiorite are rare calcite, calcite-hematite and calcite-quartz veins that cut across fractures containing higher-temperature minerals such as biotite and epidote. These carbonate veins may represent alteration related to the current geothermal system.

The resistivity, gamma ray and density logs collected at the time of original drilling were used in combination with the petrographic analysis of Lutz *et al.* (2003) to refine the formation picks in the deeper part of the well. Figure 3 shows these data below 1,525 m (5,000 feet), and subdivides formation 6 into two parts: a section of black phyllite and schist (formation 6A) and a section of metamorphosed intrusive units (formation 6B). Also shown in this figure are the drilling penetration rate (in feet/hour) and the caliper data collected using the arms of the wellbore imaging tool (see below).

Wellbore Image Log Analysis

Schlumberger's "hot hole" Formation Microscanner (FMS) tool was run in well DP23-1 in April 2003 after injecting for ~2.5 days to determine well and reservoir hydraulic parameters (see Sanyal *et al.*, 2003) and to cool the well to ensure image quality. While running a TPS survey during the injection period, an obstruction was encountered at 1,783 m (5,850 feet) in formation 6A. This zone was sloughing into the hole during injection, and an increasing amount of fill was noted at bottomhole on subsequent tool runs. The FMS tool was run into the hole and began logging up from 2,824 m (9,265 feet); logging stopped at 1,806 m (5,924 feet) to avoid encountering the obstruction with the tool arms open. Therefore, the upper quartz monzodiorite unit (formation 5) was not logged. However, wellbore images were obtained through most of the granodiorite and a portion of the overlying pT2 units. The logged interval corresponds to the interval for which caliper data are shown in Figure 3, and is also shown by the red line in Figure 2.

The digital data for the FMS log were obtained from Schlumberger and provided to GeoMechanics International (GMI) for analysis, along with supporting data from the well, including previously collected geophysical logs, temperature logs, drilling data and well test data. Wellbore failure features were identified and analyzed to determine the stress field orientation and (in conjunction with other data) to constrain the local stress tensor, and the fracture population was analyzed in a portion of the logged interval (2,051 to 2,812 m or 6,730 to 9,228 feet).

Figure 4 presents a summary of the observed wellbore failure data. Borehole breakouts were determined from both image data and caliper data (using the FMS tool arms); tensile cracks were identified from image data. Using the caliper data, a total of 52 breakouts were identified between 1,805 and 2,315 m (5,922 and 7,594 feet), and show a dominant

direction of N128°E (39 breakouts) and a subordinate direction of N68°E (13 breakouts). As breakouts form at right angles to the direction of the maximum horizontal stress (SHmax), the dominant trend suggests an SHmax direction of N38°E. Using the image data, a total of 65 breakouts were identified between 1,956 and 2,817 m (6,418 and 9,241 feet); these suggest an SHmax direction of N27°E. A total of 170 tensile cracks were identified between 1,829 and 2,728m (6,000 and 8,949) feet; these suggest an SHmax direction of N27°E.

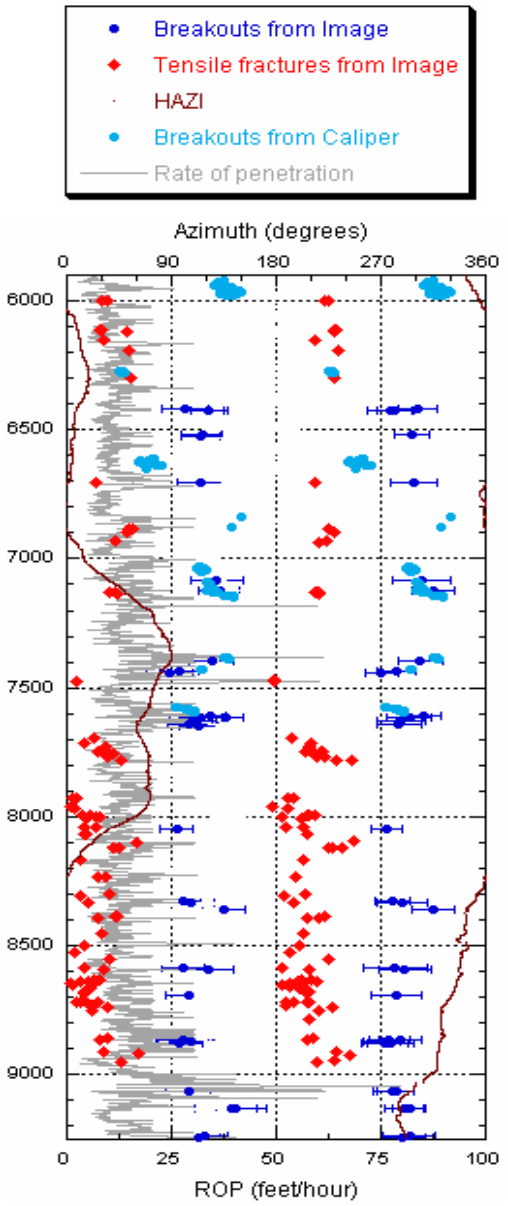

Figure 4: Observed wellbore failure features and drilling penetration rate (ROP), well DP 23-1.

Owing to budget considerations, the fracture analysis used only a portion of the logged interval; as shown in Figure 2, this covered most of the granodiorite and extended about half way through the pT2 hornblende diorite unit above it. GMI identified nearly 11,000 "fractures" in this interval; Figure 5 shows their orientation. The dominant fracture direction is NNE, dips range from 30 – 75°, and the dominant dip directions are NW and SE.

The analysis of the FMS log data leads to several observations:

- The wellbore failure data and the dominant strike of natural fractures show a stress field orientation that is not only consistent between data sets but also reflects the current stress field as indicated by both regional and local geologic data (Faulds *et al.*, 2003).
- Breakouts tend to occur where the drilling penetration rate is high (*i.e.*, in zones of weaker rock), while tensile cracks tend to occur where the drilling penetration rate is low (*i.e.*, in stronger rock).
- Significantly more tensile cracks are observed below 2,310 m (7,600 feet) than above it. Possible reasons for this include a greater amount of cooling in the portion of the well during drilling and injection, more quartz in the reservoir rock, and/or stronger rock overall below 2,310 m (7,600 feet).

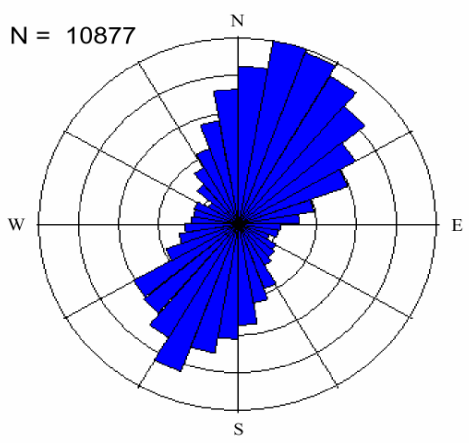

Figure 5: Orientation of natural "fractures" between 6,730 and 9,230 feet, well DP 23-1.

Hydraulic Stimulation Target Zone

The various data sets were compared to evaluate the possibility that changes in primary lithology and/or secondary mineralization may correlate with some or all of the observations made from the analysis of the image log. There is an overall decrease in secondary mineralization passing from the pT2 units into the granodiorite. XRD analyses show that the granodiorite has a relatively consistent overall composition with depth, including quartz content. Illite is minor but constant through

both the hornfelsic pT2 units and the upper part of the granodiorite. Within the granodiorite, there is a consistent decrease in chlorite and illite with depth and an overall decrease in alteration and fracturing below the lower shear zone at 2,332 m (7,650 feet). Caliper data show the hole to be "out of gauge" to a greater degree, and to have a greater variation in hole diameter on the two tool arms above this shear zone, while below it, the caliper data show a more regular borehole (Figure 3). In addition, the upper, more sericitized granodiorite drills somewhat faster than the lower granodiorite. Taken together, the competence of the rock appears to be greater below the shear zone than above it.

The temperature survey conducted during injection after re-completing the well in 1984 (the blue survey in Figure 2) shows a permeable interval at approximately 2,740 m (9,000 feet), with an isothermal interval above it to a depth of 2,057 m (6,750 feet), which is near the top of the hornblende diorite. This survey was run after cleaning and circulating the hole, running and cementing the 9-5/8-inch liner, cleaning and circulating again (about 2 weeks were spent with the rig on the hole altogether), and injecting at about 5 bpm for several hours. The presence of a permeable zone at this depth is also suggested by the fluid losses noted while cleaning the hole after setting and cementing the liner (see above).

Owing to the relatively low injection rate and short duration, the permeable zone at 2,740 m (9,000 feet) cannot be identified in the two injecting temperature surveys from the pre-logging cooling period in April 2003 (Figure 2). However, the well went on vacuum after a day of injection, and was progressively cooling deeper and deeper. Spinner surveys run concurrently with the two injecting temperature surveys show different results: the later survey appears to indicate a fluid loss zone at or below 2,740 m (9,000 feet) while the earlier does not. The reduction in spinner rate on the later survey occurs within about 100 m of the recently filled bottom of the well, leaving some ambiguity regarding its significance. Nevertheless, we believe this permeable zone exists, and that fluids will exit the well at deep levels during stimulation. There is no sign that any preferential cooling took place around the shear zone at 2,332 m (7,650 feet) on any survey.

Intrusive units are of primary interest from a hydraulic stimulation perspective. Although the upper quartz monzodiorite (formation 5) is laterally extensive and coincides with the temperature maximum in the well, it is relatively thin and is underlain by a formation that becomes unstable during injection. The lowermost pT2 (a hornblende diorite, formation 7) and the deeper, younger granodiorite (formation 8) are more massive and look mechanically attractive. The granodiorite is less altered, particularly below a shear zone at 2,332 m (7,650 feet), where a significant increase in the number of tensile cracks is observed from the image log. The rate of penetration is slightly greater and the hole is more irregular above the shear zone than below. Taken together, this information suggests that the competence of the rock below the shear zone is greater than that above it. For massive hydraulic stimulation, the lower portion of the granodiorite will be targeted. The presence of a zone of deep permeability at about 2,740 m (9,000 feet) should facilitate the stimulation over the open-hole interval.

Mini-Frac and Re-Completion of DP23-1

Having selected the lower granodiorite as the target zone for hydraulic stimulation, the next step before designing the stimulation program itself is to better constrain the stress tensor and mechanically prepare the well for stimulation. Constraining the stress tensor can be achieved through the determination of: 1) the compressive strength of cores taken from the target formation; and 2) the magnitude of the least principal stress within or near the interval of interest. Mechanical well preparation will be achieved by casing off the unstable phyllite and other intervals of the well. Both require the presence of a drilling rig, and therefore would logically be undertaken together.

A mini-frac is a series of small volume, high pressure injection tests that are undertaken while measuring downhole pressure. The parameters of interest from the mini-frac are the formation breakdown pressure and the instantaneous shut-in pressure (for details, see Hickman *et al.*, 1988). These parameters are identified by analyzing pressure versus time data collected throughout the series of injection and shut-in periods. Ideally, a mini-frac is undertaken in a relatively short, un-fractured, low-permeability interval of the well. Because of temperature effects, inflatable straddle packers (typically used to isolate the interval of interest in a mini-frac) are unlikely to seal effectively against the walls of the existing open hole in DP23-1. Therefore, we developed an alternative method that involves:

- acquiring core from TD for mechanical and sonic velocity testing;

- running a sonic velocity log through the interval to be stimulated later (from 2,350 m [7,700 feet] to TD);
- preparing for re-completion by setting a retrievable bridge plug near the top of the interval to be stimulated, topping it with two alternating layers of sand and cement;
- re-completing the well by running and cementing a 7 5/8-inch casing from 670 m (2,200 feet) to the top of the cement plug at ~2,350 m (~7,700 feet), covering the old 13-3/8 x 9 5/8 liner lap, the unstable phyllite and other formations down to the top of the target zone in the granodiorite;
- drilling out the upper cement plug at the 7-5/8-inch casing shoe and reversing out the sand, leaving a short open interval for the mini-frac;
- performing the mini-frac test with downhole pressure monitoring inside the new 7-5/8-inch casing; and
- drilling out the lower cement plug, washing out the sand, retrieving the bridge plug and cleaning out the hole to TD for later stimulation.

This approach is essentially the same as that developed for conducting mini-frac stress tests at the Dixie Valley geothermal field, also in Nevada (Hickman *et al.*, 1998). This technique was subsequently used for the Coso EGS project in well 38C-9, after setting and cementing the 13-3/8-inch production casing and drilling a short pilot hole out the bottom of this casing (Sheridan and Hickman, 2004). At Coso, the mini-frac testing was conducted at the top of the interval of interest before drilling ahead. However, since DP23-1 is an existing well, an alternative approach is required. The method we have developed will not only constrain the stress field, but also will allow the extrapolation of stress data through the interval of interest.

A rig was mobilized to the site in late September 2005 and operations began on a planned 15-day workover program. When undertaking the first phase of the operation (cleaning out the well to TD), the drill pipe became stuck. After backing off and several days of fishing, it was decided to side-track around the fish (top at 7,518 feet or 2,292 m). About 10 days were spent kicking the hole off in the granodiorite formation. Not long after the sidetrack had been successfully kicked off, the drill pipe became stuck again; subsequent fishing operations were successful. Drilling began again, but some tools were lost downhole, and a third fishing operation began, during which it became difficult to pass through the 9-5/8-inch liner lap at 810 m (2,658 feet). A downhole video showed that the liner top was damaged, and considering that the budget was nearly exhausted, operations were terminated, the rig was released and the well was secured. Further work on the well will occur in Phase II.

Future Work

The Phase I feasibility study is nearing completion, and planning is underway for the next phase of development of the field. The first major element will be repairing and completing the re-drill of DP23-1. Then, a massive hydraulic stimulation will be conducted, monitored and analyzed. This would be followed by the drilling of a second and perhaps a third well to complete an EGS doublet or triplet, and one or more periods of circulation testing. If the characteristics of underground heat exchanger are favorable, a small (3-5 MW), stand-alone binary power plant would be constructed in the third phase of the project. Power from the facility would be used either to supply the parasitic load of the power plant(s) in the hydrothermal portion of the field, or would be sold to the local utility.

While the focus to date has been on the eastern side of the field, a recently drilled well that was not commercially productive (DP27-15; see Figure 1) presents an additional opportunity for the implementation of EGS concepts at Desert Peak. Preliminary evaluation of the feasibility of using hydraulic stimulation to enhance its permeability is just getting underway. Figure 6 shows the lithology, completion, drilling penetration rate and available downhole temperature and pressure data from this well. Permeable zones often occur at the base of the rhyolite formation (pale yellow formation in Figure 6) in this portion of the field; however, this was not the case in DP27-15.

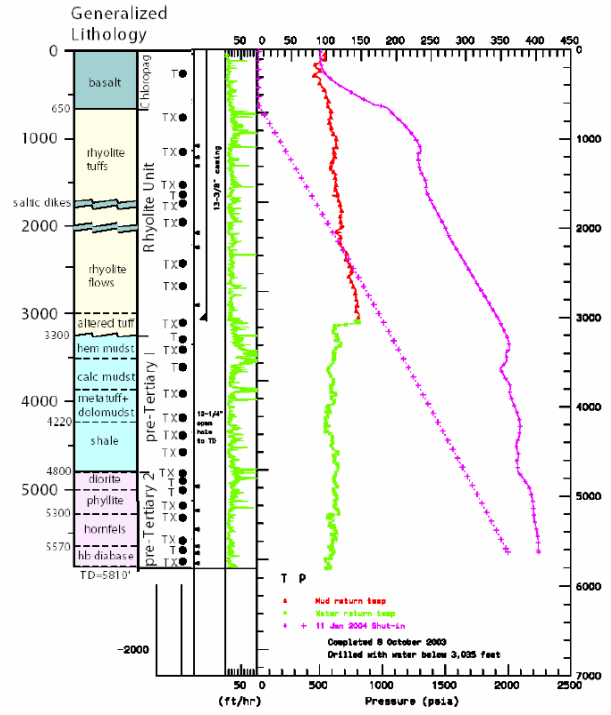

Figure 6: Data from in-field EGS candidate well DP27-15.

To evaluate the feasibility of stimulation, we plan to undertake the following program in this in-field well:

- investigate downhole conditions by running a new temperature and pressure survey;
- develop a conceptual model in the hydrothermal portion of the field by doing petrological analysis of three other newer wells (43-21, 74-21 and 77-21; see Figure 1) and several older wells (21-2, 22-22 and 29-1); and
- run geophysical logs in well DP27-15, including sonic, gamma, density, and the USGS high-temperature borehole televiewer.

These data will be analyzed to determine if chemical and/or hydraulic stimulation would result in an increase in permeability that would make the well suitable for use as a producer or injector. If this analysis is positive, then a stimulation plan would be developed, and an existing seismic monitoring network set up by Lawrence Berkeley National Laboratory (Figure 7) would be expanded by drilling three shallow core holes for deployment of geophones. Pre- and post-stimulation injection tests will be conducted and analyzed using, among others, a simple method developed in the course of this project (see Sanyal *et al.*, 2003).

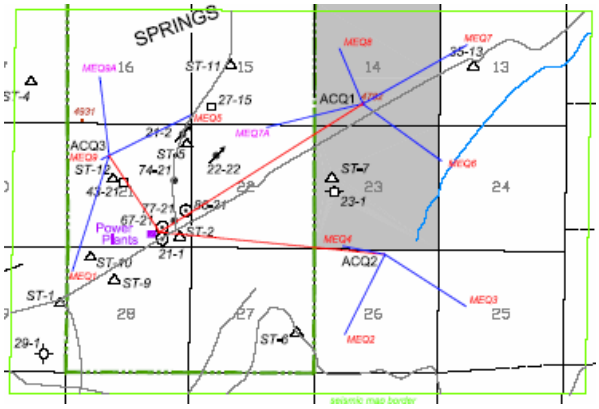

Figure 7: Seismic monitoring network at Desert Peak.

After stimulation, an integrated test will be conducted using a subset of the wells in the hydrothermal portion of the field. The plan will be developed to minimize the impact on existing well and power plant operation. Depending on the results of stimulation, the stimulated well may be used during the test as a production well, an injection well, or both. Pressure monitoring will continue in existing observation wells during the test, and PTS logs will be run in the stimulated well and perhaps others to observe specific downhole conditions. A tracer test will be an integral part of the test to assist in the evaluation of reservoir size and heat transfer capabilities.

Lessons Learned

The Desert Peak project has been developed with the benefit of experience from other EGS projects, and some of the lessons we have learned are not new. However, they are worth reviewing. The first is that basic geologic analysis is an invaluable, low-cost/high-benefit approach. Detailed petrographic analysis assists in assessing mineralogical issues, providing insight into the mechanical and hydraulic properties of target formations. Furthermore it leads to the development of a good geological picture of the target area, which is particularly important in stratigraphically and structurally complex areas such as the Basin and Range.

While the mechanical properties of sedimentary rocks are well-known, the same is not true for most EGS candidate rock types. Mechanical testing of more EGS-favorable rocks would provide a better foundation for understanding EGS development. Therefore, it is reasonable to take the time and expense to collect and analyze cores of various prospective EGS rock types.

Reservoir engineering analyses are needed, even in the early stages of a project.

Relatively simple pre- and post-stimulation tests can provide useful, practical information, and every opportunity should be taken to obtain and analyze reservoir engineering data.

Image log analysis is essential for EGS projects. Since temperature limitations of wellbore imaging tools can be problematic, such logs would ideally be run during drilling. For existing "wells of opportunity," image logs can be run after a period of injection, if no high-temperature tool is available. An approximate stress field model can be developed, even without stress magnitude data, assuming one has reasonably good well history data (drilling rate, mud weights, pressures during injection tests, etc.), a density log to assess the vertical stress, some injection testing data, and an understanding of the regional stress setting.

Similarly, analysis of pre-existing fractures is essential because the nature of the rock fabric needs to be evaluated. We have found that resistivity-based image logs may result in over-estimation of the number of fractures; however, a reasonable subset represent pre-existing cracks that can be exploited after stimulation. This kind of analysis can be used to determine what pressures are needed during stimulation. An experienced stress analysis team is essential.

A multi-disciplinary approach should be applied to EGS target selection. For the target formation, one needs to consider its extent and boundaries, its lithology and mineralogy, its initial (pre-stimulation) hydraulic characteristics, the nature and orientation of pre-existing fractures (open and closed), the stress field orientation and the rock strength, and how these change with depth. This requires input from various specialists.

Although the results are not discussed in this paper (please see Sanyal and Butler, 2005), we undertook in the course of this project (using conditions similar to those at Desert Peak) extensive numerical simulation to evaluate heat recovery for a variety of fracture spacings, well configurations and EGS system throughput. The goal of this work was to develop practical correlations that can be qualitatively applied to any EGS project. Using reasonable pressure limitations for injection pumping and production well drawdown, we determined the "net generation profile" (electrical generation over a 30-year period, taking into account all parasitic power needs and the impact of cooling on generation) for hundreds of combinations of parameters, and evaluated those that achieved less than a 15% variance in net generation during the 30-year period. For these optimized cases, we found that:

- Reducing throughput improves the net generation profile.
- Increasing the stimulated volume increases generation.
- Well geometry does not significantly affect generation vs. stimulated volume.
- Neither well geometry, fracture spacing nor fracture domain permeability have a strong impact on recovery factor, which is estimated to be quite high (about 40 to 50%) for stimulated volumes >0.1 km^3.
- To determine the economics of EGS, long-term system performance must be taken into account.

Our difficulties with the re-completion of well DP23-1 reinforce the need for excellent drilling personnel in EGS operations. High-level supervision and good communication between the drill site and EGS technical personnel are also required. Drilling budgets need a reasonable contingency (at least 25%). "Radical" bottomhole assemblies may be required to kick-off directional wells in hard rock. Despite the difficulties we had with this well, we still believe that the "wells of opportunity" approach (*i.e.*, using existing low permeability wells, perhaps on the margins on known hydrothermal systems) can advance EGS technology. Many such wells are available in the United States.

Something of interest to us (and which we hope will be discussed in the course of this workshop) is the relative contributions of industry vs. that of the academic, scientific and government communities in EGS development. A suitably motivated industrial partner could move an EGS project forward quickly and at low cost, perhaps even by taking certain short-cuts. However, to enable results to be applied to similar developments elsewhere, a high level of supporting science must be done, on paper, in the lab and in the field. This is why both groups must be involved. Government support is required to get project through the feasibility stage and to demonstrate the applicability of methodologies developed at one site to similar sites, while the support of industry pioneers is required to move technology ahead as economically as possible and show success, thus attracting other industry players.

Conclusions

In this cost-shared feasibility study for EGS development at Desert Peak, we have focused

on an existing hot, non-commercial well on the margins of a conventional hydrothermal field. Geological analysis has yielded an improved understanding of the regional and local geology, particularly the pre-Tertiary units encountered at depth in well DP23-1. Analysis of a wellbore image log has allowed the orientation of the stress field to be determined, and together with geologic and hydraulic data, has led to the identification of a target interval for hydraulic stimulation. Plans have been formulated to obtain essential stress-related data and re-complete well DP23-1 in preparation for massive hydraulic stimulation. Additional evaluations focus on enhancing the permeability of a non-productive well in the hydrothermal portion of the field.

Collaboration with specialists at the University of Nevada (Reno), the USGS and the National Laboratories, and technical contact with other EGS and HDR project teams around the world, have contributed significantly to the progress made at Desert Peak. This cooperation will expand as the project enters the next phase.

Field demonstrations such as those underway at Desert Peak and elsewhere in the world are essential steps toward EGS commercialization. For the Desert Peak EGS project, we have leveraged to the fullest extent possible the previous and ongoing work of individuals and groups already working in this field in an attempt to adapt them for commercial EGS implementation. Since ORMAT and GeothermEx are commercial entities, our participation is important for the future of wide-scale EGS development, which can provide a significant amount of base-load, renewable power in many countries. The heat reserves in the United States are significant, and they are particularly accessible in the Basin and Range, where the Desert Peak project may well serve as a blueprint for other EGS projects.

Acknowledgements

The authors gratefully acknowledge the support for this project from the U.S. Department of Energy, Assistant Secretary for Energy Efficiency and Renewable Energy, Geothermal Technologies program under a cooperative agreement with Golden Field Offices, DE-FC36-02ID14406 for EGS field projects. We also thank Judith Sheridan and Dan Moos of GeoMechanics International for many enlightening discussions of stress-related issues. We are particularly grateful to Steve Hickman of the US Geological Survey for sharing his extensive knowledge of stress data, and for his help in developing practical ways to obtain such data at Desert Peak.

References

Faulds, J.E. and L.G. Garside, 2003. Preliminary geologic map of the Desert Peak-Brady geothermal fields, Churchill County, Nevada. Nevada Bureau of Mines and Geology Open-File Report 03-27.

Faulds, J.E., L.G. Garside and G. Oppliger, 2003. Structural analysis of the Desert Peak-Brady geothermal field, western Nevada: implications for understanding linkages between NE-trending structures and geothermal anomalies in the Humboldt Structural Zone. Transactions, Geothermal Resources Council, Vol. 27, pp. 859 – 864.

Hickman, S., Zoback, M.D., and Benoit, W.R., 1998. Tectonic controls on reservoir permeability in the Dixie Valley, Nevada, geothermal field. Proceedings, 23rd Workshop on Geothermal Reservoir Engineering, Stanford University, pp. 291 - 298.

Hickman, S.H., Zoback, M.D., and Healy J.H., 1988, Continuation of a deep borehole stress measurement profile near the San Andreas Fault, I: Hydraulic fracturing stress measurements at Hi Vista, Mojave Desert, California. Journal of Geophysical Research, Vol. 93, pp. 15,183 – 15,195.

Lutz, S.J., A. Schriener Jr., D. Schochet and A. Robertson-Tait, 2003. Geologic characterization of pre-Tertiary rocks at the Desert Peak East EGS project site, Churchill County, Nevada. Transactions, Geothermal Resources Council, Vol. 27, pp.865-870.

Robertson-Tait, A., C. Morris and D. Schochet, 2005. The Desert Peak East EGS project: a progress report. Proceedings, World Geothermal Congress, Antalya, Turkey.

Robertson-Tait, A., S.J. Lutz, J. Sheridan and C.L. Morris, 2004. Selection of an interval for massive hydraulic stimulation in well DP 23 1, Desert Peak East EGS project, Nevada. Proceedings, 29th Workshop on Geothermal Reservoir Engineering, Stanford University, pp. 216 – 221.

Robertson-Tait, A., and C. Morris, 2003. Progress and future plans at the Desert Peak East EGS project. Transactions, Geothermal Resources Council, Vol. 27, pp. 871 - 877.

Sanyal, S.K. and S.J Butler, 2005. An analysis of power generation prospects from Enhanced Geothermal Systems.

Proceedings, World Geothermal Congress, Antalya, Turkey.

Sanyal, S.K., J.W. Lovekin, R.C. Henneberger, A. Robertson-Tait, P.J. Brown, C. Morris and D. Schochet, 2003. Injection testing for an Enhanced Geothermal Systems project at Desert Peak, Nevada. Transactions, Geothermal Resources Council, Vol. 27, pp. 885 – 891.

Sheridan, J.M. and S. H. Hickman, 2004. In situ stress, fracture and fluid flow analysis in well 38C-9: an Enhanced Geothermal System in the Coso geothermal field. Proceedings, 29th Workshop on Geothermal Reservoir Engineering, Stanford University, pp. 268 – 275.

ENGINE – **EN**hanced **G**eothermal **I**nnovative **N**etwork for **E**urope
Workshop 3, "Stimulation of reservoir and microseismicity"
Kartause Ittingen, Zürich, June 29 – July 1, 2006, Switzerland

Characterization of reservoir using microseismicity induced during stimulation tests: contribution from tomographic analysis and faulting mechanisms

CUENOT Nicolas, GEIE Exploitation Minière de la Chaleur, Soultz-sous-Forêts, France, cuenot@soultz.net;
CHARLéTY Jean, EOST, Strasbourg, France;
DORBATH Catherine, IPGS-EOST Strasbourg, France;
DORBATH Louis, IPGS-EOST Strasbourg, France;
HAESSLER Henri,IPGS-EOST Strasbourg, France

Abstract

Tomographic and faulting studies represent two efficient ways to characterize the behaviour of geothermal reservoirs during stimulation tests. Tomographic analysis of induced microseismicity give two types of results: the 3D distribution of seismic velocities within the medium and precise relocation of the microseismic events, using the velocity model previously found. Analysis of faulting mechanisms, especially through focal mechanisms studies, is able to give informations on the main shearing structure and the type of movements that they support.

In the case of the stimulation of EGS-type reservoir, numerous microseismic events are generally recorded; that allows performing reliable tomographic calculation. Moreover, this huge quantity of data can be used to follow the temporal evolution of the 3D distribution of the seismic velocities, which brings useful information on the effect of the circulating water on the physical properties of the reservoir. Using a velocity model that takes into account the temporal variation of the seismic velocities allows getting a very precise relocation of the microseismic events. This, combined with the analysis of the faulting mechanisms through the reservoir gives a rather good view of the shearing processes in the reservoir.

In this study, we analyses the microseismic events induced during two tests: the stimulation of GPK2 in 2000 and of GPK3 in 2003, both performed between 4.5 and 5 km depth. The temporal evolution of the 3D distribution of seismic velocities during the injections is calculated in both cases, leading to conclusions about the variations of the properties of the reservoir. The analysis of the relocated microseismic cloud demonstrates that some major structures, probably corresponding to major faults, play a dominant role in the generation of seismic events, both of small and higher magnitude.

From the focal mechanisms study, it appears that normal faulting, with a more or less pronounced strike-slip component, represent the major regime, but quasi pure strike-slip movements are also observed. From the recorded first-motion polarity data, an estimate of the stress tensor has been calculated and then applied to the nodal planes determined from focal mechanisms: orientation and dip of fractures having sheared can thus be retrieved. Moreover, all determined focal mechanisms show a double-couple solution, but from the analysis of the seismic moment tensor for several 2003 events, we have been able to quantify the proportion of the non-double-couple (NDC) component, which correspond to the proportion of opening in the shearing process. It is interesting to observe that events in the vicinity of the injection well GPK3 show a higher NDC component, than those far from the injection.

The combination of results given by all these methods, applied to two different datasets gives thus very valuable information on the mechanical processes that occur within the reservoir under stimulation conditions.

Keywords: Stimulation, Microseismicity, Tomography, Focal mechanisms, Stress.

Introduction

Since the beginning of the development of the HDR/EGS technology, it has been proved that seismology is one of the powerful tools to understand the physical processes associated with fluid injection within geothermal reservoirs. The analysis of induced microseismicity is a very convenient way to follow for example fluid circulation and

pressure wave propagation throughout the reservoir, as well as the expansion of the stimulated rock volume, which usually corresponds to the zone of permeability enhancement. Furthermore seismology can help to estimate the faulting mechanisms through the study of the failure modes on fault planes and of the state of stress within the reservoir.

The massive stimulation tests at Soultz-sous-Forêts in 2000 and 2003 generated a huge number of microseismic events, which were recorded in both cases by a surface and a downhole seismic array. The collected databases have been studied from different ways: precise events locations through tomographic procedure and the spatio-temporal distribution of seismicity, analysis of fault-plane solutions, faulting mechanisms and stress field, and evolution of seismic velocities in the reservoir during injections. The initial attempt was to understand the occurrence and behaviour of seismicity in relation with the hydrological parameters, in order to get insights about the physical processes leading to the generation of seismic events.

In this paper, we present EOST's main results obtained from the stimulation of boreholes GPK2 and GPk3 in 2000 and 2003 respectively, in terms of events spatio-temporal distribution, faulting mechanisms, stress field and velocity variations.

Tomographic studies: location of microseismic events and velocity structure

Seismological network

In 2000, the seismic network comprises around 20 stations divided into a telemetered network with eight vertical sensors, a network composed by six autonomous three-component sensors, and three four-component sensors deployed in wells at around 1.5 km depth. The latter is owned by the EEIG "Heat mining". The network changed in 2003.

Since the beginning of 2003, a field-wide permanent seismic network has been in place and has been run by a team at the Institut de Physique du Globe from Strasbourg (France). The network comprises 9 stations and covers the geothermal reservoir. The sampling rate is 6.66 ms. The frequency band of the acquisition is from 1 to 48 Hz. Three stations have three-components sensors and the others only vertical ones. Fourteen additional seismometers have supplemented the permanent network. Six stations have three-component sensors and the others only vertical ones. The three-components sensors have the same characteristics as the permanent network. The vertical seismometers have a sampling rate of 5.55 ms and the frequency band is from 1 to 60 Hz.

Hydraulic stimulations of 2000 and 2003

The aim of the 2000 stimulation was to improve the hydraulic connection between the well GPK2 and the endemic fracture system. It started on the 30th of June and lasted almost seven days. The flow-rate followed a step-wise strategy. The first step lasted less than one day with a flow-rate of 30 l.s^{-1}; the second lasted more than one day with a flow-rate of 40 l.s^{-1}; the third part lasted around 4 days with a flow-rate of 50 l.s^{-1} (figure 1 top).

The aim for the 2003 stimulation did not change but the well GPK3 was concerned: improvement of its injectivity and the relatedness between the two wells. It started on the 27th of May and lasted 11 days. The fluid injection strategy was more complex than in 2000. The flow-rate has been up to 93 l.s^{-1} on a very short period (some hours) (figure 1 bottom).

Method

Data

The data from all seismic sensors have been picked and used for the tomography. In 2000, more than 10 000 events have been recorded. More than 7000 events have been used to perform the tomography. The P and S arrival times have been manually picked (Cuenot et *al.*, 2005). For 2003 an automatic detection algorithm has been used. More than 6000 events have been detected. The data have been automatically picked by an AR-AIC algorithm (Leonard and Kennett, 1999). The tomography has been achieved with about 2250 events. Concerning the S wave arrival time picks, where shear wave birefringence was noted, the earliest S arrival was picked. S waves were picked only on horizontal components. A first location of the events was made by a hypoinverse-like algorithm with a 8 tabular layers model. This model is based on the information derived from different log-data and the calibration shot in 1987.

Tomographic algorithm

The tomography method used is based on the program simulps (Thurber, 1983). Simulps uses an iterative, damped least squares method to invert arrival times and simultaneously estimates earthquake locations

and the three-dimensional V_p and V_p/V_s fields. The velocity structures are parameterized by values defined at the nodes of a three-dimensional grid, between which the V_p and V_p/V_s values are assumed to follow trilinear functions.

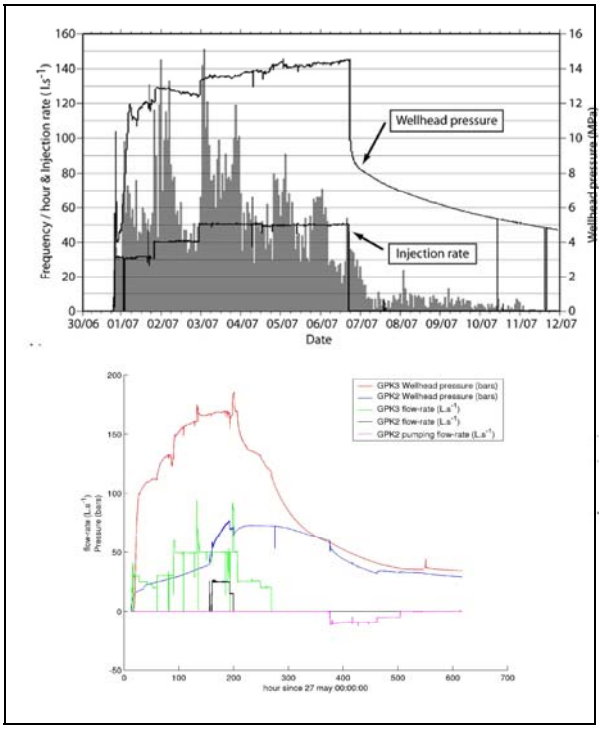

Figure 12 Injection strategy for 2000 (top) and 2003 (bottom). Top: are represented the wellhead pressure and the injection rate. In grey appears the number of seismic events per hour detected on the surface seismic network. Bottom: the wellhead pressure of GPK3 (red) and GPK2 (blue), and the flow-rate in GPK3 (green) and GPK2 (black and purple) are represented. The purple curve corresponds to the pumping strategy in GPK2.

Zhang and Thurber (2003) have developed a new method that combines both absolute and relative arrival time data. The method determines a 3D velocity model jointly with absolute and relative event locations. They developed a double difference (DD) tomography code (tomoDD) based on the DD location code hypoDD (Waldhauser, 2001). In their simultaneous inversion for velocity structure and event locations, velocity anomalies are constrained by seeking a first-order smooth model. The same smoothing weight is applied to the horizontal and vertical regions. This smoothing regularization should provide a minimum-feature model that contains only as much as structure as can be resolved above the estimated level of noise in the data.

The two different types of data are combined into one system thanks to a hierarchical weighting scheme during the inversion. We start the inversion by applying greater weight to the absolute catalog data (1 for absolute data, 0.1 for differential catalog data) to establish the large scale result. The differential catalog data are weighted more to refine the event locations and the velocity structure near the source regions (1 for differential data, 0.1 for absolute catalog data). Then we finish the inversion by weighting equivalently both catalogs. For each step, two iterations are performed. The system is solved by a LSQR algorithm for the damped least-square problem.

The tomography method has changed between 2000 and 2003. In 2000, we used the simulps methodology while in 2003, tomoDD is used. As for both years the number of events is important, we decided to divide them into temporal sets so that the evolution of the velocity structure can be imaged. For 2000, a set of data is composed by 500 events. In 2003, as a differential catalog data is also used, the number of events per sample is set to 250. In 2003 the number of events per set has been chosen in order to appreciate the effect of each injection stage: increase or decrease of the flow-rate, dual injection (injection in GPK2 and GPK3), shut-in.

The grid covered the whole area determined by the location of the seismic sensors. As the rays intercept each other in the volume of the reservoir the resolution of the tomography is good only at the depth of the injection. Thus the grid has been refined in this part.

The initial model for both tomographies is the same for each set of data and tomography.

The tomoDD code is similar to simulps if the relative catalog is not taking into account in the inversion (weight is put to 0). We have tested this approach on the first set in order to appreciate the difference between the methods. The difference in the results is quite small and it appears that the velocity values for the simulps inversion are almost always greater.

Other tests have been made. The 3D velocity model obtained is almost insensitive to starting model, event set and inversion strategy.

Results for the 2000 and 2003 stimulations

The velocity structure of each tomography is corrupted by the lack of knowledge of the velocity model before the stimulation. The region is seismically quiet so that no natural seismicity has been locally recorded prior to

the hydraulic experiments. It is also obvious that the seismicity is linked with the injection of fluid. A pre-stimulation tomography could have given us essential information on the steady state in the reservoir. Nevertheless we described the global evolution of the velocity structure in term of shape and value. We consider that as the treatment of each set is exactly the same the variation from one set to another is meaningful.

Temporal evolution of the V_P velocity structure during the 2000 stimulation test

A sequence of fourteen successive images was computed to observe the evolution of the V_P velocity in the geothermal reservoir (figure 2). On each plot are represented the corresponding 500 events used for the calculation to outline the shape and position of the microseismic cloud at that time. The trajectory of the open-hole section of the well GPK2 is also indicated. Grey zones do not have to be considered as they correspond to low-resolution areas.

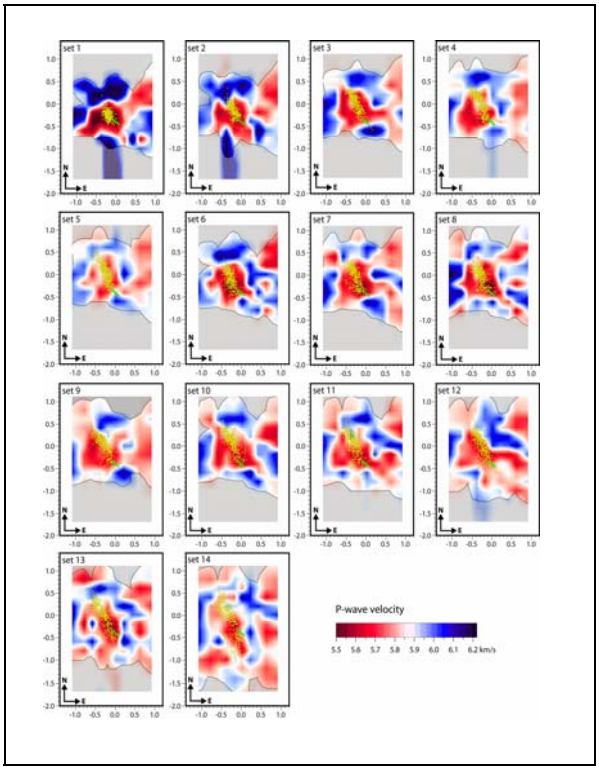

Figure 2. Evolution of the P-wave seismic velocity at 4.6 km depth during the 2000 stimulation test. Images are in chronological order from set 1 to set 14. Yellow dots represent the 500 events used in the computation for each subfigure. The green line corresponds to the open-hole section of the injection well GPK2. Grey areas do not have to be considered as they define zones of poor resolution.

Figure 2 presents the temporal evolution of the velocity structure at a depth of 4.6 km, corresponding to the location of the stimulated rock volume. Set 1 is calculated using the 500 first events of the stimulation. The dark red colour clearly denotes a significant low-velocity anomaly: the plotted microseismic cloud indicates that this anomaly corresponds to the geothermal reservoir. It is difficult to interpret this first result, as we cannot compare the present situation to that before the beginning of the injection: is the anomaly directly due to the start of the stimulation or does it actually exist before? Set 2 to set 5 show a slight increase of the velocity from 5.6 $km.s^{-1}$ to about 5.8 $km.s^{-1}$. An interesting feature appears between set 5 and set 6: on the figure 2 one can notice the reappearance of the dark red colour at the place of the geothermal reservoir, indicating a sudden decrease of the P-velocity of about 0.2 $km.s^{-1}$. Then, until the end of the recording period, velocity slowly increases in the same way as at the beginning of the experiment. What does induce the quick decrease of the velocity? It appears from the injection curve that set 6 contains events occurred just after the increase of the injection rate to 50 $l.s^{-1}$. We did not indeed observe such a variation between set 3 and set 4 although the injection rate was incremented from 30 $l.s^{-1}$ to 40 $l.s^{-1}$ between these periods. Nevertheless, we found some clear correlations between the increase of injection rate up to 50 $l.s^{-1}$ and change in the hydrological parameters and seismic activity evolution that we cannot observe after the augmentation from 30 $l.s^{-1}$ to 40 $l.s^{-1}$.

Temporal evolution of the VP and VS velocity structure during the 2003 stimulation test

A sequence of nine successive images was computed to observe the evolution of V_P velocity in the geothermal reservoir. On figure 3, are represented for each set the seismicity in black dot and a white line outlining the region where the number of rays per node is greater than or equal to 50. This number of rays commonly determines the part of the figure where the inversion resolution is good. The code tomoDD does not compute the resolution as the least square theory allows.

For the P wave velocity (figure 3), the views represent the evolution of the absolute velocity on horizontal plane at 4.6 km depth. On the first set, a large low P-wave velocity area dominates the first order spatial variation in V_p structure. This area is located around the well GPK3 near the coordinate (0;-1). This set is associated with the period where the flow-rate is not higher than 30 $l.s^{-1}$. Set 2 corresponds to

an increase of the flow rate to 50 $l.s^{-1}$. We observe that the velocity decreases and that the region affected by this change grows.

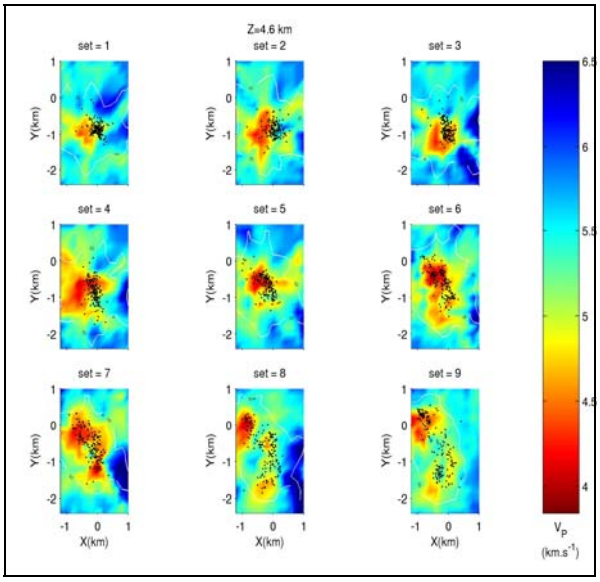

figure 3: Evolution of the P-wave seismic velocity at 4.6 km depth during the 2003 stimulation test. Images are in chronological order from set 1 to set 9. Black dots represent the 250 events used in the computation for each subfigure. The white line outlines the zone in which the number of rays per node if greater than or equal to 50, and which is supposed to be the good resolution area. North is directed toward positive Y while the East is toward positive X. GPK3 is around (0,-1) and GPK2 (-0.2,-0.5).

Then in the set 4 the velocity tends to slightly increase. The injection in both GPK2 (-0.2;-0.4) and GPK3 induces an increase of the velocity and the growth of the affected area on the northwestern part. Set 5 corresponds to the end of the dual injection. We note that the velocity increases around GPK3 and decreases around GPK2. Set 6 and 7 coincide with the end of the injection in GPK3. We can notice that the velocity remains nearly the same but the location of the maximum velocity region near GPK2 migrates to the northwestern part of the reservoir. Moreover a region where the velocity increases appears southward of GPK3. In the set 8 and 9, the low velocity zone continues its migration toward the northwest and the south away from the injection point. The set 9 corresponds to an active period since, in order to accelerate the pressure decrease, a production strategy in GPK2 has been decided.

Interpretation

The relation between flow-rate change and velocity variation is clear for both experiments. In 2000, a difference of behaviour from the geothermal reservoir appears between the flow-rate of 30-40 $l.s^{-1}$ and 50 $l.s^{-1}$. Actually, the decrease of the velocity is higher for the maximum flow-rate. This observation can also be made for 2003. Moreover for the last experiment the effect of the dual injection (injection in both well GPK2 and GPK3) appears clearly on the velocity of the P wave.

Factors that affect V_p include porosity (Wyllie *et al.*, 1956, 1958), pore pressure, partial saturation (Nur and Simmons, 1969a), phase transition (Ito *et al.*, 1979) and temperature.

The correlation between the velocity decrease and the flow-rate means that a possible mechanism for the velocity variation is the increase of pore pressure and/or porosity, because both phenomenons entail a decrease of the velocity for P wave. The schematic model for this mechanism is an increase of the pressure near the well caused by the injection. This overpressure creates microcracks through which the fluid can migrate. The microcracking generates porosity and the fluid penetration in the rock mass increases the pore pressure. The effect of pore pressure depends strongly on the saturation of the medium. Then the slow increase of the velocity afterwards can be caused by the effects of the cooling of the medium due to the injected fresh fluid and the increase of the saturation of the medium. Both mechanisms induce a velocity increase. The direction of northwest-southeast propagation fits with the direction of regional maximum horizontal stress (NNW-SSE to N-S). This direction has been determined (Tenzer *et al.*, 1991; Rummel and Baumgärtner, 1991; Klee and Rummel, 1993; Benderitter and Elsass, 1995; Helm, 1996; Cornet and Bérard, 2003) several times in the Upper Rhine Graben region.

In 2003 we note that the northwestern part of the reservoir has still a low velocity zone after the shut-in. In this region, the largest seismic events have occurred in 2000 and in 2003. The set 8 and 9 which correspond to the period after the shut-in show clearly this feature. The decrease of the velocity is due to either porosity or pore pressure. Therefore two scenarios could be guessed. The first one considers that the fluid is led to this region for some reasons so that a large part of the injected fluid remains in this area. The mechanism to invoke is so the pore pressure. The second scenario considers that as the region is submitted to a larger magnitude seismic activity (up to 3 in duration magnitude), the porosity increased and thus the P wave velocity decreased.

The 2003 tomography of allows to observe that after the hydraulic activity, the medium returns to a kind of equilibrium state. It demonstrates that the medium is perturbed by the injection and permit to consider that the first image (set 1) is fully a consequence of the injections.

The tomography used either in 2000 or in 2003 relocates the seismic events in the 3D velocity model. This relocation refines the error in latitude, longitude and depth so that the final uncertainty is around 20 to 30 meters. In 2003 the relocation of the seismic event points out the relation that exists between the seismic activity and the natural endemic fractures. The figure 4 shows the relocation of the 250 first events corresponding to the first set. The fracture represented has been imaged by UBI and the characteristic of the plane has been determined by Dezayes *et al.* (2004). This fracture absorbed around 80 % of the fluid injected as determined by a flow-log. The weakening of the fracture by the fluid entails the occurrence of a large part of the seismicity.

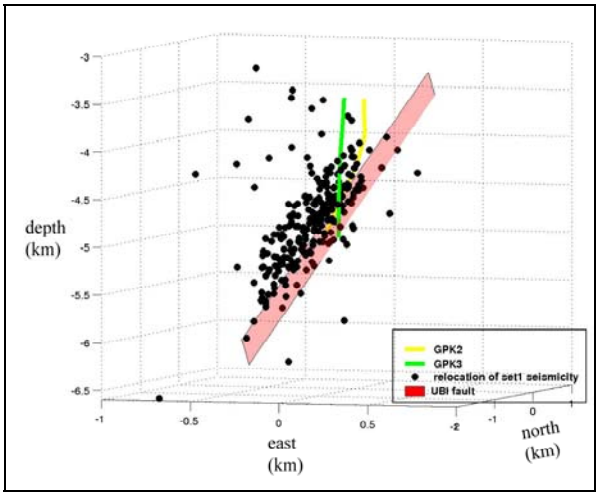

Figure 4. The seismicity relocated in the 3D model velocity determined by the tomography. This seismicity is located just above the fracture imaged by UBI (pink-red plane). The well GPK3 is in green and GPK2 in yellow.

Faulting mechanisms: fault-plane solutions, non double couple component and stress regime

Fault-plane solutions

We determine automatically several thousands of focal mechanisms using the program FPFIT (Reasenberg and Oppenheimer, 1985): nodal planes are calculated from the first-motion polarities by a maximum likelihood procedure and manually checked afterwards. More than 14 polarities are available in average for the 2000 events and more than 16 for the 2003 seismicity. Results indicate a majority of normal-faulting movements, pure or with a more or less pronounced strike-slip component. But, on the deepest part of the reservoir, a strike-slip regime seems to dominate, with some quasi-pure strike-slip events. Some representative focal mechanisms examples for the 2000 and 2003 stimulation tests are given in Fig. 5 and Fig. 6.

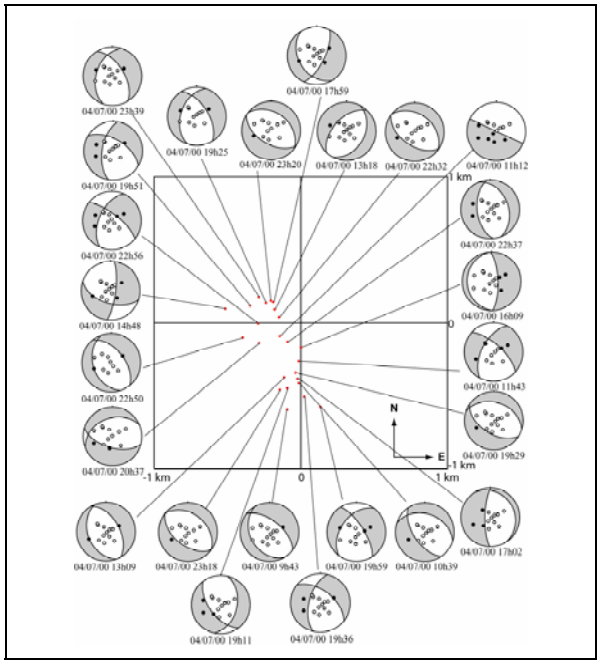

Figure 5. Representative focal mechanisms for the 2000 stimulation test.

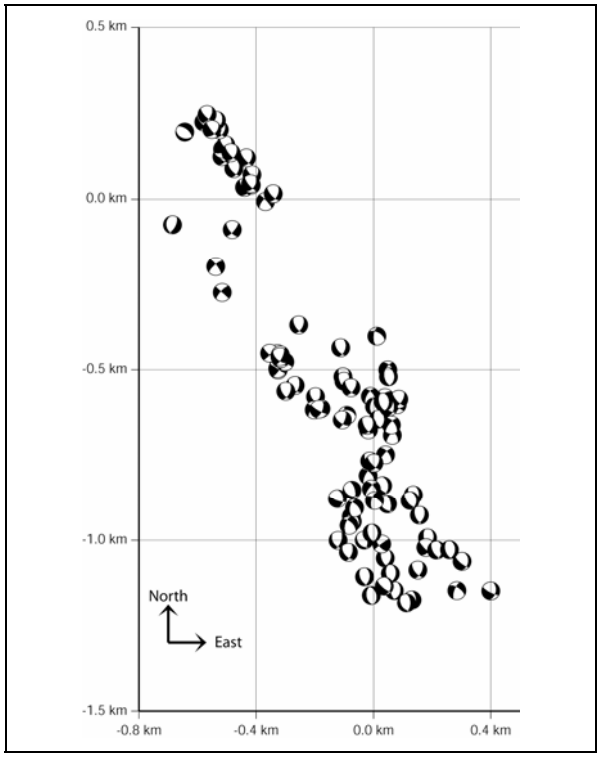

Figure 6. Representative focal mechanisms for the 2003 stimulation test.

Non Double Couple Component

From the full determination of the seismic moment tensor (1st order) we are able to describe the equivalent forces at the source, which can be correlated with the physical processes involved at the source. Moreover, the seismic moment tensor can be written as the sum of a double couple (DCC) component and a non double couple component (NDCC), which gives the proportion of tensional opening in the seismic rupture. This proportion is here expressed as a function of an index ε. ε ranges between –0.5 and 0.5. A positive ε indicates tensional opening in addition to shearing, while a negative ε describes compressive movements in addition to shearing. If $0 \leq \varepsilon \leq 0.25$, the DC component dominates. This is the case in our study, as we have been able to find a DC solution for each seismic event. However, the variations of ε between 0 and 0.25 give the proportion of NDC component in the movement. On the Figure 7, several 2003 events are presented as coloured spheres. The colours correspond to the value of ε. As all events were similarly computed, the variations of ε between each others are significant. It is striking that events occurred at the direct vicinity of the injection well GPK3 show a high value of ε. However, events occurred far from the injection well do not show such a high value of ε. Some of these latter events even have a zero ε value. It indicates that events in the vicinity of GPK3 have a non negligible NDC component, and the fractures that support the rupture may undergo tensional opening in addition to shearing. This result may be a consequence of a large overpressure increase near the well due to the massive injections, which can cause the joints to slightly open. On the contrary, if we are far away from the injection well, the fracture tensional opening component seems to be in less proportion. It would mean that the overpressure is less effective, maybe because it quickly drops with the increasing distance from injection well.

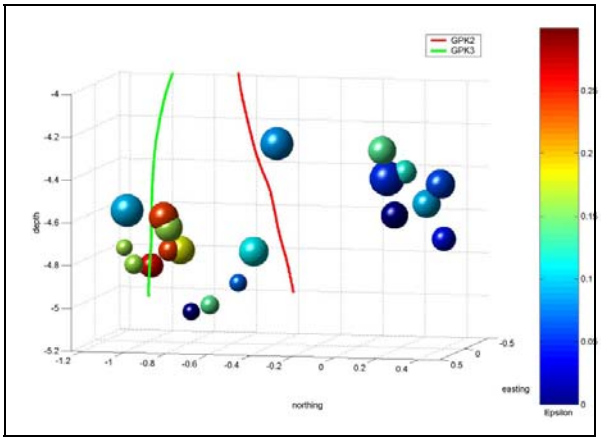

Figure 7: Non double couple component proportion for several 2003 events.

In conclusion, we determine a double couple solution for each microseismic event, which indicates that the dominant process of the faulting movements is shearing. This result seems quite common also at other HDR sites. But, by the analysis of the seismic moment tensor, we show that the rupture process involves a non double couple component. This indicates a proportion of tensional opening at the fracture planes. Moreover this NDC component is significantly higher for events in the vicinity of the injection well, probably because of greater pressure effects.

Stress tensor inversion

Two observations suggested us to perform a stress tensor inversion. First our results on focal mechanisms show a higher proportion of strike slip events in the deepest part of the geothermal reservoir. Moreover Klee and Rummel (1993) determine a stress regime profile at Soultz-sous-Forêts using hydrofracturing stress measurements. Their results show a possible cross-over between the vertical stress S_V and the maximum horizontal stress S_H at around 3500-4000 m depth. This would imply a change in the faulting regime with depth, from a normal-faulting regime to a strike-slip regime. In order to check the reliability of the assumption, we decided to perform the stress tensor inversion.

Method

We used the method of Rivera and Cisternas (1990), which involves the direct inversion of the deviatoric part of the stress tensor and of focal mechanisms from first-motion polarity data. The stress tensor is defined by three Euler angles and a shape factor, which indicates the faulting regime. From an initial trial solution (tensor and focal mechanisms), theoretical polarities are calculated and compared to the observed data at each iteration. Then the solution is modified in order to maximize a likelihood function. The quality of the solution is expressed in terms of likelihood and score (the score describes the fit between observed and theoretical polarities).

Data

We performed two inversions with two different data sets of events from the 2000 stimulation experiment. A first set contains microseisms occurred in the upper part of the reservoir (depth $\leq$ 4.5 km), the second is composed of events occurred in the bottom part of the reservoir (depth $\geq$ 5 km). For each set, about

60 microseismic events have been randomly selected among those which exhibit the largest number of available polarity data. Indeed, each selected event shows a number of polarities between 14 and 18. In order to check the reliability of the inversion, we performed several calculations with different sets containing different arrangements of events. Similar results have been obtained from the different calculations.

Results

The results of the inversion are shown in Figure 8 and Figure 9. In both figures, the picture at the top corresponds to the 100 best tensor solutions and the bottom picture gives the best estimate of the stress tensor. Figure 8 shows the inversion for the upper part of the reservoir while results of the inversion for the bottom part are displayed on Figure 9. Stresses are expressed in terms of σ_1, σ_2 and σ_3, where $\sigma_1 > \sigma_2 > \sigma_3$.

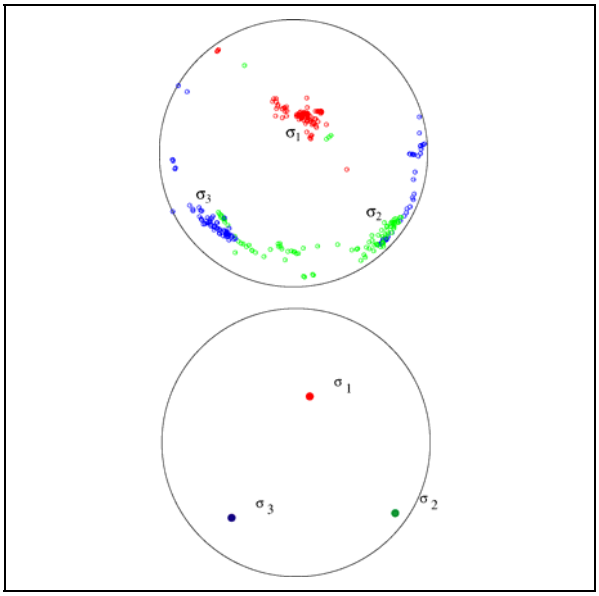

Figure 8: Results of the stress tensor inversion for the top of the reservoir. Top: 100 best tensor solutions; Bottom: best tensor solution.

A first observation is the stability of the orientation of the minimum horizontal stress S_h, which trends in both cases NE-SW to NNE-SSW. This is in agreement with the general orientation of S_h at regional scale in the upper Rhine Graben. On both figures the maximum horizontal stress S_H is oriented NW-SE to NNW-SSE. This result is also consistent with regional estimates of S_H. However, at local scale, other studies show a more N-S orientation of the maximum horizontal stress (e. g. Bérard and Cornet, 2003). The method of Rivera and Cisternas suppose that the stress tensor is homogenous over the studied region. In the case of Soultz-sous-Forêts, fluid injections may introduce strong local stress heterogeneities that we cannot see with our inversion method: our results may correspond to an "average" stress tensor, which could be more representative of the regional stress field. The relative scatter of the solutions may reflect these stress heterogeneities.

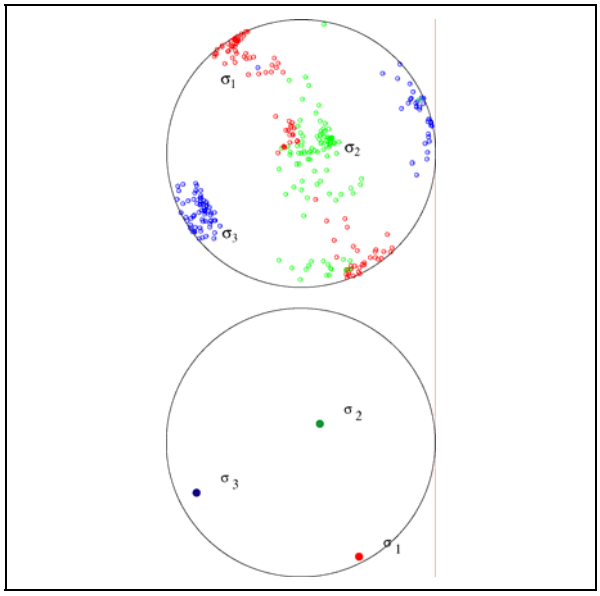

Figure 9: Results of the stress tensor inversion for the bottom of the reservoir. Top: 100 best tensor solutions; Bottom: best tensor solution.

But the most important result concerns the rotation of the maximum stress σ_1 from a subvertical orientation at the top of the reservoir (Fig. 8) to a horizontal direction (Fig. 9). We effectively observe this feature, which was predicted by other measurements. It means that the maximum horizontal stress S_H becomes the maximum stress at the bottom of the reservoir. Thus this implies a change in the failure mode. At the top of the reservoir, the dominant regime is normal-faulting whereas strike-slip is likely to occur in the deepest part of the reservoir. This result is in agreement with the results on focal mechanisms. Nevertheless, both figures 8 and 9 show a relative dispersion of the solutions. In particular on figure 9, some solutions still indicate a subvertical trend for σ_1 and a subhorizontal direction for σ_2. This suggests that the faulting regime may have not completely changed at the bottom of the reservoir, that is, the stimulated volume is located within the region of stress rotation. And moreover, this confirms the fact that the magnitudes of S_V and S_H are very close, as suggested by Klee and Rummel (1993), facilitating the stress rotation.

3-D Imaging of the fractures network

We applied the stress tensor on the nodal planes that we determine for the 2000 stimulation in order to define the plane having sheared. Figure 10 shows the result in a 3D view.

The majority of fault planes are oriented NNW-SSE to NW-SE with a dip either to the West or to the East. We can also observe that most of the planes dipping to the West are subvertical, while those dipping to the East seem more subhorizontal. In addition, several fault planes exhibit an "en echelon" structure. Nevertheless, the fracture system appears to be rather heterogeneous.

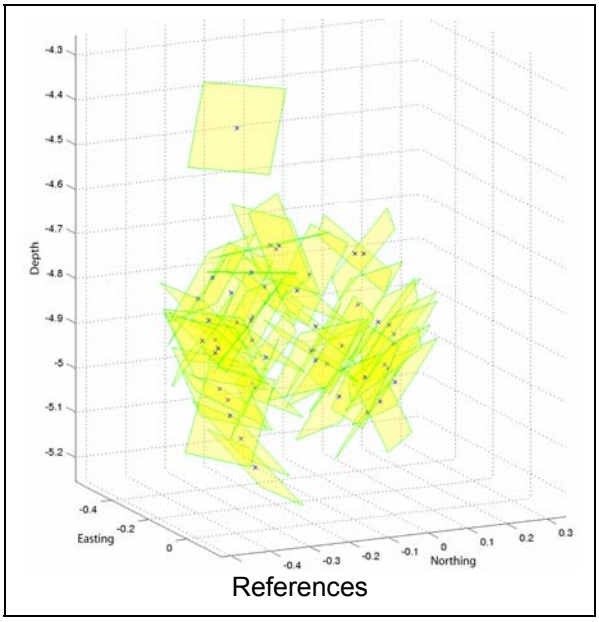

References

Figure 10: 3D representation of the fractures network.

Conclusion

In both stimulations the seismicity appears to be injection rate and volume dependant. Both experiments show that for instance an increase of the flow-rate induces an increase in number and often in magnitude of the seismic events. Furthermore, a larger proportion of larger magnitude events is observed after shutting in, although this does not lead to an increase of the number of events. As highlighted by the tomographic study, this is probably related to the variation of the physical properties inside the fault zones and in the surrounding rocks, which are due to fluid circulation, pressure variations, thermal effects and geochemical processes during fluid/rock interactions. This assumption is especially true for the vicinity of the injection well, where pressure effects are the strongest, as shown by the study of the non-double-couple component in the seismic moment tensor of several events.

The location of microseismic events seems to be highly related to the geological and tectonic settings of the region. Indeed the dimension and orientation of the microseismic cloud is in agreement with the well-known main orientation of the fracture system within the regional stress field. This is also confirmed by the fact that fault-plane solutions of events (mainly normal-faulting) correspond to what is expected from the regional tectonics. Moreover, it seems that a large part of induced seismicity, at least the stronger events, is highly related to major fault zones, which are able to drive a large proportion of the injected flow.

These observations and results shows that tomographic methods and fault-plane analysis can help understanding the behaviour of the geothermal reservoir (or at least, of the stimulated rock volume) during stimulation experiments. It can give information about the mechanical processes within the rocks and furthermore about the general tectonic conditions that are controlling shearing on fault-plane. But, some useful conclusions can also be obtained about the physical processes at the level of the rock material that are induced by injection of water. A systematic use of these methods during the course of the stimulation experiment could be a mean to check progressively the influence and effect of the injections.

Acknowledgment

This work is part of Jean Charléty's Ph.D. thesis, supported by ADEME (Agence de l'Environnement et de la maitrise de l'énergie) and Nicolas Cuenot's PhD, granted by ADEME and Conseil Général d'Alsace.

We thank also the EEIG "Heat Mining" for givingn us the hydraulic data. We also thank all the people who worked for maintaining the permanent network: Hervé Blumentritt, Michel Frogneux and Jacky Sahr.

References

Benderitter, Y., and Elsass, P. (1995), "Structural control of deep fluid circulation at the Soultz HDR site, France: a review", *Geotherm. Sci. Technol.*, vol **4**, 227-237.

Bérard, T. and Cornet, F. H. (2003), "Evidence of thermally induced borehole elongation; a case study at Soultz, France", *International Journal of Rock Mechanics and Mining Sciences*, **40**, 1121-1140.

Cuenot, N., Dorbath, C., Dorbath, L., (2005), “Analysis of the microseismicity induced by fluid injections at the Hot Dry Rock site of Soultz-sous-Forêts (Alsace, France): implications for the characterization of the geothermal reservoir properties.” *Pure and Applied Geophysics*, accepted

Dezayes, Ch., Genter, A., Homeier, G., Degouy, M., Stein, G., (2003), “Geological study of GPK3 HFR borehole (Soultz-sous-Forêts, France)”, *BRGM/RP-52311-FR*, 128 p.

Helm, J.A. (1996), “The natural seismic hazard and induced seismicity of the European Hot Dry Rock geothermal energy project at Soultz-sous-Forêts (Bas-Rhin, France)”, *Thèse de Doctorat, Ecole et Observatoire des Sciences de la Terre, Université Louis Pasteur (Strasbourg I)*, 197 p.

Ito, H., De Vilbiss, J. and Nur, A., (1979), “Compressional and shear waves in saturated rock during water-steam transition”, *Journal of Geophysical Research*, vol **84**, n° B9, 4731-4735.

Klee, G., and Rummel, F. (1993), “Hydrofrac stress data for the European HDR research project test site Soultz-sous-Forêts”, *Int. J. Rock Mech. Min. Sci. & Geomech. Abstr.*, vol **30**, 973-976.

Leonard, M., Kennett, B.L.N., (1999), “ Multi-component autoregressive techniques for the analysis of seismograms”, *Physics of the earth and Planetary Interiors*, vol. **113**, 247-263.

Nur, A., and Simmons, G. (1969a), “The effect of saturation on velocity in low porosity rocks”, *Earth Planet. Sci. Lett.* , vol **7**., 183-193.

Reasenberg, P. A. and Oppenheimer, D. (1985), “FPFIT, FPPLOT and FPPAGE: Fortran computer programs for calculating and displaying earthquake fault-plane solutions”, *U. S. Geological Survey Open-File Report 85-739*, 25 pp.

Rivera, L. and Cisternas, A. (1990), “Stress tensor and fault-plane solutions for a population of earthquakes”, *Bulletin of the Seismological Society of America*, **80**, 600-614.

Rummel, F., and Baumgärtner, J. (1991), “Hydraulic fracturing stress measurements in the GPK1 borehole, Soultz-sous-Forêts”, *Geotherm. Sci. Technol.*, vol **3**, 119-148.

Tenzer, H., Mastin, L., and Heinemann, B. (1991), “Determination of planar discontinuities and borehole geometry in the crystalline rock of borehole GPK1 at Soultz-sous-Forêts”, *Geotherm. Sci. Technol.*, vol **3**, 31-67.

Thurber, C.H., (1983), “Earthquake locations and three-dimensional crustal structure in the Coyote Lake area, central California”, *Journal of Geophysical Research*, vol **88**, 8226-8236.

Waldhauser, F., (2001), “hypoDD: a computer program to compute double difference hypocenter locations”, *U.S. Geological Survey Open File Report 01-113*, 25 p.

Wyllie, M.R., Gregory, A.R., and Gardner, L.W. (1956), Elastic wave velocities in heterogeneous and porous media, *Geophysics*, vol **21**, 41-70.

Wyllie, M.R., Gregory, A.R., and Gardner, L.W. (1958), “An experimental investigation of factors affecting elastic wave velocities in porous media”, *Geophysics*, vol ***23***, 459-493.

Zhang, H. and Thurber, C.H., (2003), “Double-difference tomography: The method and its application to the Hayward fault, California”, *Bulletin of the Seismological Society of America*, vol.**93**, n° 5, 1875-1889.

SESSION III :
Reservoir characterization during stimulation

Microseismicity and flow path identification

EVANS Keith, Swiss Federal Institute of Technology, Zürich, Switzerland, keith.evans@erdw.ethz.ch

Microseismicity constitutes the only practical tool we have of determining the likely location of flow paths in the reservoir, which is important for targeting wells to obtain satisfactory linkage between wells. However, 3-D maps of microseismic activity define regions where pore pressure has become elevated and thus is hydraulically connected to the injection well. This does not necessarily imply that the microseismically-illuminated regions contain paths that support significant flow. That is, microseismic structures are not necessarily hydrologically-significant structures. This issue of the interpretation of microseismic structures is central to the development of EGS/HDR systems. In this presentation I will examine some case histories where wells have been targeted to pass through dense microseismicity, and evaluate the success in intersecting flowing structures. I will also suggest ways of improving the ability to detect hydrologically-significant structures from microseismic observations.

ENGINE – **EN**hanced **G**eothermal **I**nnovative **N**etwork for **E**urope
Workshop 3, "Stimulation of reservoir and induced microseismicity"
Kartause Ittingen, Zürich, June 29 – July 1, 2006, Switzerland

Micro-Seismic Interpretation of Hydraulic Fracture Treatments

DE PATER Hans, Pinnacle Technologies Delft, Netherlands, hansp@pinntech.nl
WARPINSKI, N.R. , Pinnacle Technologies Delft, Netherlands
GRIFFIN, L.G. , Pinnacle Technologies Delft, Netherlands

Abstract

For completing wells in oil and gas reservoirs it is quite common to stimulate the well with a hydraulic fracture. However, the treatment is often sub-optimal because the fracture geometry is poorly known. Recent advances in micro-seismic monitoring have aided in optimizing hydraulic fractures and revealed that fracture geometry often deviates from simple modeling.

For accurate event location we need first to establish a velocity model and we will show how this can be improved by a checkshot and using initial events. Furthermore we will discuss the application in a few field cases with unexpected fracture geometry. Characterization of fracture height growth, connection with faults and complex branched fractures will be shown as examples of micro-seismic monitoring. The material in this presentation was taken from the papers by Warpinski et. al. (2003) and Griffin et. al. (2003).

Introduction

Micro-seismic imaging of fluid injection and fracturing has been pioneered in the geothermal industry. For petroleum applications, micro-seismic monitoring has become commercially available in the last decade both for reservoir monitoring and hydraulic fracture mapping. In this paper we will show a significant improvement of the location accuracy by measuring the velocity structure of the reservoir and overburden layers. A few examples will be shown of complex fracture behaviour in stimulation injections. Interaction with natural fractures and faults yields sometimes an unexpected fracture geometry. In that sense there is also a link with the first observations of geothermal stimulations (Murphy, 1986). Increasing the surface area of the fracture system is beneficial for HDR stimulation and the same applies to stimulation of very tight gas reservoirs. In many cases, however, interaction with faults hampers effective stimulation because it is difficult to pump high concentration slurry through a fracture network with width restrictions. It is likely that interaction with faults is rather common but routine treatments have only pressure measurements and then it is impossible to detect fluid channeling along faults as we will show.

Micro-seismic mapping: Location Error and Velocity Model

The location of seismic events can be accomplished by observing an event on a string of geophones and modeling the arrival times with a forward model of all the travel paths. In that way, the source location can be determined from a match between model and measurement. In addition, the phase information on the triaxial geophones can be used to determine the direction from which the waves came. Using both P and S-waves yields additional information on the source location in the inversion.

The effect of the velocity structure on the error in the locations can be illustrated with a simple case of a symmetrical, three layer system. We assume that the reservoir layer has typical sandstone compressional and shear velocities of 4500 m/sec and 3,000 m/sec, respectively, and that the bounding layers have a lower velocity of V_P and V_S of 3500 ft/sec and 2000 m/sec, respectively. For this example the ratio of the velocities is the same for both P and S waves. The best case has the array straddled over the reservoir.

The top plot of Figure 1 shows the ray paths from the microseism to each receiver. The ray paths are extremely bent by the velocity variations. The bottom plot of Figure 1 shows the locations for a constant velocity throughout the region. In one case the velocity is for the fast layer (high velocity), another is for the slow layers (low velocity), and a third is for a RMS average of both velocities. The location is found using regression on the arrival times and using a grid search approach. Both methods give the correct answer for correct velocity information, but that can be quite different depending on the error in the velocity model. The example shows that if the velocity structure is not taken

into account, the distances to the event can be in error by more than 25% of the distance to the event. Because the array is centered, however, the elevations of the events will be relatively accurate (not the case if the shale velocities are different). A worse result is obtained when the array is located above the reservoir, such as would occur if the array was placed in an older well where perforations were isolated with a bridge plug.

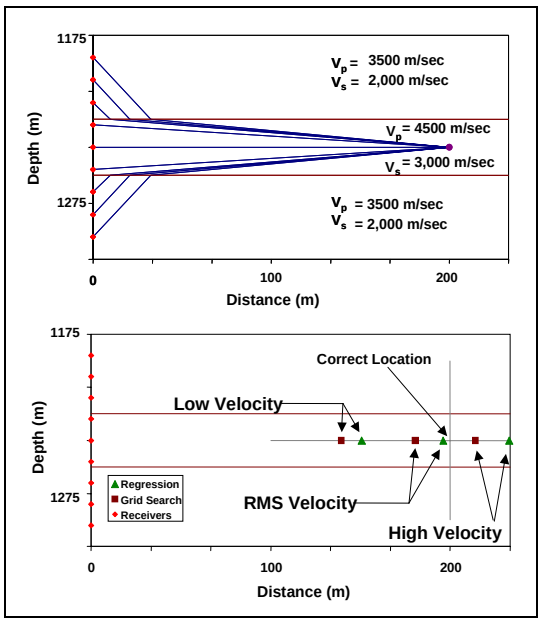

Figure 1: *Velocity-structure example for centered array.*

Formation Velocity Data

Formation velocity data can be obtained in a number of ways, but accuracy of measurement is a critical issue. Clearly, the most favorable approach is to perform a cross-well survey in order to develop P and S tomograms of the interval being studied, but even this approach is often limited to a single cross-section (lacking azimuthal information) and tomograms are seldom available for use in microseismic analysis.

In most cases the velocity is obtained from a dipole-sonic log. These logs provide high resolution of the velocity structure, but there is considerable potential for discrepancies. Most important, the measured (vertical) velocity represents the formation near the well. This may be different from the (horizontal) velocity farther from the well. A recent new development is to use VSP survey data (preferably in 3D) and combine the obtained velocity structure with the micro-seismic interpretation (Le Calvez *et. al.*, 2005). However, this is rather costly and can only be performed when there is an independent application of the VSP. Moreover, it still measures the vertical velocity.

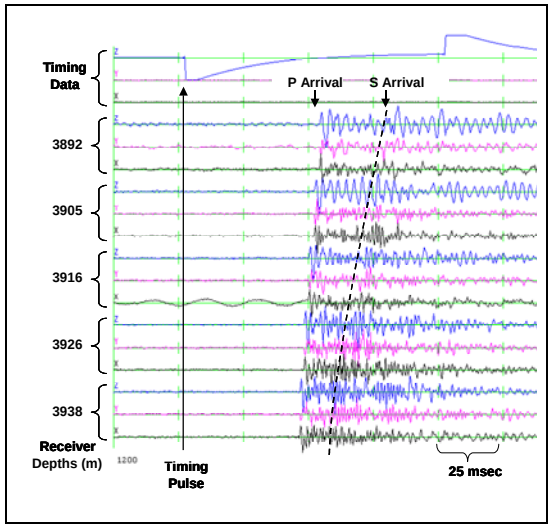

Figure 2: *Example data set from perforation with trigger pulse on zero level.*

Another approach is to jointly invert the microseismic data for both location and formation velocities. However, in petroleum applications we usually are limited to small arrays of 8-12 receivers in one or two boreholes. Systematic errors are likely to result in large inaccuracies in such cases.

A practical solution has been to use the perforation or string shot that is routinely monitored for determining the orientation of the receiver as a timed source for extracting velocity data across wells. Although we have only limited data (a few ray paths) we can determine the velocity when we assume a layered earth model. In addition we can use the velocity to calibrate more detailed sonic logs

Perforation Timing Measurements

Perforation timing measurements for velocity extraction can be made if the time that we know accurately when the perforation is fired, the arrival time at the receivers and the distance between the wells. This method has been tried by other workers, but suffered from inaccuracy in the timing of the exact perforation explosion. We have carefully investigated the sequence of events and developed an accurate electronic system for picking up the time of the perforation shot.

Data analysis results in the determination of the trigger time, the P-wave arrival times at each receiver, and the S-wave arrival times (where available) at each receiver. With perforations and string shots, the P waves are usually quite good and can be accurately detected. Often the S waves may be a problem, as these sources are not particularly good S-wave generators. However, there are

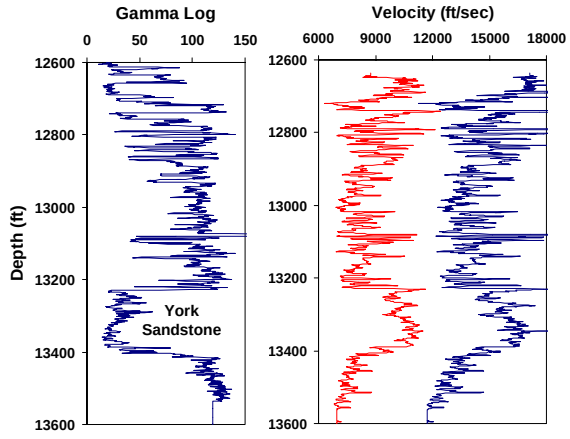

Figure 3: *Dipole sonic log of Bossier interval in example well.*

almost always some levels on which S waves can be detected. If S-waves cannot be picked clearly, we use a quick and dirty solution: we determine the S-wave velocity from the first events in a fracture injection since these will be located near the well and given this location we can determine the velocity.

In addition to the timing data, the distance between the source and each receiver must be accurately known. Accurate distance measurements require both a surface survey (or GPS measurement) and deviation surveys for both wells.

Example 1: Bossier Play

The current Bossier play is located on the western flank of the East Texas Basin. Bossier wells generally produce dry gas with little or no water production from sands embedded in the Bossier, an Upper Jurassic marine shale. Productive sands are found at depths ranging from 12,000 to 15,000 feet. Several sands are targeted in this formation, but we will show only results for the York and Bonner sands. The sand porosities generally are in the 8 to 20% range, and can have a permeability of several millidarcies, but are normally less than 0.1 mD. All producing wells in the Bossier play need hydraulic fracturing. The development of optimal fracturing procedures, therefore, has a big impact on the long-term economic viability of the play.

Velocity Measurement for Bossier Monitoring

Microseismic monitoring of hydraulic fractures in the Bossier sands is operationally difficult because of the depth and high temperature, and analysis is complicated by the complexity of the reservoirs. Figure 3 shows an example dipole sonic log run in one of the test wells in

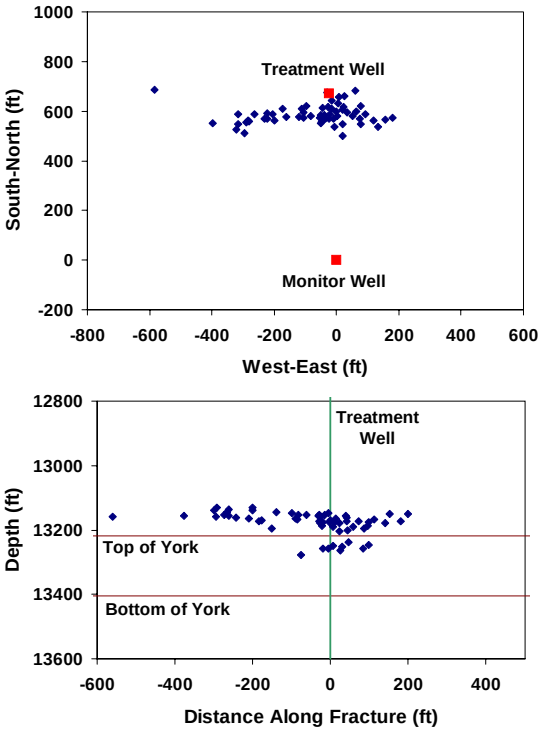

Figure 4. *Microseismic locations using 3-layer velocity structure from dipole sonic log.*

this Bossier monitoring program. Compressional-wave velocities vary from about 12,000 ft/sec to 17,000 ft/sec in the interval of interest and shear-wave velocities vary from 7,000 ft/sec to 11,000 ft/sec, based on this log. However, other sands may be present above the York sandstone in nearby offset wells, suggesting that the reservoir sizes are on the order of the well spacing.

For the first fracture treatment that was monitored in the Bossier, a limited number of high quality microseisms were selected to study velocity effects. These events were all located near or in the York sandstone. Using an initial 3-layer velocity model taken from the dipole sonic log, the maps shown in Figure 4 were obtained. As can be seen in this map, the resultant locations all appear to be too high (start well above the perforations) and too close (do not pass through the treatment well). An attempt was made to add additional layers to the velocity model, but the results did not improve significantly with even eight or ten layers.

Perforation timing measurements were performed in the treatment well as part of a three-treatment monitoring program and these data were used to calibrate the velocity structure. Only a five-level system was used because of operational constraints (a full 12-

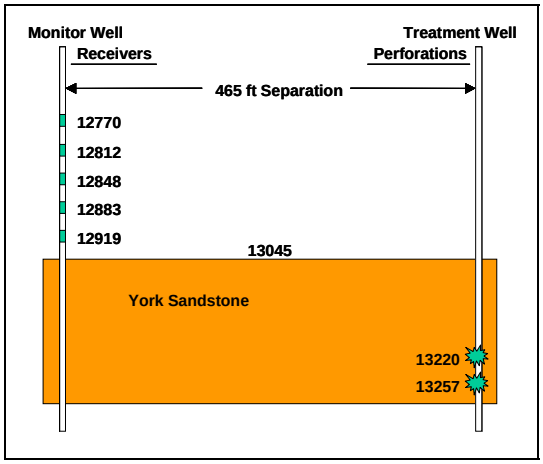

Figure 5: *Schematic layout for Bossier perforation-timing measurement.*

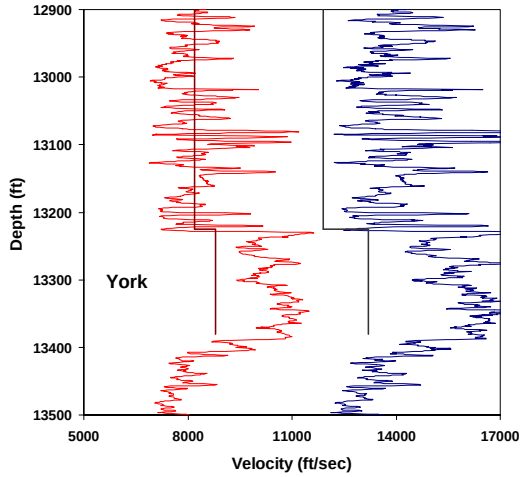

Figure 6: *Velocity comparison for Bossier test.*

level system was used for the microseismic monitoring), but two separate perforation runs were conducted, as shown schematically in Figure 5. These shots gave reasonable P-wave arrivals on all levels, but only provided clear S-wave data on a few levels of each test. From these data, it was deduced that the best-fit P-wave velocity for the York sandstone is 13,200 ft/sec and for the layers above it is about 11,900 ft/sec. For the S-wave velocities, 8,800 ft/sec and 8,200 ft/sec were determined to be appropriate velocities. A comparison is shown in Figure 6. These velocities are much different than what was obtained using the dipole sonic, but they may reflect the variability of anisotropy and sedimentary layers rather than any error in dipole-sonic measurement.

Using these perforation-timing results, the maps shown in Figure 7 were obtained. These results now start in the correct layer and pass through the treatment well, which makes the locations look much more probable. Similar behavior was observed for all three tests in this program with much more consistent locations determined using these lowered velocities. More detail was added to the velocity structure for tests having events at shallower depths, but all York and Bonner sandstone locations traversed this corrected velocity profile.

There are several potential causes for the observed discrepancy between the sonic and check-shot velocity, such as errors in the timing and distance measurement between wells. However, we see that we get a more consistent location interpretation when we use the check-shot velocity and this supports the accuracy of the perforation timing. This is generally the case when such measurements are obtained and, thus, performing perforation-timing measurements is now almost standard practice in microseismic monitoring. For most surveys we have conducted we found it critical to use the check-shot data to achieve an accurate micro-seismic event location.

APC Anderson #2 Fracture Treatment

The Bonner sand was perforated and a diagnostic injection and mini frac were conducted. Following a small acid injection the main hybrid frac was pumped in the Bonner. The injections were monitored with

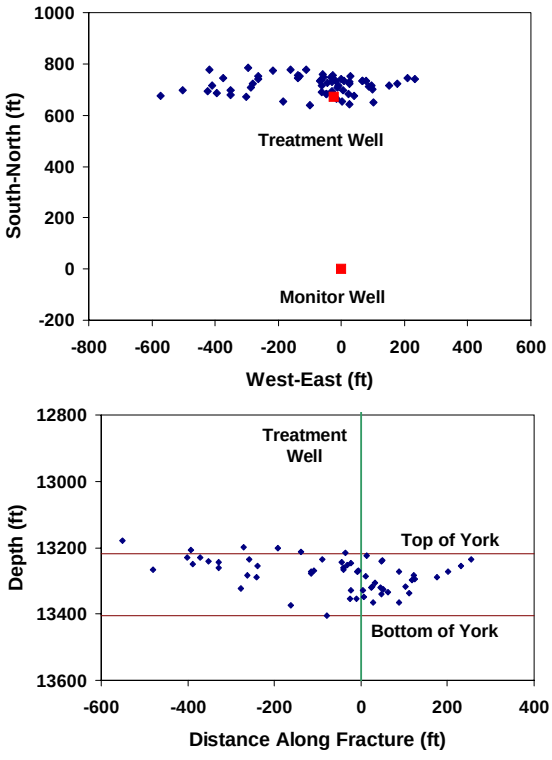

Figure 7: *Microseismic locations using 3-layer velocity structure from perforation timing.*

microseismic tools.

Figure 8 is a plot of the data collected on the Bonner stage. The 53 net feet of pay in the Bonner called for a smaller job, designed at 175,000 lbs of 20/40 proppant. We used a 35# borate gel in the crosslinked stages and the net pressure gain was over 1000 psi. Most of the net pressure rise in this treatment comes almost immediately after proppant arrives on formation, indicating a possible near-wellbore width restriction in the fracture. The relatively steep pressure increase and the instantaneous reaction to proppant indicate that this is not a tip screen-out. With the risk of a screenout with bottomhole gauges in the hole, it was decided to call flush early placing only 135,000 lbs of the designed 175,000 lbs into the created fracture.

In addition to fluid leaking off via localized faulting, the low efficiency of these jobs can also be attributed to a strong pressure dependant permeability effect in the bossier sands.

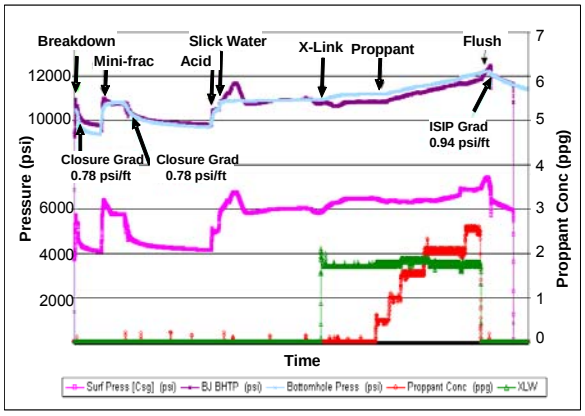

Figure 8: *Fracture treatment in the Bossier formation, Bonner sand*

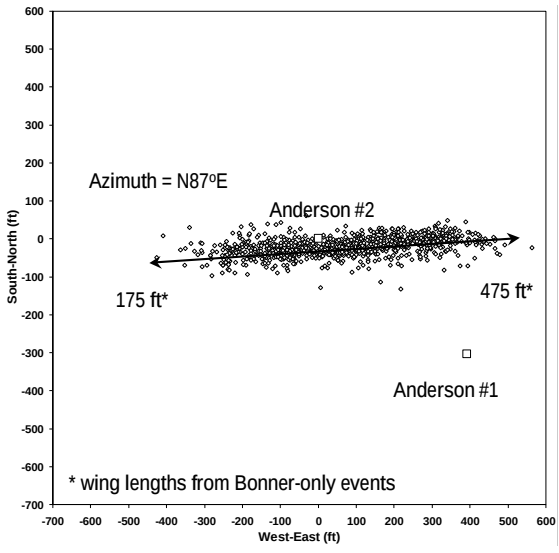

Figure 9: *APC Anderson #2 Bonner Stimulation, Microseismic Data Plan View*

Fracture Diagnostics (APC Anderson #2 Well)

Various direct and indirect fracture diagnostics were used to monitor the fracture treatments including:

- Microseismic imaging (for length, height and azimuth)
- Radioactive tagging with multiple isotopes (for near-wellbore height)
- Recording of bottomhole treatment pressure (to improve fracture simulation)
- Production logs (to evaluate effective propped fracture length and zonal coverage)

This project utilized a single microseismic imaging well to monitor the APC Anderson #2 Bonner treatments. The observation well was located 495 feet from the treatment well. Since microseisms are extremely small, a sensitive and high rate telemetry system is required to obtain accurate results. To meet these requirements, a twelve level, three-component retrievable geophone array was deployed using a fiber optic wireline unit. Once at depth, the receivers were clamped against the wellbore using mechanical arms. The tool string was configured for an aperture to adequately cover the target zones. The treatments were continuously monitored giving the capability of determining how the fractures grew with time, which proved critical for understanding the complex fracture growth.

The Bonner stimulation mapping results are shown in Figure 9 and Figure 10. The Bonner fracture also grew East/West with an azimuth

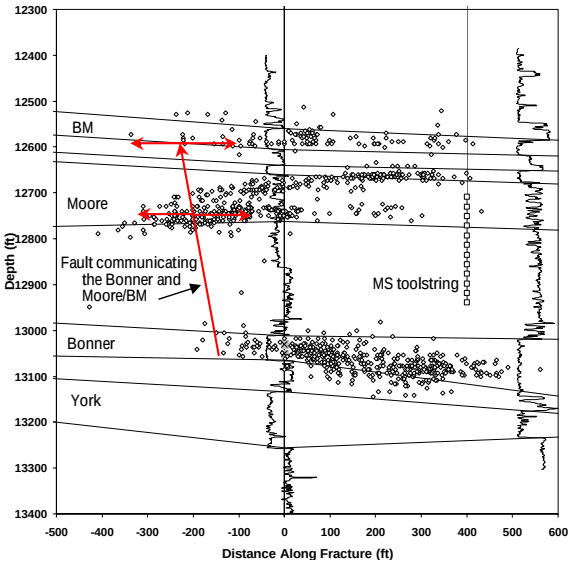

Figure 10: *APC Anderson #2 Bonner Stimulation, Microseismic Data Side View*

of N87°E. The fracture growth was asymmetrical with an east wing extending 475 feet and a west wing of 175 feet. The Bonner treatment was also observed to have communicated upward in to the Moore and Bossier Marker sands through a fault. For the Bonner stimulation a significant amount of the treatment appears to have gone out of zone.

For the Bonner stimulation, the fault closest to the wellbore was open during the stimulation and is responsible for the upward communication to the Moore and Bossier Marker sands. Interestingly, this is the same fault that was observed to be non-communicating during a previous stimulation. The westward growth of the fracture in the Bonner sand appears to have been arrested where it intersected the fault. The fracture in the Bonner does not extend to the second fault observed during the York stimulation.

Figure 11: *Plan view of microseismic map, showing a large waterfrac with extremely long and complicated fracture growth.*

Results from the tracer log do not appear to be entirely consistent with the microseismic data. This, however, is not uncommon as the tracer logs only reflect the fracture geometry very close to the wellbore.

A retrievable pressure gauge was placed at the bottom of the well to record the bottomhole treating pressure during the treatment. The gauge recorded the data and was recovered after the treatment. This data was used to help calibrate the hydraulic fracture model for both sands.

Example 2: Waterfrac

The Barnett Shale is currently one of the most prolific gas reservoirs in the United States. The Barnett shale within the Fort Worth basin ranges from 200 to 800 ft in thickness and is approximately 500 ft thick in the core area of the field. The productive formation is typically described as a black, organic-rich shale composed of fine-grained, nonsiliciclastic rocks with extremely low permeability, ranging from 0.00007 to 0.005 md. The formation is abnormally pressured, and hydraulic-fracture treatments are necessary for commercial production because of the low permeability.

There has been a rebirth of drilling and refracturing activity in recent years because of the success of waterfracture, or "light-sand," fracturing treatments. This extremely low-permeability reservoir benefits from fracture treatments that establish long and wide fracture "fairways," which result in connecting very large surface areas of the formation with an extremely complex fracture network.

Similarly to HDR stimulation, it has been realized that production benefits from a large fracture area because the gas can only be recovered from the rock adjacent to the fracture surface. The fracture conductivity does not need to be very high and the fracture area can be enhanced by injecting large volumes of water. Only a little sand is added to ensure sufficient conductivity.

Figure 11 shows a typical example of fracturing in the Barnett; the long axis of the fracture network or "fairway" (oriented ~N40E in the core area of the Fort Worth Basin) is referred to as the hydraulic fracture "fairway length" while the short axis of the rectangle (from NW to SE) is typically referred to as "fairway width". For vertical wells, these fairway dimensions can approach about 4000 ft in length and up to 1200 ft in width. Figure 11 shows a typical fracture fairway network from a vertical well in the core area of the Barnett. The microseismic events are shown as points on this plan view and the gross fracture area is immediately obvious. The points can be analyzed with time and a linear regression algorithm applied to identify events that happen sequentially and appear to be related to a specific fracture structure. These sequential linear structures are highlighted with lines representing the minimum number and size of likely fracture segments.

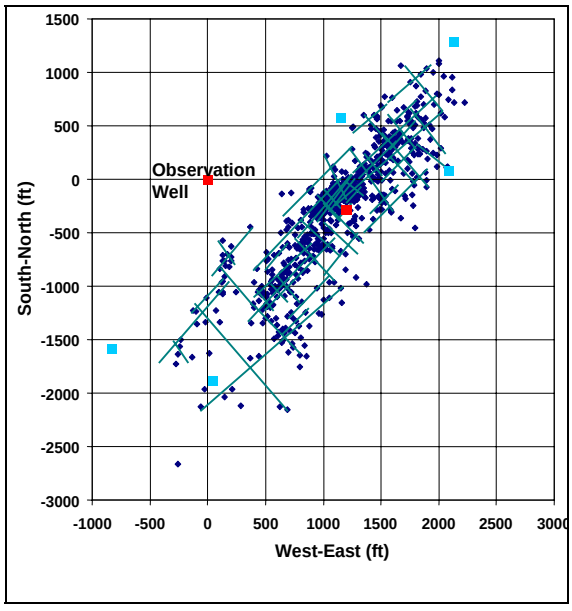

This well's fracture length is more than 4000 ft long (2000 ft half-lengths) and "fairway" width is about 1000 ft across. The individual fracture structures are shown as line segments on the

map; total fracture network length on this treatment was estimated as 30,000 ft. The five small squares seen just outside the fracture network show the locations of wells that were temporarily killed by the frac treatment on this well, confirming that the fracture network indeed extended as far as the micro-seismic cloud.

Conclusions

The perforation-timing system has been developed to use the orientation shots (perforations, string shots, or other sources) for extracting appropriate compressional and shear wave velocities for ray paths traversing interwell sections. Since the orientation shots must be performed in all tests to orient receivers, their use for velocity measurements does not impact operations, yet they provide invaluable information on crosswell velocity structure. Since the measured ray paths are similar to those of the microseisms, this type of interrogation of the reservoir provides a more accurate and more realistic velocity interpretation than using dipole-sonic logs alone. However, dipole-sonic logs still provide the high-resolution structure that perforation timing measurements cannot provide and use of the interwell velocity analysis is typically to calibrate the dipole sonic log, if possible.

Perforation-timing velocities are often considerably different than those obtained from dipole-sonic logs. In some cases the velocities are less and in other cases the velocities are greater, and there are many cases where the two velocities have been found to be relatively similar. Where the velocities are different, the perforation-timing measurements have been found to yield more consistent microseismic locations.

Nothing in this study implies that the dipole-sonic logs are not accurate; rather, the velocities that are measured with the dipole-sonic log may not be representative of the velocities that control the microseismic radiation.

The determination of an accurate velocity structure is particularly important when the array is situated above the zone where microseisms are induced. Errors in both microseismic distance and elevation can be quite large in such cases. When the array straddles the microseismic zone, all location errors are reduced considerably, but the distance to events can still be significantly miscalculated if the correct velocities are not used. The effect of these errors can be important if there is a structure to the microseismic events that needs to be evaluated (e.g., a natural fracture system that is being activated). We have shown examples of unexpected interaction between hydraulic fractures and natural fractures. Fracture mapping is crucial for characterizing such treatments. In some cases the complex fractures yield a much better stimulation than traditional propped fractures.

References

Griffin, L.G., Sullivan, R., Wolhart, S., Waltman, C., Wright, C.A., Weijers, L., and Warpinski, N.R., “Hydraulic Fracture Mapping of the High-Temperature, High-Pressure Bossier Sands in East Texas,” SPE 84489, SPE Annual Technical Conference & Exhibition, Denver, Colorado, October 5 – 8, 2003.

Le Calvez, J.H., L. Bennett, K.V. Tanner, W.D. Grant, L.. Nutt, V. Jochen, W. Underhill, J. Drew, (2005), “Monitoring microseismic fracture development to optimize stimulation and production in aging fields“, Leading Edge, p. 72, January 2005.

Murphy, H.D. and M.C. Fehler, (1986), ”Hydraulic Fracturing of Jointed Formations”, SPE 14088.

Warpinski, N.R. , R.B. Sullivan, J. E. Uhl, C. K. Waltman, and S. R. Machovoe, (2003), “Improved Microseismic Fracture Mapping Using Perforation Timing Measurements for Velocity Calibration”, SPE 84488, 2003 SPE Annual Technical Conference and Exhibition held in Denver, Colorado, U.S.A., 5 – 8 October 2003.

Fault mechanisms of induced seismicity at the superdeep KTB borehole and their relation to fault structure and stress field

BOHNHOFF Marco , GeoForschungsZentrum Potsdam, Germany, bohnhoff@gfz-potsdam.de

125 Fault plane solutions for microearthquakes induced during a long-term fluid-injection experiment at the KTB boreholes (Germany) in 2000 are investigated. A predominant strike-slip mechanism is observed, partly with components of normal but also reverse faulting. Adding 54 fault plane solutions of an earlier injection experiment at the KTB we determine the local stress field and find a subhorizontal NS orientation for the maximum principal stress and a near vertical orientation for the intermediate principal stress. The stress field exhibits no temporal or spatial variations within the resolved accuracy of 15°. However, the results of the stress tensor inversion point to heterogeneities of second order. Based on the hypocentral distribution of the induced microearthquakes and the similarity of fault mechanisms we relate our data to the fault structure at the KTB. We find that the larger faults act as pathways for the injected fluid whereas the brittle failure occurs on fault asperities of the larger mapped faults and nearby smaller faults both in agreement with the local stress field. Applying a thorough error analysis of the individual fault plane solutions we correlate the diversity of mechanisms with their strength and find that the strongest events tend to a representative mechanism that is in good correspondence with the stress field. In contrast, the diversity of fault mechanisms is larger for the smaller events indicating local stress perturbations.

Keywords: Induced seismicity, fault mechanism data, stress field, fault structure,KTB

This contribution was published as:

Bohnhoff, M., Baisch, S., Harjes, H.-P. (2004): Fault mechanisms of induced seismicity at the superdeep German Continental Deep Drilling Program (KTB) borehole and their relation to fault structure and stress field.J. Geophys. Res., 109, B02309, doi:10.1029/2003JB002528.

ENGINE – **EN**hanced **G**eothermal **I**nnovative **N**etwork for **E**urope
Workshop 3, "Stimulation of reservoir and induced microseismicity"
Kartause Ittingen, Zürich, June 29 – July 1, 2006, Switzerland

Elements governing the ratio (Hydraulic Performances)/(Induced Microseismic Nuisances) during the stimulation of "EGS Soultz type" reservoirs.

GERARD André , GEIE Exploitation Minière de la Chaleur, Soultz-sous-Forêts, France, gerard@soultz.net;
CUENOT Nicolas, GEIE Exploitation Minière de la Chaleur, Soultz-sous-Forêts, France,
CHARLéTY Jean, EOST, Strasbourg, France;
DORBATH Catherine, IPGS-EOST Strasbourg, France;
DORBATH Louis, IPGS-EOST Strasbourg, France;
GENTIER Sylvie, BRGM, Orléans, France
HAESSLER Henri,IPGS-EOST Strasbourg, France

Abstract

The results observed during the past twenty years at Soultz demonstrated that "usual" hydraulic stimulation techniques when applied in such an hydrothermal / tectonic context can provide both real, but unfortunately limited, improvements of the wells hydraulic performances and real, but fortunately up to now limited, microseismic nuisances. Seven major hydraulic stimulation tests performed at Soultz generated always large "microseismic clouds" but quite variable improvement of the wells hydraulic performances.

The questions about the possible usefulness of that induced microseismicity in the situation of Soultz came to light progressively. Despite all efforts and very large "microseismic clouds" the hydraulic results from the stimulation tests up to now resulted in injectivity indexes which were limited within a range 2 to 4 l/s/MPa (target being 10 to 20).
Those questions became definitely unavoidable after the stimulation of the well GPK3 performed at Soultz in 2003 at depth ~ 4750 m. During that test (including a dual stimulation with a second well) ~ 34 000 m^3 of water were injected in GPK3 at a mean flow ~ 50 l/s generating ~ 90 000 events [*among which 39 of magnitudes high enough* (1.9<Md<2.9) *to be felt by population*] within a cloud extending more than one km from the well. A peak of activity higher than 500 events/hour was even recorded when a flow of ~ 90 l/s was injected. Result was a null improvement of GPK3's injectivity which was ~ 3 l/s/MPa before and after that test.

This presentation aims to examine why, in fact, the apparent contradiction between the huge microseismic activity developed during more or less massive hydraulic stimulation tests and the modesty of their efficiency is not so surprising in the situation which prevails at Soultz.

The mechanisms inducing microseismicity can facilitate fluid circulation only if several conditions (such as density of events and their distance from well, fluid velocity,…) are simultaneously fulfilled. This is much easier to get in the near wellbore vicinity than in the far field.
On the contrary the development of the induced microseismic nuisances is directly related with the pressure propagation and consequently depends from conditions (such as very low fluid velocity, natural fractures density and orientations, natural porosities…) which can be easily fulfilled far from the wells.

In fact, in natural hydrothermal reservoirs of Soultz type, the relationships between enhanced water circulation(s) and pressure waves propagation during (or following) stimulation tests are quite variable, depending from the natural local conditions which are still unknown for a large part due to their complexity. Nevertheless it looks likely that hydraulic stimulations in such a medium can create sensible positive results mostly by connecting the wells to some more or less numerous and/or highly permeable natural fractures already pre-existing in their vicinity. When such a highly permeable fracture (or set of fractures) will be reached by a pressure wave during a stimulation test it will likely appear as a boundary stopping locally the progresses of the "microseismic cloud". Hydraulic results will depend how far and productive are these fractures and how their links to the wells can be cleaned/opened.

That view about the elements governing the ratio (Hydraulic Performances)/(Induced Microseismic Nuisances) during the hydraulic stimulation of "EGS Soultz type" reservoirs require now to make progresses through specific investigations (such as VSP, new logging techniques…) and innovative tests carefully designed through conceptual and digital modelling in order to optimise this key

ratio while maintaining the nuisance under a threshold which is acceptable by population.

Keywords: microseismic, Soultz

Introduction

Since more than twenty years, it is commonly considered within the frame of HDR / EGS projects, that massive hydraulic stimulation techniques, i.e. injection at various flowrates (up to 90 l/s at Soultz) of various volumes of water (up to 34 000 m^3 at Soultz) are the major tool for bringing wells from poor initial hydraulic performances to high injectivity / productivity indexes which could be generated by the development of an heat exchanger connecting more or less directly the injection and the production wells.

From twenty years of experience mainly based on such an approach at Soultz and from results obtained by series of other project (Los Alamos, Cornwall, Hijiori,…) now closed, two major sets of questions seem to become unavoidable in the case of Soultz type natural conditions.

- Is it really totally necessary to make so many efforts to develop more or less direct hydraulic connections between the wells for heat exchange through a limited volume of rocks, or is it more efficient to look as a priority for the development of the best possible connections between the wells and the surrounding natural geothermal reservoir? It can be noted that even within the second approach, *in case of pre-existing favourable natural features between the wells*, the possible development of an heat exchanger could nevertheless bring some complementary non negligible resources but could not represent any kind of priority.
- Is it expectable to develop the hydraulic connections between the wells and the surrounding reservoir with both minimum induced microseismic nuisances easily acceptable by population and enough efficiency to reach the targeted wells productivities / injectivities?

This second question requires now to consider the elements governing the ratio (Hydraulic Performances)/(Induced Microseismic Nuisances) during the stimulation of “EGS Soultz type” reservoirs.

The first major element is the present views about the natural geothermal reservoir surrounding the wells.

A conceptual reservoir model at Soultz

Taking into account the present knowledge issued from the geological / tectonic studies (1) (2) (3) and from the geochemical / petrographic investigations (4) (5) (6) towards the definition and understanding of the regional natural geothermal reservoir of the Rhine Graben it became possible to propose a conceptual reservoir model at Soultz as it is schematically described in Figure 1.

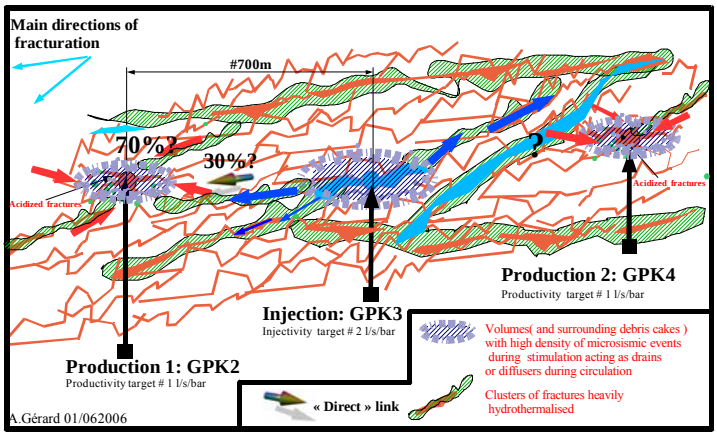

Figure 1. Horizontal plan view of a general conceptual reservoir model at Soultz

It is today demonstrated that such a highly naturally fractured system is characterised by clusters of fractures within which most of the natural circulations and associated hydrothermal phenomena occur. (1) (4)
Within these clusters hydrothermalism has either locally developed the rock porosity or randomly plugged a large proportion of the channels through which the thermal water was circulating.

Today, these views bring us to consider at the Soultz scale (i.e. a volume of several km^3 around the wells located between 1.5 and 6 km depth) a very heterogeneous natural geothermal reservoir mostly constituted by a network of fracture clusters (1) predominantly oriented close from North – Soultz (± 20º), dipping East or West close from vertical (± 20º). They are separated by distances of few hundred meters and crossing each other within distances of some kilometres forming a kind of 3D network of complex “aquifer” layers. The homogeneity of the geothermal water composition whatever is the sampling depth and the observed natural pressure distribution demonstrated that none of these clusters can be considered as being a totally closed system.

On the contrary, the observations done during drilling operations showed that:

- some clusters contain very productive fracture(s) which could be considered as being able to sustain a high "natural" geothermal production.
  As an example a fracture was crossed at 2 km depth (temperature # 140°C) while drilling GPK-2, generating total mud losses and showing no sign of reduction of its injectivity / productivity even after absorption of all the cuttings generated while drilling down to 3900 m.
- Some clusters contain large fractures showing "medium" injectivity / productivity likely affected by drilling conditions (possible impact of progressive plugging due to cuttings?). A fracture of this type was crossed at # 4750 m while drilling GPK-3.
- A large proportion of clusters showed none or only minor signs of permeability while drilling. Nevertheless hydraulic tests before stimulation demonstrated that some of them were not totally tight before stimulation.

Some major results of hydraulic stimulation tests at Soultz

The main significant experiments and their results can be summarised as follows:

- 23 500 m^3 of water were injected in GPK-2 using progressive flow values up to 50 l/s. The initial apparent productivity index of that well was increased from 0.2 l/s/MPa up to # 4 l/s/MPa by the stimulation. The maximum pressure required for injection of 50 l/s was # 130 bars.
  During a later circulation test the productivity of GPK-2 appeared to be close from 10 l/s/MPa without any clear explanation today of that huge dissymmetry between injectivity and productivity indexes (leak between open annulus and casing draining a part of the resource from 2000 m depth?, impact of the reinjection in GPK-3? other?)
- 34 000 m^3 of water were injected in GPK-3, using progressive flow values up to 50 l/s with peak values of 95 l/s during some hours. The initial apparent injectivity index of that well, 3 l/s/MPa was not obviously increased by this operation. Despite the strong initial injectivity of that well the pressure required to inject 50 l/s was up to # 150 bars.
  During a 5.5 months circulation test carried out in 2005 the apparent injectivity of GPK-3 appeared as being rather stable at # 3 l/s/MPa.
- 9 150 m^3 of water were injected at 30 l/s in GPK-4 with 3 peaks of several hours each at 45 to 40 l/s then a second stimulation test was carried out by injection of 12 500 m^3 of water at 30 l/s during 1 day then 45 l/s during 2 days then 25 l/s during one day. The apparent productivity index of the well was increased from 0.2 l/s/MPa before stimulation(s) up to around 2 l/s/MPa at termination.
  During all these tests a large microseismic activity was observed using two networks. A bottom hole network provided a magnitude threshold of # -1.5 and a surface network provided a magnitude threshold of # -0.5. Considering the most sensitive network:

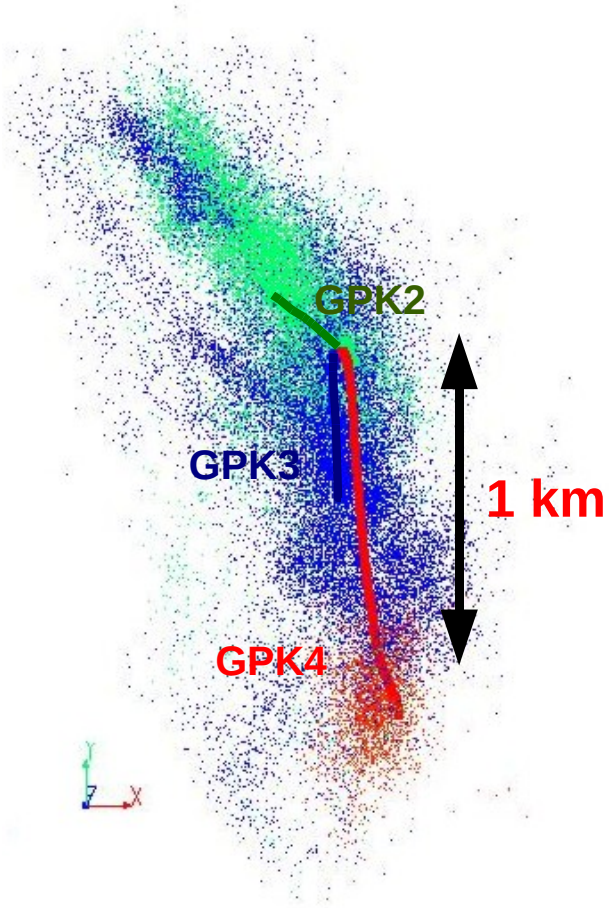

Figure 2. Horizontal plan view of the located seismic events which occurred during the stimulation campaigns. Green points: recorded during GPK-2 stimulation; blue points: recorded during GPK-3 stimulation; red points: recorded during GPK-4 stimulation.

- The stimulation of GPK-2 generated some 35 000 triggers *(within which around 25 000 appeared*

as being locatable events) among which around 40 events showed magnitudes higher than 1.9 (threshold for human reactions at Soultz) with a maximum at 2.6 generating a real emotion within the population.

- The stimulation of GPK-3 generated some 90 000 triggers (*within which around 22 000 appeared as being locatable events)* among which 36 events showed magnitudes higher than 1.9 with one event reaching 2.9 and two other 2.7 creating among the population larger emotion than during the previous test despite an intensive campaign of information.
- The stimulation of GPK-4 performed much more cautiously generated only a total of around 22 000 triggers *(~9 500 locatable events)* among which only 2 were events above 1.9 during the first stimulation. Nevertheless, even if during the second stimulation only 3 events of magnitude higher than 1.9 were generated *(among which one reached 2.6),* during the following tests performed with small flowrates (max. 30 l/s) and small volumes (max. # 5 000 m^3/test) 10 events of magnitude higher than 1.9 occurred. That is a clear indication that the well GPK-4 became hypersensitive to injections (even small) after its two first stimulations.

Summarising that main observations, it can be concluded that the best result from hydraulic stimulation was obtained for GPK-2. Its injectivity was increased up to 4 l/s/MPa with a "moderate" microseismic nuisance. For GPK-4 results (# 2 l/s/MPa) were more modest but the microseismic nuisance was also rather modest despite a worrying evolution after stimulation. For GPK-3 the microseismic nuisance appeared to be close from the maximum level of acceptability by the population and the improvement of the well's hydraulic performances was negligible.

When looking at these results, two questions arise:

- *What is really the part of the microseismic activity (if any sometimes, see the case of GPK-3) which could be useful for the improvement of the wells injectivities / productivities?*
- *Which stimulation method(s) could provide minimum nuisances and the most efficient results in "Soultz type" geothermal fields?*

This requires now to examine what are the conditions which could determine the efficiency of an hydraulic stimulation and what are those which could determine the amplitude of the microseismic nuisance.

Conditions determining the efficiency of hydraulic stimulation

For the efficiency of any hydraulic stimulation in the Soultz context two mechanisms can be considered in priority:

> ***Shearing of fractures according to criteria as for example the Mohr-Coulomb criterion or any other similar one;***
>
> ***Water cleaning of near wellbore fractures carrying flows which velocities are high enough to transport particles either resulting from the local shearing either pulled out from the fractures walls assuming these walls could be more or less fragile and sensitive to thermal chocks due to their usual high degree of hydrothermal alteration.***

The main conditions determining the efficiency of hydraulic stimulation in "Soultz type" geothermal reservoir were already described in (7). They can be briefly reminded as follows:

- ***1st condition: capacity of a crack to get its intrinsic hydraulic transmissivity locally significantly increased (i.e. increase in its local permeability)*** at the end of shearing.
  This point will very strongly depend on the parameter "amplitude of the shearing" (commonly considered) but also (and this point is more rarely considered) on the nature of the material which constitutes the walls of the crack.
  If it is, for example, dominated by clay minerals the impact of shearing on the local permeability of the crack could be poor.
  On the opposite, if the fracture is filled with a majority of quartzic minerals the results could be locally significant.
  Remains the case of shearing generating a lot of debris which could lead to local sealings, as in the case of calcite rich walls.
- ***2nd condition: evacuation of the debris and deposits which encumber the stimulated cracks.***

This condition will strongly depend on the distance which separates the stimulated cracks from the stimulated well.
Indeed, it is certain that, except for short-circuit, local velocities of the fluid injected into the cracks will be directly dependent on the distance to the stimulated well.
In the immediate vicinity of the well one can consider that the fluid velocity is very high, able to partly carry towards outside the debris generated by shearings in the course of stimulation and also to strip the walls of the hydraulically active fractures. These mechanisms could strongly increase the local permeability of the stimulated fractures close to the well, but also (and this is much less favourable) to plug with debris the more far tiny opened fractures.
Obviously, if such is really the case, the injection with large flow rates and (consequently) high pressures will offer a maximum probability for the development of kind of "mud filtration cakes" locally perforated by preferential paths which are likely to harm heat exchange in the affected areas.

- ***3rd condition: probability of hydraulically significant connections*** *(in term of flows)* ***between the stimulated cracks and the wells directly or through the network of the natural cracks***
  This probably will depend on two factors:
  - Proximity of the stimulated cracks from the wells.
  - Density of the stimulated cracks from which will depend the probability of connection of a stimulated crack with other stimulated cracks to establish paths towards the wells or the external massif.
    Indeed it is necessary that hydraulic paths sufficiently inter-connected by the operations of stimulation exist either between the stimulated crack and the wells and/or between the stimulated crack, a well and the network of the far cracks naturally interconnected at the scale of the massif. Only if it fulfils one of these conditions this crack becomes useful for hydraulic circulations from the wells to the far field or to another well.

The observation of the rapid drops of the microseismic events density (expressed for example in a number of events per million m^3) joined to the knowledge of the natural cracks network in the vicinity of the well and to what is understood about the hydrothermal deposits makes possible to infer the following forecast in the situation of Soultz:

Taking into account the three conditions described above it is not likely possible to develop **volumes containing strong density of permeable fractures** with any internal improved hydraulic efficiency around the stimulated wells beyond a distance of 100 m to 200 m. On the other hand it is not impossible to develop, by techniques wrongly intensive, some privileged paths which could inopportunely connect more or less directly an injection well to the production well generating "courts-circuits" which will be likely to strongly limit the thermal life of the system during its future exploitation. The risk of peripheral fillings by products resulting from the hydraulic stimulation could disturb considerably the essential exchanges between the natural geothermal reservoir and the volumes made more permeable around the wells.

In such a situation we have to consider the nuisance and even the risks associated with a microseismic activity which seems of questionable efficiency for its far field part.

The propagation of microseismic activity during stimulation

Due to the now well-known general characteristics of the Soultz natural geothermal reservoir surrounding the wells, it seems that the microseismicity can propagate within very large volumes far from the wells due to the propagation of over pressures through several clusters of fractures more or less sealed by hydrothermal deposits and acting as "storage volumes" during high flowrates (i.e. high pressure) hydraulic stimulations.

On another hand, as soon as the injected water either leaves the well's vicinity either flows out of one "storage" volume (when it finds connection(s) with highly permeable natural fractures), its velocity locally increases, the friction losses make the pressure dropping rapidly, and the seismic activity does not propagate beyond that limits.

Consequently it appears that the most hydraulically active parts of the reservoir during stimulation are not the most microseismically active zones which appear more as storage volumes than as regions where the water circulates.

These "realistic" views of the reservoir behaviour at Soultz during a stimulation can be summarized on figure 3,a and 3,b.

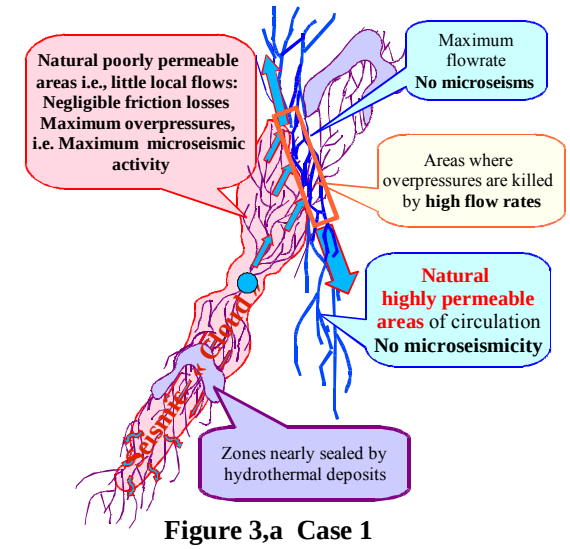

Figure 3,a Case 1
Could be ~ GPK2 or GPK4?

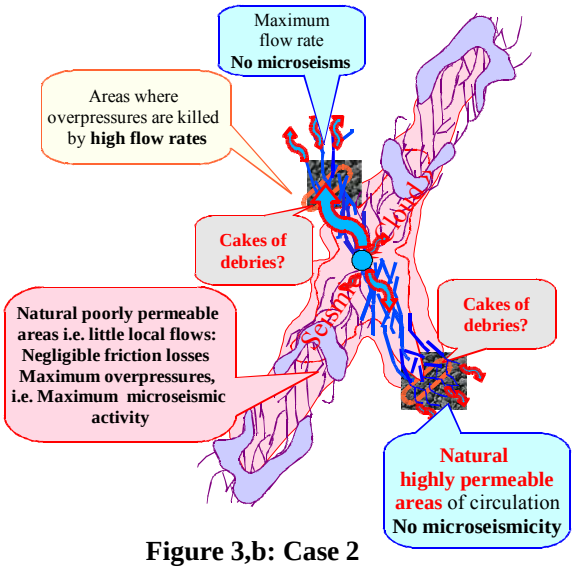

Figure 3,b: Case 2
Could be ~ GPK3?

Figures 3,a and 3,b. Basic features governing the microseismic events distribution at Soultz.

Consequences

Consequences are that, except in the near wellbore vicinity, it is unlikely at Soultz that microseismicity can be correlated with any large water flows through the reservoir during stimulation and a huge microseismic activity far from the well could represent much more a simple nuisance than a phenomenon of any interest for the wells productivities / injectivities. This is a situation quite different from the one which was prevailing in conventional HDR projects as in Los Alamos or in Cornwall where the rock was tight enough for a possible close association between water flows and pressure waves propagations and where it was possible to consider the microseisms locations as an indicator of the main paths trajectories of water flows towards the far field.

At Soultz, the huge microseismic activity developed far from the wells (and even close of them for a part) during hydraulic stimulation tests appears much more as being a simple nuisance associated with "dead" storages volumes than as indicating the development of the wells productivities / injectivities.

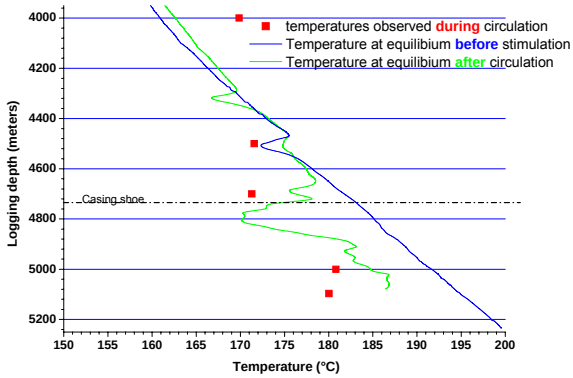

Figure 4. Temperature observations in the deepest part of GPK4:
Blue: profile at equilibrium after drilling
Green: profile "at pseudo equilibrium" after stimulation followed by 5.5 months of hot brine production.
Red dots: values observed during circulation ~2 months after beginning

This point, which could appear as rather controversial, can be demonstrated by the permanence of cooled zones in the near wellbore vicinity after stimulation, then production. The example of GPK-4 on figure 4 **shows that cold fresh water was stored here during the stimulation** but this zone was poorly drained later even after more than 40 000 m^3 of hot water production containing 75% to 85% of geothermal brine during the last two months of the circulation test.

This point can also be confirmed by the microseismic activity during the 5.5 months circulation test performed in 2005 using GPK-3 as an injector and both GPK4 and GPK2 as producers. The microseismicity was generated by over pressures in GPK-3 and occurred for a large part not only under GPK-3 but also under the production well GPK-2 (figure 5) despite the drainage due to GPK-2's production. This can be understood as a closed volume over pressurised from GPK3 and extending down towards just under GPK-2.

Such a volume appears as being one of the "dead" storage zones whose existence is considered as being very likely according with the previous considerations.

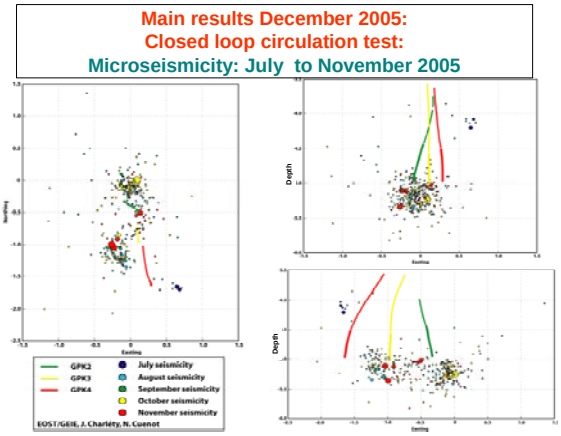

Figure 5. Microseismicity generated under the production well GPK-2 over pressures in GPK-3

Conclusions

From observations and results up to now performed in the "Soultz type" intensively fractured and hydrothermalised geothermal reservoir, it cannot be concluded that there is any demonstrated link between the far field microseismic activity and the main water circulation paths during an hydraulic stimulation.
On the contrary such a link, which was creadible in conventional HDR projects in rather homogeneous and tight poorly naturally fractured massifs appears as much more questionable in natural geothermal reservoirs of Soultz type.

It appears that massive hydraulic stimulation techniques consisting of large volumes of water injected at high flowrates in the natural geothermal reservoir at Soultz will certainly generate large microseismic nuisances in extended volumes upsetting a part of local populations[*)]. On another hand, in the present status of our comprehension of the local natural environment at Soultz (maybe insufficient) there is no obvious indication making us thinking that large seismic clouds propagated towards the far field provide a strong indication that it could be likely to get results highly positive with this method. It seems difficult to justify at present to use again this expensive and disturbing technique before to have fully tested other methods aiming at similar results through different approaches.

Among other methods much more "seismically harmless" which are up to now at the beginning of testing, chemical stimulation seems very promising after the recent success of preliminary tests using that method. After a moderate hydraulic stimulation of GPK4 the use of chemical stimulation made its apparent injectivity grossly multiplied by two, i.e. brought to a value close from what was obtained after the massive hydraulic stimulation of GPK2 but with much less nuisances. Future associations between chemistry and hydraulics ("acid frac" as an example) or as proposed in (7) look also of potential interest.

This could open a debate from which major consequences for the future of "Soultz type" EGS projects could follow.
To guide such a debate towards useful conclusions, we need to improve at the best possible level and as far as possible from the wells our comprehension of the local natural environment. A programme of **V**ertical **S**eismic **P**rofiling is already under preparation for that purpose, but testing the reactions of the medium to other harmless operations (for example cleaning or dissolving cuttings or debris encumbering the main fracture which controls the injectivity of GPK-3, circulating or mini hydraulic stimulation tests associated with chemical agents, other chemical stimulation tests,…), could provide useful guidelines.

References

(1) Genter A., Dezayes Ch., Gentier S., Ledésert B and Sausse J. (1998): *Conceptual fracture model at Soultz based on geological data.* International Conference 4th HDR Forum, Strasbourg Forum 1998 – Published in Geologisches Jahresbuch: Sonderhefte.

(2) Evans K., Genter A. and Sausse J. (2005): *Direct evidence that stimulation is restricted to hydrothermally altered zones.*

(3) Gentier S. (2004): *Les massifs rocheux fracturés : de la fracture à la géothermie – Mémoire d'habilitation à diriger des recherches :* Université Bordeaux I.

(4) Surma F. and Geraud Y. (2003): *Porosity and thermal conductivity of the Soultz-sous-Forêts granite. Pure and applied geophysics 160 (2003)* 1125 – 11360033-4553/03/061125-12.

(5) Baldeyrou-Bailly A., Surma F. & Fritz B. (2004) : Geophysical and mineralogical

*) *In case of "activation" (triggering effect?) of large tectonic features that nuisance could reach locally maximal magnitudes but the appreciation of such a possible risk is complex. BCSF (Bureau Central Sismologique Français is in charge to appreciate it.*

impacts of fluid injection in a geothermal Soultz-sous-Forêts, France. *In: Energy, Waste and the Environment – A geochemical perspective.* Reto Gieré and Peter Stille (Editors). Geol. Soc. Special Publ. 236, pp. 355-367.

(6) Durst P. & Vuataz F-D (2001): *Geochemical modeling of the Soultz-sous-Forêts Hot Dry Rock system, brine rock interactions in a deep hot fracture granite reservoir,* 26th Workshop on Geothermal Reservoir Engineering, system : the Hot Fractured Rock site in Stanford University, Stanford, California, SGP-TR-168.

(7) Gérard A., Charléty J., Cuenot N., Dorbath C., Dorbath L., Gentier S., Haessler H., Genter A., Dezayes C., Géraud Y. & Rosener M. (2005): *Elements towards an optimal efficiency and minimum risk of microseismic nuisances for the development of the geothermal power production at Soultz.* EHDRA Scientific Conference 17 – 18 March 2005 – Proceedings.

ENGINE – **EN**hanced **G**eothermal **I**nnovative **N**etwork for **E**urope
Workshop 3, "Stimulation of reservoir and microseismicity"
Kartause Ittingen, Zürich, June 29 – July 1, 2006, Switzerland

Analysis of induced microseismic events from HDR/EGS reservoirs by super resolution mapping techniques

ASANUMA Hiroshi, Graduate School of Environmental Studies, Tohoku University, Japan, hasanuma@msj.biglobe.ne.jp;
KUMANO Yusuke, Graduate School of Environmental Studies, Tohoku University, Japan,
NIITSUMA Hiroaki, Graduate School of Environmental Studies, Tohoku University, Japan,
BARIA Roy, MIL-TECH;
WYBORN Doone, Geodynamics, Australia;
TEZUKA Kazuhiko, JAPEX Research Center, Japan

Abstract

Microseismic monitoring has been used in worldwide hot dry rock (HDR) and engineered geothermal systems (EGS) projects as one of the standard techniques to monitor stimulation. The authors have been investigating "super resolution mapping techniques" of the microseismic events to obtain more reliable location of the hypocenter. In this paper, we will show concept of Coherence Collapsing method and double differential (DD) method and application to data sets collected during the stimulation.

Keywords: Coherence Collapsing, double differential method, super resolution mapping

Introduction

It has been widely accepted that the microseismic mapping/imaging method is one of the few methods that can estimate time/spatial distribution of HDR, HWR, HFR, and EGS systems. The mapping of the locations of the microseismicity is the most fundamental analysis process in the microseismic method and studies for improvement of accuracy and reliability of mapping has been carried out in worldwide project which is referred to as "MTC/MURPHY International Collaborative Project" (Murphy et al., 2000).

Most of the mapping techniques are developed to estimate the "absolute" location of the hypocenter. Because of uncertainty in the velocity structure and observational errors in picking of arrivals, it is believed that the absolute locations typically have errors in the order of several tens of metres for microseismic locations in the case of seismic mapping of engineered geothermal systems. The joint hypocenter determination method (JHD; Frohlich, 1979) has been developed in global seismology to reduce the uncertainty caused by the velocity structure. The JHD is one of the standard methods for absolute mapping although it still has uncertainty mainly due to the error in picking. Jones and Stewart (1997) developed an optimizing relocation method which is referred to as the "collapsing method" (original collapsing method). However, because of the initial assumption that the original seismic structure is a point, the ability to resolve structures that are comparable to or smaller than the spatial confidence ellipsoid is not high in the original collapsing method.

Some of the seismic events are known to have very similar waveforms although their origin times have wide separations. These events are referred to as "Multiplets" and highly precise relative mapping techniques or their location have been investigated (Moriya et al., 2002).

The authors have been investigating a mapping method that tries to bridge collapsing and multiplet analysis techniques utilizing the advantages of each of the methods. The objective of the development of this version is to offer similar information as multiplet analysis in the comparable analyzing time as JHD or collapsing method. It is hoped that this new method will provide better locations and so a more meaningful interpretation of the physical meaning of the seismic cloud. Because coherency among events is used as input, we named this variation of the collapsing method as "Coherence Collapsing" (Asanuma et al., 2003).

On the other hand, a multiplet is assumed to arise from repeated shear slip on one fracture, because highly similar waveforms can only be produced through a combination of similar source mechanism and nearly identical source-to-receiver raypaths. We capitalize on waveform similarity for precise estimation of differential travel times among events at each receiver; these differential times are used as input into the relative location technique. Because raypaths are nearly identical among multiplet members, the relative location

technique eliminates location errors introduced by velocity model inaccuracies over most of the path, providing improved accuracy for relative locations within the source region (Waldhauser et al., 2000). This technique is referred to as "double differential method" (DD method) and as considered to be one of the standard mapping techniques in the global seismology.

In this paper, the authors will discuss potential of these newly developed mapping techniques using data sets collected while stimulation of engineered geothermal systems and gas field.

Coherence Collapsing method

Principles

In the Original Collapsing method, an event is selected as a target event and it is moved slightly toward the centre of gravity of all the events that are located within its confidence ellipsoid, implicitly assuming that the original seismic structure was a point. The movement is normalized by the size of the spatial confidence ellipsoid. The process is repeated for all events in the data set and a new "generation" of locations is formed in this way. This procedure is repeated for several generations until the distribution of normalized movement fits to the Chi distribution with three degrees of freedom.

The movement of events in the Original Collapsing is determined only by residual and location of neighboring events, without any relationship to waveforms. However the multiplet analysis has already resolved that a part of dataset, which has higher mutual coherency, is relocated to a very small seismic structure. This suggests that it is reasonable to correlate the movement in the Original Collapsing method to the similarity of events. Thus the concepts of the Coherent Collapsing are,

a) The events which has higher mutual coherency are relocated to a point (or to very small structure), and

b) The events with lower mutual coherency are relocated to reduce uncertainty of whole seismic cloud.

The main procedure of the Coherence Collapsing is based on that of the Original Collapsing. The coherence of the events to the target event is used as a weight coefficient in the calculation of the centre of gravity. It is reasonable to use the coherence to multiply the weighting factor as we expect these events to come from small scale structures, however the optimum weight is unknown. We decided to determine the optimum weight using synthetic study and currently using 8th power of the coherency (Asanuma et al., 2003).

Application to data set collected at Soutlz and Cooper Basin.

The Coherence Collapsing method was applied to data set collected during the stimulation of reservoirs at Soultz, France (Baria et al., 2000, Asanuma et al, 2002, 2004) and Cooper Basin, Australia (Asanuma et al., 2004). The location of microseismic events by JHD, the original collapsing, and the coherence collapsing for data sets from simulations at Soultz in 2003, and that from Cooper Basin in 2003 are shown in Figures 1 and 2.

The extension process of a part of the shallow reservoir created at Soultz in 1993 has been interpreted by an integrated analysis of microseismicity, logging data and hydraulic record (Niitsuma et al., 2002). The seismic location in this part of the reservoir is magnified in Figure 3. The location of the highly coherent seismicity was in good agreement with that from the multiplet analysis (Moriya et al., 2002). The location of events with higher coherency shows sub-vertical linear seismic structure, which is interpreted as a firstly stimulated pre-existing fractured zone. The data from Soultz in 2000 and 2003 are collected during the creation of deep reservoir, which has more hydraulically "closed" nature than the shallow one (Asanuma et al., 2002, 2004). The location of events with higher coherence is more widely/uniformly distributed than the shallower reservoir suggesting the lower density and higher stiffness of the pre-existing fractures in the Soultz deep reservoir.

Because of the horizontal maximum stress and sub-horizontal pre-existing fractures, it is expected that a horizontal over-pressured fracture, which was not plugged in the drilling, and its subset fractures are stimulated in the Cooper Basin HFR Project, Australia. The location of microseismic events in the fracture initiation tests and main stimulation in 2003 showed sub-horizontal seismic cloud extending horizontally approximately 1500m from the injection well with thickness around 150m (Asanuma et al., 2004). The coherence collapsing method, applied to this dataset, showed several sub-horizontal seismic structures. Because it is accepted that multiplets are correlated to single fracture with multiple slip, this result suggests the existence of a set of sub-horizontal fractures in this site.

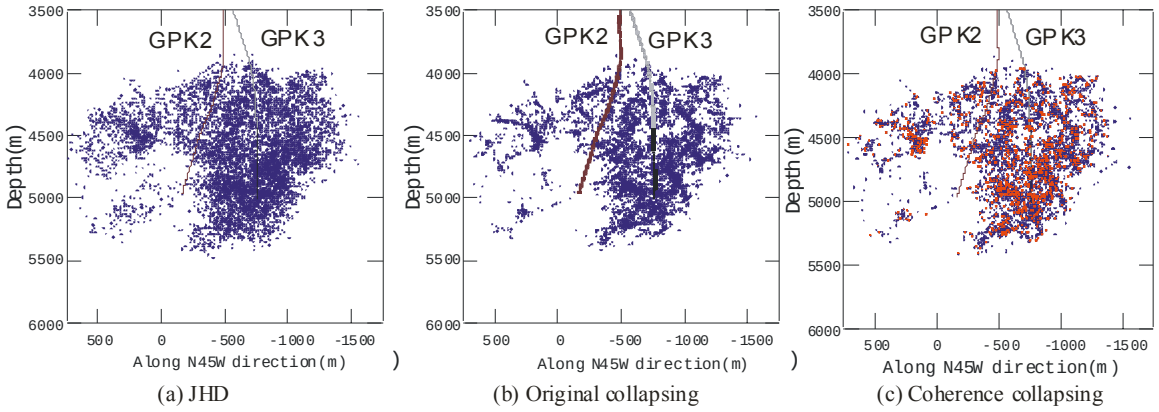

Figure. 1. Relocation of the microseismic data collected at Soultz in 2003.

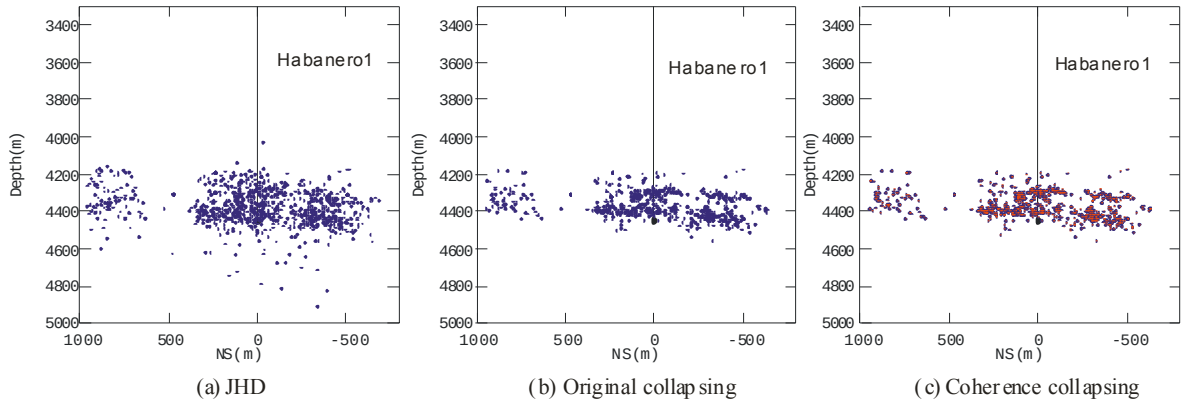

Figure. 2. Relocation of the microseismic data collected at Cooper Basin in 2003.

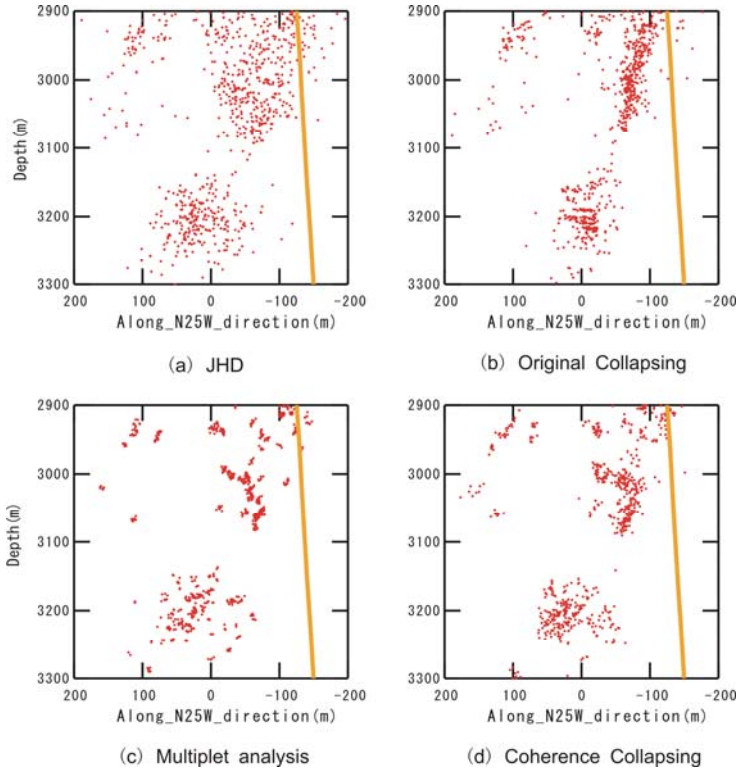

Figure. 3. Relocation of the microseismic data collected at Soultz in 1993.

DD method

Principles

The DD method is a precise relative location technique (Waldhauser et al., 2000) using relative time of arrival for a group of events. A double differential equation from the relative delays is solved to obtain the absolute location of the microseismic events. Because relative time of arrival is used as an input, it is believed that the ability of the DD to estimate absolute location is lower that for relative location.

There are several methods to estimate the relative time of arrival among a set of events. Cross spectra and coherence can bring the most accurate information on the delay and similarity of the events, although processing time may longer than the other techniques in time domain. Because the DD method can be used as a pre-processing of the multiplet analysis to estimate orientation and behavior of each fracture, the authors have been using the cross spectra for the delay estimation (Moriya et al., 2002).

Application to data set collected at Cooper Basin and Yufutsu Gas field.

Because number of the events with higher similarity was large (>10,000) in the data collected at Cooper Basin in 2003, we selected a part of the seismic cloud where more complex seismic/reservoir structure is expected from the conventional single event location (SED) technique. A total of 3,687 events were located using SED. Approximately 30% of the located events did not have adequate signal to enable determination of waveform similarity. We discuss here the remaining 70%, whose source locations we adjusted using the DD method (Kumano et al., 2006). Figure 4(b) shows the result of DD re- location in the western part of the microseismic cloud. The re-located hypocenters illuminate sub-horizontal, quasi-parallel, planar clusters that dip ~15° toward the West. The thickness of each cluster is less than 50 m, and the horizontal extent is as great as 100 m. The location of the same data set by the Coherence Collapsing is shown in Figure 4(c). The locations from the DD and the Coherence Collapsing method show detailed reservoir structure which was not delineated by the conventional SED method.

At Yufutsu gas field, Hokkaido, Japan, natural gas lies within a reservoir composed of naturally pre-existing fractures distributed in granitic basement and the upper conglomerate formations. 14 boreholes have been drilled into the reservoir, and FMI logging has been conducted at ten of them. The FMI images suggest that the boreholes with large gas production penetrate fractures with large apertures and that smaller fractures are not contributing significantly to gas production.

A hydraulic stimulation was conducted at one of the boreholes, in May, 2005. 5,628 m^3 of sea water was injected during 3 stages (1st step injection, the main injection, and 2nd step injection) for a week. The injection interval was from 4078mMD (Measured Depth) to 4220mMD in a conglomerate formation. We have monitored microseismic events using 4 downhole detectors at depths around 3100-3600m (Kumano et al., 2006)

Figure5 (b) shows the source distribution for events re-located using DD. In this figure, events are reclassified into multiplet clusters using a coherence criterion of 0.8, and each cluster is represented by a different color. Sub-parallel streaks represent each multiplet; these appear to be dipping to the SW with inclinations between 40 to 60 degrees.

To examine the reliability of the source distribution determined by DD we numerically calculated travel times using virtual source locations distributed on a sphere of radius 10 m around the feed point. The result indicates that DD technique cannot improve the source location in the direction that is consistent with direction of the streaks.

The geometry of the network is nearly planar; its normal is consistent with the direction of our multiplet streaks. Thus, we conclude that the source ‘streaks’ produced in this study using the DD method are artifacts arising from the planar geometry of the sensor network.

Summary

As described in this paper, coherence of the microseismic events is one of the parameters of importance to understand structure and extension process of stimulated zone. In this paper we introduced two mapping methods which uses information on coherency. The Coherence Collapsing method uses absolute picking of each event and a table of coherency among all the events. These inputs can be prepared in semi-realtime basis, and CPU time for the determination of the hypocenters is as small as that for JHD and original collapsing. The Coherence Collapsing method has an ability to provide absolute location of the multiplet groups but can not resolve seicmic structure of each multiplet groups. This means that orientation and stress state of the fracture with multiple slip can not be estimated. On the other hand, the DD has ability to precisely estimate relative location of the multiplets.

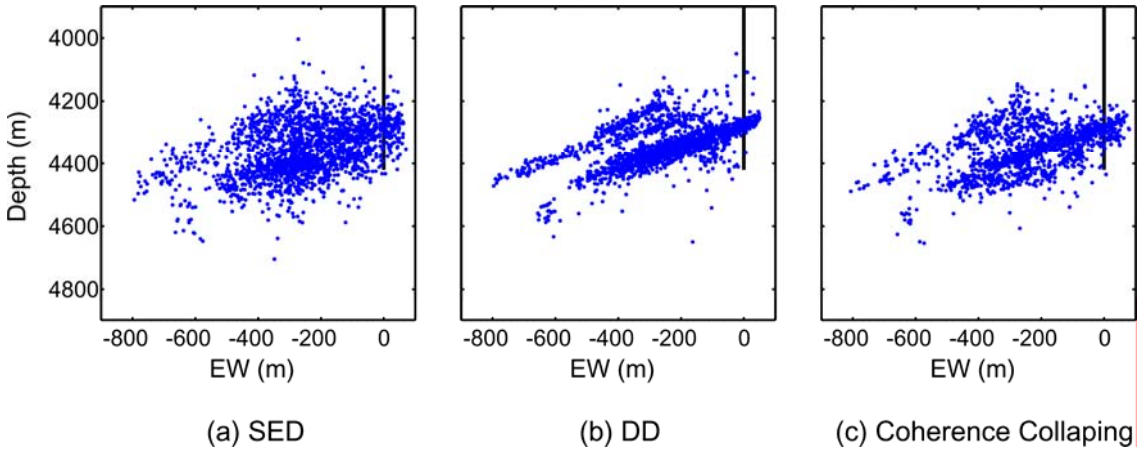

Figure. 4. Location of the microseismic data collected at Cooper Bain in 2003 by the SED, the DD, and the Coherence Collapsing.

However this method does not have realtime nature because of complex process to estimate relative time of arrivals. As shown in this paper, the distribution of the multiplets may be affected by the arrangement of the stations especially in the case of downhole sparse network. The absolute location by the DD is normally less reliable than relative locations.

Considering above mentioned advantages and disadvantages, we are currently using Coherence Collapsing method in realtime or semi-realtime monitoring as well as identification and clustering of mutiplet groups. After clustering the multiplets, precise relative picking is made to some groups of multiplets and DD is used to determine seismic structure of multiplets.

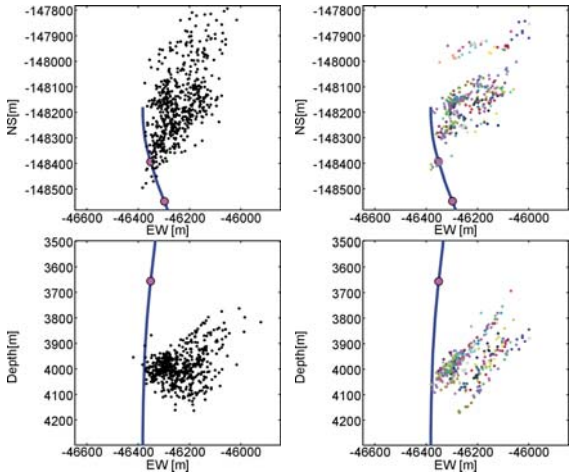

Fig.5 Comparison of source location

References

Asanuma, H., Izumi, T., Niitsuma, H., Jones, R., and Baria, R., Development of coherence collapsing method and its application to microseismicity collected at Soultz, Trans. GRC (2003), 27, 349-353.

Asanuma, H., Kumano, Y., Izumi, T., Soma, N., Kaieda, H., Aoyagi, Y., Tezuka, K., Wyborn, D., and Niitsuma, H., Microseismic monitoring of a stimulation of HDR reservoir at Cooper Basin, Australia, Trans. GRC (2004), 191-195.

Asanuma, H., Izumi, T., Kumano, Y., Soma, N., Niitsuma, H., Baria, R., and Michelet, S., Data acquisition and analysis of microseismicity from simulation at Soultz in 2003 by Tohoku University and AIST, Japan, Trans. GRC (2004) 187-190.

Asanuma, H., Mochiduki, S., Nakazato, K., Soma, N., Niitsuma, H., and Baria, R., Relocation of microseismicity from a stimulation of a deep reservoir at Soultz by a variation of the collapsing method, Trans. GRC, 26, (2002), 209 – 214.

Baria, R., Baumgartner, J., Gerad, A., and Garnish, J., The European HDR programme: main targets and results of the deepening of the well GPK-2 to 5000m, Proc. WGC 2000, (2000), 3643-3652.

Frohlich, C., An efficient method for joint hypocenter determination for large groups of earthquakes, Comput. Geosci., 5, (1979), 387-389.

Jones, R. H., and Stewart, R. C., A method for determining significant structures in a cloud of earthquakes, JGR, 102, (1997), 8245-8254.

Kumano, Y., Asanuma, H., Niitsuma, H., Tezuka, K., Kamitsuji, R., Reservoir structure

at Yufutsu gas field, JAPAN determined by analysis of induced microseismic multiplets, SEG Expanded Abstracts, (2006) (in-press)

Moriya, H., Nakazato, K., Niitsuma, H., and Baria, R., Detailed fracture system of the Soultz-sous-Forets HDR Field evaluated using microseismic multiplet analysis, Pure Applied Geophysics, 159, (2002), 517 – 541.

Niitsuma, H., Moriya, H., Asanuma, H., Evans, K., Jones, R. Jung, R. and Baria, R., Hydraulically created permeable structures in the Soultz HDR site by super resolution seismic mapping techniques, Proc. 24th NZ Geothermal Workshop, (2002), 153-157.

Murphy, H., Niitsuma, H., and Asanuma, H.: The more-than-cloud and successor projects: international joint research on new mapping and HDR/HWR reservoir development technologies, Proc. WGC 2000, (2000), 3813-1817.

Waldhauser, F. and Ellsworth, W. L., A double-difference earthquake location algorithm: method and application to the Northern Hayward Fault, California, BSSA, 90, (2000), 1353-1368.

Acknowledgments

The authors wish to acknowledge to the other members of the MTC/MURPHY International Collaborative Project for their discussion, advice and encouragement. We would like to thank GEIE for its cooperation for offering hydraulic/geological data from the European HDR site at Soultz which is supported mainly by the European Community, BMBF (Germany) and ADEME (France). We would also thank to the help from Geodynamics, which is conducting the Cooper Basin HDR/HFR Project, especially from Dr. B. de Graaf.

ENGINE – **EN**hanced **G**eothermal **I**nnovative **N**etwork for **E**urope
Workshop 3, "Stimulation of reservoir and induced microseismicity"
Kartause Ittingen, Zürich, June 29 – July 1, 2006, Switzerland

A Methodology for the hydro-mechanical characterisation of EGS reservoirs

MÉGEL Thomas, Geowatt AG, Zürich, Switzerland, megel@geowatt.ch
KOHL Thomas, Geowatt AG, Zürich, Switzerland

Abstract

The development of an EGS power plant depends vitally on the understanding of hydraulic, thermal, chemical and mechanical processes and properties of a fractured reservoir. But it is a fact that the knowledge about the leading parameters of an EGS reservoir behaviour - especially the spatial distribution of fractures or flow paths - is usually rather poor. The treatment of this problem in the hydro-mechanical code HEX-S will be discussed.

Keywords: stochastic, hydro-mechanical processes, fractured reservoir

Introduction

The development of an EGS power plant depends vitally on the understanding of hydraulic, thermal, chemical and mechanical processes and properties of a fractured reservoir. From an engineering point of view we would like to know all relevant parameters for characterising the actual state of a reservoir which would allow us to predict the results of a stimulation test and finally of long-term energy extraction.

Making predictions about a specific physical behaviour of a reservoir due to a change of boundary conditions - as e.g. during a stimulation test or during circulation - means applying a mathematical model in which as far as possible all existing information about the reservoir is integrated.

Despite the fact that a lot of progress has been made in the acquisition of information through hydraulic tests, microseismic measurements, well-logging and other methods, the underground system still remains highly under-determined during all phases of an EGS life-cycle. One method could be to integrate all known parameters deterministically into a model and treat unknown but relevant parameters in a stochastic manner. Especially the spatial distribution of fractures or flow paths is of crucial importance but usually very poorly known. How this problem can be treated shall be exemplified with the hydro-mechanical code HEX-S.

The hydro-mechanical code HEX-S

The hydro-mechanical code HEX-S has been developed to calculate the stimulation processes in a fractured reservoir during a massive injection into a borehole. The code takes into account the aperture change of each fracture in the model due to the corresponding overpressure resulting from the injection. The propagation of the overpressure in the reservoir as well as the development of the highly anisotropic reservoir permeability as a result of the fracture apertures is calculated as a time-dependent process. Hence the reaction of the reservoir permeability due to an arbitrary injection rate history can be calculated. Fig. 1 illustrates the typical transient development of a 0.1 mm aperture change in a fractured reservoir due to hydraulic injection.

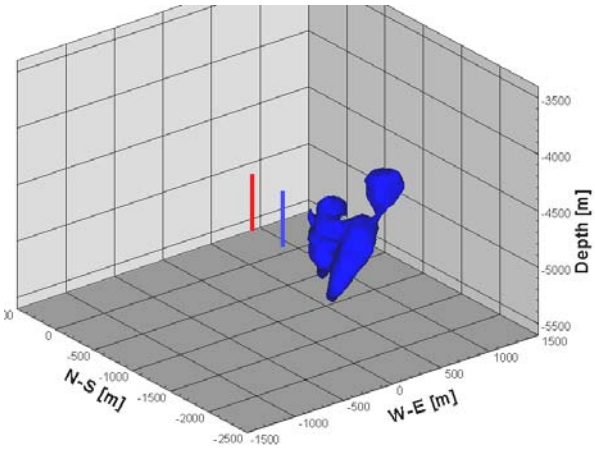

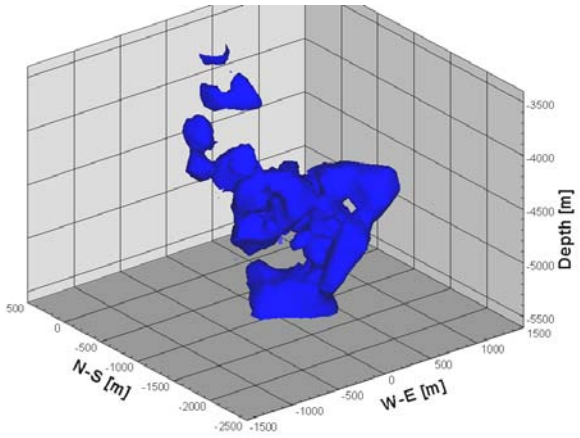

Fig. 1.: Calculated iso-surface of the 0.1 mm fracture aperture after 5 hours (top) and 20 hours (bottom) of injection into GPK4 for the 5 km deep reservoir domain at Soultz-sous-Forêts

Generation of the fracture network

The permeability distribution in a HEX S model depends essentially on the location, orientation and aperture of the incorporated fractures. HEX S allows defining an arbitrary number of both, stochastic and deterministic, fracture sets. Experience from various EGS test sites demonstrates that microseismic events often follow planar structures (i.e. Asanuma 2004, Evans et al. 2005; Cuenot et al. 2005). Since we assume that in most cases an induced microseismic event represents the shear failure of a along an area of a fracture ("slip patch"), the locations of the calculated shearing events can be compared with the microseismic clouds. In contrary, possible mode I events (normal stress variations) remain unidentified.

In HEX S every fracture or fracture zone is represented by a number of circular slip patches with small, predefined radii, generated by subdivision of a planar, and so far circular fracture zone. The aperture of each specific slip patch contributes to the final permeability distribution in the model. Starting from an initial value (see below), the aperture change of a fracture depends on the orientation, the local effective stress field and its defined mechanical parameters.

Each fracture zone in HEX S can be generated from deterministic or stochastic data, with the following detailed properties:

1. Deterministic fracture zones of defined radii, orientations and classes of mechanical behaviour for their slip patches: The corresponding data is generally derived from borehole logs (e.g. FMS, UBI) but may also include post-experimental interpretation of individual, microseismically active planar structures (Fig. 2).

2. Stochastic generation of fracture zones with random location and orientation: The statistical distribution of the orientation of fracture zones seen in borehole logs is used as the input parameter for the stochastic generation. Each random seed number generates a new distribution of fracture zones in the model (Fig. 3). Each stochastically generated model, independent from the random seed number, has the same distribution of orientations of fracture zones. Stochastically generated fracture zones are generally reasonably used at locations with little information (i.e. at greater distance from the boreholes). The herewith-defined model domain is filled-up until a predefined fracture (or slip patch) density is reached. Generally, sets of >20'000 slip patches are generated in this way.

The initial aperture of each slip patch is proportional to its radius and adjusted with an overall factor in such a way that the whole reservoir model has a predefined average permeability.

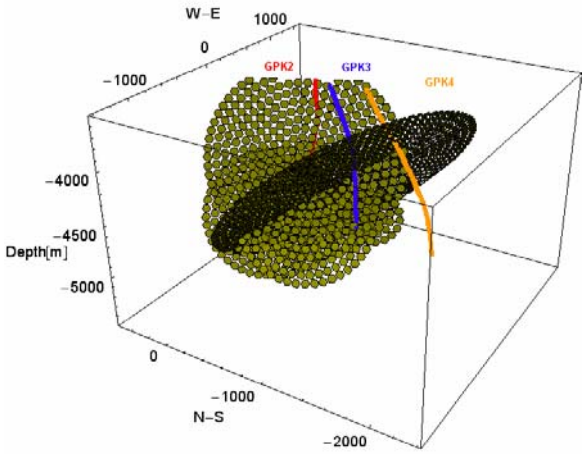

Fig. 2: Example of a model with deterministic fracture zones subdivided into slip patches for the 5 km deep reservoir domain at Soultz-sous-Forêts. Also indicated are the boreholes GPK2, GPK and GPK4

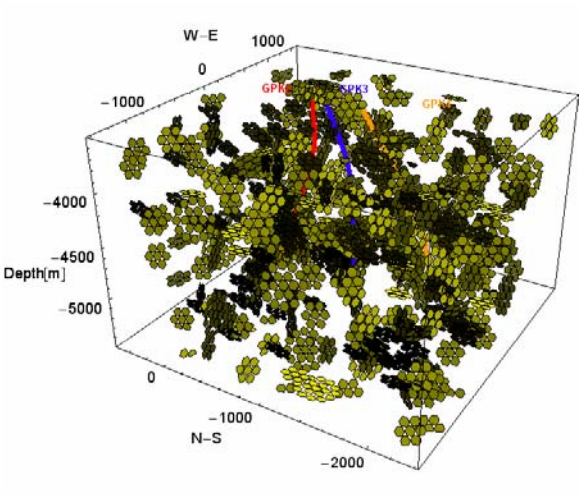

Fig. 3: Example of stochastically generated fracture zones for the 5 km deep reservoir domain at Soultz-sous-Forêts. Also indicated are the boreholes GPK2, GPK and GPK4

Implemented fracture aperture laws

The implemented aperture laws for the fractures or slip patches are basically of analytical kind (Willis-Richards et al., 1996, Jing et al., 1998, Bächler et al., 2001). The aperture of a fracture depends on three sets of parameters:

1. The mechanical properties of the fracture
2. The fluid pressure in the fracture space
3. The normal and the shear stress on the fracture plane

The effective normal stress $\sigma_{n,eff}$ and the effective shear stress τ_{eff} on the plane of a fracture are derived from the three regional principal stress components and the fluid pressure P at the fracture location. Depending on the pore and fracture fluid pressure P, the fracture aperture at a given location is assumed to react:

a) By compliance only

b) By compliance and shearing

c) By jacking and shearing

a. Compliance only

Under the condition of low effective shear stress, τ_{eff} , only a compliant reaction of the fracture walls to fluid pressure will affect the aperture. The conditions for this behaviour are

$$\sigma_{n,eff} > 0$$

$$\Delta\tau = \tau_{eff} - \sigma_{n,eff} \cdot \tan(\Phi) \quad < 0$$

(Mohr-Coulomb criterion)

As convention, stress is positive for compression. The friction angle Φ of the fracture walls is implemented as a function of $\sigma_{n,eff}$. The aperture increase is treated as reversible and vanishes as soon the pressure declines after the end of injection.

b. Compliance and shearing

If the effective shear stress τ_{eff} at the fracture walls exceeds the friction resistance, i.e. $\Delta\tau$ >0, and the effective normal stress $\sigma_{n,eff}$ still is positive, the fracture fails. The additional "shear" aperture change, a_s, due to the shear offset, U, is

$$a_s = U \cdot \tan(\Phi_{dil})$$

The shear dilation angle of the fracture wall, Φ_{dil}, is also implemented as function of $\sigma_{n,eff}$. The shear offset is defined from fracture shear stiffness, K_s, as:

$$U = \Delta\tau / K_s$$

This portion of the aperture increase is considered to be irreversible when injection test has stopped and the pressure field in the reservoir has reached its ambient value.

c. Jacking and shearing

In the case the effective normal stress, $\sigma_{n,eff}$, becomes negative, the fracture walls separate and the friction forces acting on them disappear. In addition to the shear aperture change, a contribution from jacking conditions, a_j, arises. Clearly, a_j is considered to be fully reversible.

Although the shear induced, mode II, aperture change of a fracture is the only permanent effect after an injection test has ended, the contributions from jacking and compliance are also of major importance for the propagation of the pressure front during the stimulation process.

Hydraulic processes

The time-dependent pressure calculation in HEX-S is performed with a new finite element (FE) algorithm which is a further development of the FRACTure code (Kohl & Hopkirk, 1995). The main advantages of the FE algorithm are in efficient and flexible formulations:

- Local mesh refinement at specified locations in the reservoir domain such as boreholes,
- Utilization of an implicit time-step procedure for the transient calculation
- Easy extension to further physical processes or constitutive laws

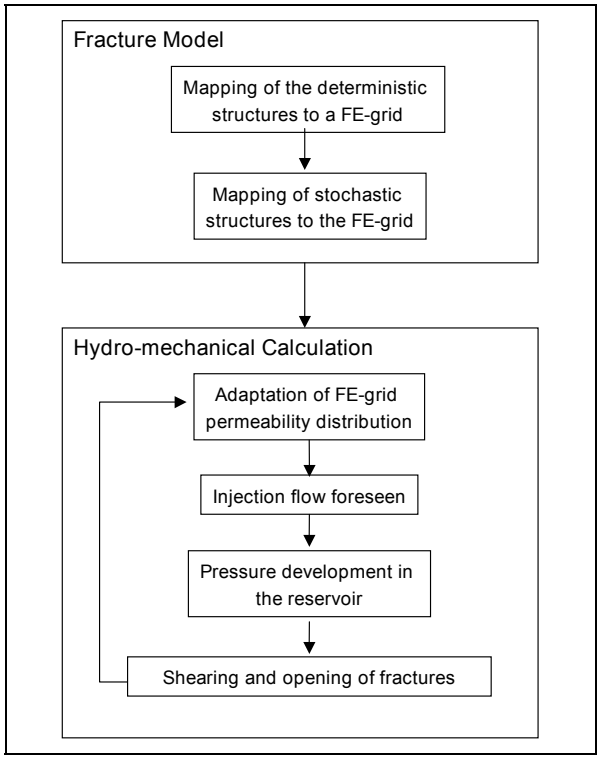

Fig. 4: Principle flow chart of HEX-S

The hydraulic conductivity for each element is derived from the apertures of the intersecting slip patches by a specific mapping procedure. The intersection of the discrete fractures with the continuous FE grid is calculated using a "Rock-to-Fracture volumetric index", RFVI. The mapping results in individual FE volumes of strongly anisotropic properties. Thereby, the hydraulic properties of the FE grid are modified after each time-step. HEX-S calculates the pressure in the model and determines the new apertures of the slip patches. When the hydraulic conductivities of the elements have been updated from the corresponding slip patch apertures, a next time-step is carried out (Fig. 4).

References

Asanuma, H., T. Izumi, Y. Kumano, N. Soma, H. Niitsuma, R. Baria, and S. Michelet, 2003, Data Acquisition and Analysis of Microseismicity from the Stimulation at Soultz in 2003 by Tohoku University and AIST, Japan., *Geothermal Resource Council, 2004*, Palm Spring Sep. 2004

Bächler D., Evans K., Hopkirk R., Kohl T., Mégel T., Rybach L., Data Analysis and controls towards understanding reservoir behaviour and the creation of a conceptual model, Final Report to the Bundesamt für Bildung und Wissenschaft, Projekt 98.0008-1 - EU Project No. JOR3-CT98-0313, Bern, Switzerland

Cuenot N., Dorbath C., Dorbath, L., 2005, Analysis of the microseismicity induced by fluid injections at the Hot Dry Rock site of Soultz-sous-Forêts (Alsace, France): implications for the characterization of the geothermal reservoir properties, *Pure and Applied Geophysics*, submitted

Kohl, T. and Hopkirk, R.J., 1995. "FRACTure" a simulation code for forced fluid flow and transport in fractured porous rock. *Geothermics*, 24(3): 345-359.

Evans K.F., Moriya H., Niitsuma H., Jones R. H., Phillips W. S., Genter A., Sausse J., Jung R., Baria R., 2005, Microseismicity and permeability enhancement of hydrogeologic structures during massive fluid injections into granite at 3 km depth at the Soultz HDR site, *Geophys. J. Int.*, 160: 388–412.

Jing, Z., Watanabe, K., Willis-Richards, J. and Hashida, T., 2002. A 3-D water/rock chemical interaction model for prediction of HDR/HWR geothermal reservoir performance. *Geothermics*, 31: 1-28.

Willis-Richards, J., Watanabe, K. and Takahashi, H., 1996. Progress toward a stochastic rock mechanics model of engineered geothermal systems. *Journal of Geophysical Research*, 101(B8): 17,481-17,496.

ENGINE – **EN**hanced **G**eothermal **I**nnovative **N**etwork for **E**urope
Workshop 3, "Stimulation of reservoir and microseismicity"
Kartause Ittingen, Zürich, June 29 – July 1, 2006, Switzerland

Hydro-mechanical behaviour of GPK3 and GPK4 during the hydraulic stimulation tests – Influence of the stress field

RACHEZ Xavier, BRGM, Orléans, France, x.rachez@brgm.fr
GENTIER Sylvie, BRGM, France
BLAISONNEAU Arnold, BRGM, France

Abstract

A study, started several years ago, aimed to construct a 3D hydro-mechanical model of the stimulation of the fracture network around each stimulated wells for the deep geothermal reservoir at Soultz-Sous-Forêts. A numerical approach based on the distinct element method (3DEC code) has been developed in order to understand and to explain the physical mechanisms which are at the origin of the hydraulic behaviour observed during stimulation tests conducted in the various wells. Previous studies have shown that there was a significant correlation between the orientations of the permeable fractures in relationship with the orientation of the in situ stresses. Knowing the most appropriate in-situ stresses is then a key issue.

This paper deals with the hydro-mechanical modelling of the stimulation tests performed in GPK3 and GPK4. Two stress fields are taken into account: the classical one used up to now, determined by Klee and Rummel (1993), and the new one determined by Cornet & al. (2006). Their influence in terms of shearing in the main fractures of the rock mass during hydraulic stimulations is analyzed.

Keywords: deep fractured crystalline reservoir, hydro-mechanical behaviour, hydraulic stimulation

Introduction

Our current 3DEC models focus on the hydro-mechanical behaviour of the deep wells GPK3 and GPK4 during hydraulic stimulations. At this stage of our modelling work, we do not take into account the effect of a hydraulic stimulation performed in a well on the response of the hydraulic stimulation of another well, nor the thermal impact of the injection of a cold fluid in the hot rock. These two assumptions will be taken care of in a later modelling.

3D Hydro-mechanical modeling

We used the 3DEC code (Itasca, 2003) in order to model the hydraulic stimulation in the fracture network around the wells. This code is based on the Distinct Element Method. Initially devoted to the modelling of three dimensions mechanical problems, 3DEC has been extended in order to simulate hydro-mechanical process due to fluid flows in deformable joints cutting three dimensions solids. Thus, it allows us to simulate interactions between the mechanical process (deformations, stresses, …) and hydraulic process (pressures, apertures, …) in a rock mass cut by discrete discontinuities which correspond to a realistic geometry of the fracture network. The resulting blocks are considered in 3DEC to be deformable, but impermeable. Indeed, the fluid flow occurs only in the joints and there's no porous flow in the rock matrix. The fluid low is laminar, obeying to a cubic law, and monophasic: the joints either are fully saturated or totally dry. This assumption is considered true for the Soultz-sous-Forêts granite as the matrix permeability is negligible.

From a mechanical point of view, the behaviour of the fractures is assumed to be elasto-plastic, the elastic part of the behaviour of the joints being governed by a normal and a tangential stiffness. The elastic behaviour of the joints is limited by a standard Mohr Coulomb criterion above which the shear behaviour of the joints is perfectly plastic with dilation. The blocks are also deformable and are assumed to display an elastic behaviour.

Concerning the numerical aspects, the blocks are discretized into tetrahedral elements and the fractures into elementary domains. The numerical resolution of the transient flows is done by using a finite difference scheme. At each time step, the flows between nets induced by the pressure field are calculated. At constant time the excess (or loss) of fluid volume in each elementary domain is modified by running mechanical cycles during which the fluid pressure is modified proportionally to the "non-equilibrated" volume. The modification of the pressure field results in a modification of the actual stresses applied to the surrounding formations, which may themselves cause changes in the openings of the fractures and hence of the pressure field. Since the calculation method in 3DEC is incremental

with preset time steps, equilibrium in the model is assumed to occur when the pressure and stress fields no longer change between two consecutive time steps.

The mechanical deformations in the normal direction (U_n) and hydraulic apertures (a) are related by the expression above in which (a_0) represent the initial hydraulic aperture defined for each discontinuity:

$a = a_0 + U_n$ (1)

Hydraulic stimulation tests

Preamble

To simplify access and data readability, we gathered in this chapter all the common features between the GPK4 and GPK3 models. Specific features, such as the fracture geometries, or the fractures hydro-mechanical properties are detailed in each corresponding GPK3 or GPK4 paragraph.

Size of the models

The numerical models are a parallelepiped volume, centred on the open hole of each studied well. The model size is 400m*400m*1000m. At this stage, the open hole of each well is considered as vertical. The Y-origin is located at the centre of each model which is extended over the range of - 500m to + 500m.

Initial hydro-mechanical conditions

The aim of our study is to analyze the influence of the stress field on the deep wells hydro-mechanical response during hydraulic stimulation. We hence performed two sets of numerical models where we assumed as initial stresses in the model, either the classical stress field used up to now, determined by Klee and Rummel (1993), or the new stress field determined by Cornet et al (2006).

The stress field determined in the nineties by Klee and Rummel is the following:

$\sigma_h = 15.8_{[MPa]} + 0.0149_{[MPa/m]}$ (depth$_{[m]}$-1458)

$\sigma_H = 23.7_{[MPa]} + 0.0336_{[MPa/m]}$ (depth$_{[m]}$-1458) (2)

$\sigma_v = 33.8_{[MPa]} + 0.0255_{[MPa/m]}$ (depth$_{[m]}$-1377)

where σ_h and σ_H represent respectively the minimal and maximal horizontal principal stress; and σ_v the vertical principal stress. The direction of the maximal horizontal principal stress σ_H is N170°E ± 15°.

This natural stress had been determined for depths between 1450m and 3500m. However, as the open holes of the three deep wells GPK2, GPK3, and GPK4 were located at a 4000m to 5000m depth, and as there were, up to recently, no other stress field data, it had been assumed that one could extend the validity of this stress field below 3500m depth.

More recently, in 2005, Cornet et al. (2006) determined the following stress field:

$\sigma_h = (0.54 +/- 0.02)* \sigma_v$

$\sigma_H = (0.95 +/- 0.05)* \sigma_v$,

oriented N175°E +/- 6° (3)

$\sigma_v = 1377*0.024_{[MPa]} + 0.0255_{[MPa/m]}$ (depth$_{[m]}$-1377)

where σ_h and σ_H represent respectively the minimal and maximal horizontal principal stress; and σ_v the vertical principal stress. The direction of the maximal horizontal principal stress σ_H is N175°E ± 6°.

Figure 1 shows the variations of σ_h, σ_H and σ_v with depth for the two stress fields: n°1 determined by Klee and Rummel, and n°2 determined by Cornet et al. The main difference between these two stress fields is that the stress regime differs for depths below 3000m: with the 2nd stress field, the stress regime remains a normal fault stress regime ($\sigma_h < \sigma_H < \sigma_v$) whereas with the first stress field, one has a normal fault stress regime for depths above 3000 m that change into strike slip regime ($\sigma_h < \sigma_v < \sigma_H$) for deeper depths. With the stress field n°1, the sub-vertical fractures in the deep Soultz granite are less horizontally constrained than with the 2nd stress field. This should obviously change their hydro-mechanical behaviour when one performs the hydraulic stimulation.

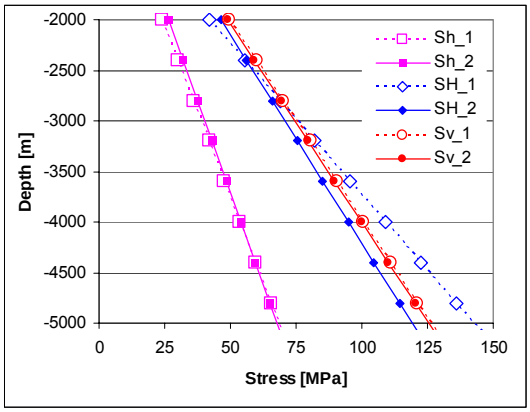

Figure 1. Stress regimes at Soultz-sous-Forêts. Comparison of stress fields n°1 and n°2.

For the two sets of numerical models, we assume that the distribution of the initial fluid pressures in the fracture network obeys to a hydrostatic field as indicated in the equation below:

$P = \rho * g * y$ (4)

where ρ represent the density of water, g is gravity and y is the depth.

Boundary hydro-mechanical conditions

The hydro-mechanical boundary conditions, shown Figure 2, are the following:

- Zero displacements are imposed at the North, West and bottom faces,

- Stresses, corresponding to the given stress field n°1 or n°2 are applied on the South, East and top faces,

The hydrostatic pressure (Eq. 4) is fixed on each face of the rectangular model.

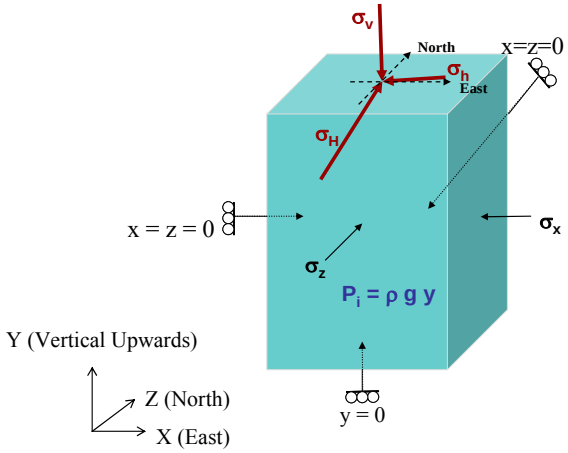

Figure 2. Initial and boundary hydro-mechanical conditions assumed in the model

Hydro-mechanical behaviour of blocks and fractures

In all the models, blocks are considered as elastic with the mechanical properties given Table 1.

Density (kg/m^3)	Young Modulus (MPa)	Poisson's ratio υ
2680	52000	0.29

Table 1. Blocks mechanical properties

All the fractures have the same mechanical constitutive law. The normal mechanical behaviour is elastic linear while the fracture is in compression; tensile strength is null. The tangential mechanical behaviour is elasto-plastic. It follows a Mohr Coulomb failure criterion with dilation effect. The shear strength of the joint verifies:

$$\tau_s \leq c + \sigma_n * \tan(\phi) \qquad (5)$$

Where c is the joint cohesion, σ_n is the normal stress applied on the joint, ϕ is the joint friction angle.

The effect of dilation appears as soon as the maximum shear strength is reached. When the joint is slipping, the increase of the walls joint normal displacement $\Delta U_{n\text{-}dil}$ due to the dilatation is governed by the following equation:

$$\Delta U_{n\text{-}dil} = \Delta U_s * \tan(\psi) \qquad (6)$$

Where ΔU_s is the tangential displacement increment and ψ is the dilation angle

In order to avoid an infinite opening of the joint when shear displacements are long, the dilation effect is cancelled in 3DEC as soon as the tangential displacement reaches a threshold called Z_dil. The shear behaviour is illustrated in Figure 3 in the case of a null cohesion.

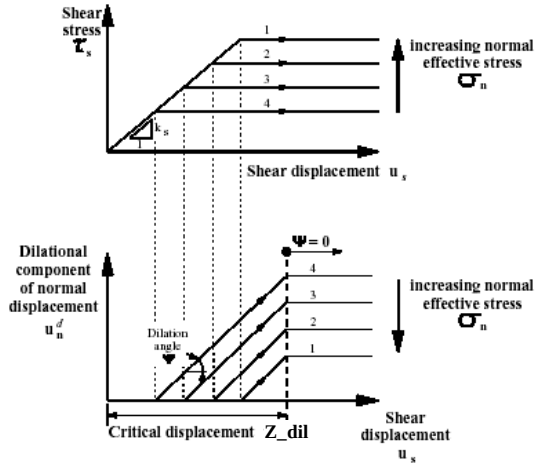

Figure 3. Illustration of the Mohr-Coulomb model with dilation effect (for a null cohesion) (ITASCA, 2003)

The fractures hydro-mechanical parameters for GPK3 and GPK4 are detailed in each corresponding paragraph.

Hydraulic stimulation of the deep wells

The simulation of the hydraulic test is carried out by adding an overpressure (ΔP) in the open part of the well (Figure 4). For each overpressure stage, a specific hydro-mechanical coupling procedure, developed with the macro language FISH, allows us to:

- calculate the flow rate injected in the well throughout the fracture network and the flow rate at the external boundaries,

stop automatically the run when there is equilibrium between the injected flow and the flow that goes out of the model.

The several overpressure stages are defined from the in situ experimental stimulation tests. However, in order to avoid any numerical instability, we apply intermediate stages of

overpressure instead of the two or three real overpressure values that have been applied during the real stimulation test (Table 2).

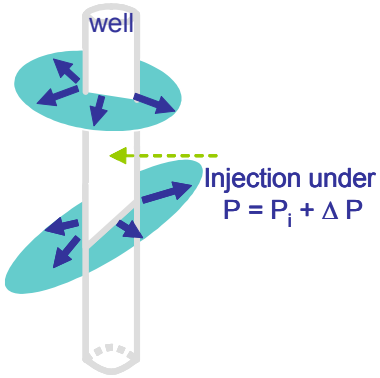

Figure 4. Overpressure conditions used in the simulation of the hydraulic stimulation

Overpressure stages applied in GPK3 [MPa]	Overpressure stages applied in GPK4 [MPa]
2.5	3.0
5.0	6.0
10.5*	9.0
12.5*	**13.75***
15.0*	15.5
17.0	**18.3***

*** Reference overpressure values issued from *in situ* measurement in the wells**

Table 2. Overpressure stages applied in the wells for modelling

GPK4 hydraulic stimulation test

GPK4 - fractures data

In this deep well, very little data is available. A preliminary fracture network has been defined essentially by comparing the thermal anomalies issued from the temperature log (July 2004) with the UBI (Gentier et al. 2005). Nine fractures have been selected and introduced in the GPK4 3DEC model. Their geometry is detailed Table 3. The GPK4 3DEC model, shown Figure 5, is centred on Fracture F6, at 4797m depth. Fractures are roughly sub-vertical and parallel to the maximum horizontal stress.

Fracture N°	Depth (m)	Dip (°)	Dip Direction (°)
F1	4797 - 244	86	274
F2	4797 - 146	83	281
F3	4797 - 99	80	272
F4	4797 - 62	85	257
F5	4797 - 23	75	75
F6	4797 - 0	66	57
F7	4797 + 27	69	255
F8	4797 + 61	70	263
F9	4797 + 162	78	290

Table 3. GPK4 fractures planes geometry

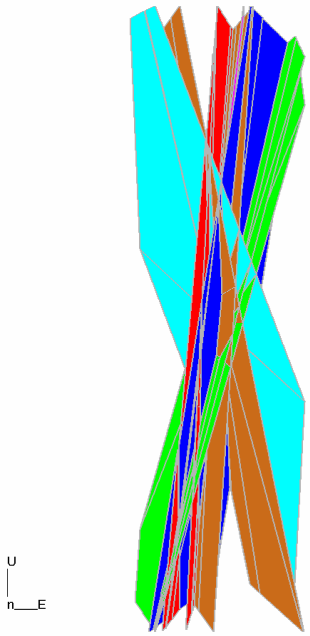

Figure 5. GPK4 3DEC model fractures perspective view

We use a 45° friction angle (Table 4) and a 5.0 μm initial hydraulic aperture a_0 (Table 5).

K_n [MPa/m]	Ks [MPa/m]	Cohesion [MPa]	Friction angle	Dilation angle	Z_dil [mm]
80000	80000	0	45°	1°	10

Table 4. GPK4 basic set of fractures mechanical properties

Initial aperture a_0 [μm]	Residual aperture a_{res} [μm]	Maximum aperture a_{max} [μm]
5.0	2.5	150

Table 5. GPK4 basic set of fractures hydraulic properties

GPK4 - influence of the stress field

We performed two numerical hydraulic stimulation tests:

- Case1, corresponding to the stress field n°1 proposed by Klee and Rummel,
- Case2, corresponding to the stress field n°2, proposed by Cornet et *al.*

Figure 6 represents the Flowrate (Q) vs Overpressure stages (ΔP) stimulation curves obtained with 3DEC for the two cases and the one obtained in-situ. At the 18.3 MPa overpressure stage, the flowrates injected in the well are very much comparable between the two stress fields: 60.7 l/s for stress field n°1, and 63.1 l/s for stress field n°2, whereas the in-situ injected flowrate is about 45 l/s. Although one does not have a very good fit of the in-situ Q-ΔP stimulation curve with these fractures hydro-mechanical properties (Table 4 & Table 5), taking into account the first or the second stress field does not change much the total flowrate in the well.

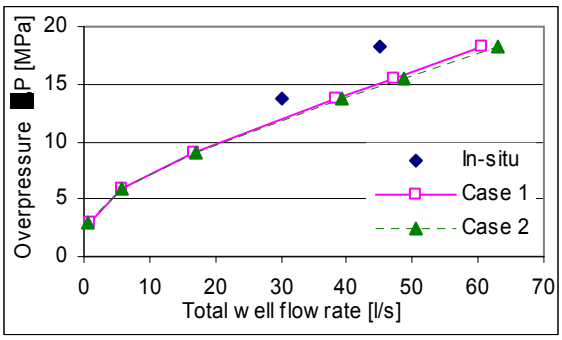

Figure 6. GPK4 – Case 1 & 2 – Evolution of the total well flowrate as a function of the overpressure stages ΔP applied into GPK4 – Comparison of the two stress fields n°1 & n°2

Figure7 represents the flow contribution, in percentage, of each fracture to the total flow in the well for each overpressure stage (ΔP). One can see that the flowrates distribution along the 9 fractures does not drastically change between the two stress fields. Moreover, the small differences become negligible when the overpressure ΔP increases. Also, for the two stress fields, the flow contribution of each fractures get smoother while the overpressure ΔP increases. For the first numerical overpressure stage, 3 MPa, the main part of the flow goes trough the first two fractures that are located on the top of the model: F2 (48-50%) and F1 (25-30%), the flow contribution of the other fractures being negligible (<10% in F3 as well as in F4, and <2% in each deeper fracture). For the last overpressure stage, 18.3 MPa, the flow distribution is much more homogenous between the 9 fractures: 17-19% in F1, 14-16% in F2 and F4, 9-10% in F6, F7, F8, F9, 8% in F3 and 6% in F5. Only fracture F4 seems to have a different behaviour than the other fractures. As soon as starts the stimulation test, F4 gives a non negligible flow contribution, 8%, and gives after the second overpressure stage a constant flow contribution whereas the flow contribution of the other fractures change with the overpressure stages. The flow contributions of fractures F1, F2, F3, located above F4, decrease when the overpressure increases, whereas the flow contributions of fractures F6 F7, F8 and F9 increase when the overpressure increases.

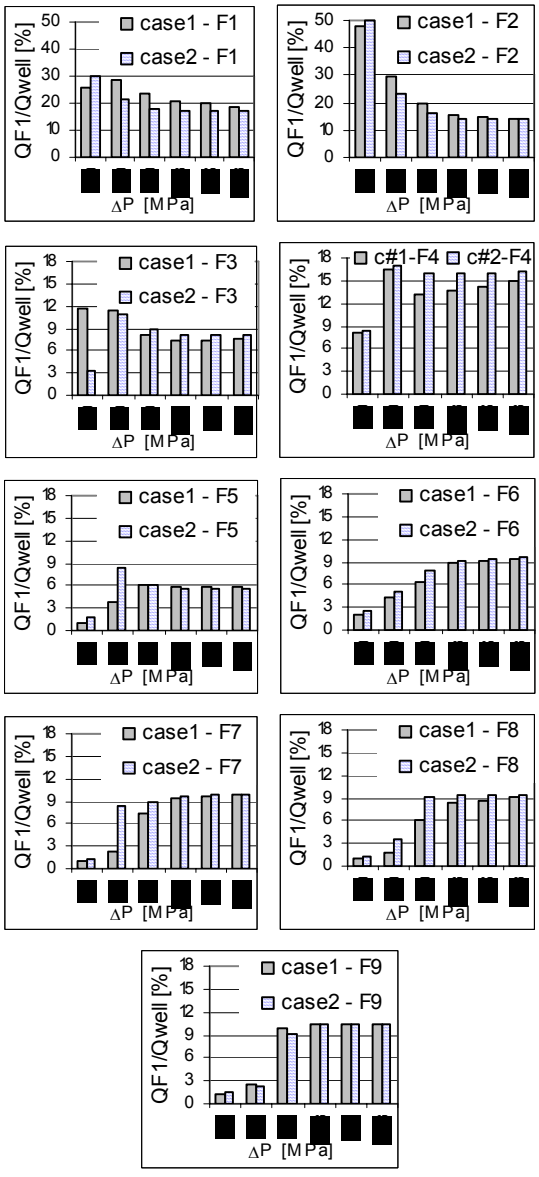

Figure 7. GPK4 – Case 1 & 2 – Flowrate percentages in each fracture vs. overpressure stages ΔP applied into GPK4 – Comparison of the two stress fields n°1 & n°2

If there is very little difference in terms of flow in the well between the two stress fields, the mechanical behaviour is on the contrary really different. Table 6 summarizes the values of

the maximum shear displacements in the fractures planes measured, at the 18.3 MPa overpressure stage, in the entire model, as well as in a set of 7 vertical cross sections parallel to the West-East axis. The highest values of shear displacements are measured in cross sections close to the model centre, far away from the external faces that have zero displacements boundaries (West and North) or fixed stress boundaries (East and South). However, these maximum values are not measured in the cross section that goes through the well. With the stress field n°1, which corresponds to a strike slip stress regime for depth greater than 3000m, it is not surprising that the fractures shear displacements are greater than with the second stress field which allows the fractures to remain in a normal fault regime. The maximum shear displacements in the fractures planes obtained with the first stress field is about 12.9 cm, twice as much as the maximum shear displacements obtained with the second stress field: 6.15 cm.

	Vertical cross section, located at z =							Entire model
	156 m	96 m	36 m	0 m	-24 m	-84 m	-144 m	
Case1	4.25	7.19	12.67	6.59	5.97	4.48	3.83	12.91
Case2	2.62	4.33	5.63	5.22	5.32	4.56	2.87	6.15

Table 6. GPK4 – Case 1 & 2 – Maximum shear displacements [cm] in the fractures planes, measured in the entire model and in a set of 7 vertical cross sections, parallel to the West-East axis at ⊿P = 18.3 MPa – Comparison of the 2 stress fields

Figure 8 represents the shear displacement vectors along the fractures in one of the studied vertical cross section, parallel to the West-East axis, located at z = +36 m (towards North), at the 18.3 MPa overpressure stage. These shear displacement vectors give a very useful information on the shearing directions and help understanding the overall model mechanical behaviour. One can see here that the shearing directions in F1 and F4 are almost along the vertical axis, whereas the shearing direction in F9 is more horizontal and perpendicular to the cross section. The maximum shear displacements obtained in this cross section located at z = +36 m, respectively 12.7 cm and 5.6 cm for stress fields n°1 & 2, correspond roughly to the maximum shear displacements obtained in the entire model. This great shearing for this cross section is mainly located in fractures planes F1 and F4.

Figure 9 to Figure 11 represent, for the two stress fields n°1 and n°2, the shear displacement contours in fractures planes F1, F2 and F4, at the 18.3 MPa overpressure stage. These contours confirm somehow the shear displacements vectors drawn Figure and clearly indicate that for the first stress field, used up to now in the modelling of the stimulations tests, the maximum shearing does not occur so close to the well. The maximum shear displacements do not appear round the well, but are located in some faces that are delimited by intersections with other fractures:

- in F1, the maximum shear displacements are in the area delimited by the intersections with F4 and F5,
- in F2, they are located in the area delimited by the intersections with F3 and F4,
- in F4, they are located in the area delimited by the intersections with F1 and F2, but also in the area between the intersection with F1 and the external boundary limit (note that the grey colour used by 3DEC for drawing some shear displacements contours in F4 correspond to values that are greater than the maximum value of 11 cm specified by the user. The maximum shear displacement in F4, located in the grey contour, is therefore greater than 11 cm and corresponds to the maximum of 12.9 cm measured in the entire model).

Figure 12 shows a perspective view of the blocks displacements vectors at the 18.3 MPa overpressure stage. For the two stress fields, there is a global movement of the blocks delimited by F4 and F5. For the stress field n°2, the maximum block displacement is about 7 cm, whereas with the first stress field the maximum block displacement is over 10 cm. However, with the stress field n°1, the displacement vectors point towards the South vertical face, which has fixed stress boundaries, whereas with the stress field n°2, the displacement vectors are not so horizontally spread and they point towards the bottom. This shows that the rock mass with the first stress field n°1 and the 18.3 MPa overpressure stage is almost unstable, whereas, with the second stress field, it is more likely to remain stable even with greater overpressures stages.

This 12.9 cm fracture shear displacement obtained with the first stress field corresponds therefore to some rock mass instability. This leads us to conclude that the first stress field is not the best appropriate for modelling the Soultz-sous-Forêts stress regime at 5000 m depths.

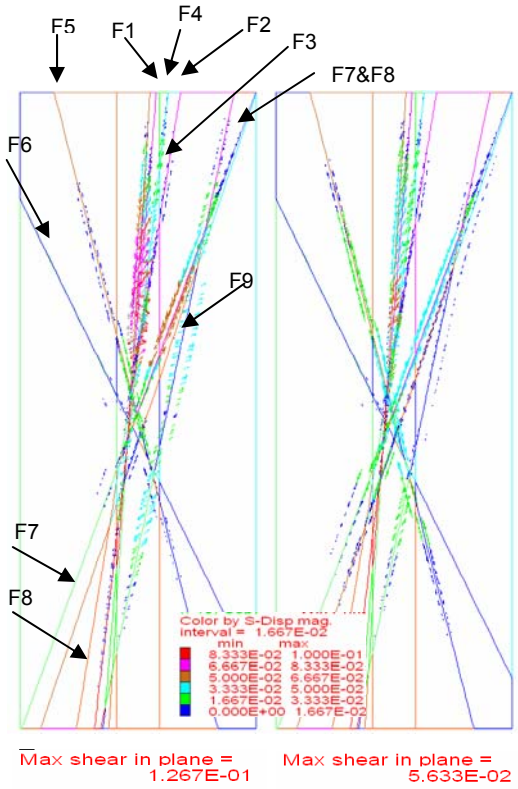

Case 1 (stress field n°1) Case 2 (stress field n°2)

Figure 8. GPK4 – Case 1 & 2 – Shear displacements vectors in a vertical plane, // to the East axis & located at z = 36m, at ΔP = 18.3 MPa – Comparison of the 2 stress fields

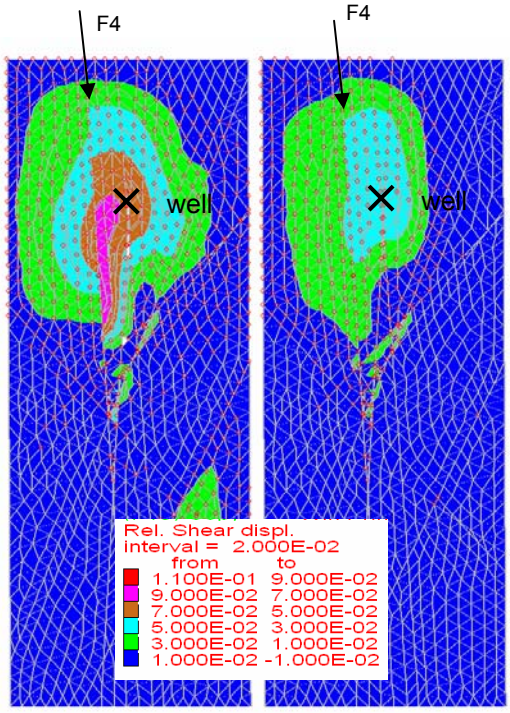

Case 1 (stress field n°1) Case 2 (stress field n°2)

Figure 9. GPK4 – Case 1 & 2 – Shear displacements contours in F1 at ΔP = 18.3 MPa – Comparison of the 2 stress fields

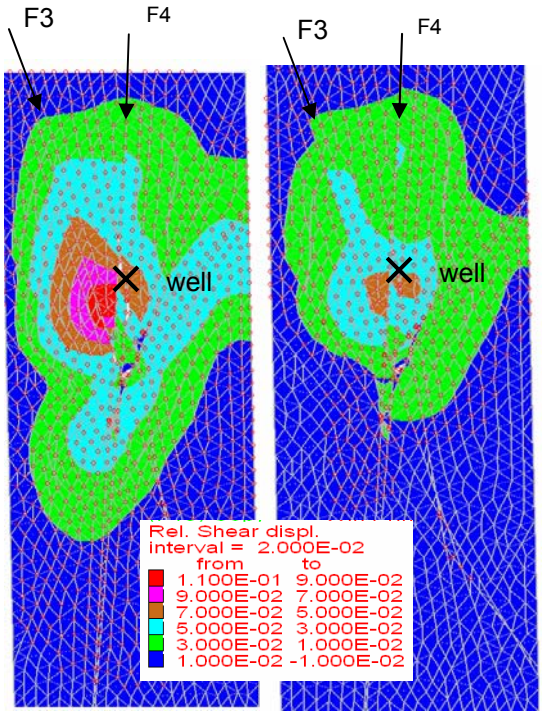

Case 1 (stress field n°1) Case 2 (stress field n°2)

Figure 10. GPK4 – Case 1 & 2 – Shear displacements contours in F2 at ΔP = 18.3 MPa – Comparison of the 2 stress fields

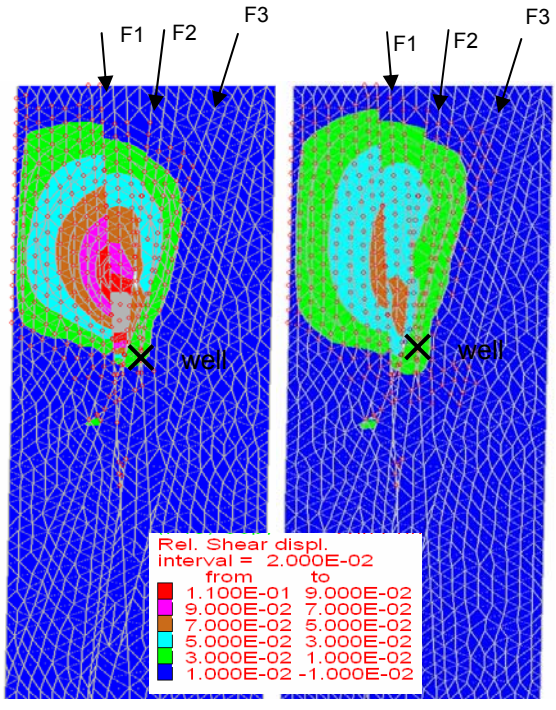

Case 1 (stress field n°1) Case 2 (stress field n°2)

Figure 11. GPK4 – Case 1 & 2 – Shear displacements contours in F4 at ΔP = 18.3 MPa – Comparison of the 2 stress fields

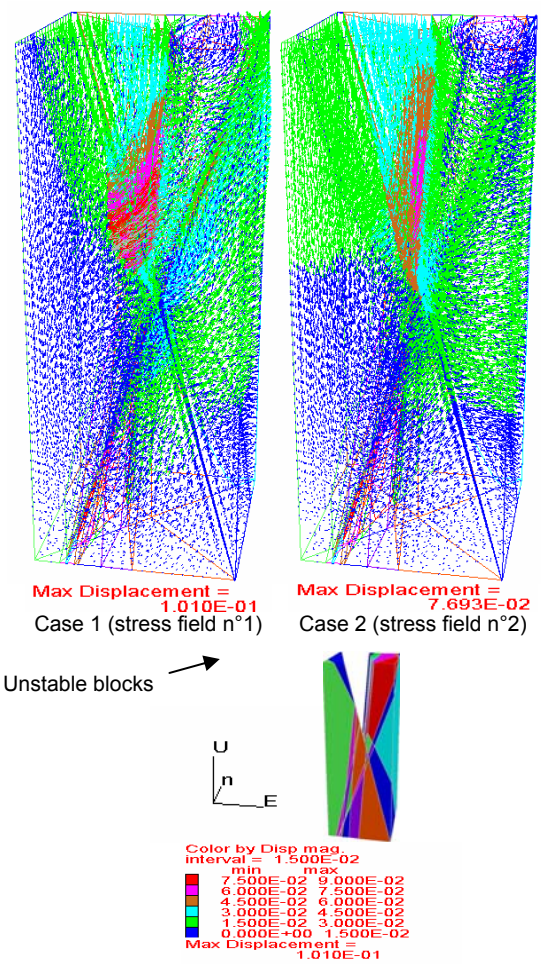

Figure 12. GPK4 – Case 1 & 2 – Perspective view of the displacement vectors in blocks at ΔP = 18.3 MPa – Comparison of the 2 stress fields

Best fit of the GPK4 hydraulic stimulation test

The total well flowrates obtained with either the first or with the second stress fields were too high compared to the in-situ injected flowrate (Figure 6). We tried to obtain a better fit of the Q-ΔP stimulation curve by choosing more appropriate fractures hydro-mechanical properties (Table 7).

Without any flow logs, we used only the UBI logs available. As F1 and F9 seemed to be less damaged than the other fractures, we decreased by a factor of 10 the hydraulic apertures used for the basic cases, case 1 and 2. As the UBI logs for F3, F4, F7 and F8 show regions much more fractured than for F2 and F5, we decided to keep constant the hydro-mechanical properties for F2 and F5, and to reduce the friction angle from 45° to 40° for fractures F3, F4, F7 and F8. For F4, we also decreased by a factor of 2 the hydraulic apertures.

With the modified fractures hydro-mechanical properties given Table 7, we performed two numerical hydraulic stimulation tests:

- Case3, corresponding to the stress field n°1,
- Case4, corresponding to the stress field n°2.

Figure 13 represents the Flowrate (Q) vs. Overpressure stages (ΔP) stimulation curves obtained with 3DEC for the two cases and the one obtained in-situ. At the 18.3 MPa overpressure stage, the flowrates injected in the well are still very much comparable between the two stress fields, but they also exactly match with the in-situ injected flowrate.

The maximum fractures shear displacements obtained in the models are respectively 7.3 cm for case 3 and 8.3 cm for case 4 (Table 8). These values are not located in the same fractures:

- for case 3, the maximum fracture shear displacement is measured in F2, around the well (Figure 15),
- for case 4, it is located in F7 (Figure 17).

Reducing the F4 hydro-mechanical properties (Table 7) changes drastically the mechanical behaviour of the rock mass. The shear displacements in F4 are less than 4 cm (Figure 16), and there is no instability of the blocks delimited by fractures F4 and F5 like with the basic set of hydro-mechanical properties (cases 1 & 2). Also, in the vertical cross sections, the shear displacements are of the same order of magnitude between the two stress fields (Table 8).

Whatever the fractures hydro-mechanical properties are, it is interesting to note that the maximum shear displacements obtained in a model are not automatically located around the well, but far away from it, in some areas of fractures planes delimited by intersections with other fractures. For case 4, one can see that the maximum shear displacement is obtained in F7, more than 100 m from the well. However, we need to perform some more detailed analysis to check if this is due to an instability and if this 40° friction angle is realistic.

	Fracture N°	Initial aperture a_0 [μm]	Resid. aperture a_{res} [μm]	Max. aperture a_{max} [μm]	Friction angle φ (°)
Case 1 & Case 2	F1 to F9	5.0	2.5	150	45
Case 3 & Case 4	F1	**0.5**	**0.25**	**15**	45
	F2	5.0	2.50	150	45
	F3	5.0	2.50	150	**40**
	F4	**2.5**	**1.25**	**75**	**40**
	F5	5.0	2.50	150	45
	F6	5.0	2.50	150	**40**
	F7	5.0	2.50	150	**40**
	F8	5.0	2.50	150	**40**
	F9	**0.5**	**0.25**	**15**	45

Table 7 – GPK4 – Changes fractures hydro-mechanical properties

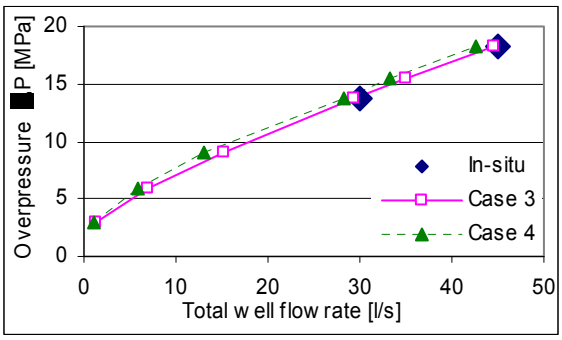

Figure 13. GPK4 – Best fit of Qwell-ΔP - stimulation curve Cases 3 & 4, respectively with the two stress fields n°1 & n°2

	Vertical cross section, located at z =							Entire model
	156 m	96 m	36 m	0 m	-24 m	-84 m	-144 m	
Case3	2.40	4.50	6.68	7.25	6.75	5.57	4.30	7.31
Case4	2.96	5.92	6.90	7.26	7.45	8.16	7.18	8.32

Table 8. GPK4 – Case 3 & 4 – Maximum shear displacements [cm] in the fractures planes, measured in the entire model and in a set of 7 vertical cross sections, parallel to the West-East axis at ΔP = 18.3 MPa – Comparison of the 2 stress fields

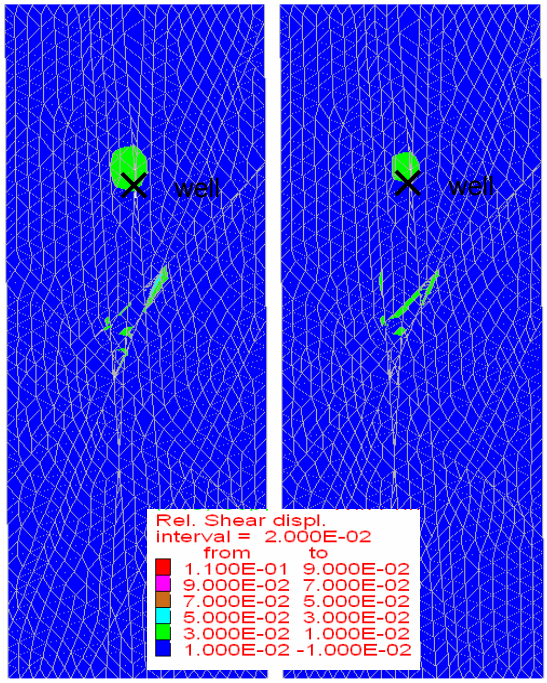

Case 1 (stress field n°1) Case 2 (stress field n°2)

Figure 14. GPK4 – Case 3 & 4 – Shear displacements contours in F1 at ΔP = 18.3 MPa – Comparison of the 2 stress fields

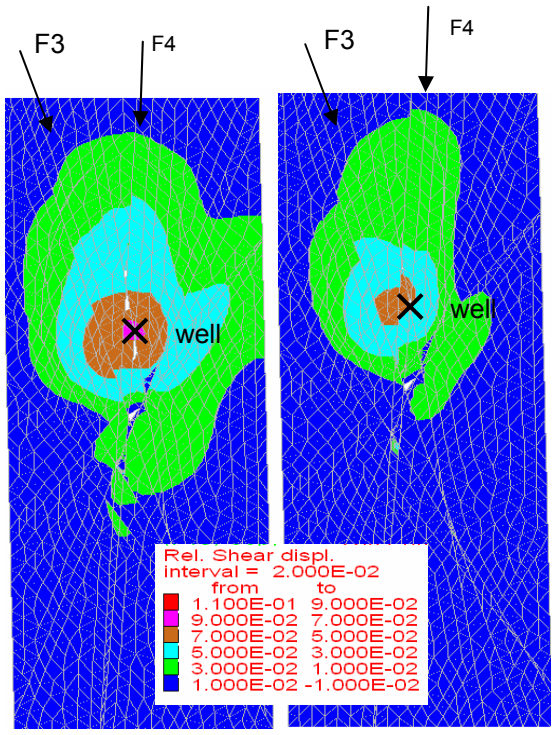

Case 1 (stress field n°1) Case 2 (stress field n°2)

Figure 15. GPK4 – Case 3 & 4 – Shear displacements contours in F2 at ΔP = 18.3 MPa – Comparison of the 2 stress fields

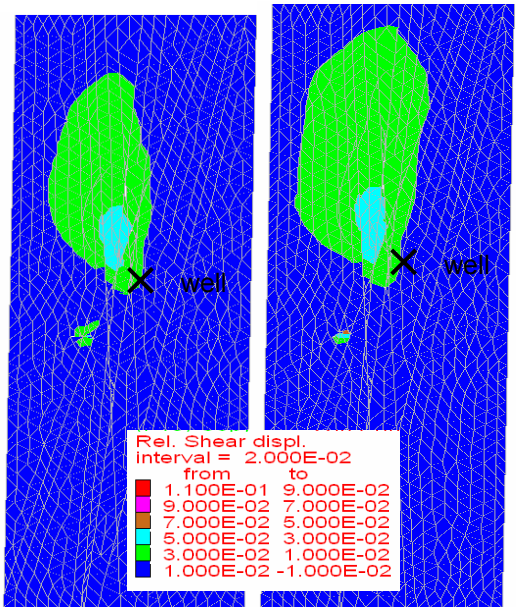

Case 1 (stress field n°1) Case 2 (stress field n°2)

Figure 16. GPK4 – Case 3 & 4 – Shear displacements contours in F4 at ΔP = 18.3 MPa – Comparison of the 2 stress fields

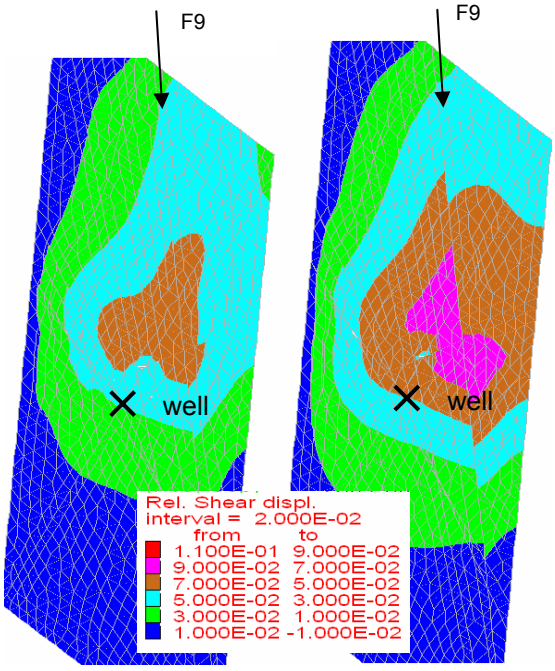

Case 1 (stress field n°1) Case 2 (stress field n°2)

Figure 17. GPK4 – Case 3 & 4 – Shear displacements contours in F7 at ΔP = 18.3 MPa – Comparison of the 2 stress fields

GPK3 hydraulic stimulation test

GPK3 fractures data

In order to study the influence of the stress field on the GPK3 stimulation test, we used the GPK3 geometry, as well as the hydro-mechanical parameters, that have been used in the previous studies of the GPK3 stimulation test (Gentier et al. 2003). For easier access and readability, we give the several parameters hereafter.

The GPK3 3DEC model has been built on the base of eight fracture zones identified on UBI data and temperature logs. As there was no data on the F0 geometry, one had performed in the previous studies some tests on the F0 geometry. Table 9 gives the fractures planes geometry used in our GPK3 models cases 1 and 2 where we apply either the first stress field or the second stress field. The GPK3 3DEC model is centred on Fracture F3, at 4900m depth (Figure 18).

Fracture N°	Depth (m)	Dip (°)	Dip Direction (°)
F0	4900 -	66	30
F1	4900 -	64	234
F2	4900 - 40	78	57
F3	4900 - 0	74	262
F4	4900 + 20	71	263
F5	4900 + 60	72	47
F6	4900 + 80	79	270
F7	4900 +	66	292

Table 9. GPK3 – fractures planes geometry

The fractures hydro-mechanical properties used are given Table 10. Note that the normal and tangential stiffnesses, the dilation angle and Z_dil are the same as the one used for the GPK4 stimulation test (given Table 4). The F1 hydro-mechanical properties correspond to a very thick permeable fracture zone (25 m), observed on the UBI data.

	Fracture N°	Initial aperture a_0 [μm]	Resid. aperture a_{res} [μm]	Max. aperture a_{max} [μm]	Friction angle φ (°)
Case 1 & Case 2	F0	5.0	2.50	250	52
	F1	140.0	70.0	12000	48
	F2 to F7	5.0	2.50	150	54

Table 10. GPK3 – fractures hydro-mechanical properties

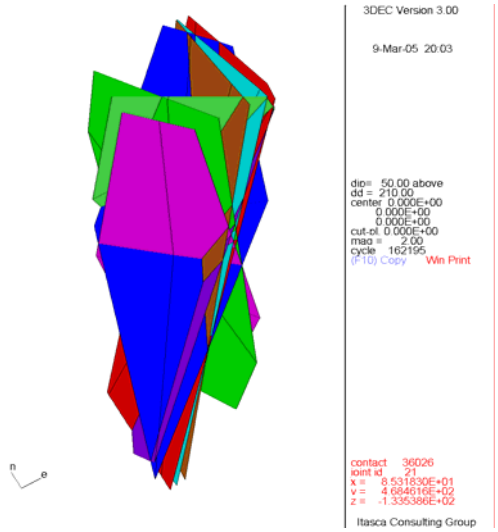

Figure 18. GPK3 – 3DEC model – fractures perspective view

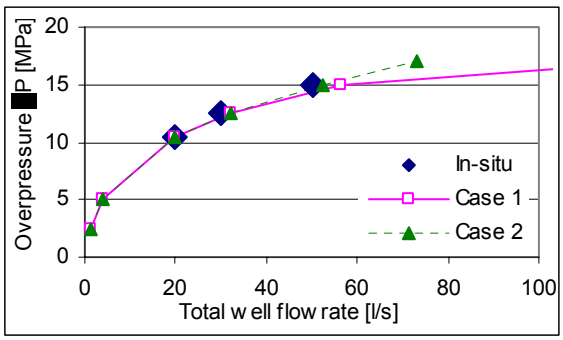

Figure 19. GPK3 – Evolution of the total well flowrate as a function of the overpressure stages ΔP applied into GPK3 – Comparison of the two stress fields n°1 & n°2

GPK3 – Influence of the stress field

As for GPK4, we performed two numerical hydraulic stimulation tests:

- Case1, corresponding to the stress field n°1 proposed by Klee and Rummel,
- Case2, corresponding to the stress field n°2, proposed by Cornet et *al.*

Figure 19 represents the Flowrate (Q) vs. Overpressure stages (ΔP) stimulation curves obtained with 3DEC for the two cases and the one obtained in-situ. For GPK3, three overpressure stages have been applied in situ. We applied in 3DEC the six overpressure stages given Table 2. Until the 15.0 MPa overpressure stage, the flowrate injected in the well is very much comparable between the two stress fields. For the last overpressure stage, 17 MPa, which has not been applied in-situ, the flowrate calculated with the second stress field seems to be in accordance with the general slope of the curve Q-ΔP, whereas with the first stress field one can observe that there is a high increase in the injected flowrate (over 100 l/s instead of 70 l/s).

Figure 20 represents the flow contribution, in percentage, of each fracture to the total flow in the well for each overpressure stage (ΔP). Except for the last overpressure stages, the flowrates distribution along the 8 fractures is comparable between the two stress fields. Due to its great initial hydraulic aperture, the strong F1 contribution to the global response is obvious. F6 is the most permeable fracture and F5 the less permeable one whatever the overpressure in the well is. Between the last two overpressure stages 15 and 17 MPa, the F1 flow contribution remains constant with the second stress field, whereas it increases from 60% to 80% with the first stress field. This results, for this first stress field, in a decrease of each fracture flow contribution to the total flowrate.

The block displacements as well as the fractures shear displacements remain very small compared to the GPK4 stimulation test. The existence of the very permeable fracture F1 limits the possibility of shearing in the other plans of fracture located below. At the 15 MPa overpressure stage, the displacements are comparable between the two stress fields, and remain below 1 cm (Table 11). The shearing is hence very limited, and it increases only for the highest overpressure stage 17 MPa applied with 3DEC into the well (note this overpressure stage has not been applied in-situ). For such an overpressure stage, the maximum fractures shear displacements reach 2.7 cm for stress field n°1 and 1.4 cm for stress field n°2 (Table 11)

Note that this shearing is not located in the same fractures for the 2 stress fields:

- the 2.7 cm maximum fracture shear displacement is obtained in F1 (Figure 21) and F2 (Figure 22) for stress field n°1, whereas

- the maximum 1.4 cm fracture shear displacement is obtained in F3 (Figure 23) for stress field n°2.

	Maximum blocks displacements in entire model [mm]		Maximum fractures shear displacements in entire model [mm]	
	ΔP= 15 MPa	ΔP= 17 MPa	ΔP= 15 MPa	ΔP= 17 MPa
Case 1	5.6	17.2	9.9	27.2
Case 2	4.7	9.6	7.1	14.0

Table 11. GPK3 – Case 1 & 2 – Maximum blocks and fractures shear displacements for two overpressure stages 15 and 17 MPa – Comparison of the 2 stress fields

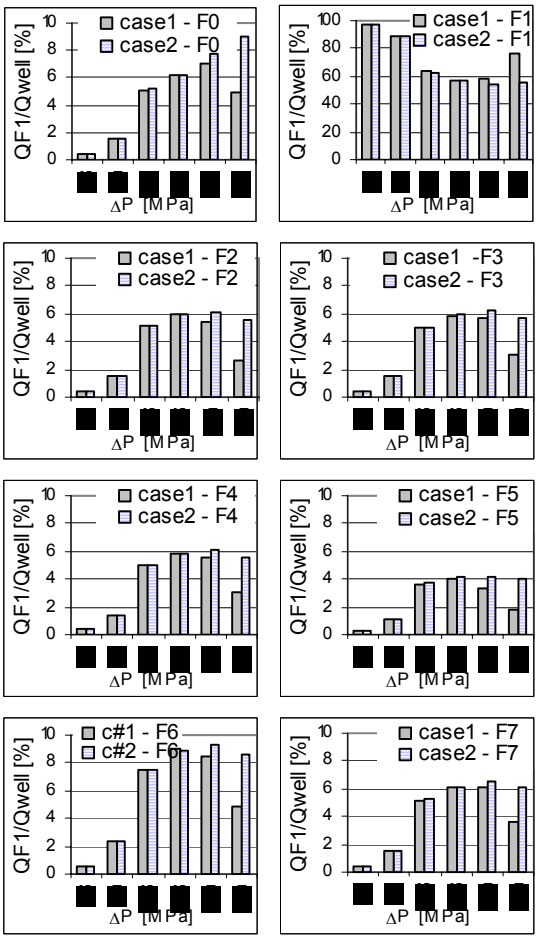

Figure 20. GPK3 – Flowrate percentages in each fracture vs overpressure stages ΔP applied into GPK3 – Comparison of the two stress fields n°1 & n°2

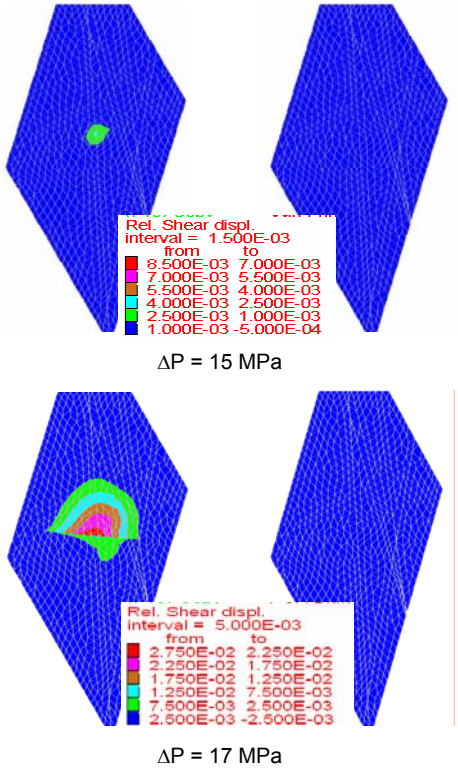

Figure 21. GPK3 – Shear displacements contours in F1 at ΔP = 15 MPa & 17 MPa – Comparison of the 2 stress fields

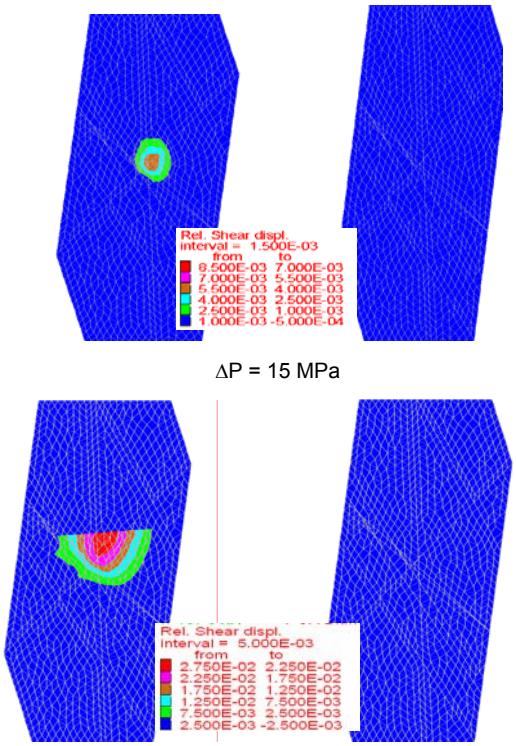

Figure 22. GPK3 – Shear displacements contours in F2 at ΔP = 15 MPa & 17 MPa – Comparison of the 2 stress fields

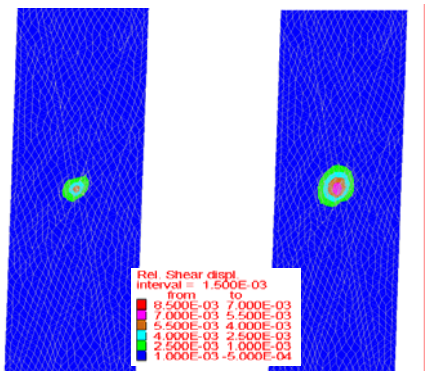

ΔP = 15 MPa

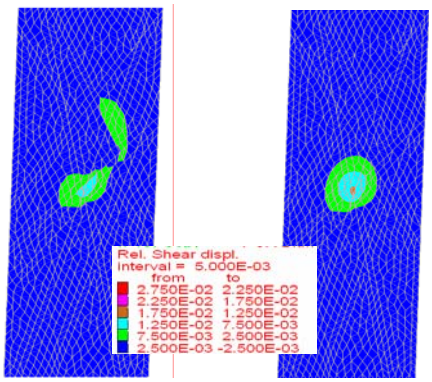

ΔP = 17 MPa

Case 1 (stress field n°1) Case 2 (stress field n°2)

Figure 23. GPK3 – Shear displacements contours in F3 at ΔP = 15 MPa & 17 MPa – Comparison of the 2 stress fields

Developments in progress

The fractures mechanical constitutive law we have used up to now is the Mohr-Coulomb slip model with dilation effect. We are aware that with this constitutive law, we may not be able to reproduce a shut-down hydraulic test, as we may not have significant irreversible permeability increase with the Mohr-Coulomb model. We plan to use another constitutive law, the Continuously Yielding Joint Model that is available in the 3DEC code, which takes into account the fracture damage associated to the shearing of the fractures.

Then, we plan to enlarge our model size and modify our hydro-mechanical coupling procedure in order simulate several wells. Thus, we will be able to take into account the effect of a hydraulic stimulation performed in a well on the response of the hydraulic stimulation of another well.

At last, we plan also to take into account the thermal impact of the injection of a cold fluid in the hot rock.

Conclusion

In the current phase of this program we studied the influence of the stress field on the hydro-mechanical behaviour of the rock mass during hydraulic stimulations. We performed with 3DEC some hydro-mechanical modelling of the stimulation tests performed in GPK3 and GPK4 and took into account two stress fields: the classical one used up to now, determined by Klee and Rummel (1993), and the new one determined by Cornet & al. (2006). We analyzed their influence in terms of shearing in the main fractures of the rock mass, and showed that, with the classical stress field, the shear displacements could be two times larger than with the second stress field. We showed that for GPK4, these large displacements were not located close to the well, but at a great distance from the well and were due to some block instabilities.

References

Cornet & al. (2006), to be published

Gentier & al. (2005), Thermo-Hydro-Mechanical modelling of the deep geothermal wells at Soultz-sous-Forêts. *Proceedings of the European Hot Dry Rock Association Scientific Conference, March 2005*

Klee, G. and Rummel, F. (1993), Hydrofrac stress data for the European HDR research test site Soultz-sous-Forêts. *Int. J. Rock Mech. Sci. & Geomech. Abstr.*, **30**, n°7, 973-976.

ITASCA (2003). 3DEC Version 3.0, 3 Dimensional Distinct Element Code. *User's Manual*. Itasca Consulting Group Inc., Minneapolis, MN., June 2003.

AUTHORS' INDEX

Design: Direction de la communication et des éditions BRGM

Layout : Geowatt AG
E-mail : engine@geowatt.ch

http://engine.brgm.fr

The ENGINE Workshop 3
Stimulation of reservoir and induced microseismicity
is sponsored by:

The ENGINE partners:

Document edited for the European
ENGINE Workshop 3
Kartause Ittingen - Switzerland
29 June - 1 July 2006

GEOWATT AG
DohlenWeg, 28
CH-8050 Zürich - Switzerland
Phone: +41 (0)44 242 14 54
Fax: +41 (0)44 242 14 58

GEOWATT AG
SWISS GEOTHERMAL EXPERT GROUP
GEOTHERMAL ENERGY HYDROGEOLOGY ENGINEERING NUMERICS